METHODS IN MOLECULAR BIOLOGY™ 303

NanoBiotechnology Protocols

Edited by

Sandra J. Rosenthal
David W. Wright

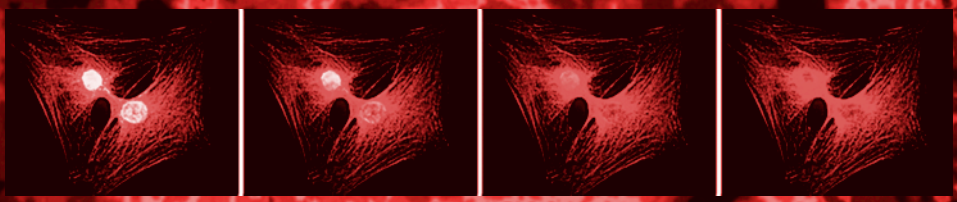

Includes Companion CD

HUMANA PRESS

NanoBiotechnology Protocols

METHODS IN MOLECULAR BIOLOGY™

John M. Walker, SERIES EDITOR

316. Bioinformatics and Drug Discovery, edited by *Richard S. Larson, 2005*

315. Mast Cells: *Methods and Protocols*, edited by *Guha Krishnaswamy and David S. Chi, 2005*

314. DNA Repair Protocols: *Mammalian Systems, Second Edition*, edited by *Daryl S. Henderson, 2005*

313. Yeast Protocols: *Second Edition*, edited by *Wei Xiao, 2005*

312. Calcium Signaling Protocols: *Second Edition*, edited by *David G. Lambert, 2005*

311. Pharmacogenomics: *Methods and Applications*, edited by *Federico Innocenti, 2005*

310. Chemical Genomics: *Reviews and Protocols*, edited by *Edward D. Zanders, 2005*

309. RNA Silencing: *Methods and Protocols*, edited by *Gordon Carmichael, 2005*

308. Therapeutic Proteins: *Methods and Protocols*, edited by *C. Mark Smales and David C. James, 2005*

307.Phosphodiesterase Methods and Protocols, edited by *Claire Lugnier, 2005*

306. Receptor Binding Techniques: *Second Edition*, edited by *Anthony P. Davenport, 2005*

305.Protein–Ligand Interactions: *Methods and Protocols*, edited by *G. Ulrich Nienhaus, 2005*

304. Human Retrovirus Protocols: *Virology and Molecular Biology*, edited by *Tuofu Zhu, 2005*

303. NanoBiotechnology Protocols, edited by *Sandra J. Rosenthal and David W. Wright, 2005*

302. Handbook of ELISPOT: Methods and Protocols, edited by *Alexander E. Kalyuzhny, 2005*

301. Ubiquitin–Proteasome Protocols, edited by *Cam Patterson and Douglas M. Cyr, 2005*

300. Protein Nanotechnology: *Protocols, Instrumentation, and Applications*, edited by *Tuan Vo-Dinh, 2005*

299. Amyloid Proteins: *Methods and Protocols*, edited by *Einar M. Sigurdsson, 2005*

298. Peptide Synthesis and Application, edited by *John Howl, 2005*

297. Forensic DNA Typing Protocols, edited by *Angel Carracedo, 2005*

296. Cell Cycle Protocols, edited by *Tim Humphrey and Gavin Brooks, 2005*

295. Immunochemical Protocols, *Third Edition*, edited by *Robert Burns, 2005*

294. Cell Migration: *Developmental Methods and Protocols*, edited by *Jun-Lin Guan, 2005*

293. Laser Capture Microdissection: *Methods and Protocols*, edited by *Graeme I. Murray and Stephanie Curran, 2005*

292. DNA Viruses: *Methods and Protocols*, edited by *Paul M. Lieberman, 2005*

291. Molecular Toxicology Protocols, edited by *Phouthone Keohavong and Stephen G. Grant, 2005*

290. Basic Cell Culture, *Third Edition*, edited by *Cheryl D. Helgason and Cindy Miller, 2005*

289. Epidermal Cells, *Methods and Applications*, edited by *Kursad Turksen, 2005*

288. Oligonucleotide Synthesis, *Methods and Applications*, edited by *Piet Herdewijn, 2005*

287. Epigenetics Protocols, edited by *Trygve O. Tollefsbol, 2004*

286. Transgenic Plants: *Methods and Protocols*, edited by *Leandro Peña, 2005*

285. Cell Cycle Control and Dysregulation Protocols: *Cyclins, Cyclin-Dependent Kinases, and Other Factors*, edited by *Antonio Giordano and Gaetano Romano, 2004*

284. Signal Transduction Protocols, *Second Edition*, edited by *Robert C. Dickson and Michael D. Mendenhall, 2004*

283. Bioconjugation Protocols, edited by *Christof M. Niemeyer, 2004*

282. Apoptosis Methods and Protocols, edited by *Hugh J. M. Brady, 2004*

281. Checkpoint Controls and Cancer, Volume 2: *Activation and Regulation Protocols*, edited by *Axel H. Schönthal, 2004*

280. Checkpoint Controls and Cancer, Volume 1: *Reviews and Model Systems*, edited by *Axel H. Schönthal, 2004*

279. Nitric Oxide Protocols, *Second Edition*, edited by *Aviv Hassid, 2004*

278. Protein NMR Techniques, *Second Edition*, edited by *A. Kristina Downing, 2004*

277. Trinucleotide Repeat Protocols, edited by *Yoshinori Kohwi, 2004*

276. Capillary Electrophoresis of Proteins and Peptides, edited by *Mark A. Strege and Avinash L. Lagu, 2004*

275. Chemoinformatics, edited by *Jürgen Bajorath, 2004*

274. Photosynthesis Research Protocols, edited by *Robert Carpentier, 2004*

273. Platelets and Megakaryocytes, Volume 2: *Perspectives and Techniques*, edited by *Jonathan M. Gibbins and Martyn P. Mahaut-Smith, 2004*

272. Platelets and Megakaryocytes, Volume 1: *Functional Assays*, edited by *Jonathan M. Gibbins and Martyn P. Mahaut-Smith, 2004*

271. B Cell Protocols, edited by *Hua Gu and Klaus Rajewsky, 2004*

270. Parasite Genomics Protocols, edited by *Sara E. Melville, 2004*

269. Vaccina Virus and Poxvirology: *Methods and Protocols*,edited by *Stuart N. Isaacs, 2004*

268. Public Health Microbiology: *Methods and Protocols*, edited by *John F. T. Spencer and Alicia L. Ragout de Spencer, 2004*

METHODS IN MOLECULAR BIOLOGY™

NanoBiotechnology Protocols

Edited by

Sandra J. Rosenthal

and

David W. Wright

The Department of Chemistry, Vanderbilt University, Nashville, TN

HUMANA PRESS TOTOWA, NEW JERSEY

999 Riverview Drive, Suite 208
Totowa, New Jersey 07512

www.humanapress.com

This publication is printed on acid-free paper. ♾
ANSI Z39.48-1984 (American Standards Institute)

Permanence of Paper for Printed Library Materials.

Production Editor: C. Tirpak
Cover design by Patricia F. Cleary

Cover Illustration: From Fig. 2, Chapter 1, "Applications of Quantum Dots in Biology: An Overview," by Charles Z. Hotz and from Fig. 3, Chapter 13, "Nanostructured DNA Templates," by Jeffery L. Coffer, Russell F. Pnizzotto, and Young Gyu Rho.

For additional copies, pricing for bulk purchases, and/or information about other Humana titles, contact Humana at the above address or at any of the following numbers: Tel: 973-256-1699; Fax: 973-256-8341; E-mail: orders@humanapr.com; or visit our Website: www.humanapress.com

Printed in the United States of America. 10 9 8 7 6 5 4 3 2 1

ISSN 1064-3745

E-ISBN 1-59259-901-X

Library of Congress Cataloging-in-Publication Data

Nanobiotechnology protocols / edited by Sandra J. Rosenthal and David W. Wright.

p. cm. -- (Methods in molecular biology ; 303)

Includes bibliographical references and index.

ISBN 1-58829-276-2 (alk. paper)

1. Nanotechnology--Laboratory manuals. 2. Biotechnology--Laboratory manuals. I. Rosenthal, Sandra Jean, 1966- II. Wright, David W. III. Series: Methods in molecular biology (Clifton, N.J.) ; 303.

TP248.25.N35N35 2005

660.6--dc22

2005000473

Preface

Increasingly, researchers find themselves involved in discipline-spanning science that a decade ago was simply inconceivable. Nowhere is this more apparent than at the cusp of two rapidly developing fields, nanoscience and biotechnology. The resulting hybrid of nanobiotechnology holds the promise of providing revolutionary insight into aspects of biology ranging from fundamental questions of receptor function to drug discovery and personal medicine. As with many fields fraught with increasing hyperbole, it is essential that the underlying approaches be based on solid, reproducible methods. It is the goal of *NanoBiotechnology Protocols* to provide novice and experienced researchers alike a cross-section of the methods employed in significant frontier areas of nanobiotechnology.

In a rapidly developing field such as biotechnology, it is difficult to predict at what mature endpoint a field will arrive. Today, nanobiotechnology is making significant advances in three broad areas: novel materials synthesis, dynamic cellular imaging, and biological assays. As a testament to the true nature of interdisciplinary research involved in nanobiotechnology, each of these areas is being driven by rapid advances in the others: New materials are enabling the imaging of cellular processes for longer durations, leading to high-throughput cellular-based screens for drug discovery, drug delivery, and diagnostic applications.

NanoBiotechnology Protocols addresses methods in each of these areas. Two overview chapters are provided for perspective for those beginning investigations in nanobiotechnology. Throughout this volume, there is a deliberate emphasis on the use of nanoparticles. As functionalized materials, they represent one of the fundamental enabling nanoscale components for these technologies. Consequently, many of the protocols highlight diverse strategies to synthesize and functionalize these probes for biological applications. Other chapters focus on the use of biological components (peptides, antibodies, and DNA) to synthesize and organize nanoparticles to be used as building blocks in larger assemblies. The methods described herein are by no means complete;

nor are they necessarily intended to be. Every day seems to produce new applications of nanotechnology to biological systems. It is our hope that this volume provides a detailed, hands-on perspective of nanobiotechnology to encourage scientists working in interdisciplinary fields to recognize the utility of this emerging technology.

Sandra J. Rosenthal
David W. Wright

Contents

Contributors

GEORGE P. ANDERSON • *Center for Bio/Molecular Science and Engineering Naval Research Laboratory, Washington DC*

FRANZ BAUDENBACHER • *Department of Physics, Vanderbilt University, Nashville, TN*

RANDY D. BLAKELY • *Department of Pharmacology, Vanderbilt University School of Medicine, Vanderbilt University, Nashville, TN*

SUNG-WOOK CHOI • *Division of Chemical Engineering and Biotechnology, Yonsei University, Seoul, Korea*

DAVID E. CLIFFEL • *Department of Chemistry, Vanderbilt University, Nashville, TN*

JEFFERY L. COFFER • *Department of Chemistry, Texas Christian University, Fort Worth, TX*

JENNIFER EDL • *Department of Biochemistry, Vanderbilt University, Nashville, TN*

SVEN E. EKLUND • *Department of Chemistry, Vanderbilt University, Nashville, TN*

DANIEL L. FELDHEIM • *Department of Chemistry, North Carolina State University, Raleigh, NC*

STEFAN FRANZEN •*Department of Chemistry, North Carolina State University, Raleigh, NC*

R. GRIFFITH FREEMAN • *Nanoplex Technologies Inc., Menlo Park, CA*

XIAOHU GAO • *Departments of Biomedical Engineering, Chemistry, Hematology and Oncology, Emory University, Atlanta, GA*

WILHELM R. GLOMM • *Department of Chemistry, North Carolina State University, Raleigh, NC*

ELLEN R. GOLDMAN • *Center for Bio/Molecular Science and Engineering Naval Research Laboratory, Washington DC*

MICHAEL A. GUILLORN • *Molecular-Scale Engineering and Nanoscale Technologies Research Group, Oak Ridge National Laboratory, Oak Ridge, TN*

NAOMI J. HALAS • *Department of Electrical and Computer Engineering and Department of Chemistry, Rice University Houston, TX*
LIN HE • *Nanoplex Technologies Inc., Menlo Park, CA*
LEE R. HIRSCH • *Department of Bioengineering, Rice University, Houston, TX*
CHARLES Z. HOTZ • *Quantum Dot Corporation, Hayward, CA*
JUNG-HYUN KIM •*Nanosphere Process and Technology Laboratory, Yonsei University, Seoul, Korea*
WOO-SIK KIM • *Division of Chemical Engineering and Biotechnology, Yonsei University, Seoul, Korea*
EUGENE KOZLOV • *Department of Chemical Engineering, Vanderbilt University, Nashville, TN*
DOUGLAS H. LOWNDES • *Thin Film and Nanostructured Materials Physics Group, Oak Ridge National Laboratory, Oak Ridge, TN*
RAHINA MAHTAB • *Department of Physical Sciences, South Carolina State University, Orangeburg, SC*
JOHN N. MASON • *Department of Pharmacology, Vanderbilt University School of Medicine, Vanderbilt University, Nashville, TN*
HEDI MATTOUSSI • *Center for Bio/Molecular Science and Engineering Naval Research Laboratory, Washington DC*
J. MATTHEW MAURO • *Center for Bio/Molecular Science and Engineering Naval Research Laboratory, Washington DC*
TIMOTHY E. MCKNIGHT • *Molecular-Scale Engineering and Nanoscale Technologies Research Group, Oak Ridge National Laboratory, Oak Ridge, TN*
IGOR L. MEDINTZ • *Center for Bio/Molecular Science and Engineering Naval Research Laboratory, Washington DC*
ANATOLI V. MELECHKO • *Molecular-Scale Engineering and Nanoscale Technologies Research Group, Oak Ridge National Laboratory, Oak Ridge, Tennessee and Electrical and Computer Engineering Department, University of Tennessee, Knoxville, TN*
VLADIMIR I. MERKULOV • *Molecular-Scale Engineering and Nanoscale Technologies Research Group, Oak Ridge National Laboratory, Oak Ridge, TN*
RAY MERNAUGH • *Department of Biochemistry Vanderbilt University, Nashville, TN*
CATHERINE J. MURPHY • *Department of Chemistry and Biochemistry, University of South Carolina, Columbia, SC*
MICHAEL J. NATAN • *Nanoplex Technologies Inc., Menlo Park, CA*
SHUMING NIE • *Departments of Biomedical Engineering, Chemistry, Hematology and Oncology, Emory University and Georgia Institute of Technology, Atlanta, GA*

SCOTT M. NORTON • *Nanoplex Technologies Inc., Menlo Park, CA*
SHARRON G. PENN • *Nanoplex Technologies Inc., Menlo Park, CA*
RUSSELL F. PINIZZOTTO• *Department of Physics, Merrimack College, North Andover, MA*
PAUL A. RAJU • *Nanoplex Technologies Inc., Menlo Park, CA*
YOUNG GYU RHO • *Department of Physics, University of North Texas, Denton, TX*
SANDRA J. ROSENTHAL • *Department of Chemistry, Vanderbilt University, Nashville, TN*
JOSEPH RYAN • *Department of Chemistry, North Carolina State University, Raleigh, NC*
NADRIAN C. SEEMAN • *Department of Chemistry, New York University, New York, NY*
MICHAEL Y. SHA • *Nanoplex Technologies Inc., Menlo Park, CA*
MICHAEL L. SIMPSON • *Molecular-Scale Engineering and Nanoscale Technologies Research Group, Oak Ridge National Laboratory, Oak Ridge, Tennessee, Materials Science and Engineering Department and Center for Environmental Biotechnology University of Tennessee, Knoxville, TN*
JOSEPH M. SLOCIK • *Department of Chemistry, Vanderbilt University, Nashville, TN*
PATRICK C. SMITH • *Nanoplex Technologies Inc., Menlo Park, CA*
DALE E. TAYLOR • *Department of Chemistry, Vanderbilt University, Nashville, TN*
ALEXANDER TKACHENKO • *Department of Chemistry, North Carolina State University, Raleigh, NC*
IAN D. TOMLINSON • *Department of Chemistry, Vanderbilt University, Nashville, TN*
IAN D. WALTON • *Nanoplex Technologies Inc., Menlo Park, CA*
JENNIFER L. WEST • *Department of Bioengineering, Rice University, Houston, TX*
DAVID W. WRIGHT • *Department of Chemistry, Vanderbilt University, Nashville TN*
HUAN XIE • *Department of Chemistry, North Carolina State University, Raleigh, NC*

Companion CD

To view color figures, please refer to the companion CD. The images are best viewed on a high-resolution (1280 x 1280) color (24 bit or higher true color) computer monitor.

1

Applications of Quantum Dots in Biology

An Overview

Charles Z. Hotz

Summary

This chapter summarizes the properties of fluorescent semiconductor nanocrystals (quantum dots), and their relationship to performance in biological assays. The properties of quantum dots (optical, structural, compositional, etc.) are described. Recent work employing these entities in biological studies (immunofluorescent labeling, imaging, microscopy in vivo applications, encoding) is discussed.

Key Words

Quantum dot; semiconductor nanocrystal; labeling; biological imaging; immunohistochemistry; fluorescence microscopy; multiplexing.

1. Introduction

Highly luminescent, colloidal semiconductor nanocrystals, or quantum dots, have been known since the early 1990s ***(1–3)***; however, not until 1998 were these materials were first utilized as biological probes ***(4,5)***. The emission wavelength of these unique fluorescent probes can be altered with a change in the size of the quantum dot, allowing their emission to be tuned to any wavelength within a range determined by the semiconductor composition. Although there have been a number of reports of biological applications of quantum dots since the pioneering articles, it is clear that the use of these novel probes is still in its infancy. Both protocols for using quantum dots and the methods for preparing these reagents are continually being improved. Because many of the properties of quantum dots differ from those of other fluorescent biological probes, quantum dots can be enabling for a given application. These key properties are discussed in relation to their performance in biological applications.

From: *Methods in Molecular Biology, vol. 303: NanoBiotechnology Protocols*
Edited by: S. J. Rosenthal and D. W. Wright © Humana Press Inc., Totowa, NJ

2. General Properties

2.1. Optical Properties

2.1.1. Absorbance Characteristics

Quantum dots absorb light differently than dye molecules. Fluorescent dyes typically absorb light efficiently in an absorbance band that has a slightly shorter wavelength than the emission (*see* **Fig. 1A**). This can be advantageous for selective excitation of a fluorophore but also requires that each fluorescent dye be excited separately when multiple colors are used together (multiplex). This can decrease throughput and increase instrument cost, particularly when lasers are required for excitation. The absorbance band of a fluorescent dye is usually spectrally close to the light emitted, making efficient collection of the emitted light more difficult owing to scatter, autofluorescence, and the need for precise optical filters.

Quantum dots, by comparison, absorb light at all wavelengths shorter than the emission (**Fig. 1B**). This allows multiple colors of quantum dots to be effectively excited by a single source of light (e.g., lamp, laser, LED) far from the emission of any color. The effective "Stokes shift," or wavelength difference between maximum absorbance and maximum emission (typically ~15–30 nm for organic dyes), can be hundreds of nanometers for a quantum dot.

Not only can quantum dots be excited far from where they emit, but extinction coefficients (i.e., the measure of absorbed light) are much larger than for typical fluorescent dyes and, thus, absorb light much more efficiently (**Fig. 1D**). For example, the extinction coefficients for some common dyes compared to quantum dots are provided in **Table 1**.

In addition, the use of many colors of quantum dots simultaneously (multiplexing) requires only one excitation source to excite all colors efficiently. This can be particularly valuable in multicolor fluorescence microscopy, enabling one to visualize simultaneously many colors of quantum dot-labeled probes.

2.1.2. Emission Characteristics

2.1.2.1. Shape of Emission Spectrum

By their nature, quantum dots exist in polydisperse collections of nanocrystals of slightly different sizes. The emission spectrum of a solution of quantum dots is the sum of the spectra of many individual quantum dots that differ slightly in size. Consequently, the width of the observable emission spectrum depends on the uniformity of the quantum dot size distribution (*see* **Subheading 2.2.**). A sample that has a very uniform quantum dot size distribution will have a narrower composite emission spectrum than a sample that is less uniform. Typically, the size distribution is nearly normally distributed and the emission spectrum nearly Gaussian shaped. This is in contrast to most fluorescent dyes that display

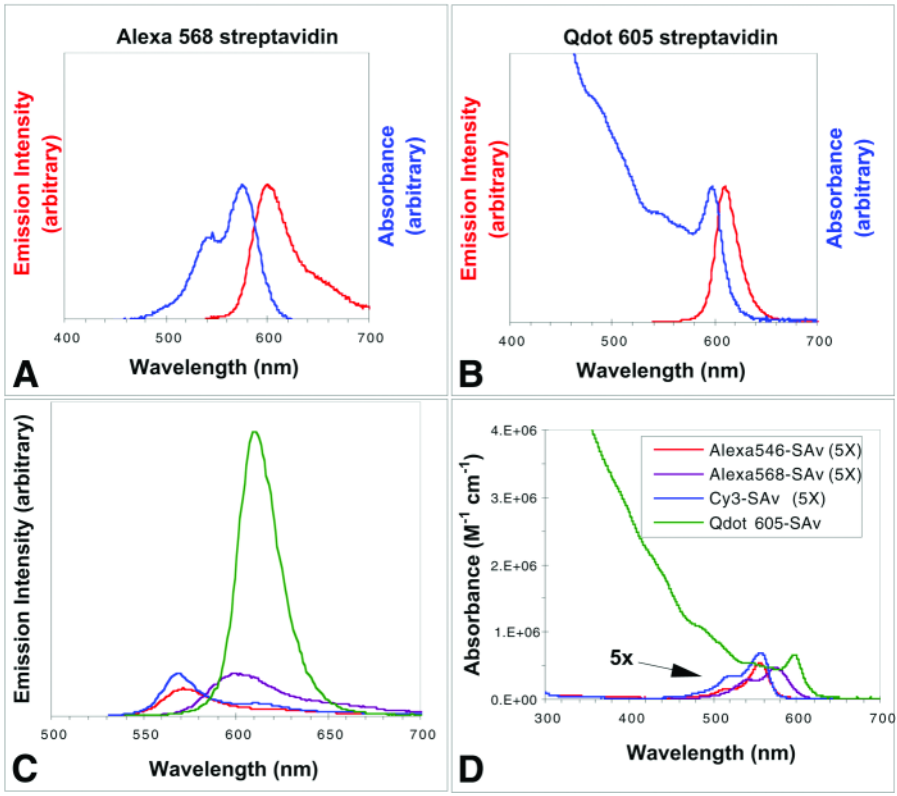

Fig. 1. Comparison of absorbance and emission spectra (normalized) of **(A)** Alexa® 568 streptavidin conjugate and **(B)** Qdot® 605 streptavidin conjugate. Note that the quantum dot conjugate can absorb light efficiently far to the blue of the emission. **(C)** Comparison of emission spectra (nonnormalized) of streptavidin conjugates of Qdot 605 (—), Alexa 546 (—), Alexa 568 (—), and Cy3® (—). The spectra were taken under conditions in which each fluorophore absorbed the same amount of excitation light. The measured quantum yields of the conjugates were 55, 8, 16, and 11%, respectively. **(D)** Comparison of absorbance spectra (nonnormalized, each 1 μ*M* flurophore) of Qdot 605 streptavidin conjugate (—), Cy3 streptavidin conjugate (—), Alexa 546 streptavidin conjugate (—), and Alexa 568 streptavidin conjugate (—). Note that all dye spectra are enhanced fivefold for clarity. Alexa, Cy3, and Qdot are registered trademarks of Molecular Probes, Amersham Biosciences, and Quantum Dot Corporation, respectively.

asymmetric emission spectra that tail (sometimes dramatically) to the red (*see* **Fig. 1C**). Additionally, typical high-quality quantum dot size distributions result in emission spectrum widths (at half maximum) of 20–35 nm, which is noticeably narrower than for comparable dyes. These narrow, symmetric emission

Table 1
Optical Properties of Quantum Dots Compared to Common Dyes[a]

Fluorescent dye	$\lambda_{excitation}$ (nm)	$\lambda_{emission}$ (nm)	$\varepsilon(mol^{-1}\text{-}cm^{-1})$
Qdot 525	400	525	280,000
Alexa 488	495	519	78,000
Fluorescein	494	518	79,000
Qdot 565	400	565	960,000
Cy3	550	570	130,000
Alexa 555	555	565	112,000
Qdot 585	400	585	1,840,000
R-Phycoerythrin	565	578	1,960,000
TMR	555	580	90,000
Qdot 605	400	605	2,320,000
Alexa 568	578	603	88,000
Texas Red	595	615	96,000
Qdot 655	400	655	4,720,000
APC	650	660	700,000
Alexa 647	650	668	250,000
Cy5	649	670	200,000
Alexa 647-PE	565	668	1,960,000

[a]The extinction coefficients (ε) are generally much larger for quantum dots than for fluorescent dyes. Furthermore, the excitation wavelength ($\lambda_{excitation}$) can be much farther from the emission ($\lambda_{emission}$).

spectra make possible detection of multiple colors of quantum dots together (multiplexing) with low cross-talk between detection channels.

2.1.2.2. Quantum Yield

Quantum yield is a measure of the "brightness" of a fluorophore and is defined as the ratio of light emitted to light absorbed by a fluorescent material. Some organic dyes have quantum yields approaching 100%, but conjugates (from biological affinity molecules) made from these dyes generally have a significantly lower quantum yield. Quantum dots retain their high quantum yield even after conjugation to biological affinity molecules (**Fig. 1C**).

2.1.2.3. Photostability

Fluorescent dyes tend to be organic molecules that are steadily bleached (degraded) by the light used to excite them, progressively emitting less light over time. Although a wide range of photostability is observed in various

fluorescent dye molecules, the stability does not approach that observed in quantum dots (*see* **Fig. 2**). Even under conditions of intense illumination (e.g., in a confocal microscope or flow cytometer), little if any degradation is observed ***(6)***. This property makes quantum dots enabling in applications requiring continuous observation of the probe (cell tracking, some imaging applications, and so on), and potentially more valuable as quantitative reagents.

2.1.2.4. Fluorescence Lifetime

Quantum dots have somewhat longer fluorescence lifetimes than typical organic fluorophores (approx 20–40 vs <5 ns, respectively) ***(7)***. While this lifetime is shorter than "long-lifetime" fluorophores, such as lanthanides (hundreds of microseconds), the difference could be exploited to reduce autofluorescence background in some measurements, such as those made on polymer substrates. A short delay between excitation and collection of the emitted light can nearly eliminate autofluorescence of polymeric substrates (or potentially other media such as blood) and still allow collection of the majority of the quantum dot-emitted light (Quantum Dot Corporation, unpublished data). Additionally, the relatively short lifetime of quantum dots does not significantly reduce emission at high excitation power owing to saturation.

2.2. Physical Properties

2.2.1. Structure

Quantum dot conjugates are complex, multilayered structures, and many process steps are required to produce a useful, biological conjugate (**Fig. 3**). Some terminology that is used in describing quantum dot structures is as follows:

1. Core quantum dot: The central quantum dot nanocrystal, and what determines the optical properties of the final structure. Most preparations produce core quantum dots that are hydrophobic.
2. Core-shell quantum dot: Core nanocrystals that have a crystalline inorganic shell. These materials are bright, stable, and, like cores, are hydrophobic and only soluble in organic solvents.
3. Water-soluble quantum dot: Core-shell quantum dots that are hydrophilic and are soluble in water and biological buffers. Commercially available water-soluble quantum dots have a hydrophilic polymer coating.
4. Quantum dot bioconjugate: Coupling a water-soluble quantum dot to affinity molecules produces a quantum dot bioconjugate.

Unlike samples of dye molecules in which every molecule is identical, each core quantum dot in a sample contains a slightly different number of atoms and thus can be slightly different in some of the properties (*see* **Subheading 2.3.**). Consequently, the methods developed to synthesize quantum dot cores are

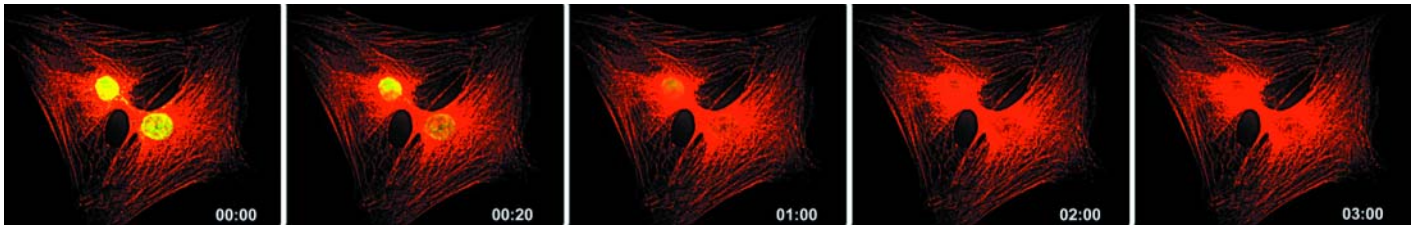

Fig. 2. Comparison of photostability between Qdot® 605 and Alexa Fluor® 488 streptavidin conjugates. Actin filaments in two 3T3 mouse fibroblast cells were labeled with Qdot 605 streptavidin conjugate (red), and the nuclei were stained with Alexa Fluor 488 streptavidin (green). The specimens were continuously illuminated for 3 min with light from a 100-W mercury lamp under a ×100 1.30 oil objective. An excitation filter (excitation: 485 ± 20 nm) was used to excite both Alexa 488 and Qdot 605. Emission filters (emission: 535 ± 10 and em 605 ± 10 nm) on a motorized filter wheel were used to collect Alexa 488 and Qdot 605 signals, respectively. Images were captured with a cooled charge-coupled device camera at 10-s intervals for each color automatically. Images at 0, 20, 60, 120, and 180 s are shown. Whereas Alexa 488 labeling signal faded quickly and became undetectable within 2 min, the Qdot 605 signal showed no obvious change for the entire 3-min illumination period.

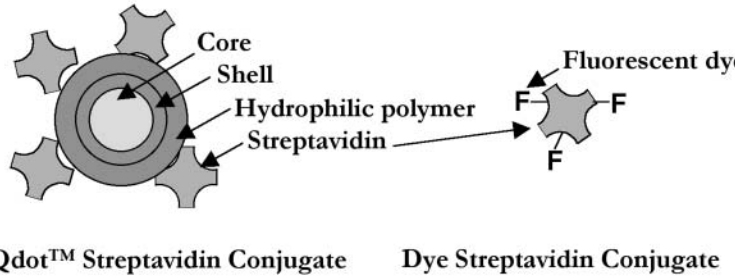

Fig. 3. Schematic of Qdot™ Nanocrystal Probe compared to a typically labeled fluorescent dye protein conjugate (see text for descriptions). Proteins generally carry several fluorescent dye labels (F). By contrast, each quantum dot is conjugated to multiple protein molecules.

continually being optimized to produce more uniform materials ***(8,9)***. This increased uniformity of size and shape produces samples that have narrower (sharper) emission spectra, allowing colors that are closer in wavelength (color) to be used together.

Although these "core" quantum dots determine the optical properties of the conjugate, they are by themselves unsuitable for biological probes owing to their poor stability and quantum yield. In fact, the quantum yield of quantum dot cores has been reported to be very sensitive to the presence of particular ions in solution ***(10)***. Highly luminescent quantum dots are prepared by coating these core quantum dots with another material (in the case of cadmium selenide cores, zinc sulfide or cadmium sulfide is generally used), resulting in "core-shell" quantum dots that are much brighter, and more stable in various chemical environments ***(3,11)***. These core-shell quantum dots are hydrophobic and only organic soluble as prepared.

A number of methods have been reported to convert these hydrophobic "core-shells" into aqueous-soluble, biologically useful versions ***(4,5,12,13)***. Although a comprehensive comparison of these approaches does not exist, there are significant differences in the stability and brightness, and therefore the performance of the resulting aqueous materials. Frequently, investigators do not report quantum yields of the bioconjugates prepared, and often the limit of detection is not reported in a way that allows comparison of performance with that of another method. The stability of the conjugate, a property that is essential for a quantitative reagent, is generally not determined either. For example, some preparations lack stability toward dilution (e.g., losing brightness on dilution in buffer); other methods produce materials that exhibit poor storage stability, or that become less bright in particular chemical environments. High-quality, water-soluble quantum dots do not show significant

change in peak emission wavelength, or quantum yield, as a function of environment or time.

Other than the difference in optical properties just outlined, quantum dots differ from dye conjugates in another important respect. Quantum dots are polyfunctional; there are a number of affinity molecules (proteins, oligonucleotides, small molecules, and so on) per quantum dot. In the case of traditional fluorescent labels, there is generally a one-to-one correspondence of dye to small molecule, and more than one dye molecule per protein or other large molecule (**Fig. 3**).

2.2.2. Size

Water-soluble quantum dot conjugates are in the 10 to 20-nm size range (as measured by transmission electron microscopy, size-exclusion chromatography, and dynamic light scattering), making them similar in size to large proteins (*see* **Fig. 4**). This might preclude them from certain applications, however, their size does not prevent use in the labeling of cell surfaces and tissue sections, or from accessing intracellular targets in fixed and permeablized cells.

2.3. Material

A bulk (i.e., arbitrarily large) piece of semiconductor has a defined emission wavelength. When the size of the semiconductor particle is diminished to the nanometer scale, "quantum confinement" becomes operant, and the emission wavelength becomes dependent on the particular particle size (hence, the term *quantum dot*). Quantum confinement is due to the energy cost of confining the excited state (of an emitting quantum dot) to a smaller volume than it would ideally occupy in the bulk material. Thus, smaller core quantum dots are higher energy and emit "bluer" than larger ones. The useful consequence of this property is that a range of colored fluorescent probes can be generated from a single material simply by preparing different sizes of quantum dots. The range of wavelengths within which a quantum dot can emit is determined by the semiconductor core material.

Cadmium selenide is the material used in virtually all of the quantum dot biological labeling to date, and its emission spectrum conveniently spans the visible light range (~450–660 nm). Materials such as cadmium telluride and indium phosphide potentially allow probes in the far red (up to ~750 nm), and cadmium sulfide and zinc selenide give access to the ultraviolet. Generation of far-red and near-infrared (IR) quantum dot probes will likely be extremely valuable in whole-blood assays in which absorption by hemoglobin limits the detection of shorter-wavelength materials. Deep tissue and in vivo imaging are other areas in which near-IR probes will find use, because scatter by tissue is minimized in this region of the spectrum. A variety of semiconductor materials and the range of emission wavelengths achievable by altering their size are shown in **Fig. 5**.

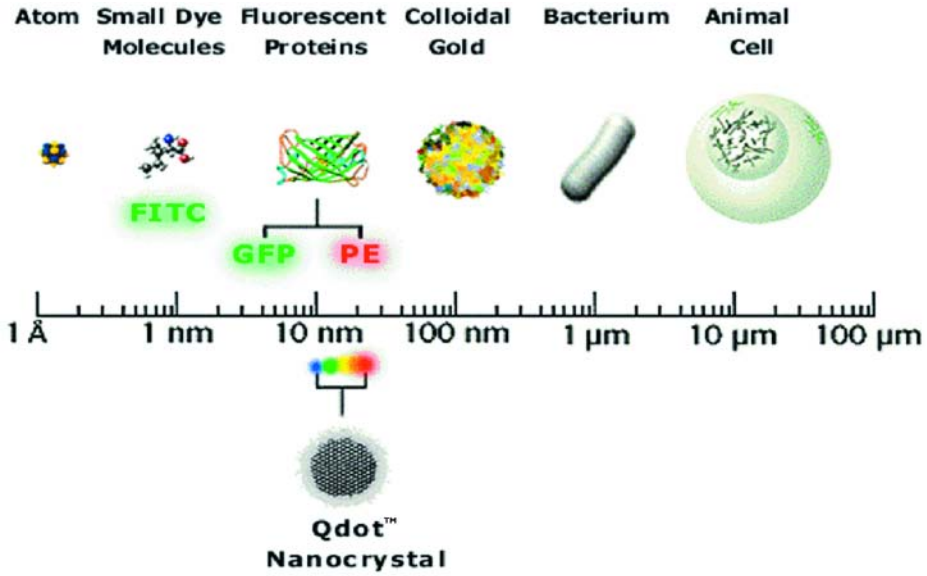

Fig. 4. Physical size of quantum dots compared to related entities.

3. Applications

3.1. Quantum Dots as Labels

For the purpose of this chapter, we define "labels" as single quantum dots conjugated to biological affinity molecules (as differentiated from encoding applications, described in **Subheading 3.2.**). These analogs to traditional fluorescent dye-labeled proteins, antibodies, oligonucleotides, and so on can be used in many biological applications, some of which are unique to quantum dots. Most of the work published on quantum dot labels to date has been "proof-of-concept" work—demonstrating the use of quantum dots in an application, but typically not solving a particular biological problem. Furthermore, the publications have used different or evolving preparations of quantum dots, making results difficult to compare among investigators.

3.1.1. Immunohistochemistry and Other Microscope-Based Techniques

A standard fluorescence microscope is an ideal tool for detection of quantum dot labels. Lamp-based excitation can be applied through a very wide excitation filter for efficient excitation of the broad quantum dot excitation spectrum. Since the emission spectrum is narrow, a narrow emission filter can be used to maximize signal to background. Alternatively, a long-pass emission filter can be used to observe several colors simultaneously. Finally, the excellent photostability provides additional time for focusing and sample inspection without bleaching.

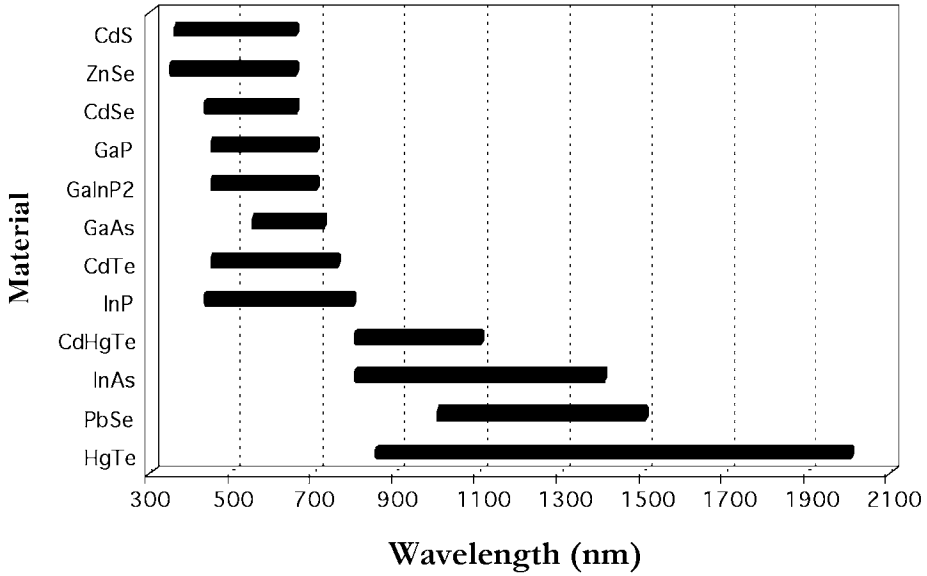

Fig. 5. Wavelength ranges obtainable by varying size of quantum dots made from a number of different semiconductor materials. Each bar approximately represents the range of wavelengths obtained from the smallest (left end) to largest (right end) quantum dot made from the material listed.

Wu et al. ***(6)*** successfully used quantum dots conjugated to immunoglobulin G (IgG) and streptavidin to label the breast cancer marker Her2 on the surface of cancer cells, stain actin and microtubule fibers in the cytoplasm, and detect nuclear antigens. Labeling was shown to be specific for intended targets, brighter, and significantly more photostable than comparable organic dyes. Using quantum dots of different colors conjugated to IgG and streptavidin, the investigators detected two cellular targets with one excitation wavelength. Although the number of simultaneously observable targets is limited in this study, the number will increase as the number of available quantum dot colors coupled to different affinity molecules increases.

Pathak et al. ***(14)*** used quantum dots coupled to oligonucleotides in *in situ* hybridization. They successfully detected hybridization to the Y chromosome of fixed human sperm cells, although no comparison was made to fluorescent dye fluorescent *in situ* hybridization.

Quantum dots have been shown to be enabling in the area of multiphoton microscopy ***(15)***. Quantum dot probes were reported to have the largest two-photon cross-sections (a measure of the ability to absorb light at twice the normal excitation wavelength) of any probe—close to the theoretical maximum

value. The cross-sections are 2 to 3 orders of magnitude larger than conventional fluorescent probes now in use. With the use of two-photon imaging, quantum dots were intravenously injected into mice and used to dynamically visualize capillaries hundreds of microns deep through scattering media (skin and adipose tissue).

3.1.2. Live Cell Labeling

Quantum dots have been used to label live cells. Jaiswal et al. ***(16)*** demonstrated that a number of cell lines endocytosed quantum dots over a 2 to 3 h period, and the quantum dots became localized in endosomes. These labeled cells were shown to be stable for as long as 12 d in culture. The investigators also labeled live cells by membrane biotinylation, followed by incubation with quantum dot–avidin conjugate, although this method also resulted in quantum dot endocytosis in the cell lines studied. They used the labeling procedure to study the effect of starvation on aggregation of developing *Dictyostelium discoideum* cells that were starved for various durations. Cells starved for different durations were labeled with different colored quantum dots, mixed, and the labeled cells were imaged for 2-s intervals every 2 min for 8 h. It was concluded that the cells' propensity to aggregate is an "on-off" phenomenon, not a continuous function of the degree of starvation. More generally, the work represents the use of quantum dot labels to solve a new biological problem not addressable by conventional fluorescent labeling.

Dubertret et al. ***(17)*** has reported the preparation of quantum dots functionalized with polyethylene glycol (PEG) to study development in *Xenopus* embryos. The quantum dots were microinjected into individual cells of the growing embryo, and because the fluorescence was confined to the progeny of the injected cells, this allowed the embryonic development to be studied for many individual cells. It was found that the quantum dots were stable and had little toxicity.

Quantum dots have also been used to measure cell motility by imaging of phagokinetic tracks ***(18)***. It was demonstrated that cells were capable of engulfing nanocrystals, through an undefined mechanism, as they travel, leaving behind a history of their migratory track. Future research will explore the use of the multiple emission colors of quantum dots to monitor cell motility and migration and simultaneously track specific proteins tagged with complementary fluorescent probes.

3.1.3. In Vivo Applications

Several reports have appeared utilizing quantum dots in vivo. This work is typically accomplished with fluorescent polymers, such as rhodamine green

dextran, or with fluorescent proteins, such as green fluorescent protein. The lack of photostability and brightness of these reagents limits their utility in longer-duration imaging experiments.

Akerman et al. ***(19)*** conducted specific targeting of quantum dot–peptide bioconjugates in mice. Peptides that specifically target lung blood vessel endothelial cells, tumor cell blood vessels, and tumor cell lymphatic vessels were conjugated to quantum dots and intravenously injected into mice. Specific targeting to the lung and tumor vasculature was observed with the appropriate conjugates, and no acute toxicity was observed after 24 h of circulation. The investigators also observed that the quantum dots accumulated in the liver and spleen in addition to the targeted tissues, unless the quantum dot was coconjugated with PEG. While the quantum dot conjugates were specific for the tumor targets, they did not accumulate in the tumor cells, instead remaining in the blood vessel endothelia. The investigators speculated as to the possible causes: the size of the quantum dots, the stability of the mercaptoacetic acid–stabilized quantum dot conjugates used, or slow endocytosis into tumor cells.

3.1.4. Small-Molecule Conjugates

A limitation of traditional small-molecule fluorescent dyes is in the labeling of other small molecules, drugs, transporters, and small-molecule probes to cell-surface receptors. Conjugates of dyes to these small molecules often lack sensitivity or specificity in the detection of the desired targets. Conjugates of small molecules to quantum dots produce conjugates with much greater light output per binding event, owing to the increased absorbance and emission of the quantum dot. Furthermore, there is the possibility of improved avidity compared to a dye conjugate, owing to the combined effect of many molecules of the binding ligand on the surface of the quantum dot. Rosenthal et al. ***(20)*** applied this concept to the study of the neurotransmitter serotonin. They coupled approx 160 serotonin molecules/quantum dot via a short linker and characterized these probes by their interaction with serotonin transporters, electrophysiology measurements, as well as fluorescence imaging. While the results for these initial conjugates show somewhat lower selectivity than high-affinity antagonists, they do show utility in the imaging of membrane proteins in living cells.

3.1.5. Microplate-Based Assays

Assays in microtiter plates are analogous to high-throughput screening. The properties of quantum dots allow a lower limit of detection than other fluorescent dyes, as well as assay simplification compared to enzymatic methods of plate-based detection when used in multiplex format. While many solution-phase fluorescent microplate assays exist, immunosorbant assays, in which the analyte is only present bound to the surface of the plate, are typically accomplished

with enzymatic amplification (enzyme-linked immunosorbent assay technique). We have shown that the limit of detection of 605 nm of streptavidin conjugate is at least an order of magnitude lower than phycoerythrin-streptavidin conjugate when used in a microplate reader using 250 nm of excitation for the quantum dot (Quantum Dot Corporation, unpublished data). The use of direct fluorescent detection (as opposed to enzymatic amplification) also allows multiplexed detection without sequential wash and amplification steps. Traditional fluorophores do not give adequate signal to allow their use in these assays.

Goldman et al. ***(21)*** have developed a series of assays for infectious diseases and explosives using quantum dot conjugates. Systematic efforts have resulted in a well-characterized system of producing conjugates as well as measurement of their performance in assays. Reports by these investigators have shown the current limit of detection for cholera and staphylococcal toxins to be 60 and 15 ng/mL, respectively.

3.2. Encoding

Using single colors to "color-code," or identify, objects; only a relatively small number of objects (probably less than 20) can be uniquely identified. However, using combinations of several colors can produce many distinguishable spectral codes. Quantum dots have several practical advantages when used to produce spectral codes. They have narrow, symmetrical emission spectra, are very photostable; and many colors can be excited by a single wavelength of light. The result is that quantum dot spectral codes can be used effectively for multiplexed assays. Because they are much smaller than objects that scientists would like to define uniquely (cells, latex beads for immuno- or other assays), quantum dots can be combined in colors and ratios to encode these objects by providing a unique spectral "fingerprint" (**Fig. 6**). The encoded entities can be conveniently decoded using imaging methods or flow-based methods to determine their characteristic fluorescence spectra. This concept applied to fluorescent dye–encoded polymer beads has been developed into a commercial system ***(22)***. However, this requires the use of multiple lasers for excitation and limits the number of codes practically attainable by such a system. Using quantum dots for polymer bead encoding has significant advantages in single excitation, such as more closely packed colors and a greater number of colors overall, thus making access to higher numbers of codes more likely ***(23)***. A recent report ***(24)*** describes the use of quantum dot–encoded beads to determine 10 cytochrome P450 genotypes on 94 patient samples. The results show that the call accuracy was higher than with gel-based sequencing.

Living cells can also be encoded using multiple colors of quantum dots together to create codes. A method for encoding cells that is based on the intracellular delivery of quantum dots into live cells was developed ***(25)***. The

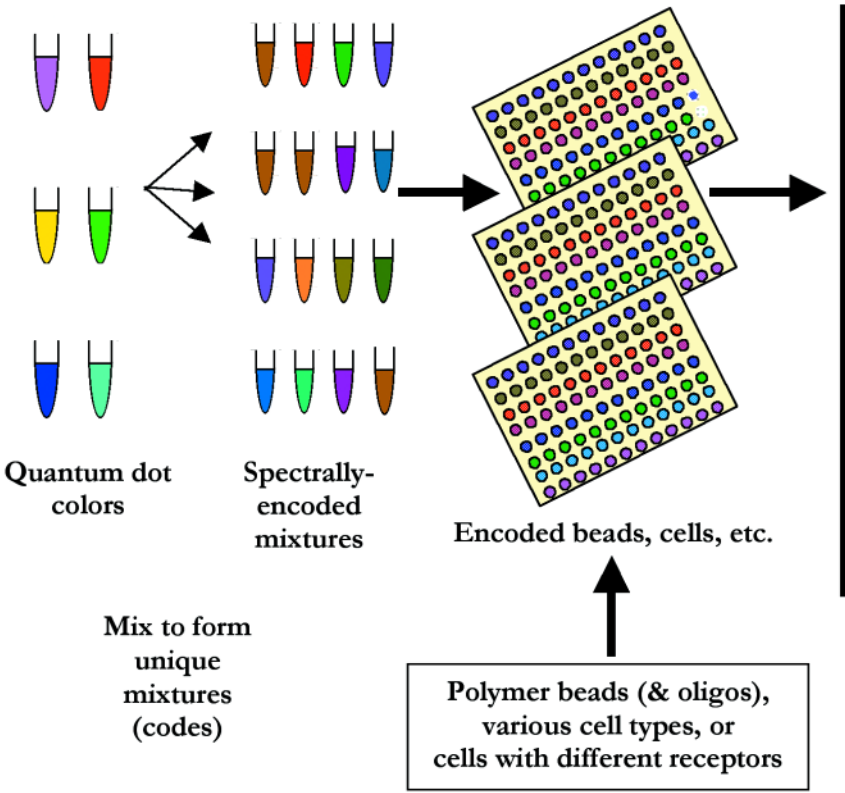

Application	Format
Multiplexed gene expression	Encoded beads each with gene-specific oligos
Multiplexed SNP genotyping	Encoded beads with allele-specific oligos
Multiplexed immunoassays	Encoded beads with antibodies
Multiplexed cell-based assays	Mixed cell types encoded with quantum dots
Multiplexed reporter assays	Encoded cell lines expressing various receptors

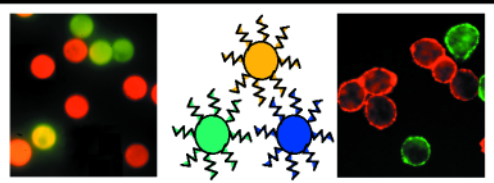

Fig. 6. Concept of encoding using quantum dots. Quantum dot colors can be mixed to produce spectral codes. These mixtures can be combined with polymer beads to produce encoded beads that can be subsequently coupled to distinct oligonucleotides or other affinity molecules. Alternatively, the quantum dot spectral codes can be used to label cells to differentiate cell lines, or cell lines bearing different receptors. SNP, single nucleotide polymorphism.

quantum dots are nontoxic, photostable, and can be imaged using conventional fluorescence microscopy or analyzed using flow cytometric systems. Unique fluorescent codes for a variety of mammalian cell types were generated, and the potential to create >100 codes was demonstrated. The quantum dot cell codes are relatively inert and do not impact most types of cell-based assays including immunostaining, competition binding, reporter gene, receptor internalization, and intracellular calcium release. A multiplexed calcium assay for G protein-coupled receptors using quantum dots was also demonstrated. The ability to spectrally encode individual cells with unique fluorescent bar codes should open new opportunities in multiplexed assay development and greatly facilitate the study of cell/cell interactions and other complex phenotypes in mixed cell populations.

4. Future Perspectives

Given the unique set of properties that quantum dots offer—that they have demonstrated superior utility in some existing applications and show enabling performance in others—it is likely that new, enabling biological applications will be discovered and developed. The photostability may bring unprecedented means of sample archival to existing applications, as well as continuous imaging for very long durations. The brightness and stability may allow levels of detection previously unachievable and make single-molecule detection more approachable to biological applications. The use of intrinsic properties such as fluorescence resonance energy transfer (FRET) and fluorescence lifetime has been virtually unaddressed, let alone developed. Using quantum dots to encode has the potential to revolutionize high-throughput biology, but little more than simple demonstrations have been made to date. Although detection of quantum dots is possible and easy on conventional instrumentation, the development of quantum dot-specific instrumentation (that takes advantage of unique quantum dot properties) will lead to improved sensitivity, multiplexing, and throughput. Possibilities are DNA microarray detection, flow cytometry, and instrumentation to decode quantum dot-encoded objects. Although quantum dots may not provide advantages in every application, it seems likely that they will become a dominant fluorescent reporter in biology over the next several years.

References

1. Kortan, A. R., Hull, R., Opila, R. L., Bawendi, M. G., Steigerwald, M. L., Carrol, P. J., and Brus, L. E. (1990) Nucleation and growth of CdSe on ZnS quantum crystallite seeds, and vice versa, in inverse micelle media. *J. Am. Chem. Soc.* **112,** 1327–1332.

2. Danek, M., Jensen, K. F., Murray, C. B., and Bawendi, M. G. (1996) Synthesis of luminescent thin-film CdSe/ZnSe quantum dot composites using CdSe quantum dots passivated with an overlayer of ZnSe. *Chem. Mater.* **8,** 173–180.
3. Hines, M. A. and Guyot-Sionnest, P. (1996) Synthesis and characterization of strongly luminescing ZnS-capped CdSe nanocrystals. *J. Phys. Chem.* **100,** 468–471.
4. Bruchez, M., Jr., Moronne, M., Gin, P., Weiss, S., and Alivasatos, A. P. (1998) Semiconductor nanocrystals as fluorescent biological labels. *Science* **281,** 2013–2015.
5. Chan, W. C. W. and Nie, S. M. (1998) Quantum dot bioconjugates for ultrasensitive nonisotopic biological detection. *Science* **281,** 2016–2018.
6. Wu, X., Liu, H., Liu, J., Haley, K. N., Treadway, J. A., Larson, J. P., Ge, N., Peale, F., and Bruchez, M. P. (2003) Immunofluorescent labeling of cancer marker Her2 and other cellular targets with semiconductor quantum dots. *Nat. Biotechnol.* **21,** 41–46.
7. Dahan, M., Laurence, T., Pinaud, F., Chemia, D. S., Alivasatos, A. P., Sauer, M., and Weiss, S. (2001) Time-gated biological imaging by use of colloidal quantum dots. *Opt. Lett.* **26,** 825–827.
8. Qu, L., Peng, Z. A., and Peng, X. (2001) Alternative routes toward high quality CdSe nanocrystals. *Nano Lett.* **1,** 333–337.
9. Peng, Z. A. and Peng, X. (2002) Nearly monodisperse and shape-controlled CdSe nanocrystals via alternative routes: nucleation and growth. *J. Am. Chem. Soc.* **124,** 3343–3353.
10. Chen, Y. and Rosenzweig, Z. (2002) Luminescent CdS quantum dots as selective ion probes. *Anal. Chem.* **74,** 5132–5138.
11. Dabboussi, B. O., Rodriguez-Viejo, J., Mikulec, F. V., Heine, J. R., Mattoussi, H., Ober, R., Jensen, K. F., and Bawendi, M. G. (1997) (CdSe)ZnS core-shell quantum dots: synthesis and characterization of a size series of highly luminescent nanocrystallites. *J. Phys. Chem. B* **101,** 9463–9475.
12. Mattoussi, H., Mauro, J. M., Goldman, E. R., Anderson, G. P., Sundar, V., Mikulec, F. V., and Bawendi, M. G. (2000) Self-assembly of CdSe-ZnS quantum dot bioconjugates using an engineered recombinant protein. *J. Am. Chem. Soc.* **122,** 12,142–12,150.
13. Potapova, I., Mruk, R., Prehl, S., Zentel, R., Basche, T., and Mews, A. (2002) Semiconductor nanocrystals with multifunctional polymer ligands. *J. Am. Chem. Soc.* **125,** 320–321.
14. Pathak, S., Choi, S., Arnheim, N., and Thompson, M. E. (2001) Hydroxylated quantum dots as luminescent probes for in situ hybridization. *J. Am. Chem. Soc.* **123,** 4103–4104.
15. Larson, D. R., Zipfel, W. R., Williams, R. M., Clark, S. W., Bruchez, M. P., Wise, F. W., and Webb, W. W. (2003) Water-soluble quantum dots with large two-photon cross-sections for multiphoton fluorescence imaging in vivo. *Science* **300,** 1434–1436.

16. Jaiswal, J. K., Mattoussi, H., Mauro, J. M., and Simon, S. M. (2003) Long-term multiple color imaging of live cells using quantum dot bioconjugates. *Nat. Biotechnol.* **21,** 47–51.
17. Dubertret, B., Skourides, P., Norris, D. J., Noireaux, V., Brivanlou, A. H., and Libchaber, A. (2002) *Science* **298,** 1759–1762.
18. Parak, W. J., Boudreau, R., Le Gros, M., Gerion, D., Zanchet, D., Micheel, C. M., Williams, S. C., Alivasatos, A. P., and Larabel, C. (2002) Cell motility and metastatic potential studies based on quantum dot imaging of phagokinetic tracks. *Adv. Mater.* **14(12),** 882–885.
19. Akerman, M. E., Chan, W. C. W., Laakkonen, P., Bhatia, S. N., and Ruoslahti, E. (2002) Nanocrystal targeting in vivo. *Proc. Nat. Acad. Sci. USA* **99,** 12,617–12,621.
20. Rosenthal, S. J., Tomlinson, I., Adkins, E. M., Schroeter, S., Adams, S., Swafford, L., McBride, J., Wang, Y., DeFelice, L. J., and Blakely, R. D. (2002) Targeting cell surface receptors with ligand-conjugated nanocrystals. *J. Am. Chem. Soc.* **124,** 4586–4594.
21. Goldman, E. R., Balighian, E. D., Mattoussi, H., Kuno, M. K., Mauro, J. M., Tran, P. T., and Anderson, G. P. (2002) Avidin: a natural bridge for quantum dot–antibody conjugates. *J. Am. Chem. Soc.* **124,** 6378–6382.
22. Kettman, J. R., Davies, T., Chandler, D., Oliver, K. G., and Fulton, R. J. (1998) Classification and properties of 64 multiplexed microsphere sets. *Cytometry* **33,** 234–243.
23. Han, M., Gao, X., Su, J. Z., and Nie, S. (2001) Quantum-dot-tagged microbeads for multiplexed optical coding of biomolecules. *Nat. Biotechnol.* **19,** 631–635.
24. Xu, H., Sha, M. Y., Wong, E. Y., et al. (2003) Multiplexed SNP genotyping using the Qbead™ system: a quantum dot–encoded microsphere-based assay. *Nucleic Acids Res.* **31(8),** e43.
25. Mattheakis, L. C., Dias, J. M., Choi, Y. J., Gong, J., Bruchez, M. P., Liu, J., and Wang, E. (2004) Optical coding of mammalian cells using semiconductor quantum dots. *Anal. Biochem.* **327,** 1200–1208.

2

Fluoroimmunoassays Using Antibody-Conjugated Quantum Dots

Ellen R. Goldman, Hedi Mattoussi, George P. Anderson, Igor L. Medintz, and J. Matthew Mauro

Summary

Luminescent colloidal semiconductor nanocrystals (quantum dots) are robust inorganic fluorophores that have the potential to circumvent some of the functional limitations encountered by organic dyes in sensing and biotechnological applications. Quantum dots exhibit size-dependent tunable, narrow fluorescence emission spectra that span the visible spectrum and have broad absorption spectra. This allows simultaneous excitation of several particle sizes at a single wavelength with emission at multiple wavelengths. Quantum dots also provide a high-resistance threshold to chemical degradation and photodegradation. We have developed a conjugation strategy for the attachment of antibodies to quantum dots based on electrostatic interactions between negatively charged dihydrolipoic acid (DHLA)-capped CdSe-ZnS core-shell quantum dots and positively charged proteins (natural or engineered) that serve to bridge the quantum dot and antibody. This chapter details the materials and methods for synthesis of the DHLA-capped CdSe-ZnS core-shell quantum dots, the construction and preparation of recombinant proteins, the conjugation of antibodies to quantum dots, and the use of antibody-coated quantum dots in a fluoroimmunoassay.

Key Words

Quantum dots; fluoroimmunoassay; nanocrystals; dihydrolipoic acid; leucine zipper.

1. Introduction

Luminescent colloidal semiconductor nanocrystals (quantum dots) provide an alternative to conventional organic fluorophores for use in a variety of biotechnological applications. The CdSe-ZnS core-shell quantum dots used in our studies exhibit size-dependent tunable photoluminescence with narrow emission bandwidths (full width at half maximum of 25–45 nm) that span the visible spectrum along with broad absorption spectra, which allow simultaneous excitation of several particle sizes at a single wavelength ***(1–5)***. In addition,

From: *Methods in Molecular Biology, vol. 303: NanoBiotechnology Protocols*
Edited by: S. J. Rosenthal and D. W. Wright © Humana Press Inc., Totowa, NJ

quantum dots have high photochemical stability, and a good fluorescence quantum yield. Photoluminescence from these quantum dots can be detected at concentrations comparable to standard fluorescent organic dyes using conventional fluorescence methods ***(6)***.

We have developed protocols for the conjugation of quantum dots to antibodies for use in fluoroimmunoassays for the detection of proteins or small molecules. Our conjugation strategy is based on electrostatic self-assembly between negatively charged dihydrolipoic acid (DHLA)-capped CdSe-ZnS core-shell quantum dots and positively charged proteins (natural or engineered) that serve to bridge the quantum dot and antibody ***(7,8)***. To facilitate easy separation of the desired quantum dot–antibody product from unlabeled antibody, we employ a mixed surface strategy in which both an antibody-bridging protein and a purification tool protein are immobilized on each quantum dot. This electrostatic noncovalent self-assembly approach to conjugate luminescent quantum dots with proteins extends and complements existing quantum dot-labeling methods ***(9,10)***. Conjugate preparation is simple, highly reproducible, and easily achieved.

We engineered proteins to interact with DHLA-capped quantum dots by appending a positively charged leucine zipper ***(11)*** interaction domain onto the C-terminus of recombinant proteins. Antibodies were conjugated to quantum dots either through the use of an engineered bridging protein consisting of the immunoglobulin G (IgG)-binding β2 domain of streptococcal protein G modified by genetic fusion with the positively charged leucine zipper interaction domain (PG-zb), or through the use of the positively charged protein avidin. A genetically engineered maltose-binding protein appended with the charged leucine zipper (MBP-zb) was used as a purification tool in conjunction with both types of bridging proteins. By using affinity chromatography, excess unconjugated antibody can be separated from the complete quantum dot immunoreagent. **Figure 1** shows schematic representations of the mixed-surface quantum dots with antibodies coupled using the engineered PG-zb or avidin as a bridge. Protocols for conjugation of quantum dots to antibodies using this scheme, as well as the use of antibody-conjugated quantum dots in fluoroimmunoassays for the detection protein targets, are described in the following sections.

2. Materials

2.1. Synthesis of Quantum Dots

1. Selenium (99.99%).
2. Dimethyl cadmium ($CdMe_2$).
3. Trioctylphosphine (TOP) (90–95%).
4. Trioctylphosphine oxide (TOPO).
5. Inert gas (nitrogen or argon).

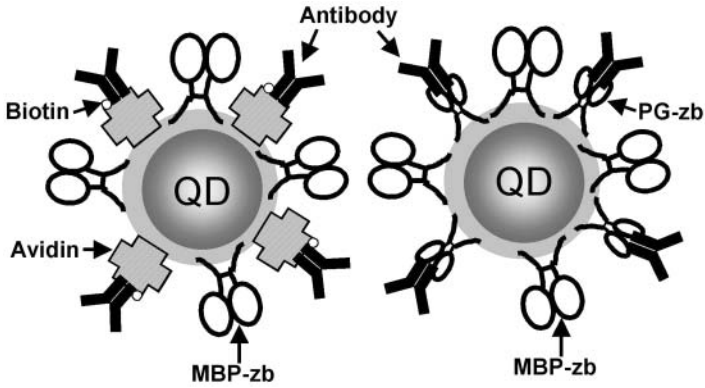

Fig. 1. Schematic of a mixed-surface quantum dot–antibody conjugate in which avidin bridges CdSe-ZnS core-shell nanocrystal quantum dot (capped with a negatively charged DHLA surface) and biotinylated antibody (**Left**). Schematic of a mixed-surface composition quantum dot–antibody conjugate in which the PG-zb (IgG-binding β2 domain of streptococcal protein G modified by genetic fusion with a dimer-forming positively charged tail) acts as a molecular adaptor to connect DHLA-capped CdSe-ZnS core-shell with Fc region of the IgG. **(Right)** In both quantum dot constructs, the MBP-zb (maltose-binding protein appended with the dimer-forming positively charged tail) serves as a purification tool for separating quantum dot–IgG conjugate away from excess IgG through affinity chromatography using crosslinked amylose resin. The exact numbers of avidin, PG-zb, and MBP-zb per quantum dot are not known; the image is not drawn to scale.

6. Glove box.
7. Schlenk line.
8. Solvents (hexane, toluene, butanol, ethanol, methanol, dimethylformamide [DMF]).
9. Diethylzinc ($ZnEt_2$).
10. Hexamethyldisilathiane (TMS_2S).
11. Tthioctic acid.
12. Potassium-*tert*-butoxide (KTB).
13. Ultrafree centrifugal filtration device, molecular weight cutoff of 50,000 (Millipore, Bedford, MA).
14. DHLA. This is prepared from distilled thioctic acid by borohydride reduction ***(12)***.

2.2. Construction of DNA Vector and Expression of Protein

1. pMal-c2 plasmid (New England Biolabs, Beverly, MA).
2. Cloning enzymes (polymerases and endonucleases).
3. QIAquick gel extraction kit (Qiagen, Valencia, CA)
4. pBad/HisB protein expression kit (Invitrogen, Carlsbad, CA).
5. *Escherichia coli* TOP 10 (Invitrogen).

6. Luria Broth Base (LB, Invitrogen).
7. Ampicillin.
8. Isopropyl β-D-thiogalactoside (IPTG).
9. L-(+)Arabinose (Sigma, St. Louis, MO).

2.3. Purification of Protein

1. Buffer A: 100 m*M* NaH_2PO_4, 10 m*M* Tris, 6 *M* guanidine HCl; adjust pH to 8.0 using NaOH.
2. NiNTA resin (Qiagen).
3. Oak Ridge polypropylene centrifuge tubes (50 mL).
4. Buffer B: 100 m*M* NaH_2PO_4, 10 m*M* Tris, 8 *M* urea; adjust pH to 8.0 with NaOH *immediately prior to use*.
5. Buffer C: 100 m*M* NaH_2PO_4, 10 m*M* Tris, 8 *M* urea; adjust pH to 6.3 with NaOH *immediately prior to use*.
6. Phosphate-buffered saline (PBS): 200 m*M* NaCl, 2.7 m*M* KCl, 8.2 m*M* Na_2HPO_4, 4.2 m*M* NaH_2PO_4, 1.15 m*M* K_2HPO_4, pH 7.4.
7. Buffer D: 50 m*M* NaH_2PO_4, 300 m*M* NaCl, 250 m*M* imidazole; adjust pH to 6.5 with HCl.
8. Dialysis tubing (12- to 14-kDa cutoff).
9. Centriprep and/or Centricon (Millipore).
10. Syringe filter (0.22 μ) compatible with protein samples.

2.4. Immunoassays

1. Borate buffer: 10 m*M* sodium borate, pH 9.0.
2. Amylose affinity resin (New England Biolabs).
3. Maltose (Sigma).
4. Small columns (such as Bio-Spin columns or Micro-Bio-Spin columns; Bio-Rad, Hercules, CA).
5. PBS (*see* **Subheading 2.3., item 6**).
6. 96-Well white microtiter plates (FluoroNunc™ Plates MaxiSorp™ surface, Nalge Nunc, Rochester, NY).
7. Fluorescence microtiter plate reader.
8. Appropriate antibodies and antigens.

3. Methods

3.1. Synthesis of Quantum Dots

3.1.1. CdSe Core

1. Prepare a 1 *M* stock solution of TOP:selenide (TOP:Se) by dissolving 7.9 g of Se (99.99%) into 100 mL of TOP (90–95%) (*see* **Note 1**).
2. Add 170–250 μL of $CdMe_2$ and 3.5–4 mL of 1 *M* TOP:Se to about 15 mL of TOP.
3. Mix under inert atmosphere in a glove box.
4. Load into a syringe equipped with a large-gage needle for injection. Store in the glove box until **step 9**.

5. Load 20–30 g of TOPO (90%) into a 100-mL three-neck flask.
6. Use a Schlenk line to heat TOPO to 150–180°C for 2 h under vacuum while stirring. This dries and degases the TOPO.
7. Backfill with inert gas (typically nitrogen or argon).
8. Raise the temperature to 300–350°C in preparation for precursor injection.
9. Remove the flask from the heating source. Retrieve the syringe from the inert chamber (glove box) and quickly inject the syringe content into the 100-mL flask.
10. Keep the temperature below 200°C for a few minutes (to avoid growth) and take an absorption spectrum. The spectrum should show resolved features with the peak of the first transition (band edge absorption) usually located approx 490 nm.
11. Raise the temperature to 280–300°C. These higher temperatures allow growth and annealing of the quantum dots.
12. During growth, periodically remove samples and take their ultraviolet (UV)/visible absorption spectra. Monitor the position of the first absorption peak and its relative width; this is usually indicative of a sample's size distribution. If spectra indicate that growth has stopped, raise the temperature by several degrees (if desired).
13. Once the location of the first absorption peak reaches a wavelength indicative of a desired size, drop the temperature to below 100°C to arrest crystal growth.
14. Store the growth solution in a mixture of butanol and hexane (or toluene).

3.1.2. Purification

To isolate quantum dots with TOP/TOPO-capping ligands and to obtain a sample with a more narrow size distribution, CdSe quantum dots are often purified using size-selective precipitation, which makes use of preferential Van der Waals interactions ***(1)***.

1. Retrieve a fraction of the growth solution (usually containing a mixture of quantum dots, TOP, TOPO, butanol, and hexane [or toluene]).
2. Slowly add a "bad" solvent for the TOP/TOPO-capped nanocrystals, such as methanol or ethanol.
3. Precipitate the mixture.
4. Redisperse the precipitate in hexane or toluene.
5. Precipitate again using methanol or ethanol.

These steps should provide solutions of quantum dots with very low concentrations of free TOP/TOPO ligands. Repeating this operation without inducing macroscopic precipitations can substantially reduce the overall size distribution of the quantum dots; however, it reduces product yield ***(1)***.

3.1.3. ZnS Overcoating

In the mid-1990s, a few reports ***(4,5)*** showed that overcoating CdSe quantum dots with ZnS improved quantum yields to values of 30–50%. This is owing to the fact that passivating the quantum dots with an additional layer made of a

wider band-gap semiconductor provides a better passivation of surface states and results in a dramatic enhancement of the fluorescence quantum yield.

The procedure for overcoating colloidal CdSe quantum dots with a thin layer of ZnS can be carried out as follows: A dilute solution of quantum dots (containing Cd concentrations of approx 0.5 mmol or smaller) is dispersed in a TOPO-coordinating solvent. The temperature of the solution is raised to about 150°C but kept lower than 200°C to prevent further growth of the quantum dots. A dilute solution of Zn (or Cd) and S precursors is then slowly introduced into the hot stirring quantum dot solution. A typical ZnS overcoating includes the following steps:

1. Mount a round-bottomed flask (100 mL or larger) along with a separate addition funnel.
2. Load 20–30 g of TOPO into the round-bottomed flask and let it dry and degas (as described in **Subheading 3.1.1., step 6**) for 2 to 3 h under vacuum.
3. Add purified CdSe quantum dot solution (dispersed in hexane or toluene) at 70–80°C to a final Cd concentration of 0.5 mmol or smaller.
4. Evaporate the solvent under vacuum.
5. Increase the temperature of the quantum dot/TOPO solution to between 140 and 180°C, depending on the initial core radius (lower temperature for smaller core size).
6. In parallel, add equimolar amounts of $ZnEt_2$ and TMS_2S precursors that correspond to the desired overcoating layer for the appropriate CdSe nanocrystal radius to a vial containing 4 to 5 mL of TOP. Use an inert atmosphere (e.g., a glove box) to carry out this operation, because precursors are volatile and hazardous.
7. Load the Zn and S precursor solution from **step 6** into a syringe (in the glove box).
8. Retrieve the syringe containing the solution from the inert chamber and transfer the content to the addition funnel.
9. Slowly add through the addition funnel the Zn/S precursor solution to the quantum dot/TOPO solution at a rate of about 0.5 mL/min (about 1 drop every 3–5 s).
10. Once the addition is complete, lower the solution temperature to 80°C, and leave the mixture undisturbed for several hours.
11. Add a small amount of solvent (e.g., butanol and hexane), and precipitate the ZnS-overcoated quantum dots with methanol to recover the quantum dot product.

3.1.4. DHLA Cap and Water Solubilization

Water-soluble CdSe-ZnS nanoparticles, compatible with aqueous conjugation conditions, can be prepared using a stepwise procedure. A relatively thick ZnS overcoating of five to seven monolayers should be used to prepare the water-compatible quantum dots.

1. Purify TOP/TOPO-capped CdSe-ZnS core-shell quantum dots by two to three rounds of size-selection precipitation (*see* **Subheading 3.1.2.**).

2. Suspend 100–500 mg of purified TOP/TOPO-capped quantum dots in 300–1000 µL of freshly prepared DHLA. Heat the mixture to 60–80°C for a few hours, while stirring.
3. Dilute the quantum dot solution in 3–5 mL of DMF or methanol.
4. Deprotonate the terminal lipoic acid-COOH groups by slowly adding excess KTB. A precipitate is formed, consisting of the nanoparticles and released TOP/TOPO reagents.
5. Sediment the precipitate by centrifugation and discard the supernatant solvent.
6. Disperse the precipitate in water. The quantum dots with the new DHLA caps should disperse well in the water.
7. *Optional:* Conduct centrifugation or filtration of the dispersion (using a 0.5-µm disposable filter) to permit removal of the TOP/TOPO and provide a clear dispersion of the alkyl-COOH-capped nanocrystals.
8. Use an ultrafree centrifugal filtration device (M_W cutoff of approx 50,000) to separate the DHLA-capped quantum dots from excess hydrolyzed KTB and residual DMF. This will also remove the TOP/TOPO if **step 7** is skipped.
9. Repeat the centrifugation cycle using the centrifugal filtration device four times, taking up the quantum dot solution in water using a concentration/dilution of 10:1.
10. Disperse the final material in deionized water or buffer at basic pH.

Dispersions of quantum dots in aqueous suspension with concentrations of 5–30 µ*M* are prepared using this approach. The aqueous quantum dot suspensions are stable for months if stored at 4°C.

3.2. Construction of DNA Vector and Expression of Protein

3.2.1. Construction of MBP-zb DNA Vector and Expression of Protein

The coding DNA sequence for the two-domain maltose-binding protein–basic zipper fusion protein (MBP-zb) was constructed using standard gene assembly and cloning techniques. **Figure 2** illustrates the idealized MBP-zb dimer and the detailed nucleotide coding and primary amino acid sequences of the version of MBP-zb lacking a HIS tail.

1. Amplify DNA coding for the basic zipper from the plasmid pCRIIBasic (kindly supplied by H. C. Chang of Harvard University; ***[13]***) using polymerase chain reaction (PCR) with the following conditions: 25 cycles (30 s at 94°C, 90 s at 60°C, and 90 s at 72°C) using primers 1 and 2 (primer 1: 5′-TGCGGTGGCT CACTCAGTTG-3′; primer 2: 5′-GCTCTAGATTAATCCCCACCTGGGCGAG TTTC-3′) and pfu DNA polymerase (Stratagene).
2. Digest the amplified DNA with *Xba*I endonuclease.
3. Ligate into the *Xmn*I/*Xba*I sites within the polylinker downsteam of the *mal E* gene in the commercially available pMal-c2 vector to produce the plasmid pMBP-zb.

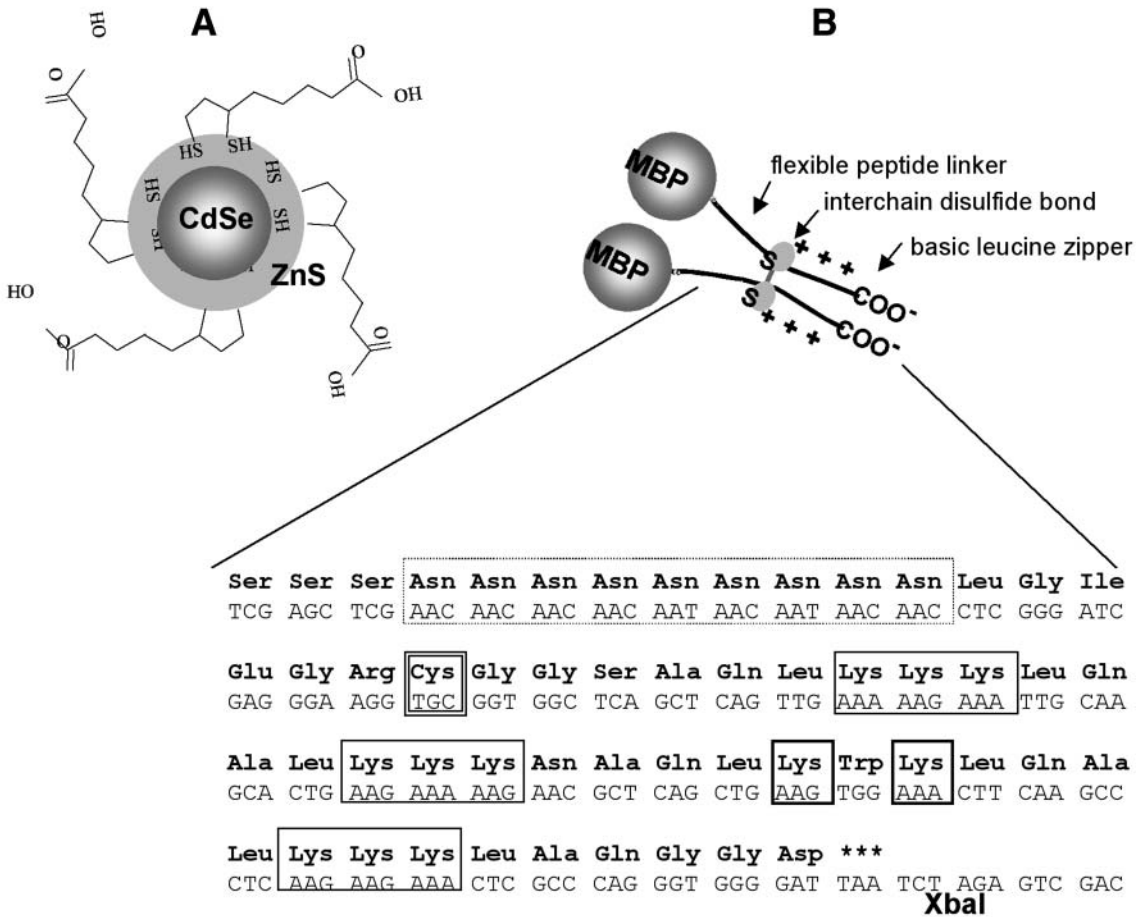
A
B
CdSe
ZnS
HO
OH
SH
MBP
MBP
flexible peptide linker
interchain disulfide bond
basic leucine zipper
S
COO-
Ser Ser Ser Asn Asn Asn Asn Asn Asn Asn Asn Asn Leu Gly Ile
TCG AGC TCG AAC AAC AAC AAC AAT AAC AAT AAC AAC CTC GGG ATC
Glu Gly Arg Cys Gly Gly Ser Ala Gln Leu Lys Lys Lys Leu Gln
GAG GGA AGG TGC GGT GGC TCA GCT CAG TTG AAA AAG AAA TTG CAA
Ala Leu Lys Lys Lys Asn Ala Gln Leu Lys Trp Lys Leu Gln Ala
GCA CTG AAG AAA AAG AAC GCT CAG CTG AAG TGG AAA CTT CAA GCC
Leu Lys Lys Lys Leu Ala Gln Gly Gly Asp ***
CTC AAG AAG AAA CTC GCC CAG GGT GGG GAT TAA TCT AGA GTC GAC
XbaI

The coding sequence for the C-terminus of MBP-zb (**Fig. 2**) was remodeled using standard DNA manipulation and cloning techniques to include a short spacer element linked to a hexahistidine affinity tag. The finally obtained C-terminus in pMBP-zb-his was identical to the C-terminal sequence of PG-zb shown in **Fig. 3**.

The following protocol for protein expression can be used with either the pMBP-zb or pMBP-zb-his vector construct. We performed the majority of our work using the pMBP-zb-his vector. The protein purification protocol detailed in **Subheading 3.3.** is for the his-tag-containing protein.

1. Inoculate 10 mL of LB medium (100 µg/mL of ampicillin) with a single colony of *E. coli* (strain TOP 10; Invitrogen) freshly transformed with the MBP-zb-his vector.
2. Grow with shaking at 37°C overnight (about 15 h).
3. Inoculate 5 mL of the overnight culture into 0.5 L of LB (100 µg/mL of ampicillin).
4. Continue to grow at 37°C until an OD_{600} of about 0.5 is reached. Induce protein production by adding IPTG (from a 1 *M* sterile stock) to a final concentration of 1 m*M*.
5. Grow an additional 2 h at 37°C with shaking.
6. Pellet the cells by centrifugating 4,000 rpm at 4°C, and store the resulting cell pellet frozen at –80°C.

3.2.2. Construction of PG-zb DNA Vector and Protein Expression

The two-domain protein G-basic leucine zipper (PG-zb) fusion protein was constructed using standard gene assembly and cloning techniques. **Figure 3** shows a schematic representation and the coding sequence of the PG-zb construct.

1. Use PCR to amplify the β2 IgG-binding domain of streptococcal protein G (PG; ***[14]***) and to introduce sites for cloning with the following conditions: 25 cycles (45 s at 94°C, 45 s at 55°C, and 45 s at 72°C) using primers GNCO199 (CAACGCTAAAATCGCCATGGCTTACAAACTTGTTATTAAT) and GSAC199 (GGTACCAGATCACGAGCTCTCAGTTACCGTAAAGGTCTT); *Nco*I, *Sac*I, and *Kpn*I sites are underlined.

Fig. 2. *(previous page)* **(A)** Schematic of CdSe-ZnS core-shell nanoparticle with DHLA surface capping groups; **(B)** schematic of S-S-linked MBP-zb homodimer and detail showing nucleotide and primary amino acid sequence of C-terminal basic leucine zipper interaction domain. Poly-Asn flexible linker is boxed with dashed lines, unique engineered cysteine is double boxed, and lysine residues contributing to net positive charge of leucine zipper are single boxed. (Reprinted from **ref. *6***. Copyright [2000] American Chemical Society.)

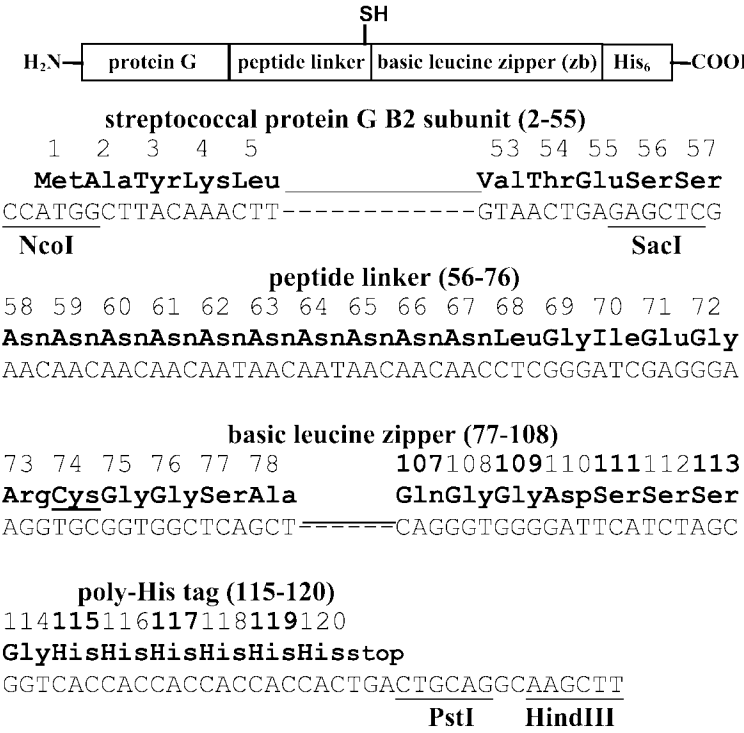

Fig. 3. Schematic of PG-zb protein with DNA and translated protein sequences of relevant region of pBadG-zb. (Reprinted in part from **ref. *7***. Copyright [2002] American Chemical Society.)

2. Extract the *Nco*I-*Kpn*I fragment containing the PG coding sequence from a 2% agarose gel (QIAquick gel extraction kit; Qiagen) and ligate into the *Nco*I/*Kpn*I sites of expression vector pBad/HisB (Invitrogen) to produce the plasmid pBadG.
3. Ligate the purified *Sac*I-*Hin*dIII DNA fragment (from pMBP-zb-his) containing the coding sequences for the poly-Asn linker (from the pMal plasmid series; New England Biolabs), a dimer-promoting cysteine, the basic leucine zipper, and the C-terminal hexahistidine tag into the *Sac*I/*Hin*dIII sites of pBadG to produce pBadG-zb.
4. Select or screen for the appropriately cloned insert.

The following protocol details protein expression for the PG-zb protein.

1. Inoculate 10 mL of LB medium (50 μg/mL of ampicillin) with a single colony of *E. coli* (strain TOP 10; Invitrogen) freshly transformed with pBadG-zb.
2. Grow with shaking at 37°C overnight (about 15 h).

3. Dilute the overnight 1/100 into LB medium (50 μg/mL of ampicillin).
4. Grow with shaking at 37°C until an OD_{600} of approx 0.5 is reached. Induce protein production with the addition of L-(+)arabinose to a final concentration of 0.002% (w/v).
5. Grow an additional 2 h at 37°C with shaking.
6. Pellet the cells by centrifugating at 4,000 rpm, and store the resulting cell pellet frozen at –80°C.

3.3. Purification of Protein

The following protocol can be used for protein purification of both the MBP-zb and PG-zb proteins containing the his tail. This is a denaturing protein preparation and serves to eliminate the copurification of nucleic acids and significant amounts of very active protease(s) that occur under nondenaturing conditions using the cytoplasmic protein fraction from cell lysis and a metal affinity column chromatography.

1. Resuspend the frozen cell pellet from the 500-mL *E. coli* culture (approx 2.5 g of wet cells) in 12.5 mL of denaturing buffer A. Stir the resuspended cells vigorously for 1 h at room temperature using a magnetic stirrer (avoid excess foaming).
2. Place the suspension in a polypropylene Oak Ridge tube (50 mL), and centrifuge at 15,000 rpm for 30 min at room temperature (4°C is also fine).
3. Transfer the supernatant to a clean tube. Add 6 mL of NiNTA resin (about 50% slurry) previously equilibrated two times with 15 mL of buffer A. Tumble the suspension for 45 min at room temperature.
4. Load a 1- to 1.5-cm-diameter column with the protein-charged resin and allow the fluid to flow through. Collect and save the flow-through for possible later analysis.
5. Wash the settled resin in the column two times with 15 mL of buffer A.
6. Wash the resin two times with 15 mL of buffer B.
7. Wash the resin four times with buffer C.
8. Wash the resin four times with 15 mL of PBS buffer (pH 7.4).
9. Elute the protein at about 1 mL/min with 26 mL of buffer D. Collect 1- to 2-mL fractions. Store the fractions at 4°C until dialysis.
10. Analyze the fractions by absorption A_{280} and A_{260} and/or sodium dodecyl sulfate polyacrylamide gel electrophoresis (SDS-PAGE).
11. Dialyze the pooled purified fractions against 4 L of PBS at 4°C for 2 to 3 h, change the buffer, and dialyze against 4 L of fresh PBS overnight.
12. Centrifugally concentrate the dialyzed protein solution to about 2 to 3 mL using Centriprep and/or Centricon devices at 4°C.
13. Pass the concentrated material through a buffer-washed 0.22-μ*m* syringe filter into a sterile plastic tube for storage. Aliquots can be stored short term at 4°C or quick frozen in a dry ice–ethanol bath for storage at –80°C.
14. Read the final A_{280} on the properly diluted sample. The molar extinction coefficients for the MBP-zb and PG-zb dimers are 166,200 and 35,400 $M^{-1}cm^{-1}$,

respectively. Run a denaturing SDS-PAGE gel ± reducing agent on the final concentrated product. Estimate and record the approximate covalent monomer/dimer ratio based on the gel results.

3.4. Immunoassays

3.4.1. Preparation of MBP-zb/Avidin/IgG-Coated Quantum Dots

This section describes the preparation of antibody-conjugated quantum dots using avidin to bridge quantum dots and biotinylated antibody. Quantum dots are mixed with avidin and a purification tool protein (MBP-zb). The protein-coated quantum dots are loaded onto an amylose column and biotinylated antibody is bound to the avidin quantum dots on the column. The MBP-zb facilitates purification of the final quantum dot/antibody reagent from excess free antibody. The left panel of **Fig. 1** shows a representation of the MBP-zb/avidin/IgG-coated quantum dot product produced through this protocol.

1. To 200 µL of borate buffer add 0.43 nmol of MBP-zb, 15 µg of avidin (about 0.22 nmol), and 0.1 nmol of quantum dots. Mix gently and incubate at room temperature for about 15 min (*see* **Notes 2** and **3**).
2. Add a second aliquot of 0.22 nmol of MBP-zb to the dot-protein mix. Mix gently and incubate for another 15 min at room temperature. At this point, the quantum dots can be stored overnight in a refrigerator.
3. Prepare an amylose column by mixing the resin and transferring 0.5 mL/column.
4. Wash the column with 1 mL of buffer (PBS).
5. Add the MBP-zb/avidin-coated quantum dots to the top of the column.
6. Wash the column with 1 mL of PBS.
7. Add biotinylated antibody (20 µg) to the top of the column. Let it just run into the resin and cap the column to stop the flow (*see* **Note 4**).
8. Add 50 µL of PBS to the top of the resin so that it does not dry. Allow the biotinylated antibody to interact with the quantum dot–conjugate on the column for about 1 h.
9. Remove the cap, let the PBS on top run into the column, and then wash the resin with 1 mL of PBS.
10. Elute the MBP-zb/avidin/IgG-coated quantum dots with 1 mL of 10 m*M* maltose in PBS. The elution can be monitored with a hand-held UV light (365 nm). These MBP-zb/avidin/IgG-coated quantum dots can be stored in a refrigerator for at least a few days before use.

3.4.2. Preparation of PG-zb/MBP-zb/IgG-Coated Quantum Dots

This section describes the preparation of antibody-conjugated quantum dots prepared using the engineered protein PG-zb to bridge quantum dots and IgG antibody. Quantum dots are mixed with PG-zb, the purification tool protein (MBP-zb), and IgG. The protein-coated quantum dots are loaded onto an

amylose column used to purifiy the final quantum dot/antibody reagent from free antibody. The right panel of **Fig. 1** shows a representation of the PG-zb/MBP-zb/IgG-coated quantum dot product produced via this protocol.

1. To 200 µL of borate buffer add 0.25 nmol of MBP-zb, 0.22 nmol of PG-zb, and 0.1 nmol of quantum dots. Mix gently and incubate at room temperature for about 15 min (*see* **Note 5**).
2. Add a second aliquot of 0.33 nmol of MBP-zb to the dot-protein mix. Mix gently and incubate for another 5 min at room temperature.
3. Add about 35 µg of IgG to the quantum dot-protein mix. Incubate at 4°C for 1 h (*see* **Note 6**).
4. Prepare an amylose column by mixing the resin and transferring 0.5 mL/column.
5. Wash the column with 1 mL of buffer (PBS).
6. Add the MBP-zb/PG-zb/IgG quantum dots to the top of the column.
7. Wash the column with 2 mL of PBS.
8. Elute the MBP-zb/PG-zb/IgG-coated quantum dots with 1 mL of 10 m*M* maltose in PBS. The elution can be monitored with a hand-held UV light.

3.4.3. Protocol for Sandwich Immunoassays

Figure 4 shows data from a sandwich immunoassay for cholera toxin. Goat anti-cholera toxin (Biogenesis, Kingston, NH) was used as the capture antibody adsorbed onto the wells of plates. Rabbit anti-cholera toxin antibody (Biogenesis) was coupled to 550-nm emitting quantum dots using the PG-zb conjugation strategy detailed in **Subheading 3.4.2.** Concentrations of cholera toxin down to 3 ng/mL were visualized in this assay. Control wells in which no cholera toxin was added to capture antibody-coated wells were also examined.

1. Coat plates overnight at 4°C with 10 µg/mL of appropriate capture antibody diluted into 0.1 *M* sodium bicarbonate, pH 8.6, using 100 µL/well.
2. The next day remove the capture antibody and block the plates with 4% (w/v) powdered nonfat milk in PBS. Blocking can be done for 1 h at room temperature or for several hours at 4°C.
3. After blocking, wash the plates twice with PBS plus 0.1% Tween-20 (PBST).
4. Add 100 µL of antigen solution (diluted in PBS) to the wells of the plates, usually a dilution series with a highest value of 1–10 µg/mL of antigen. Remember to include control wells with no antigen. Test and control wells should be plated in at least triplicate.
5. Rock the plates gently at room temperature for 1 h.
6. Wash the plates twice with PBST.
7. Add 50–100 µL of antibody-conjugated quantum dot reagent (in PBS). Usually the quantum dots eluted in **Subheadings 3.4.1.** or **3.4.2.** are diluted to three to four times the elution volume.
8. Rock the plates gently at room temperature for 1 h.

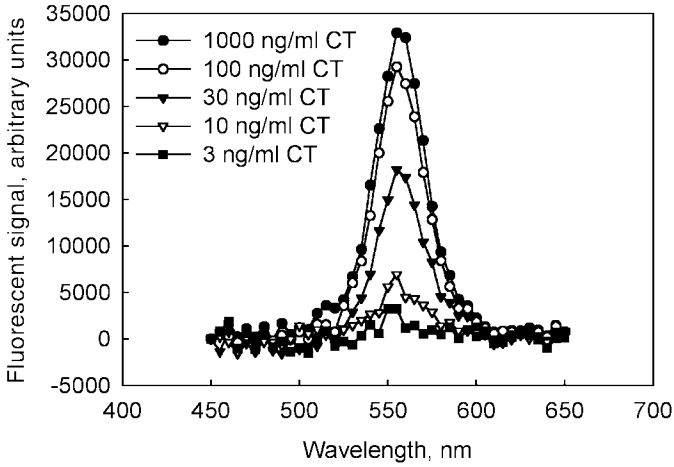

Fig. 4. Sandwich assay for detection of cholera toxin (CT). Goat anti-cholera toxin (Biogenesis) was adsorbed onto wells of the 96-well plate as a capture antibody. Concentrations of cholera toxin ranging from 3 to 1000 ng/mL were incubated with the capture antibody. Rabbit anti-cholera toxin antibody (Biogenesis) coupled to 550-nm emitting quantum dots using the PG-zb adaptor (detailed in **Subheading 3.4.2.**) was used as the signal-producing reagent. Each concentration was measured in triplicate, and the average signal is shown.

9. Wash the plates twice with borate buffer (pH 9.0), and add a final 50–100 µL of borate buffer to the plates (*see* **Notes 7** and **8**).
10. Read the fluorescence in a fluorescent microplate reader. We use an excitation of 330 nm; however, the broad excitation spectra of the quantum dots allows a wide choice of excitation. Choice of emission setting/filter depends on the emission spectra of the quantum dots used in the assay. If the control wells have a high nonspecific signal from the quantum dots, wells may be washed several more times with the borate buffer to reduce further nonspecific signal.

4. Notes

1. Peng and colleagues ***(15,16)*** have developed a modified organometallic synthesis that is less dependent on the purity of the TOPO and avoids the use of pyrophoric $CdMe_2$ precursor. High-purity TOPO and controlled amounts of cadmium-coordinating ligands such as hexylphosphonic acid or tetradecylphosphonic acid, are combined in the preparation flask. Cadmium compounds (e.g., cadmium oxide or cadmium acetate) are added at a relatively low temperature (140°C). The mixture is heated to generate Cd^{2+} ions before the addition of TOP : Se results in nanocrystal nucleation and growth.
2. Mercaptoundecanoic acid- and mercaptoacetic acid-capped CdSe-ZnS quantum dots have also worked with this conjugation method based on electrostatic

self-assembly. Any cap that leads to a negatively charged surface on the quantum dot should also work.

3. Recently, it has been observed that the MBP appended with a 5-HIS tail can be conjugated to CdSe-ZnS core-shell DHLA-capped quantum dots and used as a purification tool protein.
4. Biotinylated antibody is bound to avidin-coated quantum dots on the column to prevent the formation of crosslinked aggregates.
5. By varying the amount of PG-zb per quantum dot, the number of antibodies per quantum dot can be tuned. Problems with the amylose purification however, can arise if there are too few of the purification proteins (MBP-zb) per quantum dot.
6. If less antibody is added than there are available PG-zbs for binding antibody, generic IgG (goat IgG) can be added to the reagent before use to prevent free PG-zbs on the quantum dot surface from binding to capture antibody in a sandwich assay.
7. These quantum dots contain cadmium and selenium in an inorganic crystalline form. Dispose of quantum dot waste in compliance with applicable local, state, and federal regulations for disposal of this kind of material.
8. The quantum dots may be stabilized by washing with borate buffer containing 1% bovine serum albumin and reading the plates dry.

Acknowledgments

We thank the Office of the Naval Research for research support. The views, opinions, and/or findings described in this chapter are those of the authors and should not be construed as official Department of the Navy positions, policies, or decisions.

References

1. Murray, C. B., Norris, D. J., and Bawendi, M. G. (1993) Synthesis and characterization of nearly monodisperse CdE (E = S, SE, TE) semiconductor nanocrystallites. *J. Am. Chem. Soc.* **115,** 8706–8715.
2. Mattoussi, H., Radzilowski, L. H., Dabbousi, B. O., Thomas, E. L., Bawendi, M. G., and Rubner, M. F. (1998) Electroluminescence from heterostructures of poly(phenylene vinylene) and inorganic CdSe nanocrystals. *J. Appl. Phys.* **83,** 7965–7974.
3. Rodriguez-Viejo, J., Mattoussi, H., Heine, J. R., Kuno, M. K., Michel, J., Bawendi, M. G., and Jensen, K. F. J. (2000) Evidence of photo- and electrodarkening of (CdSe)ZnS quantum dot composites. *Appl. Phys.* **87,** 8526–8534.
4. Hines, M. A. and Guyot-Sionnest, P. (1996) Synthesis and characterization of strongly luminescing ZnS-capped CdSe nanocrystals. *J. Phys. Chem.* **100,** 468–471.
5. Dabbousi, B. O., Rodrigez-Viejo, J., Mikulec, F. V., Heine, J. R., Mattoussi, H., Ober, R., Jensen, K. F., and Bawendi, M. G. (1997) (CdSe)ZnS core-shell quantum dots: Synthesis and characterization of a size series of highly luminescent nanocrystallites. *J. Phys. Chem. B* **101,** 9463–9475.

6. Mattoussi, H., Mauro, J. M., Goldman, E. R., Anderson, G. P., Sundar, V. C., Mikulec, F. V., and Bawendi, M. G. (2000) Self-assembly of CdSe-ZnS quantum dot bioconjugates using an engineered recombinant protein. *J. Am. Chem. Soc.* **122,** 12,142–12,150.
7. Goldman, E. R., Anderson, G. P., Tran, P. T., Mattoussi, H., Charles, P. T., and Mauro, J. M. (2002) Conjugation of luminescent quantum dots with antibodies using an engineered adaptor protein to provide new reagents for fluoroimmunoassays. *Anal. Chem.* **74,** 841–847.
8. Goldman, E. R., Balighian, E. D., Mattoussi, H., Kuno, M. K., Mauro, J. M., Tran, P. T., and Anderson, G. P. (2002) Avidin: A natural bridge for quantum dot-antibody conjugates. *J. Am. Chem. Soc.* **124,** 6378–6382.
9. Bruchez, M., Jr., Moronne, M., Gin, P., Weiss, S., and Alivisatos, A. P. (1998) Semiconductor nanocrystals as fluorescent biological labels. *Science* **281,** 2013–2016.
10. Chan, W. C. W. and Nie, S. M. (1998) Quantum dot bioconjugates for ultrasensitive nonisotopic detection. *Science* **281,** 2016–2018.
11. O'Shea, E. K., Lumb, K. J., and Kim, P. S. (1993) Peptide velcro—design of a heterodimeric coiled-coil. *Curr. Biol.* **3,** 658–667.
12. Gunsalus, I. C., Barton, L. S., and Gruber, W. J. (1956) Biosynthesis and structure of lipoic acid derivatives. *J. Am. Chem. Soc.* **78,** 1763–1768.
13. Chang, H. C., Bao, Z. Z., Yao, Y., et al. (1994) A general-method for facilitating heterodimeric pairing between 2 proteins—applications to expression of alpha-T-cell and beta-T-cell receptor extracellular segments. *Proc. Natl. Acad. Sci. USA* **91,** 11,408–11,412.
14. Mauro, J. M., Cao, L. K., Kondracki, L. M., Walz, S. E., and Campbell, J. R. (1996) Fiber-optic fluorometric sensing of polymerase chain reaction–amplified DNA using an immobilized DNA capture protein. *Anal. Biochem.* **235,** 61–72.
15. Peng, Z. A. and Peng, X. G. (2001) Formation of high-quality CdTe, CdSe, and CdS nanocrystals using CdO as precursor. *J. Am. Chem. Soc.* **123,** 183, 184.
16. Qu, L., Peng, Z. A., and Peng, X. G. (2001) Alternative routes toward high quality CdSe nanocrystals. *Nano Lett.* **1,** 333–337.

3

Labeling Cell-Surface Proteins Via Antibody Quantum Dot Streptavidin Conjugates

John N. Mason, Ian D. Tomlinson, Sandra J. Rosenthal, and Randy D. Blakely

Summary

The quantum dot is a novel fluorescent platform that has the potential to become an alternative to conventional organic dyes used to label biological probes such as antibodies or ligands. Compared to typical fluorescent organic dyes, cadmium selenide/zinc sulfide core-shell nanocrystals, or quantum dots, have greater photostability, resist metabolic and chemical degradation, are nontoxic, and display broad emission and narrow excitation bands. When conjugated to generic adaptor molecules such as streptavidin, quantum dots can be used to label different biotinylated antibodies or ligands without having to customize the quantum dot surface chemistry for each antibody or ligand. In this chapter, we outline the methodology for using streptavidin quantum dots to label biotinylated antibodies that target cell-surface ectodomain proteins on both living and fixed cells.

Key Words

Streptavidin; quantum dots; biotinylation; cell-surface proteins; imaging.

1. Introduction

The conjugation of highly luminescent semiconductor cadmium selenide/zinc sulfide core-shell nanocrystals (quantum dots) conjugated to biorecognition molecules has produced a new class of fluorescent labels that has the potential to revolutionize biological imaging. Compared with conventional fluorescent organic dyes, quantum dots display a narrow emission band that is tunable, have a broad excitation spectrum, are resistant to chemical and metabolic degradation, display photostablility, and offer versatility in attachment of biorecognition molecules ***(1–4)***. In this chapter, we demonstrate that streptavidin can serve as a bridge for binding biotinylated antibodies when conjugated to the surface of quantum dots. We also illustrate that the streptavidin quantum dots

From: *Methods in Molecular Biology, vol. 303: NanoBiotechnology Protocols*
Edited by: S. J. Rosenthal and D. W. Wright © Humana Press Inc., Totowa, NJ

(SA-quantum dots) can be used to detect biotinylated antibodies used to label specific neuronal surface proteins on living cells.

2. Materials

1. Papain (Worthington, Lakewood, NJ).
2. Bovine serum albumin (BSA) (Sigma, St. Louis, MO).
3. DNase I (Sigma).
4. Hank's buffer (Gibco-BRL, Rockville, MD).
5. Nembutal (Abbott, North Chicago, IL).
6. Trypsin (Sigma).
7. Penicillin-streptomycin (Invitrogen, Carlsbad, CA).
8. Poly-D-lysine (Sigma-Aldrich, St. Louis, MO).
9. Laminin-coated cover slips (BD Biosciences, Bedford, MA).
10. Dulbecco's modified Eagle's medium (Gibco-BRL).
11. Basal medium (F-12 nutrient mixture, HAM) (Gibco-BRL).
12. Dialyzed fetal bovine serum (FBS) (Sigma-Aldrich).
13. Glutamine (Sigma-Aldrich).
14. Supplement B27 (Gibco-BRL).
15. CO_2-controlled incubator.
16. 70% Alcohol.
17. Angle-neck flasks (40 mL) (Nalgen Nunc, Rochester, NY).
18. Hemacytometer (Improved Neubauer) (BD Biosciences).
19. Inverted light microscope.
20. Phosphate-buffered saline (PBS) (1X solution): 0.1 *M* NaCl, 2.7 m*M* KCl, 1.5 m*M* KH_2PO_4, 8.5 m*M* Na_2HPO_4, 1 m*M* $MgCl_2$, 0.1 m*M* $CaCl_2$; pH to 7.4.
21. EZ-Link™ sulfo-NHS-Biotin (Pierce, Rockford, IL).
22. Nonenzymatic dissociation solution (Sigma-Aldrich).
23. Glycine (Sigma-Aldrich).
24. Microcentrifuge tube with screw cap (2 mL) (Fisher brand no. 05-669-23; Fisher, Pittsburg, PA).
25. Stir bar (0.25 in.) (Fisher).
26. Halothane (Abbott).
27. Dimethyl sulfoxide (DMSO), anhydrous (Fisher).
28. Sodium bicarbonate (Sigma-Aldrich).
29. MicroSpin G-25 spin columns (Amersham Biosciences, Piscataway, NJ).
30. G-25 purification resin (Amersham Biosciences).
31. Hank's balanced salt solution (HBSS), Ca^{+2} + Mg^{+2} free, 10X (no. 14186-012; Gibco-BRL).
32. Excitation/emission filter: 485/520 and 580–630.
33. Glass collection tubes (13 × 100 mm) (Fisher).
34. Swinging-bucket centrifuge.
35. KRH buffer: 60 m*M* NaCl, 2 m*M* KCl, 0.6 m*M* KH_2PO_4, 4 m*M* HEPES.
36. Rotating shaker (Stoval, Greensboro, NC).
37. Biotinylated secondary anti-rabbit IgG (Vector, Burlingame, CA).

38. SA-quantum dots (Quantum Dot, Hayward, CA).
39. SA-Alexa Red™ (Molecular Probes, Eugene, OR).
40. Borate buffer (Polysciences, Warrington, PA).
41. Mercury lamp HBO 100 (Zeiss, Oberkochen, Germany).
42. Charge-coupled device (CCD) digital video camera (Roper, Tucson, AZ).
43. Human norepinephrine transporter (hNET)-expressing HEK293 cell line (Dr. Randy Blakely, Vanderbilt University, Nashville, TN).
44. Monoclonal antibody (MAb) to limbic-associated membrane protein (LAMP) (Dr. Pat Levitt, Vanderbilt University).
45. Polyclonal antibody to hNET ectodomain (Dr. Randy Blakely, Vanderbilt University).
46. HEK293 parental cells (American Type Tissue Collection [ATTC], Manassas, VA).
47. Pregnant rat (Sprague-Dawley®; Harlan, Indianapolis, IN).
48. Polypropylene conical tubes (50 mL) (Becton Dickinson, Franklin lakes, NJ).
49. Glass-bottomed microwell dishes (MatTek, Ashland, MA).

3. Methods

The following methods describe how to grow dispersed primary neurons and a continuous cell line culture, biotinylation of cell-surface proteins and MAbs, cell-surface protein immunocytochemistry using a biotinylated monoclonal and an anti-rabbit IgG, detection of biotinylated antibody-labeled proteins with SA-quantum dots and SA-Alexa flurophores™, and fluorescent imaging of SA-quantum dots and SA-Alexa flurophores.

3.1. Tissue Culture

The growth and maintenance of a primary neuronal (hippocampal) culture and a continuous cell line (HEK293) culture are described next. Each procedure can be adapted for use with other tissues (*see* **Note 1**).

3.1.1. Culture of Dissociated Primary Hippocampal Neuron Monolayer

1. Euthanize an 18-d pregnant rat (Sprague-Dawley) with halothane, nembutal, or other approved means.
2. Surgically remove the pups from the mother.
3. Perform each of the following steps using aseptic technique in a laminar flow hood (*see* **Note 2**). Remove the brain from the skull and immerse in HBSS to prevent the tissue from drying. Place the brain on a glass culture dish on a dissecting scope illuminated from below.
4. The following briefly describes how to dissect the hippocampus; for a more detailed discussion *see* **ref. *5***. Dissect the hippocampus and incubate for 30 min at 37°C in 20 U/mL of papain and 100 U/mL of DNase I in Ca^{+2}/Mg^{+2}-free Hank's buffer. Briefly rinse the tissue twice with HBSS containing 1 mg/mL of trypsin inhibitor, 100 U/mL of DNase, and 1 mg/mL of BSA; allow to dissociate in growth medium consisting of basal medium, with supplement B27, 10% FBS, 0.5 m*M* glutamine, and 0.5 m*M* penicillin-streptomycin.

5. Plate the dissociated cells on a poly-D-lysine and laminin-coated cover glass of a MatTek culture dish at a density of 20,000 cells and incubate in a 5% CO_2 incubator at 37°C. After 3 h, flood the plates with 1 mL of growth medium. After 3 d of culturing, feed the cells with growth medium containing FBS, and culture the cells for another 5 d.

3.1.2. Culture of HEK Cell Line Monolayer

Human embryonic kidney (HEK293) cells, a parental line and a stable line expressing hNET (Dr. Randy Blakely, Vanderbilt University), were frozen on dry ice in cryogenic vials at a concentration of 1×10^8/mL. The vials were stored immediately in liquid nitrogen for later use. At the time of use, the vials were removed from the liquid nitrogen and freeze-thawed on ice. While thawing, flasks were labeled as either HEK293/parental or HEK293/hNET. Cell medium, previously stored at 4°C, was removed and placed in a 37°C water bath until needed.

In the remainder of this section, each step was performed using aseptic technique inside a laminar flow hood (*see* **Note 2**). Ten milliliters of medium was transferred by pipet into each labeled flask. Thawed vials were then sterilized by swabbing with alcohol. The vials were slowly opened, and the medium with the cells was transferred by pipet into the appropriately labeled flask. The flasks were next placed in a 37°C incubator at 5% CO_2, and the cells were allowed to grow until confluent.

Once confluent, the medium was aspirated off and the cells well rinsed with PBS, and then 3 mL of 0.1% trypsin was added. After approx 1 to 2 min, or when the cells began to round up and detach, 3 mL of medium was added to disperse the cells and to inhibit the trypsin (*see* **Note 3**). Cells from each flask were then transferred to an appropriately labeled 50-mL conical tube and centrifuged at 500*g* for 5 min. The supernatant was aspirated off, and the cells were resuspended in fresh medium.

Using a hemacytometer, the cells were counted and their concentration was determined (*see* **Note 4**). The cell solution was next diluted to 1×10^5 cells/mL and 150 µL was added to the glass cover slip of poly-D-lysine-coated sterile MatTek microwell dishes. The cells were incubated at 37°C with 5% CO_2 for 3 h to allow the cells to attach. Once the cells had attached, 2 mL of additional medium was added to the dish. The dishes were then returned to the incubator and allowed to grow for 3 d or until 50% confluent.

3.2. Biotinylation

The following protocols describe procedures for conjugating cell-surface proteins and antibodies to biotin. Once conjugated, the biotin acts as a bridge for attaching SA-quantum dots or SA-fluorophores. Streptavidin has an

exceptionally high affinity for biotin ($Ka = 10^{14}$ mol^{-1}) and therefore binds essentially irreversibly ***(6)***.

Because each cell line may vary in its nonspecific adsorption of SA-quantum dots, and because we have observed that SA-quantum dot integrity is compromised after long periods of storage, we recommend first conducting a control experiment using biotinylated cells to confirm the integrity of SA-quantum dots and to determine their signal over background for the cell line being used (*see* **Fig. 1**). **Subheadings 3.2.1.** and **3.2.2.** describe a biotinylation procedure for both dispersed primary neuronal and continuous cell line cultures.

Subheading 3.2.3. describes the step-by-step process for covalent coupling of biotinyl groups to the MAb LAMP. This procedure may also be used with other antibodies (IgG and different Ig classes) (*see* **Note 5**). Most secondary antibodies are commercially available with biotin already attached (i.e., Vector).

3.2.1. Cell-Surface Biotinylation

1. Seed poly-D-lysine-coated microwell dishes with parental HEK-293 cells at 50,000 cells/well, and incubate for 48 h as described in **Subheading 3.1.2.**
2. Remove the dishes from the incubator and wash quickly with 37°C KRH.
3. Treat the cells with EZ-Link sulfo-NHS-Biotin at 1.5 mg/mL at 4°C for 1 h in PBS/Ca^{+2} + Mg^{+2}.
4. After incubation, remove the biotinylating reagents and quench by washing twice with ice-cold 100 m*M* glycine in PBS/Ca^{+2} + Mg^{+2}.
5. Quench the reaction further by incubating with 100 m*M* ice-cold glycine for 30 min.
6. Rapidly wash the cells three times with PBS/Ca^{+2} + Mg^{+2}.

3.2.2. Primary Cultures

1. Culture primary hippocampal neurons as described in **Subheading 3.1.1.**
2. After neuronal growth has reached confluence and/or 8 d in age (*see* **Note 6**), perform **steps 3–6** in **Subheading 3.2.1.**.

3.2.3. Antibody Biotinylation

1. Transfer 200 µL of a 1.0 mg/mL antibody solution to a 2-mL tube containing a stir bar, place on a stir plate, and set the magnetic stirrer at 50 rpm (*see* **Note 7**).
2. To this tube add 20 µL of 1 *M* sodium bicarbonate (freshly made).
3. To a 2-mL reaction tube add 200 µg of DSB-X biotin succinimidyl ester (*see* **Note 8**).
4. To this tube add 40 µL of DMSO and mix by pipetting up and down (*see* **Note 9**).
5. Add 3 µL of this mix to the 2-mL tube with antibody that is stirring in **step 1**.
6. Allow the reaction mix to stir for 1 to 1.5 h at room temperature.
7. While the reaction mixture is stirring, perform **steps 8–13**.

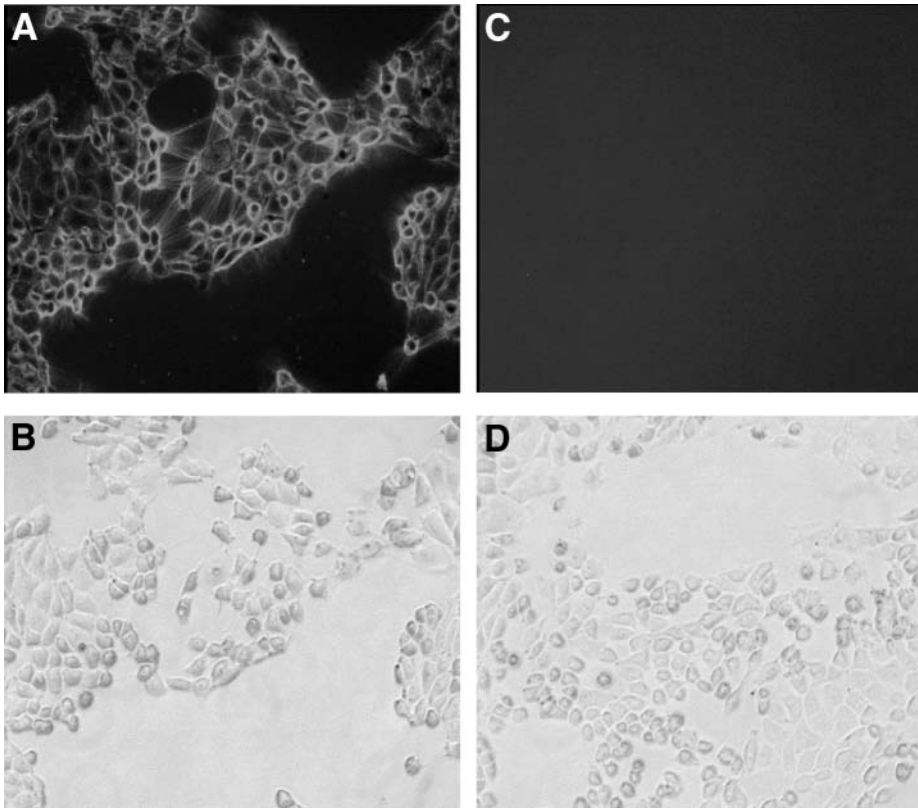

Fig. 1. Labeling of biotinylated HEK293 cells with SA-quantum dots (magnification: ×10). Three-day-old HEK293 cells cultured on poly-D-lysine glass-bottomed microwell dishes were biotinylated as described in **Subheading 3.2.1. (A,B)** Biotinylated HEK293 cells incubated with SA-quantum dots (50 n*M*); **(C,D)** biotinylated HEK293 cells labeled with SA-quantum dots after preincubating with 2 mg/mL of biotin.

8. Place a spin column into a 13 × 100 mm glass tube.
9. Stir the purification resin using a clean plastic tube.
10. Add 1 mL of the purification resin to the spin column.
11. Allow the resin to settle, and then add more resin until the bed volume is approx 1.5 m while allowing the column buffer to drain into the 13 × 100 mm glass tube.
12. Place the spin column into a collection tube.
13. Centrifuge the spin column with the collection tube for 3 min at 1100*g* using a swinging-bucket rotor.
14. Load the reaction mixture from **step 6** (~200 µL) onto the center of the spin column and allow it to be absorbed (*see* **Note 10**).

15. Place the spin column into an empty collection tube and centrifuge for 5 min at 1100*g*. The eluate in the bottom of the tube contains the biotinylated antibody in 20 m*M* PBS, pH 7.4. We determined the concentration of biotinylated antibody to be 800 µg/mL (*see* **Note 11**).

3.3. Immunocytochemistry

In **Subheading 3.3.1.** and **3.3.2.**, we describe respectively how to label a specific cell-surface protein by using a biotinylated MAb for direct detection and by indirect labeling using a nonbiotinylated polyclonal antibody followed by a secondary biotinylated anti-rabbit IgG.

3.3.1. Detection with Biotinylated Primary Antibody

1. Quickly wash with room temperature KRH dissociated primary hippocampal neurons (*see* **Note 12**) grown to confluency on microwell dishes (*see* **Subheading 3.1.1.**).
2. Remove the excess KRH present on the cover glass surface by aspiration.
3. Add 100 µL of biotinylated LAMP primary antibody (diluted to a concentration of 8 µg/mL) to the cells attached to the cover slip glass of the microwell dishes.
4. Incubate the dishes at room temperature for 1 h on a rotating shaker at 50 rpm.
5. After 1 h, wash the dishes three times for 5 min with KRH while rotating on a shaker at 50 rpm.
6. Aspirate the excess KRH from the cover glass, and label the attached cells using either SA-quantum dots or SA-Alexa Red (*see* **Subheadings 3.4.1.** and **3.4.2.**).

3.3.2. hNET Detection in HEK-293 Cell Line With Biotinylated Secondary Antibody

1. Quickly wash with room temperature KRH HEK-293 cells cultured on the cover slip glass of each microwell dish (*see* **Subheading 3.1.2.**).
2. Remove the excess KRH present on the cover glass surface by aspiration.
3. Add 100 µL of polyclonal anti-hNET (5 µg/mL) to the cells covering the microwell dish cover slip glass.
4. Incubate the cells for 1 h on a rotating shaker at 50 rpm.
5. Wash the dishes three times for 5 min with KRH while rotating on a shaker at 50 rpm.
6. Add 1.5 µg/mL of biotinylated anti-rabbit.
7. Incubate the dishes at room temperature for 1 h on a rotating shaker at 50 rpm.
8. Wash the dishes three times for 5 min with KRH while rotating at 50 rpm on the shaker. The cells on the cover slip glass are now ready to be labeled using either SA–quantum dots or SA–Alexa Red (*see* **Subheadings 3.4.1** and **3.4.2.**).

3.4. Detection Using SA-Quantum Dots and SA-Alexa Fluor™

Biotinylated antibodies are detected using quantum dots conjugated to streptavidin (SA-quantum dots) and the streptavidin-labeled fluorophore Alexa Red™

594 as a control. **Subheadings 3.4.1.** and **3.4.2.** describe a procedure that was developed for detecting biotinylated antibodies with either SA-quantum dots or SA-Alexa Red. Depending on the cell type, it may be necessary first to pre-incubate cells with a blocking solution when labeling with SA-quantum dots (*see* **Note 13**).

3.4.1. SA-Quantum Dots

1. Aspirate the excess KRH buffer on the cells covering the cover slip glass of the microwell dishes from **Subheadings 3.3.1.** and/or **3.3.2.**, being careful to avoid removing any of the attached cells.
2. Add 50 µL of SA-quantum dots (50 n*M*) in borate buffer (pH 8.0) to the cover slip glass of the microwell dishes.
3. Incubate the dishes at room temperature for 10 min with no agitation (*see* **Note 14**).
4. Quickly rinse the dishes three times with KRH.
5. Add 100 µL of KRH to the cells covering the cover slip glass of the microwell dishes.
6. Immediately image the SA-quantum dot-labeled cells (*see* **Subheading 3.5.**).

3.4.2. SA-Fluorophore (Alexa Red)

1. Aspirate off the excess KRH buffer from the cells covering the cover slip glass of the microwell dishes from **Subheadings 3.3.1.** and/or **3.3.2.**, being careful to avoid removing any of the attached cells.
2. Add 50 µL of SA-Alexa Red (300 µg/mL) in KRH buffer (pH 7.4) to the cover slip glass of the microwell dishes.
3. Incubate the dishes at room temperature for 10 min with no agitation.
4. Quickly rinse the dishes three times with KRH.
5. Add 100 µL of KRH to the cells on the cover slip glass well of the microwell dishes.
6. Immediately image the SA-Alexa Red-labeled cells (*see* **Subheading 3.5.**).

3.5. Fluorescent Imaging

To fluorescently image labeled cells on the cover glass of microwell dishes after incubation with SA-quantum dots or SA-Alexa Red requires an inverted fluorescent microscope equipped with a transmitted-light illumination system, for the initial bright-field examination; an incident-light illuminator, for the excitation of fluorophores; and a filter cube with the appropriate filter set (*see* **Fig. 2**). For convenience, the microscope should also have a phototube for mounting either a conventional 35-mm or an electronic CCD digital video camera that can be interfaced with a computer. The steps for imaging SA-quantum dot- and SA-Alexa Red-labeled cells from **Subheadings 3.4.1.** and **3.4.2.** using an Axiovert 110 (Zeiss) equipped with an HBO 100 mercury lamp (Zeiss) and a

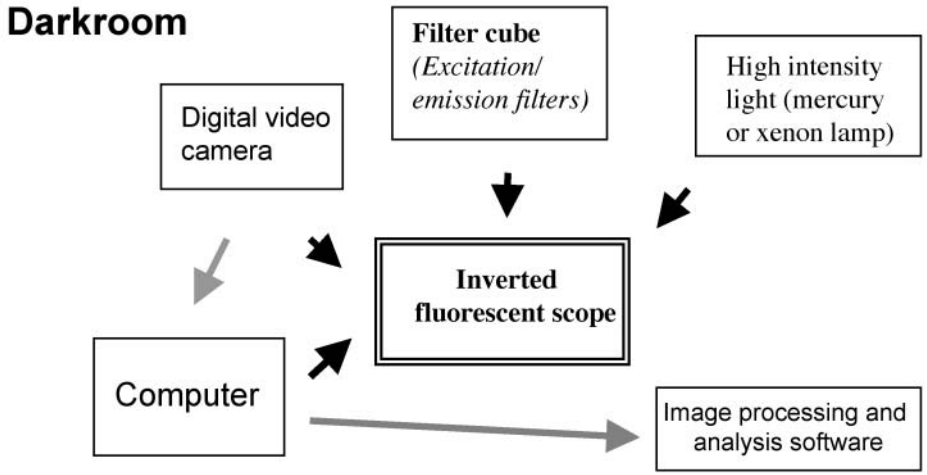

Fig. 2. Components required for fluorescent imaging. An inverted fluorescent microscope equipped with the appropriate excitation/emission filter(s) and camera insertion site also should include a mercury or xenon lamp for fluorophore excitation and a digital camera. The computer selected should have sufficient memory to process and to analyze digital images using analysis software. All equipment shown should be set up in a room in which lighting can be shut off without inconveniencing other laboratory operations.

Photometric Cool Snap™ digital CCD camera (Roper) are described next. However, these steps can be repeated using a comparable imaging system.

3.5.1. Fluorescent Imaging

1. Position cells on the cover glass of microwell dishes labeled with either SA-quantum dots or SA-Alexa Red on the stage of an inverted fluorescent microscope.
2. Using transmitted light, bring into focus the cells on the cover glass and capture a bright-field image using a CCD digital video camera.
3. Using 488 nm of incident light, excite the cells labeled by SA-quantum dots or SA-Alexa Red, and observe the fluorescence produced though a 485/20 and 580–630 band-pass filter.
4. Before capturing an image, illuminate the SA-quantum dot-labeled cells on the cover glass of the dishes with incident light for a minimum of 2 min to induce maximal fluorescence (*see* **Note 15**). Immediately capture images of SA-Alexa Red-labeled dishes to avoid bleaching.
5. To ensure that SA-quantum dots used to label cells have not aggregated while labeling, examine imaging fields for SA-quantum dot clusters that are not colocalized with cells (*see* **Fig. 4C**). When aggregates or clusters are present, it is assumed that SA-quantum dots did not remain in the solution while labeling and

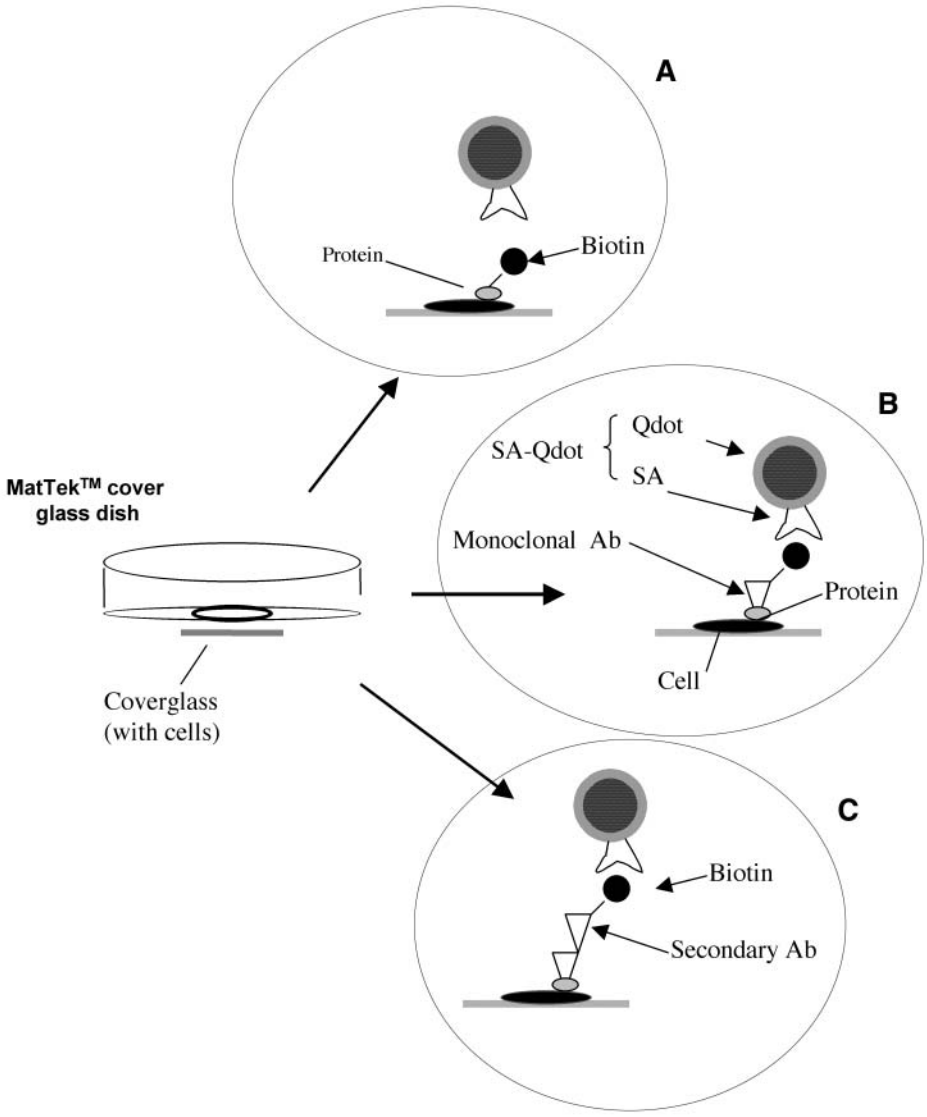

Fig. 3. Direct and indirect labeling of live cells by SA-quantum dots (SA-Qdot). **(A)** Biotinylated cell-surface proteins are labeled directly by SA-quantum dots. **(B)** Biotinylated MAb used to detect cell-surface protein is labeled by SA-quantum dots. **(C)** Biotinylated secondary antibody used to detect polyclonal antibody attached to the cell-surface protein is labeled by SA-quantum dot.

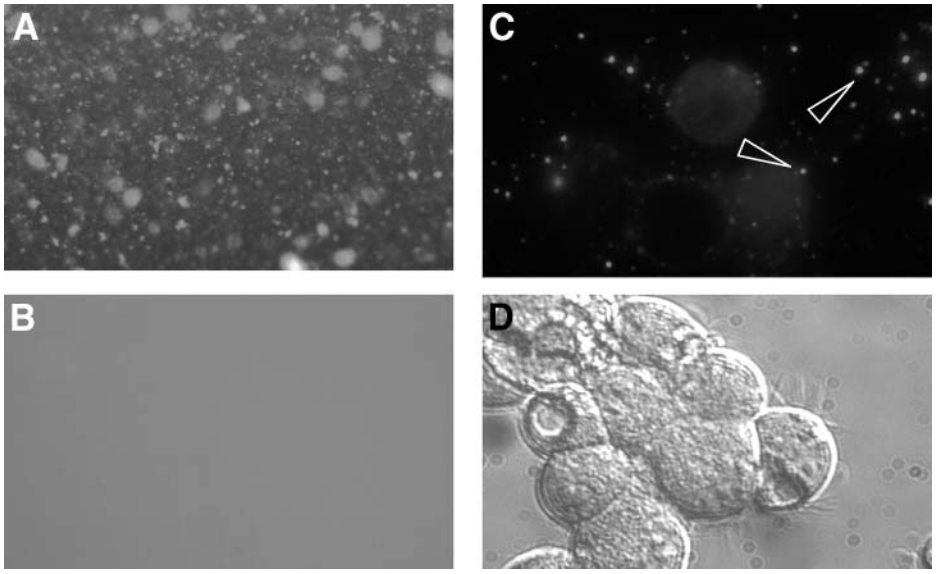

Fig. 4. Evidence for quantum dot aggregation (magnification: ×40): **(A)** fluorescent image of aggregated SA-quantum dots in absence of cells; **(B)** image of nonaggregated SA-quantum dots in absence of cells; **(C)** image of cells surrounded by aggregated SA-quantum dots (arrowheads); **(D)** bright-field image.

that labeling of the biotin-modified targets with SA-quantum dots was compromised (*see* **Note 16**).

4. Notes

1. Depending on which type of cell line is cultured, the growth medium used may vary. Whether or not a cell-line type expresses a particular protein in culture can be controlled by the nutritional constitution of the medium, such as hormones and other inducer or repressor substances, as well as the interaction between cells and their substrate. Most media are based on balanced salt solutions to which are added amino acids, vitamins, and other nutrients at concentrations roughly similar to those found in serum. The composition of the media commonly used in cell culture is provided in standard texts and in catalogs from companies that sell supplies for tissue culture ***(7,8)***. Suggested growth media that is commercially available for most cell culture lines is also listed with the ATTC ***(9)***. Because the requirements for dissociated primary tissue growth media can be specific, it is best to obtain media requirement details that optimize growth by referring to the materials and methods sections of publication(s) in which the tissue you are interested in has already been cultured. Reviews of culture techniques for specific cell types are available ***(10,11)***.

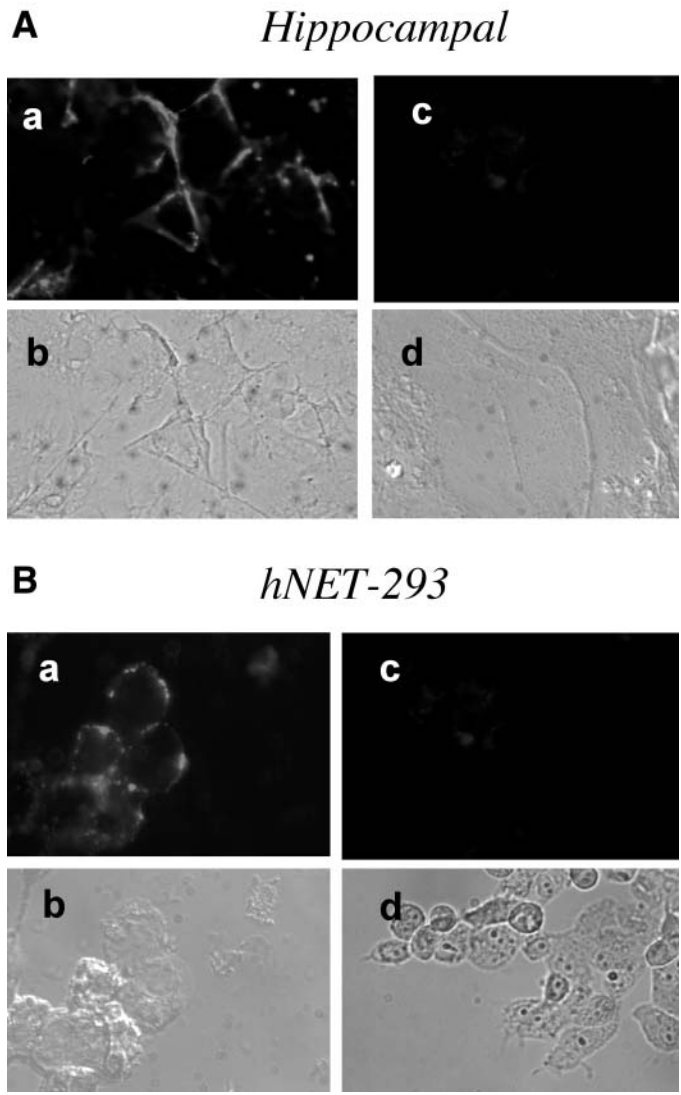

Fig. 5. SA-quantum dots and SA-Alexa Red recognize biotin-modified antibody-labeled cultures. **(A)** Eight-day-old *fixed* primary hippocampal cultures incubated with anti-LAMP followed by SA-quantum dots (a, b) or SA-quantum dots alone (c, d); **(B)** labeling of live hNET-293 cells with anti-hNET + biotinylated anti-rabbit IgG followed by SA-quantum dots (a, b) or SA-quantum dots alone (c, d).

2. In spite of the introduction of antibiotics, contamination by microorganisms remains a major problem in tissue culture. Correct aseptic technique should provide a barrier between microorganisms in the environment outside the culture. The procedure used for equipping and practicing aseptic technique in a laboratory has been described in a number of sources ***(7,11)***. Inability to follow steps in aseptic technique will likely result in bacterial contamination that may alter the biochemical behavior and cell-surface protein expression of the cell line. Taking time to obtain advice from personnel of other laboratories experienced in aseptic technique can greatly facilitate success in this area.
3. Although some cell lines can be dislodged from the bottom of the flask by gently pipetting the medium over the cells repeatedly, trypsinizing cells has the advantage of producing a single cell suspension. However, overtrypsinizing may reduce viability, and undertrypsinizing can result in cell clumps. Furthermore, cells treated with trypsin may require one or more days after plating before reexpression of surface proteins. If viability is a concern, commercially available nonenzymatic dissociation solutions can be used (e.g., from Sigma-Aldrich). These dissociation solutions are calcium free.
4. The concentration of a cell suspension may be determined by placing cells in an optically flat chamber, known as a hemacytometer, which is placed under a microscope. The cell number within a defined area of the hemacytometer can then be counted and the cell concentration derived from this count. Detailed instructions on how to use a hemacytometer (Improved Neubauer) are described elsewhere ***(12)***. An alternative approach to the hemacytometer is electronic particle counting. This method requires the use of an automated system called a Coulter Counter. In this system, cells in suspension are drawn though a fine orifice. As each cell passes though the orifice, it causes a change in current. This change produces a series of pulses, which are then counted ***(5)***.
5. Because the coupling conditions are mild, biotinylation normally does not have any adverse effect on the antibody. However, if a free amino group forms at a position on the protein that is essential for activity (i.e., the antigen-combining site), biotinylation will lower or destroy the activity of the antibody ***(13,14)***.
6. Dissociated primary tissue neurons are typically fastidious in their growth requirements. Failure to provide the appropriate growth factor or combination of factors can cause the neurons to die within a few days. Altering the composition of the medium can determine whether a protein is or is not expressed. One approach is to allow the cultured cells to produce their own growth factors. Most types of glia cells and neurons secrete growth factors in vitro. Thus, if appropriate mixtures of the cells are grown at high density, adequate amounts of the needed growth factor may accumulate. Another approach is to add growth factors directly to the medium. Various classes of neuronal growth factors have been used in culture. For a more complete discussion of required growth factors and their sources, *see* **refs. *5*** and ***7***.
7. If the purified antibody is in dilute buffer, such as 10–20 m*M* PBS, it may be used directly in the protocol. However, if the antibody is in a buffer containing

extraneous primary amines (i.e., Tris or glycine) or ammonium ions, then it must be desalted by dialyzing against PBS, or by using a spin column ***(15)***.

8. In our experiments, we had success when using the biotin succinimide ester DSB-X™ (Molecular Probes). Many biotinylated succinimide esters are now available. Most of these variations alter the size and characteristic of the spacer arm between the succinimide-coupling group and the biotin. However, all the esters are handled in a manner similar to that described in this protocol ***(14)***.
9. To ensure the reactivity of the succinimidyl ester, the solution in DMSO should be made immediately before use. This is to prevent precipitation of the biotin ester, which will occur if the final concentration of DMSO drops below 5%.
10. If any precipitation has occurred during the reaction, the sample must be centrifuged for 5 min to pellet the precipitate before loading. Only the supernatant should be loaded onto the column ***(15)***.
11. Typically, about 80–90% of the antibody in the reaction is recovered as a biotin conjugate.
12. It is necessary to separate out all nonneuronal cells in a neuronal preparation. Nonneuronal cells have a tendency to proliferate, displacing the neuronal cells. If nonneuronal proliferation impedes the detection of the neuronal cells, an antimitotic drug such as cytosine arabinofuranoside can be added (1–5 μ*M*). However, this may result in injury to the neuronal cells and should, therefore, be used at its minimum concentration ***(16)***.
13. Our experience is that the adsorbtion of quantum dots by cells can be cell-type specific. Therefore, preincubating cells and quantum dots with a blocking reagent before application may be necessary ***(17)***. Some reagents that we and others have found to be successful include BSA ***(18)***, 5% normal goat serum (Jackson Immunoresearch), and 0.1% cold-water fish skin gelatin (Amersham Life Bioscience) ***(4)***.
14. Depending on the cell type, rapid agitation may cause cells to detach; therefore, we recommend gently rotating dishes manually. Because borate buffer is harsh on cells, we incubated cells for no more than 15 min to prevent dissociation. However, this will vary with the cell type and number of days that they are cultured. Cells tend to dissociate most readily if cultured less than 2 d and/or grown past confluence.
15. When imaging quantum dots, it is necessary to illuminate for 2 to 3 min before maximum fluorescent intensity will be reached. The rate of quantum dot bleaching is approx 2%/min when illuminated continuously after reaching maximum fluorescence intensity. This is in contrast to conventional fluorophores, which are typically bleached entirely within minutes of illuminating ***(19)***.
16. When imaging, it is important to recognize when aggregates have formed. Our experience is that aggregates can occur unpredictably. Before adding quantum dots for labeling, we advise placing SA-quantum dots on the cover glass of a clean microwell dish and imaging at ×40 to determine whether aggregates have already formed (*see* **Fig. 4A,B**). This assay will confirm whether the SA-quantum dots should be used for labeling. If SA-quantum dots are not aggregated before

adding but aggregate after incubation with cells (*see* **Fig. 4C,D**) then the problem resides with the incubation step. Note that quantum dots when conjugated to certain proteins, such as transferrin, can be internalized by the cell though activation of transferrin receptors. Thus, proper controls should be included to distinguish surface labeling from potential internalization ***(20)***.

References

1. Jaiswal, J. K., Mattoussi, H., Mauro, J. M., and Simon, S. M. (2003) Long-term multiple color imaging of live cells using quantum dot bioconjugates. *Nat. Biotechnol.* **21,(1),** 47–51.
2. Akerman, M. E., Chan, W. C., Laakkonen, P., Bhatia, S. N., and Ruoslahti, E. (2002) Nanocrystal targeting in vivo. *Proc. Natl. Acad. Sci. USA* **99(20),** 12,617–12,621.
3. Goldman, E. R., Balighian, E. D., Mattoussi, H., Kuno, M. K., Mauro, J. M., Tran, P. T., and Anderson, G. P. (2002) Avidin: a natural bridge for quantum dot–antibody conjugates. *J. Am. Chem. Soc.* **124(22),** 6378–6382.
4. Rosenthal, S. J., Tomlinson, I., Adkins, E. M., Schoeter, S., Adams, S., Swafford, L., McBride, J., Wang, Y., DeFelice, L. J., and Blakely, R. D. (2002) Targeting cell surface receptors with ligand-conjugated nanocrystals. *J. Am. Chem. Soc.* **124,** 4586–4594.
5. Banker, G. and Goslin, K. (1998) *Culturing Nerve Cells*, 2nd ed., MIT Press, Cambridge, MA.
6. Green, N. M. (1990) Avidin and streptavidin. *Methods Enzymol.* **184,** 51–67.
7. Freshney, R. I. (1991) *Culture of Animal Cells: A Manual of Basic Technique*, 2nd ed., Wiley-Liss, New York.
8. Gibco-BRL. (2002) *Products and Reference Guide 2001–2002*, Gibco-BRL, Rockville, MD.
9. American Type Tissue Collection. (2002) Catalogue, ATTC, Manassas, VA.
10. Jacoby, W. B. and Pastan, I. H. (1979) Cell culture, in *Methods in Enzymology, vol. LVIII* (Colowick, S. P. and Kaplan, N. D., eds.), Academic, New York, pp. 1–64.
11. Kruse, P. and Patterson, M. K. (1973) *Tissue Culture Techniques and Applications*, Academic, New York.
12. BD Biosciences. (2002) *Hemocytometer Reference Guide*, Palo Alto, CA.
13. Bayer, E. A. and Wilchek, M. (1979) The biotin transport system in yeast. *Methods Enzymol.* **62,** 371–378.
14. Harlow, E. and Lane, D. (1999) *Using Antibodies: A Laboratory Manual*, Cold Spring Harbor Laboratory Press, Cold Spring Harbor, New York.
15. Amersham Biosciences. (2002) Spin column instructions, Amersham Biosciences, Piscataway, NJ.
16. Patel, M. N. and McNamara, J. O. (1995) A novel way of removing quiescent astrocytes in a culture of subcortical neurons grown in a chemically defined medium. *Neuroscience* **69,** 763–770.
17. Quantum Dot. (2002) Immunofluorescent labeling of tissue sections with quantum dot-streptavidin, protocol from Quantum Dot, Hayward, CA.

18. Mason, J. N., Farmer, H., Tomlinson, I. D., Schwartz, J. W., Savchenko, V., DeFelice, L. J., Rosenthal, S. J., and Blakely, R. D. (2005) Novel fluorescence-based approaches for the study of biogenic amine transporter localization, activity, and regulation. *J. Neurosci. Methods*, in press.
19. Wu, X., Liu, H., Liu, J., Haley, K. N., Treadway, J. A., Larson, J. P., Ge, N., Peale, F., and Bruchez, M. P. (2003) Immunofluorescent labeling of cancer marker Her2 and other cellular targets with semiconductor quantum dots. *Nat. Biotechnol.* **21(1),** 41–46.
20. Chan, C. W. W. and Nie, S. (1998) Quantum dot bioconjugates for ultrasensitive nonisotopic detection. *Science* **281(5385),** 2016–2018.

4

Peptide-Conjugated Quantum Dots

Imaging the Angiotensin Type 1 Receptor in Living Cells

Ian D. Tomlinson, John N. Mason, Randy D. Blakely, and Sandra J. Rosenthal

Summary

Peptide–quantum dot conjugates have been prepared by attaching angiotensin II (Ang II) to cadmium selenide/zinc sulfide core-shell nanocrystals using an 1-[3-(Dimethyamino)propyl]-3-ethylcarbo diimide hydrochloride (EDC) coupling. These conjugates have been used to image angiotensin I–expressing Chinese hamster ovary (CHO) cells in vitro. When CHO cells were incubated with Ang II before incubating with Ang II-conjugated quantum dots, we were able to block the binding of the dots. The Ang II–quantum dot conjugates did not bind to parental cells and showed similar staining patterns when compared with a commercially available Ang II Alexa 488™ conjugate.

Key Words

Nanocrystals; quantum dot; angiotensin II; peptide; fluorescence; Chinese hamster ovary cells; Alexa 488™.

1. Introduction

Cadmium selenide/zinc sulfide core-shell nanocrystals (quantum dots) are composed of a crystalline cadmium selenide core (2–7 nm in diameter) surrounded by a zinc sulfide shell (approx 1.5 nm thick). The small size of the core gives rise to unique properties that are not observed in bulk material. The fluorescent properties of quantum dots have potential applications in biological imaging and drug development. When compared to conventional dyes, it has been shown that quantum dots have several unique advantages, including increased quantum yields; increased photostability; narrower, Gaussian-shaped emission bands; and a continuous absorption above the first excitation feature

From: *Methods in Molecular Biology, vol. 303: NanoBiotechnology Protocols*
Edited by: S. J. Rosenthal and D. W. Wright © Humana Press Inc., Totowa, NJ

(1–5). The fluorescence emission of quantum dots is size tunable: small quantum dots give rise to fluorescence toward the blue end of the spectrum and large quantum dots give rise to a fluorescence emission towards the red end of the spectrum ***(6–8)***.

Several groups have reported conjugating antibodies, proteins, peptides, and nucleic acids to quantum dots ***(9–18)***. In our laboratory, we have synthesized conjugates composed of small molecules and short peptides attached to quantum dots via either electrostatic interactions, acid base interactions, or direct covalent attachment ***(19–21)***. Our interests include the G protein-coupled receptors. This is a very broad family of receptors that regulates a wide range of physiological functions. Their ligands may be small molecules such as serotonin and dopamine or peptides such as angiotensin II (Ang II) and somatostatin. Because of the wide variety and different functions of peptide hormones, we have developed a methodology for attaching peptides to quantum dots. In this chapter, we describe how angiotensin II may be covalently attached to the surface of polymer-coated (AMP™) quantum dots. These peptide-nanoconjugates have been used to successfully image live Chinese hamster ovary (CHO) cells expressing the angiotensin I receptor.

2. Materials

1. AMP-coated cadmium selenide/zinc sulfide core-shell nanocrystals (Quantum Dot, Haywood, CA).
2. Borate buffer, 0.5 *M*, pH 8.5, 5X concentrate (Polysciences, Warrington, PA).
3. mPEG-Amine, mol wt = 5000, chromatographically pure (Shearwater, Huntsville, AL).
4. *N*-Hydroxysuccinimide, 1-(3-dimethylaminopropyl)-3-ethylcarbodiimide hydrochloride (Aldrich, St. Louis, MO).
5. Sephadex PD-10 columns Sephadex TM G25-M (Pharmacia, Uppsala, Sweden).
6. CHO cells (Dr. Ted Ingami, Department of Biochemistry, Vanderbilt University, TN).
7. Human ang II (Sigma-Aldrich, St. Louis, MO).
8. Trypsin (Sigma-Aldrich).
9. Ang II, Alexa Fluor® 488 conjugate (Molecular Probes, Eugene, OR).
10. Phosphate-buffered saline (PBS): (1X solution): 0.1 *M* NaCl, 2.7 m*M* KCl, 1.5 m*M* KH_2PO_4, 8.5 m*M* Na_2HPO_4, 1 m*M* $MgCl_2$, 0.1 m*M* $CaCl_2$; pH to 7.4.
11. Inverted fluorescent microscope.
12. HBO 100 mercury lamp (Zeiss, Oberkochen, Germany).
13. Charge-coupled device (CCD) digital video camera (Roper, Tucson, AZ).
14. Glass-bottomed microwell dishes (MatTek, Ashland, MA).
15. Hemacytometer (Improved Neubauer) (BD Biosciences, Bedford, MA).
16. Swinging-bucket centrifuge.
17. Laminin-coated cover slips (BD Biosciences).
18. CO_2-controlled incubator.

19. Inverted light microscope.
20. Glutamine (Sigma-Aldrich).
21. Nonenzymatic dissociation solution (Sigma-Aldrich).
22. Glycine (Sigma-Aldrich).
23. Poly-D-lysine (Sigma-Aldrich).
24. Dialyzed fetal bovine serum (Sigma-Aldrich).
25. Penicillin-streptomycin (Invitrogen, Carlsbad, CA).
26. Dulbecco's modified Eagle's medium F12 Nutrient Mixture (HAM) (Gibco-BRL, Rockville, MD).
27. Angle-neck flasks (40 mL) (Nalgen Nunc, Rochester, NY).
28. Excitation/emission filter set: 485/20 and 515–530; 546/12 and 580–630.
29. KRH buffer: 60 m*M* NaCl, 2 m*M* KCl, 0.6 m*M* KH_2PO_4, and 4 m*M* HEPES.
30. Rotating shaker (Stoval, Greensboro, NC).
31. Polypropylene conical tubes (50 mL) (Becton Dickinson, Franklin Lakes, NJ).

3. Methods

The methods described next outline (1) the synthesis of Ang II, mPEG-amine-conjugated AMP-coated water cadmium selenide/zinc sulfide core-shell nanocrystals; (2) fluorescence imaging studies of CHO cells using the Ang II conjugates; and (3) fluorescence imaging studies of CHO cells using an Ang II Alexa Fluor 488 conjugate.

3.1. Synthesis of Ang II, mPEG-Amine-Conjugated AMP-Coated Cadmium Selenide/Zinc Sulfide Core-Shell Nanocrystals

We prepared nanoconjugates of Ang II as follows: A total of 0.3 mL of a 2 μ*M* solution of AMP-coated quantum dots in borate buffer at pH 8.5 was placed in a vial. These dots had a maximum emission at 585 nm and a full width at half maximum emission (FWHM) of 22 nm. Their quantum yield was 37% and they were a gift from Quantum Dot (batch no. 228-35). Then *N*-hydroxysuccinimide (35 μg, 30 nmol) dissolved in 0.1 mL of borate buffer and 1-(3-dimethylaminopropyl)-3-ethylcarbodiimide hydrochloride (5.8 μg, 30 nmol) dissolved in borate buffer (0.1 mL) were each added, and the solution was stirred for 5 min at room temperature. mPEG-amine 5000 (0.6 mg, 12 nmol) and human Ang II (70 μg, 6 nmol) dissolved in borate buffer (0.1 mL) were next added, and the mixture was stirred at room temperature for 18 h. The conjugates were then purified using a Sephadex P-10 column eluted with borate buffer at pH 8.5. Fractions containing 0.1 mL of solution were collected from the column, and the product was shown to be in fractions three to nine, because these samples fluoresced brightly under a mercury lamp. Fractions four to eight were combined, and the concentration of the resulting nanoconjugate was determined using UV-vis spectroscopy and was determined using an extinction coefficient of 650,000 (Quantum Dot, personal

communication, September 2000). The conjugated dots were used to image cells with no further purification.

3.2. CHO Cells and Cell Cultures

CHO cells, a parental line and a stable line expressing the Ang II receptor type 1 (AT1) receptor, were a gift from Dr. Tad Inagami (Vanderbilt University, Nashville, TN). Cells were delivered frozen on dry ice in cryogenic vials at a concentration of 1×10^8/mL. On arrival, the vials were stored immediately in liquid nitrogen for later use. At the time of use, the vials were removed from the liquid nitrogen and freeze-thawed on ice. While thawing, the flasks were labeled as either CHO/parental or CHO/AT1. Cell medium, previously stored at 4°C, was removed and placed in a 37°C water bath until needed.

In the remainder of this section, each step was performed using an aseptic technique inside a laminar flow hood (*see* **Note 1**). Ten milliliters of medium was transferred by pipet into each labeled flask. Thawed vials were then sterilized by swabbing with alcohol. The vials were slowly opened, and the medium with the cells was transferred by pipet into the appropriately labeled flask. The flasks were next placed in a 37°C incubator at 5% CO_2, and the cells were allowed to grow until confluent.

Once confluent, the medium was aspirated off, the cells were rinsed with PBS, and then 3 mL of 0.1% trypsin was added. After approx 1 to 2 min, or when the cells began to round up and detach, 3 mL of medium was added to disperse the cells and to inhibit the trypsin (*see* **Note 2**). Cells from each flask were then transferred to an appropriately labeled 50-mL conical tube and centrifuged at 500*g* for 5 min. The supernatant was aspirated off, and the cells were resuspended in fresh medium. The cells were next counted with a hemacytometer and their concentration was determined (*see* **Note 3**). The cell solution was diluted to 1×10^5 cells/mL, and 150 µL was added to the glass cover slips of poly-D-lysine-coated sterile MatTek microwell dishes. Cells were then incubated at 37°C with 5% CO_2 for 3 h to allow the cells to attach. Once the cells had attached, 2 mL of additional medium was added to each of the dishes. The dishes were then returned to the incubator and allowed to grow for 3 d or until 50% confluent.

3.2.1. Detection Using Ang II-Conjugated Quantum Dots

Ang II AT1 receptors expressed on the surface of CHO cells can be detected directly by using Ang II-conjugated quantum dots and Ang II-conjugated Alexa 488 as a control. **Subheadings 3.2.1.1.** and **3.2.1.2.** describe procedures that were developed for the direct detection of the AT1 receptor on the surface of living CHO cells with angII–quantum dots and Ang II–Alexa 488, respectively.

3.2.1.1. Ang II–Quantum Dot

1. Aspirate off the excess KRH buffer on the cells covering the cover slip glass of the microwell dish, being careful to avoid removal of attached cells.
2. Add 50 µL of Ang II–quantum dots (200 n*M*) in borate buffer (pH 8.4) to the cover slip glass of the microwell dish.
3. Incubate the dish at room temperature for 5 min with no agitation (*see* **Note 4**).
4. Quickly rinse the dish three times with KRH.
5. Add 100 µL of KRH to the cells covering the cover slip glass well of the microwell dish.
6. Immediately image the Ang II–quantum dot-labeled cells.

3.2.1.2. Ang II–Fluorophore (Alexa 488)

1. Carefully aspirate off the excess KRH buffer from the cells covering the cover slip glass of the microwell dish to avoid removal of attached cells.
2. Add 50 µL of Ang II–Alexa 488 (2.5 µg/mL) in KRH buffer (pH 7.4) to the cover slip glass of the microwell dish.
3. Incubate the dish at room temperature for 5 min with no agitation.
4. Quickly rinse the dish three times with KRH.
5. Add 100 µL of KRH to the cells covering the cover slip glass well of the microwell dish.
6. Immediately image the Ang II–Alexa 488-labeled cells.

3.3. Fluorescent Imaging

To image cells fluorescently on cover glass microwell dishes labeled directly with Ang II–quantum dots or Ang II–Alexa 488 after incubation with SA-quantum dots or SA–Alexa 488 requires an inverted fluorescent microscope equipped with a transmitted-light illumination system for the initial bright-field examination, an incident-light illuminator for the excitation of fluorophores, and a filter cube with the appropriate filter set. For convenience, the scope should contain a phototube for mounting either a conventional 35-mm or an electronic CCD digital video camera. If a digital video camera is used, it must be interfaced with a computer. The steps described for imaging Ang II–quantum dot- and Ang II–Alexa 488-labeled cells in this chapter use an Axiovert 110 (Zeizz) equipped with an HBO 100 mercury lamp (Zeiss) and a Photometric CoolSnap™ digital CCD camera (Roper). However, these steps can be repeated using a comparable imaging system.

3.3.1. Imaging of CHO Cells

1. Position cells on the cover glass of microwell dishes labeled with either Ang II–quantum dots or Ang II–Alexa 488 on the stage of an inverted fluorescent microscope.

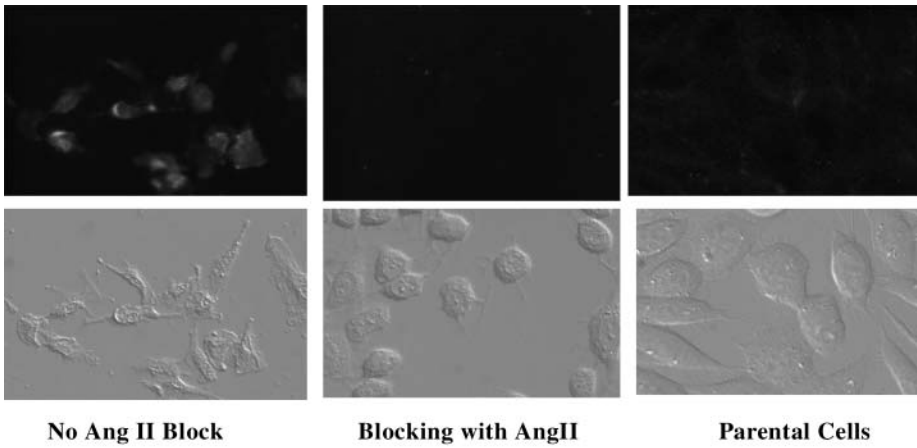

Fig. 1. Imaging CHO cells with Ang II–quantum dot conjugates. The upper panels show the fluorescence images, and the lower panels show the bright-field images. Cells are clearly visible in all of the bright-field images; however, only the cells incubated with Ang II conjugates that express the AT1 receptor are seen to be fluorescent (top left panel). When these cells were preincubated with a 100 μ*M* solution of Ang II, the binding of Ang II-conjugated quantum dots was blocked (top center panel). Finally, when parental cells that did not express the receptor were incubated with the conjugate, no fluorescence was observed (top right panel).

2. Using transmitted light, bring the cells on the cover glass into focus and capture bright-field image using a digital CCD camera.
3. Using 488 nm of incident light, excite the cells labeled by Ang II–quantum dots or Ang II–Alexa 488, and obscure the fluorescence through a 485/20 and 515–530 band-pass filter for Ang II–Alexa 488 and through a 546/12 and 580–630 filter for Ang II–quantum dots.
4. To capture an image, illuminate the Ang II–quantum dot-labeled cells on the cover glass of the dishes with incident light for a minimum of 2 min to induce maximal fluorescence (*see* **Note 5**). Immediately capture images of Ang II–Alexa 488–labeled dishes to avoid bleaching.
5. To ensure that Ang II–quantum dots used to label cells have not aggregated while labeling, examine imaging fields for Ang II–quantum dot clusters. When aggregates or clusters are present, it is assumed that Ang II–quantum dots were not in the solution while labeling and that Ang II–quantum dot labeling was compromised (*see* **Note 6**).

In our initial experiments, we were able to label CHO cells with fluorescent cadmium selenide core-shell nanocrystals that were conjugated to Ang II. We showed that this labeling was specific for cells expressing the AT1 receptor and that there was no labeling of parental cells that did not express the AT1 receptor (**Fig. 1**). Furthermore, the specific binding of Ang II-conjugated

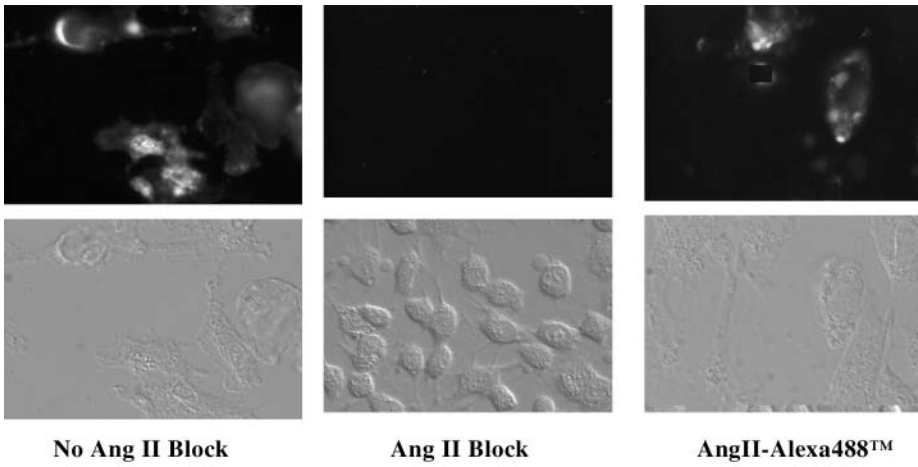

Fig. 2. Imaging CHO cells expressing AT1 receptor using Ang II–quantum dot conjugates and Ang II–Alexa 488. The upper panels show the fluorescent images, and the lower panels show the bright-field images. Cells are clearly visible in all of the bright field images. Cells expressing the AT1 receptor specifically bind Ang II–quantum dot conjugates (top left panel). Similar binding was observed when the cells were incubated with Ang II–Alexa 488 (top right panel). This specific binding of Ang II–quantum dot conjugates was blocked by preincubation of AT1-expressing cells with a 100-μ*M* solution of Ang II (top center panel).

nanocrystals to cells expressing the AT1 receptor was blocked by preincubation of cells with excess Ang II (**Fig. 1**).

The results of our initial experiment demonstrate that the Ang II-conjugated quantum dots bind specifically to the CHO cells expressing the AT1 receptor. We then compared the specificity of the Ang II–conjugated quantum dots with the angiotensin dye conjugate (Ang II–Alexa 488). Cells were incubated with each conjugate and their fluorescence was compared. These images are shown in **Fig. 2**.

4. Notes

1. In spite of the introduction of antibiotics, contamination by microorganisms remains a major problem in tissue culture. Correct aseptic technique should provide a barrier between microorganisms in the environment outside the culture. The procedure used for equipping and practicing aseptic technique in a laboratory has been described in a number of sources ***(22**,**23)***. Inability to follow the steps in aseptic technique will likely result in bacterial contamination that may alter the biochemical behavior and cell-surface protein expression of the cell line. Taking time to obtain advice from personnel of other laboratories experienced in aseptic technique can greatly facilitate success in this area.

2. Although some cell lines can be dislodged from the bottom of the flask by gentle and repeated pipetting of the medium over the cells, trypsinizing the cells has the advantage of producing a single cell suspension. However, overtrypsinizing may reduce viability, and undertrypsinizing can result in cell clumps. Furthermore, cells treated with trypsin may require one or more days after plating before reexpression of surface proteins. If viability is a concern, a commercially available nonenzymatic dissociation buffer solution can be used (e.g., from Sigma-Aldrich). These dissociation solutions lack magnesium.
3. The concentration of a cell suspension may be determined by placing cells in an optically flat chamber, known as a hemacytometer, under a microscope. The cell number within a defined area of the hemacytometer can then be counted and the cell concentration derived from the count. Detailed instructions on how to use a hemacytometer (Improved Neubauer) are described elsewhere ***(24)***. An alternative approach to the hemocytometer is electronic particle counting. This method requires the use of an automated system called a Coulter Counter. In this system, cells in suspension are drawn through a fine orifice. As each cell passes through the orifice, it causes a change in current. This change produces a series of pulses, which are then counted ***(25)***.
4. Depending on the cell type, rapid agitation may cause cells to detach; therefore, we recommend gently rotating dishes manually. Because borate buffer is harsh on cells, we incubate cells for no more than 15 min to avoid dissociation. However, this will vary with the cell type and number of days that they are cultured. Cells tend to dissociate most readily if cultured less than 2 d and/or are overgrown.
5. When imaging quantum dots, it is necessary to illuminate for 2 to 3 min before maximum fluorescent intensity is reached. The rate of quantum dot bleaching is approx 2%/min when illuminated continuously after reaching maximum fluorescence intensity. This is in contrast to conventional fluorophores, which are typically bleached entirely within minutes after beginning to illuminate ***(26)***.
6. When imaging, it is important to recognize when aggregates have formed. Our experience is that aggregates occur unpredictably. Before adding quantum dots for labeling, we advise placing Ang II–quantum dots on a clean cover glass of a dish and imaging at ×40 to determine whether aggregates have already formed. This will confirm whether the Ang II–quantum dots should be used for labeling. If Ang II–quantum dots are not aggregated before adding but aggregate after incubation with cells, then the problem resides with the incubation step.

Acknowledgments

We wish to thank Quantum Dot for supplying the core-shell nanocrystals used in this study. We also thank Dr. Marcel Bruchez of Quantum Dot for helpful advice during the course of this study. This work was supported by grants from the National Institutes of Health.

References

1. Bhargava, R. N. (2000) "Quantum-confined atoms": novel luminescent centers for future II-VI devices. *J. Crystal Growth* **214,** 926–930.
2. Klarreich, E. (2001) Biologists join the dots. *Nature* **413,** 450–452.
3. Michalet, X., Pinaud, F., Lacoste, T. D., Dahan, M., Bruchez, M. P., Alivisatos, A. P., and Weiss, S. (2001) Properties of fluorescent semiconductor nanocrystals and their application to biological labeling. *Single Molecules* **2,** 261–276.
4. Alivisatos, A. P., (1996) Perspectives on the physical chemistry of semiconductor nanocrystals. *J. Phys. Chem. B* **100,** 13,226–13,239.
5. Dabbousi, B. O., Rodriguez-Viejo, R., Mikulec, F. V., Heine, J. R., Mattoussi, H., Ober, R., Jensen, K. F., and Bawendi, M. G., (1997) (CdSe)ZnS core-shell quantum dots: synthesis and characterization of a series of highly luminescent nanocrystallites. *J. Phys. Chem. B* **101,** 9463–9475.
6. Norris, D. J. and Bawendi, M. G. (1996) Measurement and assignment of the size-dependent optical spectrum in CdSe quantum dots. *Phys. Rev. B.* **53,** 16,338–16,346.
7. Schmelz, O., Mews, A., Basché, T., Herrmann, A., and Müllen, K. (2001) Supramolecular complexes from CdSe nanocrystals and organic fluorophors. *Langmuir* **17,** 2861–2865.
8. Gerion, D., Pinaud, F., Williams, S. C., Parak, W. J., Zanchet, D., Weiss, S., and Alivisatos, A. P. (2001) Synthesis and properties of biocompatible water-soluble silica-coated CdSe/ZnS semiconductor quantum dots. *J. Phys. Chem. B* **105,** 8861–8871.
9. Zhang, C., Ma, H., Nie, S., Ding Y., Jin, L., and Chen, D. (2000) Quantum dot–labeled trichosanthin. *Analyst* **125,** 1029–1031.
10. Wu, X., Liu, H., Liu, J., Haley, K. N., Treadway, J. A., Larson, J. P., Ge, N., Peale, F., and Bruchez, M. P. (2003) Immunofluorescent labeling of cancer marker Her2 and other cellular targets with semiconductor quantum dots. *Nat. Biotechnol.* **21,** 41–46.
11. Bruchez, M., Moronne, M., Gin, P., Weiss, S., and Alivisatos, P. A. (1998) Semiconductor nanocrystals as fluorescent biological labels. *Science* **281,** 2013–2018.
12. Goldman, E. R., Anderson, G. P., Tran, P. T., Mattoussi, H., Charles, P. T., and Mauro, J. M. (2002) Conjugation of luminescent quantum dots with antibodies using an engineered adaptor protein to provide new reagents for fluoroimmunoassays. *Anal. Chem.* **74,** 841–847.
13. Chan, W. C. W., Maxwell, D. J., Gao, X., Bailey, R. E., Han, M., and Nie, S. (2002) Luminescent quantum dots for multiplexed biological detection and imaging. *Curr. Opin. Biotechnol.* **13,** 40–46.
14. Goldman, E. R., Balighian, E. D., Mattoussi, H., Kuno, M. K., Mauro, M. J., Tran, P. T., and Anderson, G. P. (2002) Avidin: a natural bridge for quantum dot–antibody conjugates. *J. Am. Chem. Soc.* **124,** 6378–6382.
15. Jyoti, K. J., Mattoussi, H., Mauro, J. M., and Simon, S. M. (2002) Long-term multiple color imaging of live cells using quantum dot bioconjugates. *Nat. Biotechnol.* **21,** 1–5.

16. Dubertret, B., Skourides, P., Norris, D. J., Noireaux, V., Brivanlou, A. H., and Libchaber, A. (2002) In vivo imaging of quantum dots encapsulated in phospholipid micelles. *Science* **298,** 1759–1762.
17. Åkerman, M. E., Chan, C., W. C., Laakkonen, P., Bhatia, S. N., and Ruoslahti, E. (2002) Nanocrystal targeting in vivo. *Proc. Natl. Acad. Sci. USA* **99,** 12,617–12,621.
18. Watson, A., Wu, X., and Bruchez, M. (2003) Lighting up cells with quantum dots. *Bioimaging* **34,** 296–303.
19. Rosenthal, S. J., Tomlinson, I. D., Adkins, E. M., Schroeter, S., Adams, S., Swafford, L., McBride, J., Wang, Y., DeFelice, L. J., and Blakely, R. D. (2002) Targeting cell surface receptors with ligand-conjugated nanocrystals. *J. Am. Chem. Soc.* **124,** 4586–4594.
20. Tomlinson, I. D., Kippeny, T., Swafford, L., Siddiqui, N. H., and Rosenthal, S. J. (2002) Novel polyethylene glycol derivatives of melatonin and serotonin: ligands for conjugation to fluorescent cadmium selenide/zinc sulfide core shells and nanocrystals. *J. Chem. Res. (M)* **203,** 525–528.
21. Tomlinson, I. D., Grey, J. L., and Rosenthal, S. J. (2002) A synthesis of 6-(2,5-dimethoxy-4-(2-aminopropyl)phenyl)-hexylthiol: a ligand for conjugation with fluorescent cadmium selenide/zinc sulfide core/shell nanocrystals and biological imaging. *Molecules* **7,** 777–790.
22. Freshney, R. I. (1991) *Culture of Animal Cells: A Manual of Basic Technique*, 2nd ed., Wiley-Liss, New York.
23. Kruse, P. and Patterson, M. K. (1973) *Tissue Culture Techniques and Applications*, Academic, New York.
24. BD Biosciences. (2002) *Hemocytometer Reference Guide*, BD Biosciences, Palo Alto, CA.
25. Jacoby, W. B. and Pastan, I. H. (1979) Cell culture, in *Methods in Enzymology*, vol LVIII (Colowick, S. P. and Kaplan, N. D., eds.), Academic, New York, pp. 1–65.
26. Mason, J. N., Farmer, H., Tomlinson, I. D., Schwartz, J. W., Savchenko, V., DeFelice, L. J., Rosenthal, S. J., and Blakely, R. D. (2005) Novel fluorescence-based approaches for the study of biogenic amine transporter localization, activity, and regulation. *J. Neurosci. Methods*, in press.

5

Quantum Dot-Encoded Beads

Xiaohu Gao and Shuming Nie

Summary

Multicolor optical coding for biological assays has been achieved by embedding semiconductor quantum dots into mesoporous and macroporous beads at precisely controlled ratios. Owing to their novel optical properties such as size-tunable emission and simultaneous excitation, quantum dots are ideal fluorophores for wavelength-and-intensity multiplexing. Kinetics study reveals that quantum dot doping of porous silica and polystyrene beads can be completed from seconds to minutes. The use of 10 intensity levels and six colors could theoretically code 1 million nucleic acid or protein sequences. Imaging and spectroscopic measurements indicate that the quantum dot-tagged beads are highly uniform and reproducible, yielding bead identification accuracies as high as 99.99% under favorable conditions. DNA hybridization studies demonstrate that the coding and target signals can be simultaneously read at the single-bead level. This spectral coding technology is expected to open new opportunities in gene expression studies, high-throughput screening, and medical diagnostics.

Key Words

Quantum dots; nanoparticles; encoding; multiplexing; spectroscopy; gene expression; decoding.

1. Introduction

Recent advances in bioanalytical sciences and bioengineering have led to the development of DNA chips ***(1,2)***, miniaturized biosensors ***(3,4)***, and microfluidic devices (e.g., microelectromechanical systems or bioMEMS) ***(5–7)***. These enabling technologies have substantially impacted many areas in biomedical research, such as gene expression profiling, drug discovery, and clinical diagnostics. As current research in genomics and proteomics produces more sequence data, there is a strong need for new and improved technologies that can rapidly screen a large number of nucleic acids and proteins. Here we report detailed protocols for preparing quantum dot-encoded beads in the size range of 100 nm to 100 μm in diameter.

From: *Methods in Molecular Biology, vol. 303: NanoBiotechnology Protocols*
Edited by: S. J. Rosenthal and D. W. Wright © Humana Press Inc., Totowa, NJ

Key steps in preparing quantum dot-encoded beads include the synthesis of highly monodisperse beads with suitable pore structures and the formulation of solvent conditions that strongly favor the partitioning of quantum dots from the solution into the pores. In this chapter, we discuss these two aspects and provide detailed procedures for three types of encoded beads: (1) polymeric nanobeads, (2) mesoporous polystyrene microbeads, and (3) mesoporous silica microbeads.

2. Materials

1. Technical grade (90%) trioctylphosphine oxide (TOPO).
2. Trioctylphosphine (99% pure).
3. Cadmium oxide (CdO) (99.7%).
4. Selenium (more than 99%).
5. Stearic acid (98%).
6. Hexamethyldisilathiane ($[TMS]_2S$).
7. Dimethlycadmium; store and use in inert air.
8. Dimethylzinc ($ZnMe_2$) (10% wt in hexane); store and use in inert air.
9. Hexadecylamine (HDA) (98%).
10. Styrene (99%); store at –80°C after removing inhibitor.
11. Divinylbenzene (80%); store at –80°C after removing inhibitor.
12. Acrylic acid (99%); store at –80°C after removing inhibitor.
13. Inhibitor remover disposable column, polyvinylpyrrolidone (PVP).
14. 2,2′-Azobisisobutyronitrile (AIBN) (98%).
15. PVP (mol wt = 40,000).
16. Polystyrene beads.
17. Silica beads (obtained from high-performance liquid chromatography column).
18. Dibutyl phthalate (DBP).
19. Sodium dodecyl sulfate (SDS) (98%).
20. Sodium nitrite (99.5%).
21. Benzoyl peroxide (70%).
22. Poly (vinyl alcohol) (mol wt = 85,000–124,000).
23. (3-Mercaptopropyl)trimethoxysilane (more than 97%).
24. Tetraethoxysilane (more than 99%).
25. Specialized equipments (*see* text).

3. Methods

Multicolor quantum dots are incorporated into *porous* polymer beads mainly via hydrophobic interactions. In this section, we describe the methods of making and reading quantum dot-tagged microbeads: preparation of quantum dots, synthesis of microbeads, bead encoding and surface functionalization, bead characterization.

3.1. Preparation of Multicolor Quantum Dots

High-quality hydrophobic quantum dots are prepared according to literature procedures with modifications ***(8–12)***.

1. Dissolve 1 mmol of CdO precursor in 1 g of stearic acid with heating until a clear solution is formed.
2. Add a TOPO and HDA mixture (10 g) as reaction solvents, and then heat to 250°C under argon for 10 min.
3. Briefly raise the temperature to 360°C, and quickly inject an equal molar selenium solution into the hot solvents. The mixture will immediately change color to orange-red, indicating the formation of quantum dots.
4. Reflux the dots for 10 min.
5. Slowly add a capping solution of 20 m*M* $ZnMe_2$ and $(TMS)_2S$ to protect the CdSe core. These ZnS-capped CdSe dots have excellent chemical and photo stability.
6. Cool the dots to room temperature, and rinse repeatedly with methanol to remove free ligands.
7. For characterization, use ultraviolet (UV) adsorption, fluorescence emission spectra, and transmission electron microscopy.

The emission spectra of quantum dots can be continuously tuned by changing particle size and component materials during synthesis (*see* **Note 1**). Spanning the visible spectrum, simultaneous excitation of 10 emission colors can be achieved with a single near-UV (350-nm) lamp ***(13)***. For microbead encoding, the dots are stored in a mixture solvent containing 5% chloroform and 95% butanol.

3.2. Synthesis of Porous Microbeads

Depending on the bead size, quantum dot-encoded beads can be used for multiplexed bioassays and multiplexed biolabeling. In the first application, optically encoded microcarriers in the size range of 3–30 μm are linked to DNA probes or antibodies for recognition and detection of target molecules in a homogeneous solution ***(14–19)***. In the second application, small beads in the size range of 100–500 nm are used for spectrally encoded tagging of cells and tissue specimens ***(20–26)***. Some of the mesoporous beads suitable for these applications are available from chromatographic or latex reagent companies such as Phenomenex (Torrance, CA) or Bangs Lab (Fisher, IN). To describe the procedures of preparing microbeads with tunable size and porosity, we outline them in the following three subsections.

3.2.1. Polystyrene-Based Nanobeads

Polystyrene nanobeads are synthesized by using emulsion polymerization ***(13)***.

1. Purify styrene, divinylbenzene, and acrylic acid with an inhibitor-remover column, and store at –80°C in small aliquots.
2. Add the three monomers into an ethanol/water mixture (8:1 [v/v]) in a ratio of 98:1:1, together with PVP as a stabilizer. Briefly sonicate the whole system and purge with N_2 for 2 min.

3. Initiate polymerization by adding AIBN (1.5 mg/mL) and heating to 70°C.
4. Shake or stir the reaction for 10 h.
5. Rinse the resulting polymer beads with ethanol for three rounds and ethanol/chloroform (9:1) for another three rounds.
6. Store the isolated beads in butanol for encoding experiments.

3.2.2. Polystyrene-Based Mesoporous Microbeads

Porous polystyrene microbeads are prepared according to literature procedures ***(27,28)***. Monodispersed nonporous polystyrene beads with a diameter of 1 μm are used as a shape template.

1. Swell the beads (60 mg) with 0.2 mL of DBP in 0.25% SDS solution for 10 h, and with a styrene emulsion (porogen) and benzoyl peroxide for another 10 h.
2. Add sodium nitrite (0.3 mg/mL) and poly (vinyl alcohol) at a final concentration of 1% to the swelled beads before purging the emulsion mixture with nitrogen. Conduct the polymerization at 70°C for 24 h.
3. Add an emulsified mixture of 5 mL of styrene, divinylbenzene, DBP, and benzoyl peroxide in 0.25% SDS solution to the reaction and mix for 10 h under stirring. Again, purge the emulsion with nitrogen and polymerize at 70°C.
4. Rinse the resulting beads with water and methanol before extracting with toluene using a Soxhlet extractor.

3.2.3. Silica-Based Mesoporous Microbeads

Mesoporous silica beads are synthesized by using pore-generating templates such as self-assembled surfactants or polymers (called porogens) ***(29)***. After synthesis, removal of the templates generates mesosized pores, which are either ordered or random depending on the template structures. In general, the porous silica beads can be prepared with a broad size range (nanometers to micrometers). Alternatively, mesoporous silica beads (5 μm diameter) with pore sizes of 10 or 32 nm are available from Phenomenex. The pore surfaces are coated with a monolayer of Si-$C_{18}H_{37}$ (octadecyl, an 18-carbon linear-chain hydrocarbon). The beads are repeatedly rinsed with ethanol and butanol before use.

3.3. Bead Tagging and Surface Functionalization

Single-color doping is accomplished by mixing porous beads with a controlled amount of quantum dots in an organic solvent mixture (butanol and chloroform). Quantum dot concentration is measured based on its fluorescence absorption profile ***(8)***. In parallel, the number of microbeads is counted using a hemacytometer. Owing to the completeness and evenness of quantum dot incorporation into porous beads, the number of quantum dots per bead can be calculated and can be used to generate working curves (**Fig. 1**). Based on these curves, intensity-coded beads can be prepared by adding predetermined

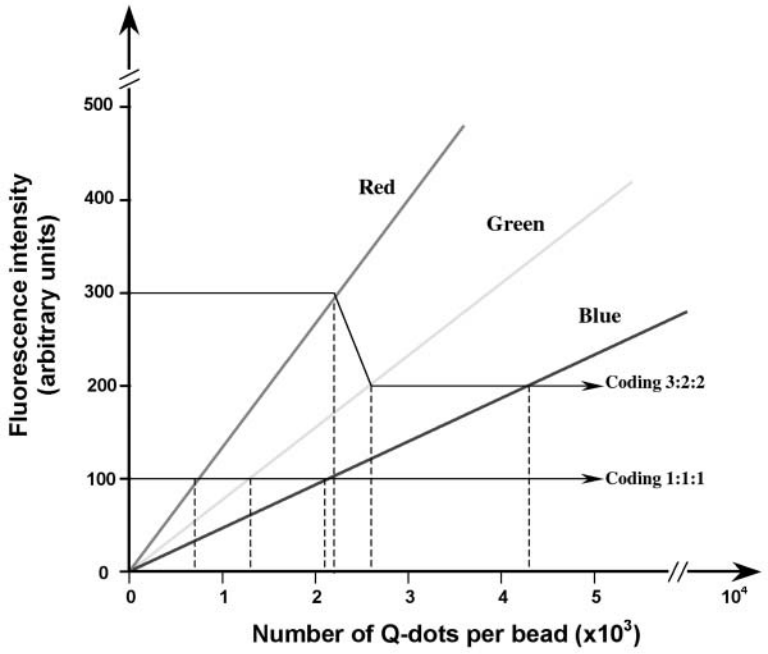

Fig. 1. Schematic drawing of working curves for preparation of multicolor quantum dot microbeads. Arrows depict two representative beads coded with intensity ratios of 1:1:1 and 3:2:2, and the number of quantum dots (or concentration) can be obtained from the *x* axis. Each single bead may contain quantum dots (Q-dots) ranging from several hundred to millions, depending on the bead size and surface area.

amounts of quantum dots in a stock solution. For beads with a pore size more than 30 nm, the doping process is complete in less than 10 min (essentially no free dots left in the supernatant). For beads with smaller pores, more extended times are used to allow quantum dot incorporation (*see* **Note 2**). For multicolor doping, different-colored quantum dots are premixed in precisely controlled ratios, determined by a fluorometer. Porous beads are then added to an aliquot of this premix solution in a similar manner to the monochromatic beads. Doped beads are isolated by centrifugation and are washed three times with ethanol.

For different applications, the encoded beads can be either used directly or sealed before conjugation to biomolecules. In one example, 3-mercaptopropyltrimethoxysilane is adsorbed onto the embedded quantum dots in ethanol, and the free compound is removed by centrifugation. The beads are then resuspended in ethanol with the addition of tetraethoxysilane (sealant). The silane compounds are polymerized inside the beads on addition of water and,

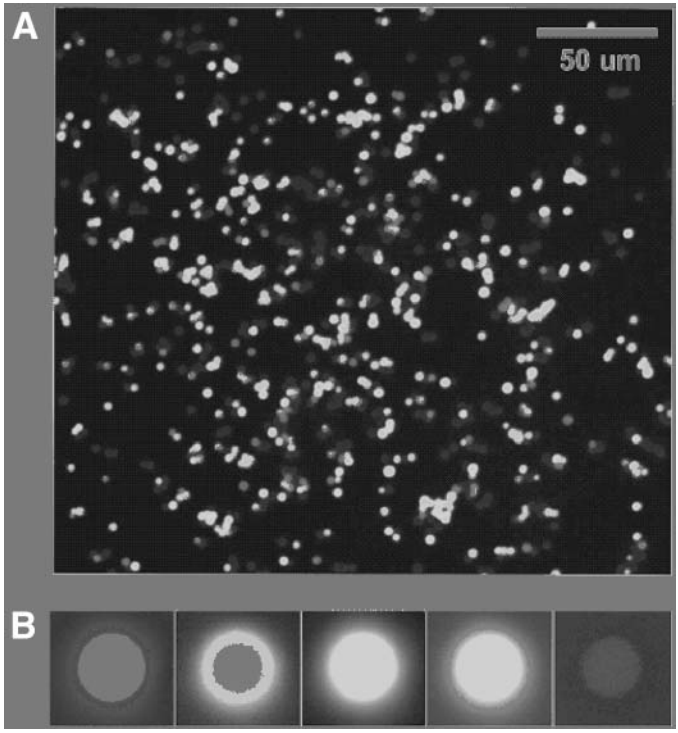

Fig. 2. Fluorescence images of mesoporous silica beads (5-μm diameter, 32-nm pore size) doped with single-color quantum dots emitting light at 488 nm, 520 nm, 550 nm, 580 nm, or 610 nm. **(A)** Wide-field view of large population of doped beads, prepared in batches and then mixed; **(B)** enlarged views of single monochromatic beads. Each bead contains up to 2 million dots of the same color.

therefore, seal the pores. A variety of sealing procedures can be used for different types of beads and applications (*see* **Note 3**).

The sealed beads can then be linked to biomolecules by covalent binding or adsorption and used for bioassays, sharing the same detection principles as the organic dye-labeled microspheres. Owing to this similarity, detailed procedures can be found in the references ***(14–26,30)*** and are thus not discussed here.

3.4. Optical Imaging and Spectroscopy

True-color fluorescence imaging is achieved with an inverted Olympus microscope (IX-70) equipped with a digital color camera (Nikon D1), a broadband UV (330- to 385-nm) light source (100-W mercury lamp), and a long-pass interference filter (DM 400; Chroma Tech, Brattleboro, VT). **Figure 2**

shows true-color fluorescence images of quantum dot–doped silica beads (5.0 ± 0.3 μm in diameter) with an average pore size of 32 ± 4 nm. These "monochromatic" beads (coded with single-color quantum dots) are mixed and spread on a glass surface for fluorescence imaging. Although only a single light source (a near-UV lamp) is used for excitation, all the doped beads are observed and are clearly distinguishable. Note that simultaneous excitation of multiple emission colors is a unique property of quantum dots and is not possible with organic dyes or lanthanide compounds. The quantum dot-doped beads are remarkably bright and can be recorded by using a digital color camera and a mercury lamp.

Wavelength-resolved spectra are obtained by using the inverted microscope coupled with a single-stage spectrometer (SpectraPro 150; Roper, Trenton, NJ). A schematic diagram of the instrument is shown in **Fig. 3**. Multicolor quantum dots are excited with a broadband excitation in the UV or blue region, and the Stoke-shifted fluorescence is passed through a long-pass filter. A pinhole is placed at the objective image plane between the spectrograph and microscope to reject the out-of-focus lights. The beads are manually positioned, and spectra are recorded with a thermoelectrically cooled charge-coupled device (CCD). The quantitative results have shown that the intensity ratios of multicolor quantum dots are remarkably uniform, leading to the development of advanced devices and algorithms to read the doped beads at high accuracies and speeds (*see* **Note 4**).

4. Notes

1. The preparation of multicolor quantum dots, especially CdSe/ZnS quantum dots, has been reported by many groups. The emission wavelengths can be tuned by several factors, such as chemical composition and particle size. For example, the use of semiconductor materials with higher band gap or preparation of dots with bigger particle size results in longer emission wavelength, and vice versa. Detailed procedures are discussed in **refs. *8–12***.
2. The key to making quantum dot-encoded microspheres is the preparation of porous microstructures, because quantum dots are much bigger than traditional organic fluorophores. It has been shown that completion of quantum dot doping can be as fast as minutes if microbeads with a pore size bigger than 30 nm are used, whereas the same process could take hours for beads with 10-nm pores ***(31)***. Beads with small pores need to be swelled before quantum dot doping. A typical solvent for this purpose is chloroform, which not only enlarges the polystyrene microbeads, but also increases the solubility of quantum dots. For hydrocarbon-capped silica beads, the addition of chloroform also improves the doping kinetics, by increasing the flexibility of hydrocarbons on the bead wall and quantum dot surface ***(13,31)***.
3. A variety of pore-sealing or surface-coating methods could be used for different applications. To seal the pores completely, polymerization can be conducted

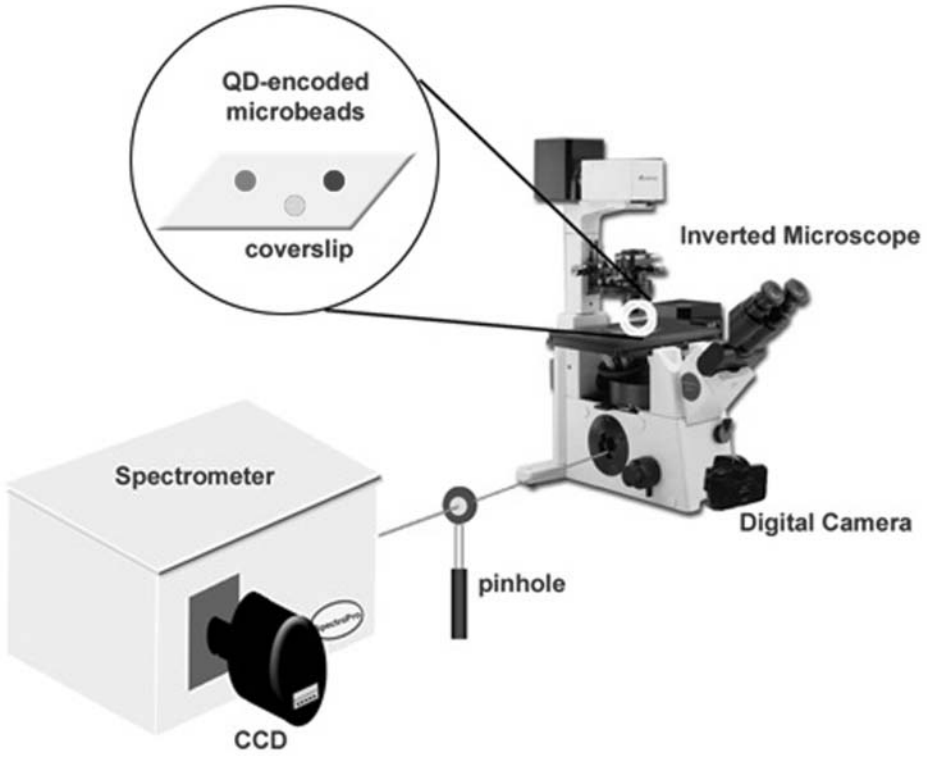

Fig. 3. Schematic diagram of integrated fluorescence imaging and spectroscopy system. The coding signals are read out by a CCD camera and a single-stage spectrometer attached to the side port of an inverted microscope.

within the pores using silanes, styrene and derivatives, and so forth. This approach completely isolates the embedded dots with the environment and protects them. However, the area for biomolecule conjugation is limited to the beads' outer surface. Another approach that can be used to protect the dots is to overcoat the pores and the embedded dots with a layer of polymers, so that bioconjugation can occur on both the interior and the outside walls of the beads.

4. The coding uniformity is mainly determined by the intrinsic variation in bead size. It has been reported previously that ratiometric measurements are considerably more reliable than absolute intensities because the ratio values are often not affected by simultaneous drifts or fluctuations in the individual signals ***(32)***. Therefore, the use of ratios for bead decoding could help in the development of advanced devices and algorithms that can read the doped beads at high accuracies and speeds.

Acknowledgments

We are grateful to Dr. Mingyong Han (Department of Materials Science, National University of Singapore) for help with the microbead synthesis and for fruitful discussions. This work was supported in part by the National Institutes of Health, the Department of Energy, and the Coulter Translational Research Program at Georgia Tech and Emory University.

References

1. Fodor, S. P. A., Read, J. L., Pirrung, M. C., Stryer, L., Lu, A. T., and Solas, D. (1991) Light-directed, spatially addressable parallel chemical synthesis. *Science* **251,** 767–773.
2. Schena, M., Shalon, D., Davis, R. W., and Brown, P. O. (1995) Quantitative monitoring of gene-expression patterns with a complementary-DNA microarray. *Science* **270,** 467–470.
3. Dickinson, T. A., Michael, K. L., Kauer, J. S., and Walt, D. R. (1999) Convergent, self-encoded bead sensor arrays in the design of an artificial nose. *Anal. Chem.* **71,** 2192–2198.
4. Clark, H. A., Hoyer, M., Philbert, M. A., and Kopelman, R. (1999) Optical nanosensors for chemical analysis inside single living cells: fabrication, characterization, and methods for intracellular delivery of PEBBLE sensors. *Anal. Chem.* **71,** 4831–4836.
5. Harrison, D. J., Fluri, K., Seiler, K., Fan, Z., Effenhauser, C. S., and Manz, A. (1993) Micromachining a miniaturized capillary electrophoresis-based chemical analysis system on a chip. *Science* **261,** 895–897.
6. Ramsey, J. M., Jacobson, S. C., and Knapp, M. R. (1995) Microfabricated chemical measurement systems. *Nat. Med.* **1,** 1093–1096.
7. Woolley, A. T. and Mathies, R. A. (1994) Ultra-high-speed DNA fragment separations using microfabricated capillary array electrophoresis chips. *Proc. Natl. Acad. Sci. USA* **91,** 11,348–11,352.
8. Murray, C. B., Norris, D. J., and Bawendi, M. G. (1993) Synthesis and characterization of nearly monodisperse CdE (E = S, Se, Te) semiconductor nanocrystallites. *J. Am. Chem. Soc.* **115,** 8706–8715.
9. Hines, M. A. and Guyot-Sionnest, P. (1996) Synthesis of strongly luminescing ZnS-capped CdSe nanocrystals. *J. Phys. Chem. B* **100,** 468–471.
10. Peng, X. G., Schlamp, M. C., Kadavanich, A. V., and Alivisatos, A. P. (1997) Epitaxial growth of highly luminescent CdSe/CdS core/shell nanocrystals with photostability and electronic accessibility. *J. Am. Chem. Soc.* **119,** 7019–7029.
11. Peng, Z. A. and Peng, X. G. (2001) Formation of high-quality CdTe, CdSe, and CdS nanocrystals using CdO as precursor. *J. Am. Chem. Soc.* **123,** 183, 184.
12. Qu, L., Peng, Z. A., and Peng, X. (2001) Alternative routes toward high quality CdSe nanocrystals. *Nano Lett.* **1,** 333–337.

13. Han, M. Y., Gao, X. H, Su, J. Z., and Nie, S. M. (2001) Quantum-dot-tagged microbeads for multiplexed optical coding of biomolecules. *Nat. Biotechnol.* **19,** 631–635.
14. Chen, J., Iannone, M. A., Li, M. S., Taylor, J. D., Rivers, P., Nelsen, A. J., Slentz-Kesler, K. A., Roses, A., and Weiner, M. P. (2000) A microsphere-based assay for multiplexed single nucleotide polymorphism analysis using single base chain extension. *Genome Res.* **10,** 549–557.
15. Fulton, R. J., McDade, R. L., Smith, P. L., Kienker, L. J., and Kettman, J. R. Jr. (1997) Advanced multiplexed analysis with the FlowMetrix™ system. *Clin. Chem.* **43,** 1749–1756.
16. Steemers, F. J., Ferguson, J. A., and Walt, D. R. (2000) Screening unlabeled DNA targets with randomly ordered fiber-optic gene arrays. *Nat. Biotechnol.* **18,** 91–94.
17. Ferguson, J. A., Boles, T. C., Adams, C. P., and Walt, D. R. (1996) A fiber-optic DNA biosensor microarray for the analysis of gene expression. *Nat. Biotechnol.* **14,** 1681–1684.
18. Ferguson, J. A., Steemers, F. J., and Walt, D. R. (2000) High-density fiber-optic DNA random microsphere arrays. *Anal. Chem.* **72,** 5618–5624.
19. Van Oosterhout, M. F., Prinzen, F. W., Sakurada, S., Glenny, R. W., and Hales, J. R., (1998) Fluorescent microspheres are superior to radioactive microspheres in chronic blood flow measurements. *Am. J. Physiol.* **275,** H110–H115.
20. Bhalgat, M. K., Haugland, R. P., Pollack, J. S., Swan, S., and Haugland, R. P. (1998) Green- and red-fluorescent nanospheres for the detection of cell surface receptors by flow cytometry. *J. Immunol. Methods* **219,** 57–68.
21. Hall, M., Kazakova, I., and Yao, Y. M. (1999) High sensitivity immunoassays using particulate fluorescent labels. *Anal. Biochem.* **272,** 165–170.
22. Zijlmans, H. J. M. A. A., Bonnet, J., Burton, J., Kardos, K., Vail, T., Niedbala, R. S., and Tanke, H. J. (1999) Detection of cell and tissue surface antigens using up-converting phosphors: a new reporter technology. *Anal. Biochem.* **267,** 30–36.
23. Kurner, J. M., Klimant, I., Krause, C., Preu, H., Kunz, W., and Wolfbeis, O. S. (2001) Inert phosphorescent nanospheres as markers for optical assays. *Bioconj. Chem.* **12,** 883–889.
24. Sondi, I., Siiman, O., Koester, S., and Matijevic, E. (2000) Preparation of aminodextran-CdS nanoparticle complexes and biologically active antibody-aminodextran-CdS nanoparticle conjugates. *Langmuir* **16,** 3107–3118.
25. Chen, Y. F., Tianhao, J., and Rosenzweig, Z. (2003) Synthesis of glyconanospheres containing luminescent CdSe-ZnS quantum dots. *Nano Lett.* **3,** 581–584.
26. Schultz, S., Smith, D. R., Mock, J. J., and Schultz, D. A. (2000) Single target molecule detection with non-bleaching multicolor optical immunolabels. *Proc. Natl. Acad. Sci. USA* **97,** 996–1001.
27. Wang, Q. C., Svec, F., and Frechet, J. M. J. (1994) Fine control of the porous structure and chromatographic properties of monodisperse macroporous poly (styrene-codivinylbenzene) beads prepared using polymer porogens. *J. Polym. Sci. Pol. Chem.* **32,13,** 2577–2588.

28. Cheng, C. M., Micale, F. J., Vanderhoff, J. W., and El-Aasser, M. S. (1992) Synthesis and characterization of monodisperse porous polymer particles. *J. Polym. Sci. Pol. Chem.* **30,** 235–244.
29. Iler, R. K. and Kirkland, J. J. (1978) Process for manufacture of macroporous microspheroids. US patent no. 4,105,426.
30. Hermanson, G. T. (1996) *Bioconjugate Techniques*, Academic, New York.
31. Gao, X. H. and Nie, S. M. (2003) Doping mesoporous materials with multicolor quantum dots. *J. Phys. Chem. B*, **107,** 11,575–11,578.
32. Deniz, A. A., Laurence, T. A., Dahan, M., Chemla, D. S., Schultz, P. G., and Weiss, S. (2001) Ratiometric single-molecule studies of freely diffusing biomolecules. *Annu. Rev. Phys. Chem.* **52,** 233–253.

6

Use of Nanobarcodes® Particles in Bioassays

R. Griffith Freeman, Paul A. Raju, Scott M. Norton, Ian D. Walton, Patrick C. Smith, Lin He, Michael J. Natan, Michael Y. Sha, and Sharron G. Penn

Summary

We have developed striped metal nanoparticles, Nanobarcodes® particles, which can act as encoded substrates in multiplexed assays. These particles are metallic, encodeable, machine-readable, durable, submicron-sized tags. The power of this technology is that the particles are intrinsically encoded by virtue of the difference in reflectivity of adjacent metal stripes. This chapter describes protocols for the attachment of biological molecules, and the subsequent use of the Nanobarcodes particles in bioassays.

Key Words

Multiplex; substrate; nanoparticles; hybridization; immunoassay; fluorescence microscopy.

1. Introduction

1.1. Needs of the Bioassay Community

The need to measure simultaneously many different molecular species in microliters of sample ***(1)*** has propelled bioassays toward multiplexation, miniaturization, and ultrasensitivity. Multiplexing affords the ability to make two or more measurements simultaneously. This has a number of advantages. It reduces the time and cost to collect the measurement. It can also often reduce the amount of sample needed to acquire the measurement. More important, it allows data to be reliably compared across multiple experiments. Additionally, multiplexing can add confidence to measurements through the incorporation of multiple internal controls. Techniques for multiplexing bioassays can be divided into two broad categories: the use of multiple quantitation tags such as

From: *Methods in Molecular Biology, vol. 303: NanoBiotechnology Protocols*
Edited by: S. J. Rosenthal and D. W. Wright © Humana Press Inc., Totowa, NJ

organic fluorophores, and the use of substrates to achieve spatial multiplexing. Our discussion here concentrates on the latter approach.

A widely used approach to spatial multiplexing is the use of a planar microarray in which the identity of the target analyte is encoded by its location, with a secondary reporter providing the quantitative data (such as an organic fluorescent dye). Many technologies make use of this approach, including oligonucleotide and cDNA microarrays ***(2)*** and protein arrays ***(3)***. An alternative to planar microarrays, which we advocate, is to use solution arrays, in which encoded nanoparticles are used to provide multiplexed data. Compared to microarray-based methods, these "suspension arrays" offer, in principle, greater flexibility (via the ability to incorporate easily a new assay via addition of a new type of bead), more rapid assay times (radial vs planar diffusion), and greater reproducibility (tens to hundreds of thousands of replicates for each assay), and they can potentially use less sample and reagent. Analyte quantitation is achieved by the use of a quantitation tag (typically an organic fluorophore).

1.2. Nanobarcodes® Particles as Encoded Nanoparticles

At Nanoplex Technologies, we have developed striped metal nanoparticles (Nanobarcodes particles) (NBCs) as encoded substrates for multiplexed assays and have previously described their use in multiplexed assays ***(4–7)***. NBCs are encodeable, machine-readable, durable, submicron-sized tags. The power of this technology is that the particles are intrinsically encoded by virtue of the difference in reflectivity of adjacent metal stripes, as shown in **Fig. 1**. The large number of striping patterns available and the development of automated software for particle identification should facilitate development of very highly multiplexed assays (i.e., hundreds to thousands). The NBCs are manufactured in a semiautomated, highly scalable process by electroplating inert metals—such as gold (Au), nickel (Ni), platinum (Pt), or silver (Ag)—into templates that define the particle diameter, and then releasing the resulting striped nanorods from the templates ***(8)***. Just as a conventional barcode is read by measuring the differential contrast between adjacent black and white lines using an optical scanner, individual NBCs are read by measuring the differential reflectivity between adjacent metal stripes within a single particle using a conventional optical microscope. The advantage of this method of encoding is its massively multiplexed capabilities (e.g., nine stripes of three metals = approx 10,000 combinations). We foresee many applications for NBCs as substrates. One potential application for this technology is the detection of unique DNA sequences for diagnostic applications, including the detection of single-nucleotide polymorphisms (SNPs).

As is the case for other bioassay substrates, such as beads and microarray slides, the active surface of the NBCs must be modified such that the particles

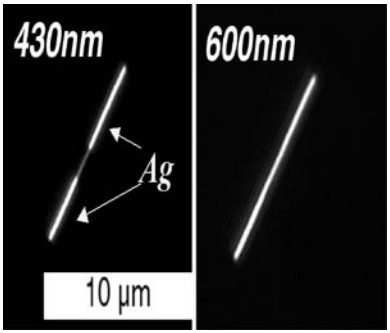

Fig. 1. Differences in reflectivity at 430 vs 600 nm for NBC sequence Ag-Au-Ag.

will bind to target biological molecules. We present here protocols for the attachment of oligonucleotides to the surface of the NBC via amine linkage, the subsequent hybridization of attached oligonucleotides, the derivatization with a universal attachment chemistry, and the subsequent quality control. In addition, we discuss methods of enumeration of particles, detection, and analysis.

2. Materials

1. Benchtop sonicator.
2. Microcentrifuge (set to 5000 rpm).
3. Analytical balance.
4. Pipetmen (P10, P100, and P1000).
5. Hemacytometer and cover slip.
6. Upright optical microscope (with ×20 objective).
7. Rotator.
8. Microcentrifuge tubes (1.5 mL).
9. NBCs in H_2O (Nanoplex Technologies, Menlo Park, CA).
10. 1-Ethyl-3-(3-dimethylaminopropyl) carbodiimide (EDC) (Pierce Biotechnology, Rockford, IL).
11. *N*-Hydroxyl sulfosuccinimide (NHS) (Pierce).
12. NeutrAvidin™ (Molecular Probes, Eugene, OR).
13. Phosphate-buffered saline (PBS), pH 7.4 (Sigma, St. Louis, MO).
14. 2(*N*-Morpholino)ethane sulfonic acid (MES), pH 5.0 (Sigma).
15. Sodium dodecyl sulfate (SDS) (Sigma).
16. 70% Ethanol (Sigma).
17. 20X saline sodium citrate (SSC) (Promega, Madison, WI).
18. PEG-8000 (Promega).
19. Formamide (Sigma).
20. Bovine serum albumin (BSA) (Sigma).
21. Molecular biology-grade distilled water (Promega).

22. EDC/NHS coupling solution: 100 n*M* EDC/40 m*M* NHS in MES buffer (pH 5.0).
23. Hybridization buffer: 6X SSC, 5% PEG-800, 40% formamide.

3. Methods

NBCs, as obtained from Nanoplex Technologies, have a self-assembled monolayer surface coating, resulting in a functionalized surface of carboxyl groups. This allows the use of carbodiimide chemistry to attach primary amine groups of the biomolecule to the carboxyl groups on the NBCs. Carbodiimides couple carboxyl groups to primary amines, resulting in the formation of amide bonds. NHS is included in the reaction in order to stabilize the *O*-acylisourea intermediate product ***(9)***.

Note that in all protocols, particles with different striping patterns are derivatized separately until the final multiplexed assay step. NBCs are supplied in ethanol, and prior to any experiment they must be exchanged into water.

3.1. Attachment of Amine-Derivatized Oligonucleotides to NBCs

Oligonucleotides can be directly attached to the surface carboxyl groups if they are modified with amine groups on the 3′ or 5′ end.

1. Centrifuge 100 µL of NBCs (5×10^6/µL) for 1 min.
2. Incubate the NBCs with 500 µL of EDC/NHS solution for 30 min in 1.5-mL Eppendorf tubes. Use a rotator to mix the reaction continuously during incubation. Alternatively, the particles can be occasionally sonicated to ensure even activation of the particle surface. It is critical that this reaction only proceed for 30 min (*see* **Note 1**).
3. Wash the NBCs with 10 m*M* PBS twice, and resuspend in 100 µL of 10 m*M* PBS.
4. Incubate the activated NBCs with 980 µL of 10 m*M* PBS and 20 µL of 10 µ*M* amine-modified oligonucleotide for 30 min at room temperature on a rotator.
5. Wash the NBCs with 10 m*M* PBS twice. Resuspend the NBCs in 100 µL of 10 m*M* PBS. NBCs derivatized with oligonucleotides can be stored for future use for approx 2 wk at 4°C.

3.2. Hybridization of Oligonucleotides Conjugated to NBCs

Following attachment of oligonucleotides to NBCs, assays often involve a hybridization step. Such an assay can be used to detect SNPs or mutations, or to measure gene expression. The following is a generic protocol for hybridization of oligonucleotides attached to NBCs.

1. To 90 µL of hybridization buffer, add 5 µL of oligonucleotide conjugated to NBCs (between 2.5 and 5×10^7 NBCs) and 5 µL of target DNA (1–10 pmol). Mix well.
2. Incubate at 42°C for 2 h while tumbling on a rotator.

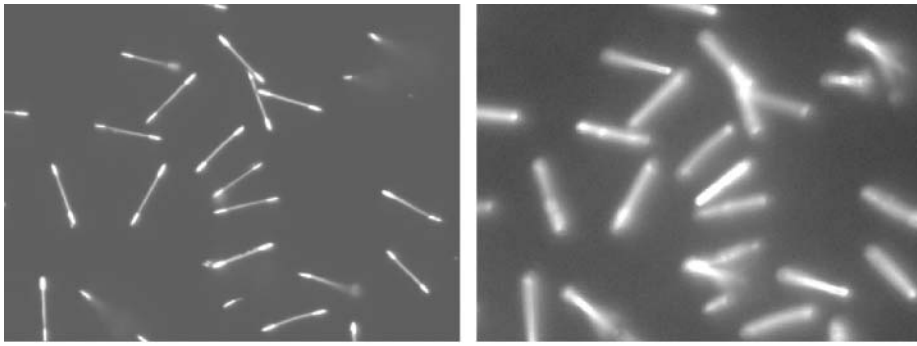

Fig. 2. Signal detection of oligonucleotide-derivatized NBCs hybridized with complementary Cy5 oligonucleotide.

3. Wash the particles with 500 µL of 1X SSC for 5 min at room temperature. Wash the particles with 500 µL of 0.1 X SSC for 5 min at room temperature. Resuspend the particles in 50 µL of 10 m*M* PBS.
4. Image with a fluorescence microscope. (For more details on imaging, *see* **Subheading 3.6.**).

Figure 2 shows a pair of optical microscope images from the protocols in **Subheadings 3.1.** and **3.2.** The left-hand image is a typical reflectance image (405 nm) for a set of particles with the striping pattern 100001. The right-hand image shows the fluorescence from the same particle (620-nm excitation, 690-nm emission) after hybridization with fluorescently labeled oligonucleotide.

3.3. NeutrAvidin Surface Coating of NBCs

A more generic derivation chemistry is to attach a modified avidin to the NBCs, allowing the attachment of any biotin-terminated species, including oligonucleotides for DNA-based assays and biotinylated antibodies for immunoassays. We choose to work with NeutrAvidin because it binds optimally to biotin at neutral pH, making it easier to work with than streptavidin, in which binding is outside physiological pH ranges. Attachment of the NeutrAvidin uses the same chemical reaction as attachment of amine-labeled oligonucleotides, the carbodiimide chemistry.

1. Follow **steps 1–3** in **Subheading 3.1.**
2. After incubation, sonicate the reaction tube to suspend the particles that have adhered to the wall and lid. Add SDS to a final concentration of 0.1% and centrifuge.

3. Wash the particles with 500 µL of 10 m*M* PBS/0.1% SDS twice. Resuspend the particles in 100 µL of 10 m*M* PBS.
4. Prepare 1 mL of 0.1 mg/mL NeutrAvidin in PBS buffer. Mix the activated particles with 800 µL of 10 m*M* PBS and 100 µL of 1 mg/mL NeutrAvidin. *Note:* Always add the particles *to* protein. Briefly sonicate, and allow the mixture to incubate for 30 min on a rotator.
5. After 30 min, sonicate the reaction vessel to suspend the particles adhering to the walls and lid. Add SDS to a final concentration of 0.1% and centrifuge.
6. Suspend the particles in enzyme-linked immunosorbent assay blocking buffer (PBS, 0.5% BSA, 0.1% sodium azide). Note that BSA should not be used at any stage prior to this step, because it will compete with the NeutrAvidin in the attachment step.
7. Wash the NBCs with 10 m*M* PBS twice. Resuspend the NBCs in 100 µL of 10 m*M* PBS. NBCs derivatized with protein can be stored for future use for approx 2 wk at 4°C.

3.4. Quality Control of NeutrAvidin Attachment Step

Quality control can be carried out using a number of approaches. The most informative is to react with fluorescently labeled biotin. However, the protocol described here can also be used to attach another biomolecule of interest, such as a biotinylated protein, an antibody, or an oligonucleotide.

1. To 1×10^6 of NBCs (10 µL NBCs at 1×10^5/µL) add 10 µL of 0.4 µ*M* dye-labeled biotin.
2. Let the reaction proceed for 20 min at room temperature. Be sure to cover the reaction chamber with aluminum foil, to eliminate photobleaching of the fluorescent dye.
3. After 20 min, add 500 µL of PBS/0.5% BSA/0.1% sodium azide with 0.1% SDS. Centrifuge, aspirate the supernatant, and wash three times.
4. Resuspend the NBCs in 100 µL of PBS/0.5% BSA/0.1% sodium azide for imaging.

3.5. Measuring Nanoparticle Concentrations (Particle Enumeration)

During both the methods development process and subsequently when performing quantitative assays, it is important to know the number of NBCs in each assay, to account for variations in particle concentration caused by manufacturing and particle derivatization procedures. We have developed a simple method for enumeration that is applicable for all nanoscale particles and uses a hemacytometer. A standard hemacytometer, normally used to count blood cells, is about the size of a regular microscope slide consisting of two chambers. The chambers are etched glass with raised sides that support a quartz cover slip. The cover slip is exactly 0.1 mm above the chamber floor. The counting chamber is etched in a total surface area of 9 mm^2. Calculation of concentration is based on the volume underneath the cover slip. In our case,

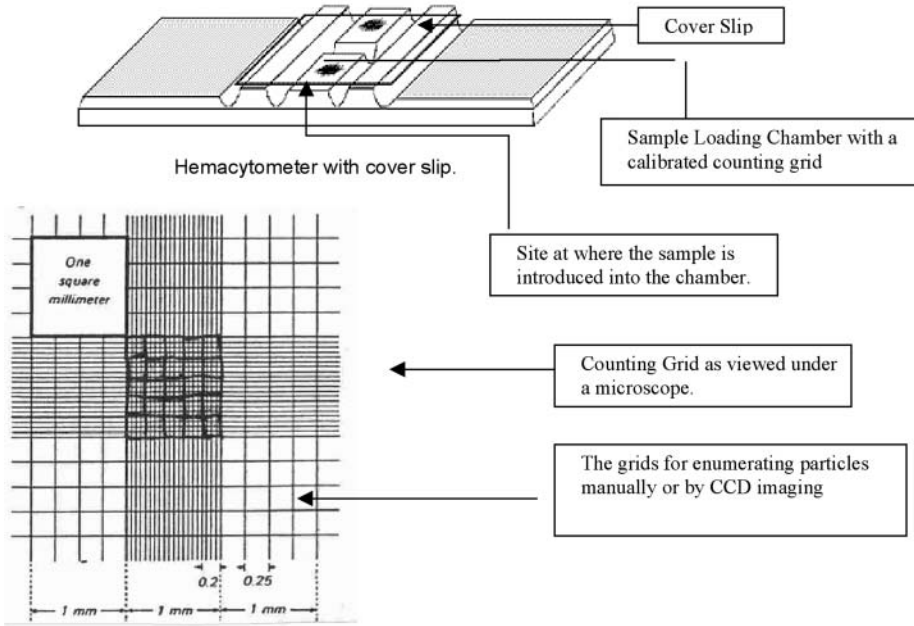

Fig. 3. Layout of hemacytometer.

one large square has a volume of 0.0001 mL (length × width × height; i.e., 0.1 × 0.1 × 0.01 cm). Each large square is divided into nine 1.0-mm squares. The NBC concentration per milliliter will be the average count per square × 10^4. **Figure 3** shows the device as layout, and **Fig. 4** a typical image.

1. Sonicate NBCs to suspend the particles that have adhered to the wall and lid.
2. Make 1:10, 1:100, and 1:1000 serial dilutions of the particles in water.
3. Using a pipetman, load the 1:100 dilution into both chambers of the hemacytometer by carefully touching the edge of the cover slip with the pipet tip and allowing the chamber to fill by capillary action. About 10 µL should be enough to load each chamber.
4. Let the particles sediment in the chamber for 5–10 min.
5. Using a ×20 objective, scan each square of the 4 × 4 squares grid (1 mm^2). Check for an even distribution of the particles.
6. Count each 1 or 2 or 3 squares such that a count of 100 particles is obtained. If a total count of 100 particles is not obtained from all 16 squares, repeat the process with the 1:10 dilution. If the particle number is much greater than 100 in a single square, repeat with the 1:1000 dilution.
7. Calculate the NBC concentration based on the dilution factor and hemacytometer dimensions.

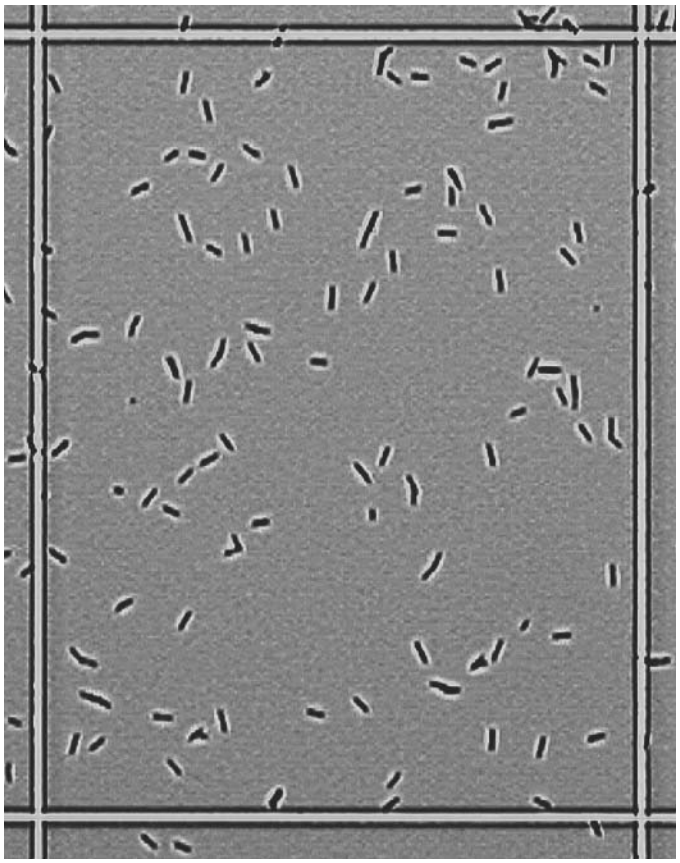

Fig. 4. NBC particles as they appear in 1 of the 16 grids (4 × 4 squares grid) using a ×20 objective lens in a hemacytometer.

3.6. Detection of NBCs

The measurement of NBCs requires the use of a reflectance microscope. If the NBCs are going to be used as substrates in bioassays, the microscope must also be capable of fluorescence measurements. The microscope can be either upright or inverted. The typical fluorescence assay image acquisition process is as follows:

1. Choose the reflectance filter set and focus on the reflectance image of the particles.
2. Acquire and save the reflectance image. Camera integration time is from 10 to 100 ms, depending on the light source and filter set used.
3. Move the sample approx 1 μm for fluorescence image. The depth of focus of a 1.4 NA objective is quite small, so there can be a focus difference between the

reflectance image acquired at 450 nm and the fluorescence image acquired at 690 nm.
4. Choose the fluorescence filter set.
5. Acquire and save the fluorescence image with shuttered light. The light source needs to be shuttered to control the fluorescence exposure time and prevent photobleaching. Typical integration times are more than 1 s.

The components of one system capable of such measurements are as follows.

1. Zeiss Axiovert 100 microscope.
2. Sutter 175-W Xe lamp.
3. Photometrics CoolSnapHQ charge-coupled device camera.
4. Prior automated xyz stages.
5. Sutter automated filter wheels for excitation and collection. The excitation wheel must have a shutter.
6. Polytec PI PIFOC® piezoelectric drive for fine focus.
7. ×63 and ×100 oil immersion objectives (1.4 NA).
8. MetaMorph™ software from Universal Imaging for system control and image capture.
9. Glass-bottomed 96- or 384-well plates.
10. Reflectance excitation filter: 400- to 460-nm filter with 10- to 40-nm bandpass.
11. Fluorescence filter set.

As described, this system is capable of acquiring a pair of reflectance and fluorescence images in <5 s. If a ×63 objective is used, one can image 100 or more particles. A good sample of any assay point comes with averaging the fluorescence from 50 to 100 particles; thus, if multiple codes are used, multiple images are required. Image acquisition in assays requires the coordinated use of all the listed components. Software packages such as MetaMorph can automate the control of all items and perform automatic focusing.

Any fluorescent dye can be used with the particles; however, the differential reflectance of the metals means that the banding pattern will appear in the fluorescent image of any dye emitting below 600 nm. Cy5 is the best dye to use, because the absorption is well away from the reflectance imaging wavelengths and thus will not photobleach during focusing. The emission of Cy5 is also well above 600 nm and, therefore, the banding pattern will not appear. Fluorescein is the dye most likely to photobleach during focusing, because its absorption spectrum is close to or contains the reflectance image wavelengths. The dichroic filters for Cy3 and Cy5 will reflect and transmit enough light for the reflectance image and an automatic dichroic filter changer is not necessary.

Both reflectance and fluorescence images of particles may be acquired on a standard glass microscope slide and using an upright microscope.

High-magnification oil immersion objectives give the best NBC detection and fluorescent sensitivity; however, they require a PIFOC microscope objective positioner for automatic focusing. For imaging of NBCs, ×63 .8NA objectives can be used and will reduce the complexity and expense of the system. The reduced resolution means a smaller number of codes can be distinguished, but the required focus accuracy is reduced considerably. Standard stepper motor-driven objective-focusing systems can be used with this objective, and the focus offset between reflectance and fluorescence can be eliminated.

3.7. Image Processing

Analysis of the reflectance and fluorescence images is carried out with a proprietary software package developed in-house at Nanoplex Technologies—BSee™ software—that rapidly decodes the identity of the particles imaged and with an extremely high level of accuracy. The automated image-processing solution for NBC images must meet the following criteria: It must handle multiple images, both in the sense of analyzing and coupling the reflectance (RFL) and fluorescent images (FL), and in the sense of amassing statistics from many RFL/FL pairs. It must work over a large range of image conditions and accept some degree of blurring and other aberrations in the images. The software is designed to consider only isolated rods. Coincident rods and large clumps are rejected, because they can confound rod identification and increase the error in fluorescence quantitation.

Processing begins with the reflectance image. A high-pass filter is first applied to the reflectance image. This kernel has the effect of both enhancing the edges of the rods and separating those rods that are in close proximity. The image noise is assessed and combined with the median background level to determine the threshold intensity level that must be applied for proper segmentation—a method of isolating objects in a binary image. Applying a threshold cutoff to the image produces a binarized image whose nonzero pixels correspond to NBCs and whose zero pixels correspond to background.

The connected nonzero regions in the binarized image are designated as "blobs" or potential NBCs. Using principal component analysis (PCA) ***(10)***, the original gray-scale image pixels in each blob, corresponding to a single NBC, are used to determine the medial axis of the NBC. In PCA analysis, the first principal axis closely matches the best-fit line used to extract the intensity level along the length of the NBC.

The intensity profile is used to match the NBC to a library of striping profiles or "flavors." Two main scoring algorithms are used. The first is based on correlating the intensity profile to synthetic profiles in the library. The second method divides the intensity profile into a given number of segments and determines the metal choice for each segment. Once the flavor of an NBC has been identified, the fluorescent intensity of the NBC is assessed using the stored fluorescent

image. More specifically, those same pixel coordinates that are used to highlight the NBC image in the reflectance image are used with modification to quantify fluorescent intensity. The software generates mean and median background subtracted values for the fluorescence. Data are then accumulated over all NBCs of the same flavor. For instance, fluorescent values corresponding to all rods with the same striping pattern are averaged together. The data are output visually in spreadsheet form as well as to a file in a text format appropriate for Excel. More information about licensing the software can be obtained from Nanoplex Technologies.

4. Note

1. Always prepare the EDC/NHS solution fresh every day.

Acknowledgment

We wish to acknowledge the Advanced Technology Program of the National Institute of Standards and Technology for funding (grant no. 70NANB1H3028).

References

1. Kitano, H. (2002) Systems biology: a brief overview. *Science* **295,** 1662–1664.
2. Howbrook, D. M., Van der Valk, A. M., O'Shaughnessy, M. C., Sarker, D. K., Baker, S. C., and Lloyd, A. W. (2003) Developments in microarray technologies. *Drug Discov. Today* **8,** 642–651.
3. Levit-Binnum, N., Lindner, A. B., Zik, O., Eshhar, Z., and Moses, E. (2003) Quantitative detection of protein microarrays. *Anal. Chem.* **75,** 1436–1441.
4. Nicewarner-Peña, S. R., Freeman, R. G., Reiss, B. D., He, L., Peña, D. J., Walton, I. D., Cromer, R., Keating, C. D., and Natan, M. J. (2001) Submicrometer metallic barcodes. *Science* **294,** 137–141.
5. Penn, S. G., He, L., and Natan, M. J. (2003) Nanoparticles in bioanalysis. *Curr. Opin. Chem. Biol.* **7,** 609–615.
6. Nicewarner-Pena, S. R., Carado, A. J., Shale, K. E., and Keating, C. D. (2003) Barcoded metal nanowires: optical reflectivity and patterned fluorescence. *J. Phys. Chem. B.* **107,** 7360–7367.
7. Walton, I. D., Norton, S. M., Balasingham, A., He, L., Oviso, D. F., Gupta, D., Raju, P. A., Natan, M. J., and Freeman, R. G. (2002) Particles for multiplexed analysis in solution: detection and identification of striped metallic particles using optical microscopy. *Anal. Chem.* **74,** 2240–2247.
8. Reiss, B. D., Freeman, R. G., Walton, I. D., Norton, S. M., Smith, P. C., Stonas, W. G., Keating, C. D., and Natan, M. J. (2002) Electrochemical synthesis and optical readout of striped metal rods with submicron features. *J. Electranal. Chem.* **522,** 95–103.
9. Wong, S. S. (1991) *Chemistry of Protein Conjugation and Cross-Linking*, CRC Press, Boca Raton, FL.
10. Fox, J. (1997) *Applied Regression Analysis, Linear Models, and Related Methods*, Sage, Thousand Oaks, CA.

7

Assembly and Characterization of Biomolecule–Gold Nanoparticle Conjugates and Their Use in Intracellular Imaging

Alexander Tkachenko, Huan Xie, Stefan Franzen, and Daniel L. Feldheim

Summary

In this chapter, we outline protocols for assembling and characterizing peptide–gold nanoparticle conjugates. We describe two strategies for attaching peptides to gold nanoparticles. One involves the covalent coupling of cysteine-terminated peptides directly to a particle surface via a sulfur-gold bond. Alternatively, peptides are coupled to bovine serum albumin (BSA) via a bifunctional molecular crosslinker. We also describe a number of characterization methods for determining the number of crosslinkers per BSA, peptides per BSA, and peptides adsorbed per particle. Finally, we show that the enormous visible light extinction properties of gold nanoparticles make them excellent imaging agents for tracking the trajectories of peptides inside living cells.

Key Words

Gold nanoparticles; cell imaging; bovine serum albumin; polyethylene glycol; peptides; microscopy.

1. Introduction

Protocols for assembling peptide–gold particle conjugates and monitoring their trajectories inside cells are detailed in this chapter. Gold particle bioconjugates are important constructs for cellular imaging, therapeutic delivery, and biomolecule detection ***(1–3)***. Because of the remarkably large scattering cross-section of metal particles (10^{-10} cm^2), individual nanoparticles can be imaged under white-light illumination. Moreover, the plasmon resonance condition of metals can be tuned across the visible spectrum and into the near infrared simply by changing particle size and shape ***(4,5)***. Thus, multicolor assays are

From: *Methods in Molecular Biology, vol. 303: NanoBiotechnology Protocols*
Edited by: S. J. Rosenthal and D. W. Wright © Humana Press Inc., Totowa, NJ

possible with a single light source, without the need for filters, and free from complications of fluorescence bleaching or blinking.

A potential application of gold particle bioconjugates is therapeutic delivery. A primary goal of modern therapeutic delivery is to create a bioconjugate capable of seeking out specific cells in vivo, traversing the cell and nuclear membranes, and releasing a therapeutic in the nucleus. Recognizing the multitude of challenges associated with nuclear targeting, and following the presumption that no single peptide will be effective at *specific* cell recognition and nuclear targeting, we have been pursuing a new approach to nuclear translocation. The general strategy has been to combine multiple membrane translocating peptides and antibodies on a *single* gold nanoparticle scaffold. Of paramount importance in the construction of multipeptide nanoparticles is understanding how to formulate peptide-gold bioconjugates that are stable in high ionic strength solutions containing exchangeable peptides and proteins found in cellular media, and how to quantitate the number of adsorbed biomolecules per gold particle (*see* **Note 1**). Protocols for performing these studies are described herein. These experiments are then followed by a description of methods for imaging gold nanoparticles inside cells using video-enhanced color differential interference contrast (VECDIC) microscopy.

2. Materials

1. Hydrogen tetrachloroaurate.
2. Sodium citrate.
3. Bovine serum albumin (BSA) (highest purity) (Roche, Indianapolis, IN).
4. 3-Maleimido benzoic acid *N*-hydroxysuccinimide (MBS) (Pierce, Rockford, IL).
5. Gold nanoparticles (20-nm diameter) (Ted Pella).
6. Dimethylformamide (DMF).
7. 50 m*M* phosphate buffer, pH 7.0, with 50 m*M* EDTA.
8. EDTA.
9. Dithiothreitol (DTT).
10. Fluorescamine (4-phenyl-spiro [furan-2(3H), 1′-phthalan]-3,3′-dione).
11. Rhodamine B isothiocyanate (RBITC).
12. Cysteine-terminated peptides.
13. Lysine.
14. Thiolated methoxy polyethylene glycol (PEG), 5000.
15. Acetone.
16. Membrane filter (0.8 μm).
17. Sephadex G-50 (Sigma, St. Louis, MO).
18. Chromatography equipment.
19. Centricon YM-30 and Microcon YM-100 (Millipore, Bedford, MA).
20. Sodium dodecyl sulfate polyacrylamide gel electrophoresis (SDS-PAGE) equipment.
21. Microplate absorbance and fluorescence reader.

22. Optical research microscope equipped with differential interference contrast (DIC) optic.
23. Scientific-grade color digital camera (at least 1 million pixels).

3. Methods

3.1. Synthesis of Gold Nanoparticles

Gold nanoparticles are synthesized in a one-step aqueous preparation in which hydrogen tetrachloroaurate is brought to boiling and reduced by rapidly adding sodium citrate ***(6)***. Particle diameter can be tuned via citrate:$[AuCl_4]^{1-}$ stoichiometry. The resulting particles are ready immediately for conjugation to peptides or proteins.

1. In a 1-L round-bottomed flask equipped with a condenser, heat 500 mL of 1 m*M* $HAuCl_4$ solution to boiling point with vigorous stirring.
2. After refluxing for 10 min, rapidly add 50 mL of 40 m*M* of trisodium citrate to the stirring solution. The color should change from a pale yellow to a deep wine red.
3. Let the solution boil for 10 min.
4. Remove from the heat and continue to boil for an additional 15 min.
5. Remove the stir bar and allow the solution to cool to room temperature.
6. Filter through an 0.8-μm membrane filter.
7. Characterize using visible spectroscopy and transmission electron microscopy (TEM). This prep yields about 12-nm-diameter particles with peak absorption at 520 nm.

3.2. Assembly of Biomolecule–Gold Nanoparticle Complexes

Two strategies for attaching cell-targeting peptides to gold nanoparticles are described (**Fig. 1**). One involves the covalent coupling of cysteine-terminated peptides directly to a particle surface via a sulfur-gold bond. Alternatively, peptides are coupled first to BSA via the bifunctional crosslinker MBS and then attached to gold nanoparticles via electrostatic interactions ***(7)***. There are advantages and disadvantages for each strategy. The direct coupling of cysteine-terminated peptides to gold particles affords a simple one-step procedure that produces particles with a high surface coverage of peptide. However, many peptides are sparingly soluble in aqueous solution or cause flocculation when attached to gold nanoparticles. Attaching peptides to BSA prior to immobilization on gold nanoparticles creates extra chemical reaction and purification steps but can increase peptide solubility and sol stability.

3.2.1. Conjugation of Peptides to BSA

Peptides are conjugated in two steps. In step 1, lysine residues of BSA are treated with the heterobifunctional crosslinker MBS. The maleimide moieties of

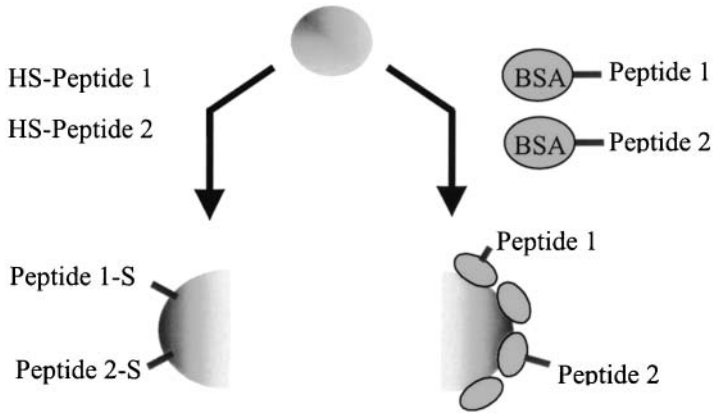

Fig. 1. Two strategies for assembling multifunctional gold particle–peptide bioconjugates.

the BSA-MBS complex react with free thiols of the peptide terminal cysteine residue. Right side of the diagram illustrates use of a protein linker, while left side shows covalent attachment via a thiol-gold bond.

1. Prepare an aqueous solution of high-purity BSA (5–10 mg/mL) in degassed 50 m*M* phosphate buffer, pH 7.0, with 50 m*M* EDTA.
2. Dissolve MBS in DMF (10 mg/mL).
3. Within 30 min add the solution of MBS to aqueous solutions containing BSA in molar ratios of the linker to BSA of between 1:2 and 1:100. (BSA contains 59 lysine residues, of which up to 35 can be used for MBS modification ***[8]***).
4. Allow the reaction to proceed for 60 min at room temperature.
5. Remove the unreacted MBS linker by gel filtration using Sephadex G-50 or by centrifugal solvent displacement (Centricon YM-30 at 5000*g*). (Maleimides can undergo hydrolysis; therefore, thiol binding should be performed within hours of purifying excess MBS from the BSA-MBS complex).
6. Dissolve 5 mg of lyophilized peptide containing terminal cysteine in degassed 50 m*M* phosphate buffer, pH 7.0, with 50 m*M* EDTA.
7. Because the sulfhydryl groups in the peptide may oxidize, it is often necessary to pretreat the peptide with a reducing reagent such as DTT prior to coupling with BSA-MBS. Mix 5 mg of peptide with 5 mg of DTT and let it react for 1 h at room temperature.
8. Separate the peptide from free DTT using an equilibrated Sephadex G10 column with 1% acetic acid. The first fraction will contain the peptide and the second fraction will contain free DTT.
9. Mix BSA-MBS conjugates with peptide solution at the desired ratio (2–50:1 peptide:BSA) and react in pH 7.4 buffer for at least 3 h at 4°C.

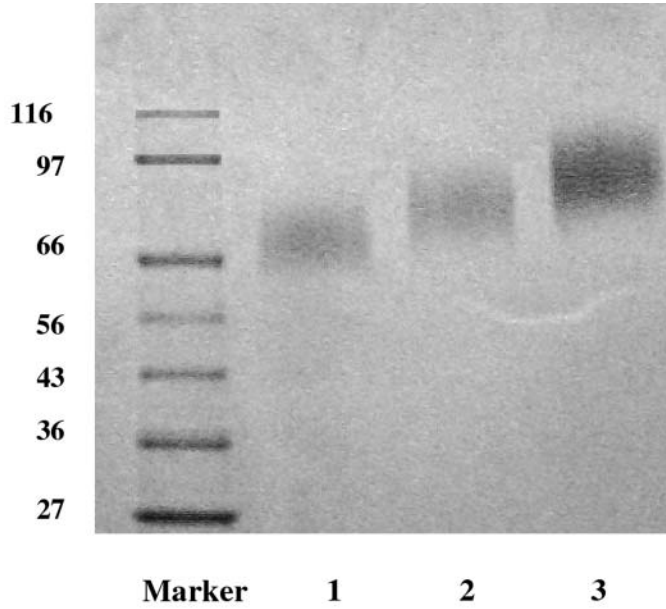

Fig. 2. Gel shift assay, 7.5%, SDS-PAGE gel: lane 1, BSA/MBS complex at 1:40 ratio; lane 2, BSA/peptide at 1:3 ± 1 ratio; lane 3, BSA/peptide at 1:6 ± 2 ratio. The broad nature of the sample bands reflects various binding efficiencies within the sample. Marker bands correspond to the molecular weight in thousands on the left.

10. Remove the unreacted peptides by dialysis or by centrifugal solvent displacement (Centricon YM-30 at 5000*g*).
11. Analyze the prepared BSA-peptide complexes using 7.5% polyacrylamide gel electrophoresis (SDS-PAGE). An example is shown in **Fig. 2**.

3.2.1.1. Characterization of BSA-MBS Complexes by Fluorescamine Assay

Because the purity of BSA varies and the binding efficiency of the *N*-hydroxysuccinimide (NHS) moiety of MBS is strongly affected by water and pH, it is important to investigate quantitatively the number of MBS ligands attached to BSA. This can be determined using a fluorescamine assay, which measures the number of unreacted lysine residues following MBS conjugation (*see* **Note 2**):

1. Dissolve fluorescamine in high-performance liquid chromatography–grade acetone (3 mg/mL) to obtain a 1 m*M* solution. (The use of acetone presents a set of unique problems, because commonly used polystyrene disposable pipets are incompatible. Glass or polypropylene materials, with their higher resistance to organic solvents should be used.)

2. Prepare appropriate lysine standards (0–500 μ*M*) and BSA-MBS (100–500 μg/mL) samples in 50 m*M*, pH 7.4 phosphate buffer.
3. Add a 250 μ*M* solution of fluorescamine to the prepared samples. (If plastic is used, the fluorescamine solution should be no more than 25% of the total reaction volume. For standard 96-well microplate assays, 50 μL of stock fluorescamine solution is added to 150 μL of sample.)
4. Mix thoroughly.
5. Read the fluorescence with a 390/30-nm excitation filter and a 460/40-nm emission filter. If samples remain sealed and protected from light, the reaction will be stable for 2 h.
6. Determine the number of bound MBS per BSA from the difference of total and unreacted lysines.

3.2.2. Attachment of Peptide-BSA Conjugates to Gold Nanoparticles

The following protocols for attaching peptide-BSA conjugates to gold nanoparticles will vary slightly depending on the particular choice of peptide. In general, to avoid particle flocculation, the pH of the peptide-BSA conjugate should be adjusted to a value close to the isoelectric point (p*I*) of the peptide prior to addition to the gold nanoparticle sol. The following example is for a peptide with a p*I* close to pH 9.0. Note that all glassware must be clean.

1. Add dropwise with rapid stirring 0.1 mL of 10 μ*M* freshly prepared peptide-BSA conjugate (in 10 m*M*, pH 9.0 carbonate buffer) to 0.9 mL of 20-nm-diameter citrate-passivated gold nanoparticles (1.16 n*M*) to achieve a ratio of approx 1000 protein molecules per gold nanoparticle ***(9)***.
2. Incubate the mixture on a shaker for 30 min.
3. Centrifuge the solution at 12,000*g* for 1 h at 4°C to separate the unbound peptide-BSA from the conjugates.
4. Carefully remove the supernatant containing unbound peptide-BSA and resuspend the pellet in carbonate buffer (10 m*M*, pH 9.0) to obtain peptide-BSA-coated gold nanoparticles.

3.2.3. Attachment of Peptides Directly to Gold Nanoparticles

Thiols form covalent bonds to metals such as gold and silver. Thiol-gold chemistry is being employed in a wide range of biomolecule-sensing strategies, including a gold particle colorimetric assay for DNA ***(10)***. One of the more appealing aspects of thiol-gold chemistry is that the reaction proceeds at room temperature in aqueous solution. Moreover, attaching many different functional thiols to a single particle is typically as simple as stirring all the ingredients together in one pot ***(11)***.

For a 20-nm colloid, the thiolated species are typically added so as to achieve a molar ratio of approx 2500 thiols per nanoparticle. To ensure monolayer coverage, this ratio can be adjusted according to the core size of the colloids; the

available number of adsorption sites is directly proportional to the total surface area and thus to the square of the particle diameter. If a mixed thiol monolayer is sought, the desired thiols may simply be stirred in solution together with gold particles and allowed to adsorb. In many cases, the mole fraction of thiols bound to nanoparticles will reflect the mole fraction added to the reaction mixture ***(11)***. Mixed monolayers of PEG and peptides are synthesized as follows. Note that all glassware must be clean.

1. Combine 72 μL of thiolated PEG (20 μ*M*) and 72 μL of peptide (20 μ*M*) to produce a molar ratio of PEG to peptide of 1:1.
2. Add 145 μL of this mixture to 1 mL of 20-nm-diameter citrate-capped gold nanoparticles (1.16 n*M*) to produce a molar ratio of thiol to gold of 2500:1.
3. Stir the mixture of gold/PEG/peptide at room temperature for 1 h to allow complete exchange of thiol with citrate on the gold nanoparticles.
4. To purify the complex, centrifuge at 12,000*g* for 30 min.
5. Decant the supernatant and resuspend the pellet in 1 mL of water.

3.3. Characterization of Peptide–Gold Nanoparticle Complexes

The number of peptide-BSA conjugates attached to gold can be determined by radiolabeling, fluorescence spectroscopy, and time-correlated single-photon counting spectroscopy (TCSPC) ***(12)***. TCSPC requires relatively sophisticated laser equipment and expertise but has the advantage of being able to probe the dynamics of protein or peptide adsorption and exchange on gold nanoparticles without separation steps. Here we focus on the more routine static fluorescence techniques used in our laboratory for characterizing protein–gold particle conjugates.

Peptide-BSA binding isotherm measurements on gold nanoparticles can be constructed as follows:

1. Label the protein (or attached peptide) with a fluorophore. In this example, BSA was modified with RBITC. Similar procotols may be used for fluorescently tagged peptides.
2. Prepare 9 × 30 μL solutions of RBITC-BSA in concentrations ranging from 0.4 to 12 μ*M* *i*n 10m*M* pH 7 phosphate buffer.
3. To each protein solution, add 450 μL of a 1.05 n*M* solution of gold nanoparticles and stir for 15 min. Native BSA may be added to each solution to increase stability against particle aggregation. Caution must be taken, however, that the exchange of the added native BSA for surface-bound protein does not occur during the course of the experiment. To improve the stability of RBITC-BSA–gold nanoparticle conjugates, 20 μL of 2 mg/mL native BSA (e.g., unlabeled BSA) was added to each solution ***(13,14)***.
4. Remove the unbound fraction of RBITC-BSA by centrifuging the solutions at 10,000*g* for 30 min. Collect the supernatant.

5. Repeat **step 4**.
6. Dilute all the supernatants to 2 mL by pH 7.0, 10 m*M* phosphate buffer. Measure the fluorescence intensity of each sample, and compare the fluorescence to a standard curve to determine the concentration of unbound RBITC-BSA in the initial mixture.
7. Calculate the amount of RBITC-BSA bound to the gold particles by subtracting free RBITC-BSA from the total amount of RBITC-BSA added initially.

An adsorption isotherm for BSA conjugates is shown in **Fig. 3**. Formally, adsorption isotherms are only valid for systems in equilibrium. Two experimental findings are suggestive of equilibrium adsorption in the systems studied here: (1) the amount of BSA adsorbed per particle did not change over the course of several hours; and (2) BSA desorbed, albeit slowly, over time. Nonlinear regression was applied to analyze the RBITC-BSA saturation curve. A one-site binding model yielded a K_d of 101.4 n*M* and a saturation coverage of 158 RBITC-BSA/gold nanoparticle ***(9)***.

This curve suggests a substantial amount of multilayer adsorption may occur for these BSA conjugates on gold nanoparticles. Thus, care must be taken to measure adsorption isotherms for each new peptide-BSA–gold nanoparticle construct.

3.4. Intracellular Imaging of Colloidal Gold With Light Microscopy

Silver and gold colloids have been of interest for thousands of years because of their unique visible optical properties. The efficiency for the extinction of light (absorption plus scattering) by metal nanoparticles surpasses by orders of magnitude that of any molecular chromophore. In addition, both absorption and scattering properties can be considerably altered by surface modification, or by electronic coupling between individual nanoparticles ***(1,15,16)***. Together with an exceptional resistance to photodegradation, such favorable optical features are making metal colloids attractive components for diagnostic, electronic, and photonic devices. Metal nanoparticles modified with many different cell-targeting agents and therapeutics could also be attractive components for therapeutic delivery ***(3,17)***.

TEM remains the best technique in terms of spatial resolution (~1 nm) for viewing colloidal nanoparticles in biological samples, but it requires laborious sample preparation and expensive equipment. Live cells, however, can only be imaged using light microscopy, and various techniques have been employed to enhance the visibility of colloidal gold particles, which are typically smaller than the resolution limit of light microscopy. With video-enhanced light microscopy, structures that are an order of magnitude smaller than the resolution limit of the light microscope can be detected ***(18,19)***. Individual gold particles of 20-nm diameter can be observed with reflection-contrast microscopy

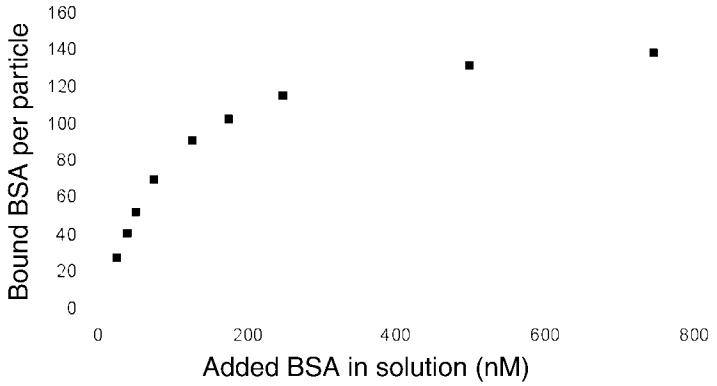

Fig. 3. Adsorption isotherm of RBITC-labeled BSA adsorbed on gold particles (20 nm in diameter).

(20,21) and high-contrast video microscopy (Nanovid) ***(22)***, and the use of video-enhanced light microscopy to image colloidal gold inside living cells has been reported ***(23–25)***.

Note, however, that there are several caveats to the optical imaging techniques just described. First, nanoparticles are only identified as an inflated diffraction image. Thus, a 20-nm-diameter particle will appear as an approx 200-nm particle in the optical image (the diffraction limit). Second, these techniques often require second-image and post-image processing to visualize cellular structures. Finally, some cellular structures such as out-of-focus dense granules may also appear in an enhanced image as bright or dark spots, and it is often difficult to distinguish these structures from nanoparticles unless polarization optics and color imaging are used ***(1,3)***.

3.4.1. VECDIC Microscopy

Introducing color into the imaging system capitalizes on the ability of nanoparticles to reflect polarized light at wavelengths different from that of the surrounding biological media; thus, silver and gold nanoparticles can be simultaneously observed inside living or fixed cells via single-pass VECDIC microscopy (**Fig. 4**).

3.4.1.1. Hardware Configuration of VECDIC Microscopy

VECDIC microscopy can be performed with any research-grade DIC-equipped microscope using Nomarski or de Sénarmont bias retardation. The light upright microscope Leica DMLB has been used routinely for these studies with a standard image-splitting prism, which can direct 0, 50, or 100% of

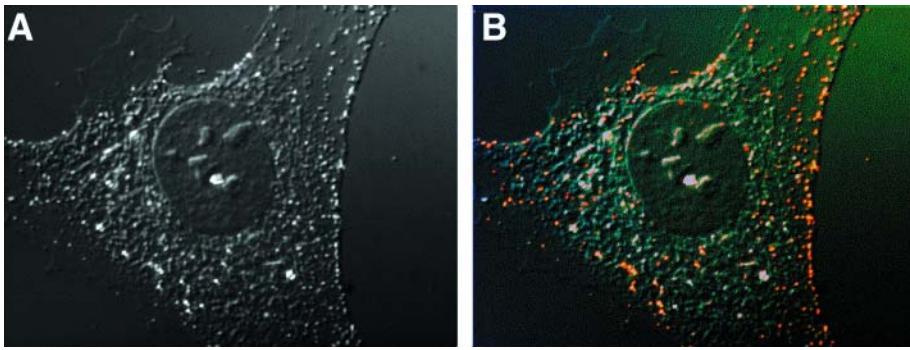

Fig. 4. Comparison of **(A)** video-enhanced black-and-white DIC microscopy and **(B)** video-enhanced color DIC microscopy. Shown are 20-nm-diameter gold-peptide-BSA complexes inside 3T3 cells. Images were taken with a Nikon DXM 1200 digital color CCD camera on a Leica DMLB DIC-equipped microscope with a ×100/1.3 NA objective.

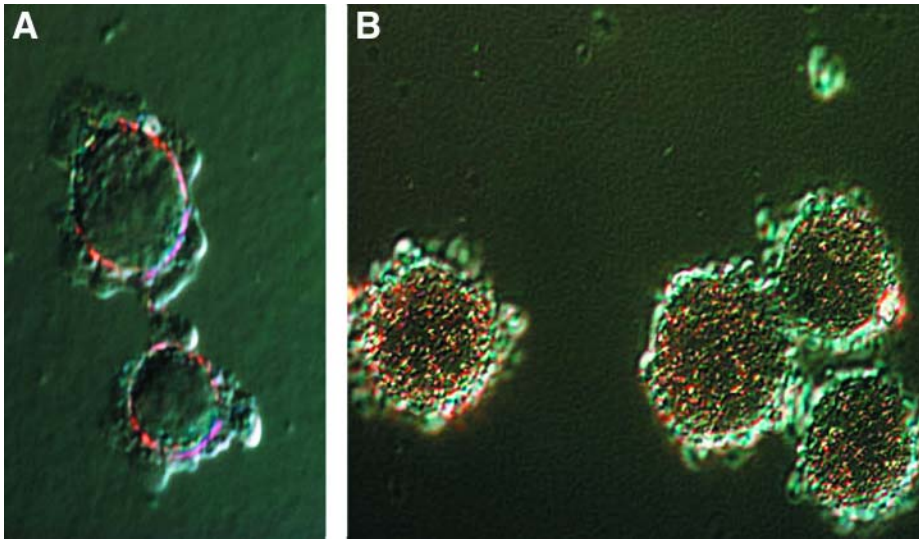

Fig. 5. Incubation of HeLa cells with 20-nm gold nanoparticles after 3 h by VECDIC microscopy. **(A)** Nanoparticle carrying Large T NLS accumulated around nuclear membrane. **(B)** Nanoparticle carrying adenovirus NLS accumulated inside nucleus.

the light into the camera. The microscope was equipped with a 0.9 numerical aperture (NA) condenser and Nomarski DIC optics. Illumination was supplied from a 100-W halogen light source. The strain-free Plan Apo ×63–100 objectives (NA 1.00–1.4) are suitable for this purpose. Oil immersion objectives

should be used to eliminate reflections from the surface-air interface of the microscopic slide. High NA oil condenser and light-scrambling techniques using fiberoptic illumination can dramatically improve resolution of VECDIC microscopy. Our video system comprises a Nikon DMX-1200 color charge-coupled device (CCD) digital camera, with software-based manual control of individual color channels and contrast enhancement on live and captured images. The ability to use video enhancement on live images is essential for video-enhanced microscopy. Manual control of the camera video enhancement setting is also necessary, because an automatic camera will continuously adjust brightness and contrast to accommodate bright spots inherent in DIC microscopy, which makes it difficult to compare acquired images.

3.4.1.2. Operation of VECDIC Microscope

A microscope should be equipped with DIC optics using Nomarski or de Senarmount bias retardation and color camera with video enhancement capabilities.

1. Adjust the microscope for Köhler illumination and switch to a high-magnification objective (×60–100).
2. Insert the polarizer and analyzer in the optical path of the microscope set up for bright field, and examine the objective rear focal plane with a phase telescope or Bertrand lens. If the polarizer and analyzer are properly positioned and the microscope perfectly aligned, a dark extinction cross will appear in the objective aperture. (This step may not be necessary if the optic was properly aligned before.)
3. With the microscope aligned for Kühler illumination and set up for DIC (the polarizer and analyzer crossed, and both prisms [objective and condenser] installed), place a sample on the stage and focus the specimen while observing the procedure through the eyepieces. In general, the specimen assumes a pseudo-three-dimensional appearance with a shadow-cast effect.
4. Rotate the objective DIC prism or rotate the polarizer (or analyzer) in the microscope equipped for de Sénarmont compensation to achieve maximum extinction. The image should appear very dark gray at maximum extinction. Gold nanoparticles >40 nm should be observed at this setting as bright yellow or red dots. Reducing the size of the condenser aperture diaphragm can significantly improve the observation of gold nanoparticles.
5. Switch the image from the viewfinder to the attached color video camera.
6. Using the video enhancement features of the camera, optimize the contrast and color setting for observation of yellow/red gold nanoparticles. Optimizing bias retardation and aperture diaphragm on the microscope will allow simultaneous observation of cellular structures and gold nanoparticles (*see* **Note 3**).

3.5. Intracellular Imaging of Peptide–Gold Nanoparticle Conjugates

The nucleus is the desired target for cancer therapies that involve DNA–drug-binding interactions, gene therapy and antisense strategies that manipulate RNA splicing. Although viruses have been adapted to deliver genes to cell nuclei, the design of safer synthetic delivery systems remains a challenge. The functionally active peptide sequences of nuclear localization signals (NLSs) of many viral proteins are known. Such peptides could be synthesized with a terminal cysteine residue and attached to a nanoparticle along with therapeutic agents. The following example demonstrates nuclear targeting of gold particles modified with NLS peptides derived from SV-40 and adenoviruses (**Fig. 5**).

1. Order the desired peptide with terminal cysteine.
2. Prepare a peptide-BSA conjugate (*see* **Subheading 3.2.1.**).
3. Attach the peptide-BSA conjugate to a 20-nm-diameter citrate-coated gold nanoparticle (*see* **Subheading 3.2.2.**).
4. Incubate the desired cell line (e.g., 3T3, HeLa) on 1.5 microscopy cover slips until they reach 60–70% confluency.
5. Add nanoparticles carrying NLS to the cell growth media.
6. Incubate the cells with the nanoparticles in growth media for 1–6 h.
7. Stop incubation at the specified time by removing the media.
8. Rinse the cells with DPBS five times to remove nanoparticles in the growth media.
9. Fix the cells in 4% paraformaldehyde for 15 min and replace with Dulbecco's phosphate buffered saline (DPBS).
10. Mount cover slips containing cells on a microscopy slide using Fluorosave mounting media.
11. Let the mounting media dry overnight.
12. Image the cells using VECDIC microscopy (*see* **Subheading 3.4.1.**).

4. Notes

1. The stability of colloidal sols is owing to a balance of forces including electrostatic repulsion, van der Waals attraction, and mixing free energy. The former two forces have been condensed into the well-known Derjaquin, Landau, Verway, Overbeck (DLVO) theory ***(26)***, which explains the stability of charged particles. The stability of colloidal sols is often improved with the use of "steric stabilizers." These are typically large proteins or polymers, placed in solution at concentrations often 1000 times the particle concentration. Proteins and polymers may adsorb to the particle surface strongly, in which case stabilization is afforded simply by the large positive free energy of desorption required prior to particle–particle fusion. Polymer chains that are free in solution, however, may also influence colloidal stability. Polymers in solution can cause particle flocculation or stabilization ***(26)***. Flocculation occurs whenever colloidal

particles approach so closely that the free polymer is excluded from the interparticle region. This is an entropic effect; the polymer leaves the interparticle region in response to the loss of configurational entropy on compression by the particles.

2. BSA has multiple lysine residues for reaction with the NHS moiety of MBS. The nonfluorescent compound fluorescamine (4-phenyl-spiro [furan-2(3H), 1′-phthalan]-3,3′-dione) reacts rapidly with primary amines in proteins, such as the terminal amino group of peptides and the ε-amino group of lysine, to form highly fluorescent pyrrolinone-type moieties ***(27)***. The number of MBS ligands coupled to BSA can thus be determined with the fluorescamine assay by measuring the number of unreacted lysine residues following MBS conjugation.
3. When tracking the trajectories of nanoparticles inside cells, it is important to be able to distinguish the relative location of particles inside (or outside) the cell in both the x-y and z directions. Because the depth of field in DIC is very shallow, optical z sectioning is possible with VECDIC. Thus, it is usually possible to discriminate between nanoparticles inside or outside the cell or nucleus. It must be remembered that DIC is a pseudo-three-dimensional imaging technique. The size of objects in the z direction is thus the result of the optics and may not be representative of the actual feature size.

References

1. Schultz, S., Smith, D. R., Mock, J. J., and Schultz, D. A. (2000) Single-target molecule detection with nonbleaching multicolor optical immunolabels. *Proc. Natl. Acad. Sci. USA* **97,** 996–1001.
2. Feldherr, C. M., Lanford, R. E., and Akin, D. (1992) Signal-mediated nuclear transport in simian-virus 40-transformed cells is regulated by large tumor-antigen. *Proc. Natl. Acad. Sci. USA* **89,** 11,002–11,005.
3. Tkachenko, A. G., Xie, H., Coleman, D., Glomm, W., Ryan, J., Anderson, M. F., Franzen, S., and Feldheim, D. L. (2003) Multifunctional gold nanoparticle-peptide complexes for nuclear targeting. *J. Am. Chem. Soc.* **125,** 4700–4701.
4. Jin, R., Cao, Y., Mirkin, C. A., Kelly, K., Schatz, G., and Zheng, J. (2001) Photoinduced conversion of silver nanospheres to nanoprisms. *Science* **294,** 1901–1903.
5. West, J. L. and Halas, N. J. (2000) Applications of nanotechnology to biotechnology—commentary. *Curr. Opin. Biotechnol.* **11,** 215–217.
6. Grabar, K. C., Freeman, R. G., Hommer, M. B., and Natan, M. J. (1995) Preparation and characterization of Au colloid monolayers. *Anal. Chem.* **67,** 735–743.
7. Lanford, R. E., Kanda, P., and Kennedy, R. C. (1986) Induction of nuclear transport with a synthetic peptide homologous to the Sv40 T-antigen transport signal. *Cell* **46,** 575–582.
8. Hermanson, G. T. (1996) *Bioconjugate Techniques*, 1st ed., Academic, New York.
9. Hayat, M. A., ed. (1989) *Colloidal Gold: Principles, Methods, and Applications*, vol. 2, Academic, New York.
10. Demers, L. M., Mirkin, C. A., Mucic, R. C., Reynolds, R. A., Letsinger, R. L., Elghanian, R., and Viswanadham, G. (2000) A fluorescence-based method for

determining the surface coverage and hybridization efficiency of thiol-capped oligonucleotides bound to gold thin films and nanoparticles. *Anal. Chem.* **72,** 5535–5541.
11. Templeton, A. C., Wuelfing, W. P., and Murray, R. W. (2000) Monolayer-protected cluster molecules. *Acc. Chem. Res.* **33,** 27–36.
12. Xie, H., Tkachenko, A., Glomm, W., Ryan, J., Brennaman, M. K., Papanikolas, J. M., Franzen, S., and Feldheim, D. (2003) Critical flocculation concentrations, binding isotherms, and ligand exchange properties of peptide-modified gold nanoparticles studied by UV-visible, fluorescence, and time-correlated single photon counting spectroscopies. *Anal. Chem.* **75,** 5797–5805.
13. Deroe, C., Courtoy, P. J., and Baudhuin, P. (1987) A model of protein colloidal gold interactions. *J. Histochem. Cytochem.* **35,** 1191–1198.
14. Horisberger, M. and Clerc, M. F. (1985) Labeling of colloidal gold with protein A: a quantitative study. *Histochemistry* **82,** 219–223.
15. Cao, Y., Jin, R., and Mirkin, C. A. (2001) DNA-modified core-shell Ag/Au nanoparticles. *J. Am. Chem. Soc.* **123,** 7961–7962.
16. Haes, A. and Van Duyne, R. (2002) A nanoscale optical biosensor: sensitivity and selectivity of an approach based on the localized surface plasmon resonance spectroscopy af triangular silver nanoparticles. *J. Am. Chem. Soc.* **124,** 10,596–10,604.
17. Tkachenko, A. G., Xie, H., Yanli, L., Coleman, D., Ryan, J., Glomm, W., Shipton, M., Franzen, S., and Feldheim, D. L. (2004) Cellular trajectories of peptide-modified gold particle complexes: comparison of nuclear localization signals and peptide transduction domains. *Bioconj. Chem.* **15,** 482–490.
18. Inoue, S. (1981) Video image processing greatly enhances contrast, quality and speed in polarization-based microscopy. *J. Cell Biol.* **89,** 346–356.
19. Inoue, S. and Spring, K. (1997) *Video Microscopy, The Fundamentals*, 2nd ed., Plenum, New York.
20. Hoefsmit, E., Korn, C., Bliliven, N., and Ploem, J. (1986) Light microscopical detection of single 5 and 20 nm particles used for immunolabelling of plasma membrane antigens with silver enhancement and reflection contrast. *J. Microsc.* **143,** 161–169.
21. De Waele, M. (1989) Silver-enhanced colloidal gold for the detection of leucocyte cell surface antigens in dark-field and epipolarization microscopy, in *Colloidal Gold: Principles, Methods, and Applications*, vol. 2 (Hayat, M. A., ed.), Academic, New York, pp. 443–467.
22. De Brabander, M., Geerts, H., Nuyens, R., Nuydens, R., and Cornelissen, F. (1993) Nanovid microscopy: imaging and quantification of colloidal gold labels in living cells, in *Electronic Light Microscopy: Techniques in Modern Biomedical Microscopy* (Shotton, D., ed.), Wiley-Liss, New York, pp. 141–155.
23. Albrecht, M. and Hodges, G., eds. (1988) *Biotechnology and Bioapplications of Colloidal Gold*, Scanning Microscopy International, Chicago, IL.
24. Ellis, I., Bell, J., and Bancroft, J. (1989) Polarized incident light microscopical enhancement of immunogold and immunogold-silver preparations: its role in immunohistology. *J. Pathol.* **159,** 13–16.

25. De Brabander, M., Geerts, H., Nuydens, R., Geuens, S., Moeremans, M., and De Mey, J. R. (1989) Detection and use of gold probes with video-enhanced contrast light microscopy, in *Immuno-Gold Labeling in Cell Biology* (Verklej, A. J. and Leunissen, J. L. M., eds.), CRC Press, Boca Raton, FL, pp. 217–222.
26. Hunter, R. J. (2001) *Foundations of Colloid Science*, 2nd ed., Oxford University Press, Oxford, UK.
27. Udenfriend, S., Stein, S., Buhlen, P., Dairman, W., Leimgruber, W., and Weigele, M. (1972) Fluorescamine: a reagent for assay of amino acids, peptides, proteins, and primary amines in the picomole range. *Science* **178,** 871–872.

8

Whole-Blood Immunoassay Facilitated by Gold Nanoshell–Conjugate Antibodies

Lee R. Hirsch, Naomi J. Halas, and Jennifer L. West

Summary

In this chapter, we outline a simple procedure using gold nanoshells as a substrate for an immunoassay that is capable of detecting subnanogram levels of analyte within whole blood on the order of minutes. Unique to metallic nanoshells is their optical tunability over a large range of wavelengths. We describe the design of nanoshells that attenuate light strongly in a region of light where blood does not (i.e., the near infrared [IR]), permitting optical detection of nanoshells in whole blood. We also describe a procedure to monitor the analyte-induced aggregation of antibody-conjugated nanoshells in whole blood using near-IR light. The immunoassay is fast and specific, requires no separation/purification steps, is simple to perform (mix and sit), and uses common laboratory equipment for detection (spectrophotometer). Preparation of the antibody-nanoshell conjugates is described, along with the design and optimization of the whole-blood nanoshell-based immunoassay system.

Key Words

Nanoshells; immunoassay; whole blood; silica cores; gold colloid.

1. Introduction

We describe a procedure using metal nanoshell technology for a new immunoassay capable of detecting analyte in whole blood with minimal sample preparation that is completed on the order of minutes ***(1)***. To date, there are very few homogeneous immunoassays capable of performing in whole blood. Existing methods often employ the agglutination of sensitized erythrocytes, which, although effective, are limited in scope owing to the difficulty of sensitizing erythrocytes. The method described herein is simple; is capable of incorporating a variety of antibody/analyte pairs; and could be extended into areas

From: *Methods in Molecular Biology, vol. 303: NanoBiotechnology Protocols*
Edited by: S. J. Rosenthal and D. W. Wright © Humana Press Inc., Totowa, NJ

such as public health or point-of-care applications where there is a strong demand for the rapid, high-throughput screening of blood-borne species.

Silica-gold nanoshells are a subclass of a larger family of metal nanoshells that consist of layered, spherical nanoparticles possessing a dielectric core (silica) surrounded by a thin metal shell (gold) ***(2)***. These nanoparticles possess a plasmon resonance that gives rise to intense optical absorption and scattering. The unique property of nanoshells is that their plasmon resonance—also their absorption resonance—is tuned by changing the relative dimensions of the core and shell, permitting peak optical extinctions spanning the visible to the mid-infrared (IR) region of the spectrum ***(3)***. The application outlined in this chapter hinges on the ability to fabricate nanoshells with intense attenuation in the near-IR (700–1300 nm), a region of light where blood provides strong optical transmission owing to its deficiency of near-IR chromophores. This situation permits the photometric detection of nanoshells in whole blood.

Development of the immunoassay begins with assembly of antibodies onto the nanoshell surfaces, forming antibody-nanoshell immunoconjugates. Then, in a manner similar to latex particle agglutination, nanoshell conjugates are placed in an analyte-containing solution, where multiple particles bind to the multivalent analyte, causing agglutination of the particles. However, unlike latex particles, the optical resonance of nanoshells is strongly modified by an additional optical absorption at longer wavelengths just as aggregation commences. This phenomenon leads to a reduction in the original near-IR extinction of the nanoshell solution (**Fig. 1**). We have reported that, over the appropriate concentration ranges, analyte induces aggregation of the particles in a concentration-dependent fashion, leading to a concentration dependent reduction in near-IR extinction, observable by photometry ***(1)***. This method provides an easy immunoassay; simply mix the nanoshell immunoconjugates with the blood sample, let them sit, and measure the extinction. A sensitive and quantitative assay is possible in approx 5 min.

2. Materials

1. Tetrakis(hydroxymethyl)phosphonium chloride (THPC) (Aldrich).
2. Chloroauric acid ($HAuCl_4$) (Aldrich).
3. Tetraethyl orthosilicate (TEOS) (Aldrich).
4. Polystyrene particles (1 μm) (2 wt%) (Aldrich).
5. Formaldehyde.
6. Antibody (analyte specific, free of stabilizing proteins, stored in amine-free buffer).
7. Analyte standards.
8. Whole-blood specimen (heparinized, 10 U/mL).
9. Whole-blood standard (heparinized, 10 U/mL, analyte free).
10. Silica-gold nanoshells (720-nm resonant, 156-nm total diameter).

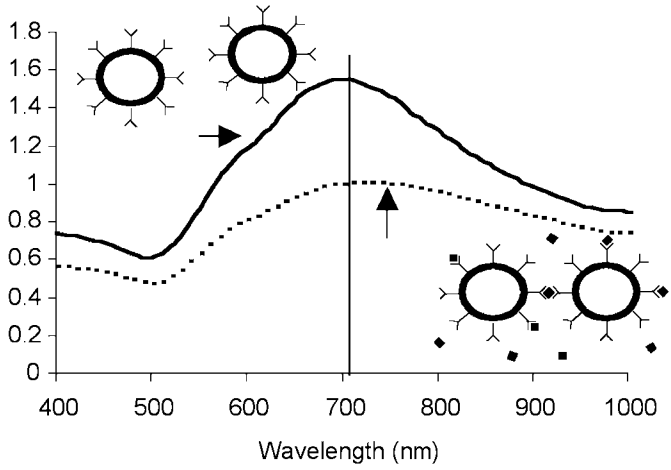

Fig. 1. Well-dispersed antibody-nanoshell conjugates in the absence of analyte possess a well-defined extinction peak in the near-IR. In the presence of the complementary analyte, multiple nanoshells bind to the analyte, causing agglutination and a corresponding reduction in the extinction peak.

11. Deionized (DI) water, 18.2 mΩ-cm purity.
12. 2-Iminothiolane (Traut's Reagent; Sigma, St. Louis, MO).
13. 5,5′-Dithio-*bis*(2-nitrobenzoic acid) (Ellman's Reagent; Sigma).
14. Polyethylene glycol (PEG)-amine (mol wt = 5000; Shearwater Polymers).
15. Dialysis membrane (500 mol wt cutoff; Spectrum).
16. Orthopyridyl disulfide-polyethylene glycol-*N*-hydroxysuccinimide (OPSS-PEG-NHS) (mol wt = 2000; Shearwater Polymers).
17. 100 m*M* Phosphate-buffered saline (PBS) (pH 7.4).
18. 1.8 m*M* Potassium carbonate buffer.
19. 10 m*M* Sodium bicarbonate buffer (pH 8.5).
20. Lysis buffer: 8 mg/mL HEPES, 26.7 mg/mL NaCl, 4.4 mg/mL EDTA, 72 mg/mL β-glycerophosphate, 6.7% Triton X.
21. X10 Protease inhibitor cocktail (Sigma).

3. Methods

3.1. Fabrication of Silica-Gold Nanoshells

The following protocol describes the fabrication of a 720-nm resonant silica-gold nanoshell with a 106-nm-diameter core and a 25-nm-thick gold shell using methods outlined by Oldenberg et al. ***(3)*** (*see* **Note 1**). The procedure begins with the growth of the silica cores. The silica particles are then functionalized with amine groups so that when the aminated particles are placed in a gold colloid solution, the colloid adsorbs to the aminated silica surface. The

gold colloid serves as nucleation sites for further electroless plating of gold. During this procedure, the gold colloid grows on the silica surface. Eventually, the gold particles begin to coalesce, forming a complete metal shell. Although this fabrication step is somewhat involved, a batch of nanoshells and its precursors are stable in solution for months, if not years, and therefore do not require recurrent synthesis. However, if desired, this step can be averted; the nanoparticles may be purchased from Nanospectra, L.L.C., Houston, TX.

3.1.1. Growth of Gold Colloid

Growth of gold colloid is performed using the method of Duff and Baiker ***(4)***. Because it must be done at least 3 wk in advance of nanoshell growth, it should be performed first.

1. In a clean 250-mL beaker, add 180 mL of DI water and 1.2 mL of 1 *M* NaOH.
2. In a separate container, make a stock solution of 400 µL of THPC in 33 mL of DI water.
3. Add 4 mL of this THPC solution to the NaOH. Stir the NaOH and THPC for 5 min.
4. Prepare a solution of 1% $HAuCl_4$. The solution must age at least 3 d.
5. To the NaOH/THPC solution, quickly add 6.75 mL of the $HAuCl_4$ under rapid vortexing. The color should instantly change to a light/midbrown. Age for 3 wk at 2–4°C. Before use the colloid needs to be concentrated 10- to 20-fold using a rotovap. This can be done either before or after aging.

3.1.2. Growth of Silica Cores

Growth of the 106-nm silica cores is done via the Stöber method ***(5)***, in which TEOS (Aldrich) is reduced in NH_4OH in ethanol. This procedure is moisture sensitive and, for best results, should be done under inert gas.

1. In a 50-mL beaker, mix 45 mL of ethanol with 2.8 mL of concentrated NH_4OH (14.8 *N*).
2. While vortexing, add 1.5 mL of TEOS. React for at least 8 h.
3. Size the particles via electron microscopy. For this application, nanoshells should possess a diameter of 106 ± 10 nm or better (*see* **Notes 2** and **3**).

3.1.3. Amination of Silica Cores

The silica cores must be functionalized with amine groups (aminated) to serve as adsorption sites for the gold colloid. Amine groups are incorporated onto the silica surface using aminopropyltriethoxy silane (APTES) as described next.

1. While vortexing the silica solution from **Subheading 3.1.2.**, add 126 µL of APTES. This is enough APTES to assemble 10 monolayers onto the particles.
2. Let react for at least 8 h.

3.1.4. Rinsing of Cores

1. Boil the aminated cores for 2 h, adding additional ethanol as necessary to maintain a 50-mL volume.
2. Centrifuge the cores at 2000*g* for 30 min. Discard the supernatant and resuspend the pellet in 50 mL of ethanol using probe sonication for at least 5 min.
3. Repeat **step 2** two more times but resuspend the aminated cores to a total volume of 10 mL during the last centrifugation (instead of 50 mL).

3.1.5. Coating of Cores With Gold Colloid

1. Determine the final concentration of aminated silica cores using the EM latex technique as follows. Mix silica particles with 1-µm polystyrene particles in DI water. Using a hemacytometer, count the polystyrene microparticle concentration in the mixture. Using scanning electron microscopy, measure the ratio of aminated cores to microparticles. Determine the aminated particle concentration by multiplying the microparticle concentration by (aminated particles/microparticles). Record the silica concentration.
2. In a 50-mL centrifuge tube, add 1×10^{12} aminated cores in ethanol.
3. Add excess gold colloid to the aminated particles. To determine the amount needed, calculate the amount of gold colloid needed to cover >150% of the silica particle surface area. For 3 nm of gold colloid, this would be $>7.5 \times 10^{15}$ particles. If the colloid were concentrated 10-fold in **Subheading 3.1.1.**, then the concentration would be about 7.5×10^{15}/mL. In this case, one would add at least 1.0 mL of gold colloid to the solution in **step 1**. Mix thoroughly. React for at least 8 h.
4. Remove excess gold colloid by first suspending the solution to 40 mL in DI water, then centrifuging at 2000*g* for 30 min. Discard the supernatant, and resuspend via probe ultrasound into 40 mL of DI water. Repeat two more times.

3.1.6. Growth of Nanoshells

1. At least 16 h prior to growth of nanoshells, prepare 200 mL of 1.8 m*M* K_2CO_3 supplemented with 3 mL of 1% $HAuCl_4$.
2. In ultraviolet-visible (UV-vis) cuvets, mix the $HAuCL_4$ from **step 1** and the silica-gold colloid suspension (**step 4** in **Subheading 3.1.5.**) at different volumetric ratios of $HAuCl_4$:silica-gold colloid (e.g., 20:1, 10:1, 5:1).
3. Add 20 µL of 30% formaldehyde to each solution. Mix thoroughly. Solutions should change color from a light red to a blue/green. The reaction should reach completion after 5–10 min.
4. Record the ratio of $HAuCl_4$:silica-gold colloid that grows a nanoshell with a peak extinction at 720 nm (*see* **Fig. 1**).
5. In a clean beaker, scale up the ratio from **step 2** to make 200 mL of nanoshells.
6. After growth, centrifuge the nanoshells once at 650*g* for 12 min. Discard the supernatant and resuspend in a solution of 1.8 m*M* K_2CO_3 at a concentration that provides an equivalent absorbance of 12.0 at 720 n*M* with a 1.0-cm path length (A^{720}) (*see* **Note 4**).

3.2. Binding of Antibodies to PEG Tethers

Antibodies are tethered to nanoshell surfaces using PEG linkers (*see* **Note 5**). These linkers are a heterobifunctional PEG compound. On one end of the PEG is an NHS that is used to couple the PEG to the antibody's amine residues, forming an amide linkage. On the other end is an OPSS whose sulfur groups bind strongly to the gold surface of the nanoshell. The use of PEG linkers serves two purposes: (1) it provides an easy method of self-assembly of antibodies onto the gold surface, for the gold-sulfide bond is much stronger than the electrostatic forces that drive protein-gold chemisorption; and (2) it helps lift the antibody off of the surface, permitting greater conformational freedom of the molecule and therefore improving antibody binding. All preparations and procedures in this section should be performed on ice.

1. Suspend antibody in 10 m*M* sodium bicarbonate (pH 8.5) at a concentration between 1 and 10 mg/mL. Antibody solution should be free of stabilizing proteins (i.e., no bovine serum albumin or other serum proteins). Additional protein will compete for binding sites onto the gold nanoshell surface and reduce the surface density of antibody on the antibody-nanoshell conjugates.
2. Prepare OPSS-PEG-NHS at a 10-fold excess concentration of the antibody in 10 m*M* sodium bicarbonate (average mol wt of IgG is ~150,000). Beware that NHS groups have a very short half-life (~20 min) in an aqueous environment and, thus, should be reacted with the antibody as quickly as possible on suspending in buffer.
3. Add 1 part OPSS-PEG-NHS to 9 parts antibody. Vortex, and let sit for >2 h.
4. Store OPSS-PEG-antibody in frozen working aliquots.

3.3. Synthesis of PEG-Thiol

PEG-thiol (PEG-SH) is a linear chain molecule capable of assembling into a densely packed monolayer on the gold nanoshell surface via the thiol residue. By occupying any remnant sites on the nanoshell surface left unoccupied by OPSS-PEG-antibody, this molecule helps both to deter nonspecific protein adsorption onto the metal surface and to stabilize sterically the nanoshells in a complex saline environment such as whole blood. Although PEG-SH is commercially available, this compound can be made from a PEG-amine precursor using simple chemistry at a considerably lower cost (*see* **Note 6**).

1. Prepare a 1 m*M* PEG-amine solution in 100 m*M* PBS.
2. Prepare Traut's Reagent at 10 m*M* in DI.
3. Mix equal parts of PEG-amine and Traut's Reagent.
4. Vortex, and react for 1 h at room temperature.
5. Dialyze the product against DI water for at least 2 h using a dialysis membrane with a molecular weight cutoff between 500 and 1000. The dialysate should be changed at least three times. Store produce in frozen aliquots at less than 0°C.

3.4. Fabrication of Antibody-Nanoshell Conjugates

Fabrication of antibody-nanoshell conjugates involves two steps: (1) determining the optimal concentration of PEG-SH necessary to stabilize sterically nanoshells in a saline environment, and (2) assembly of OPSS-PEG-antibody onto the nanoshells at the optimal concentration.

3.4.1. Determining Optimal PEG-SH Concentration to Stabilize Nanoshells in Saline

1. Serially dilute the PEG-SH prepared in **Subheading 3.3.** over a range of 1:1–1:1000 in DI water.
2. In a standard 1-cm UV-vis cuvet, add 50 µL of each PEG-SH dilution to 450 µL of nanoshells from **Subheading 3.1.6.**
3. Make two additional control samples that contain 50 µL of DI water and 450 µL of nanoshells. Mix all samples thoroughly and let sit for 1 h.
4. Add 55 µL of 10% NaCl to each sample from **step 2**, and to one of the samples in **step 3**. To the other sample in **step 3**, add 55 µL of DI water. Let sit for 30 min. The NaCl will aggregrate nanoshells possessing insufficient quantities of the sterically stabilizing PEG-SH.
5. Add an additional 3.0 mL of DI water to each sample. Mix well and record the A^{720}.
6. Report the data as the percentage decrease in absorbance from the control in **step 4** possessing no NaCl and no PEG-SH. On examining the results, there should be a PEG-SH threshold concentration at which a reduction in PEG-SH results in a dramatic decrease in absorbance. This is the cutoff concentration below which the PEG-SH is too low to stabilize the nanoshells (*see* **Note 7**). Hence, the optimal concentration for PEG-SH stabilization is the concentration just above this threshold that stabilizes the nanoshells in NaCl. Record this value.

3.4.2. Assembly of OPSS-PEG-Antibody Onto Nanoshells

For a given concentration of analyte and nanoshells, there is an optimal concentration of antibody on the nanoshells that will promote aggregation in a concentration-dependent fashion. It is the purpose of this section to determine that optimal value.

1. Prepare different concentrations of PEG-antibody in DI water, ranging between 100 and 1 µg/mL (e.g., 100, 50, 10, 5, 1 µg/mL).
2. For each concentration of PEG-antibody, add 200 µL of antibody to 1.8 mL of nanoshell solution. Vortex. One hour is sufficient time for completion of antibody-nanoshell conjugation.
3. To each sample in **step 2**, add 222 µL of PEG-SH at the optimal concentration determined in **step 6** of **Subheading 3.4.1.**
4. Prepare the analyte standard solutions. These solutions should be prepared over a concentration range that spans the expected concentration range of the unknown

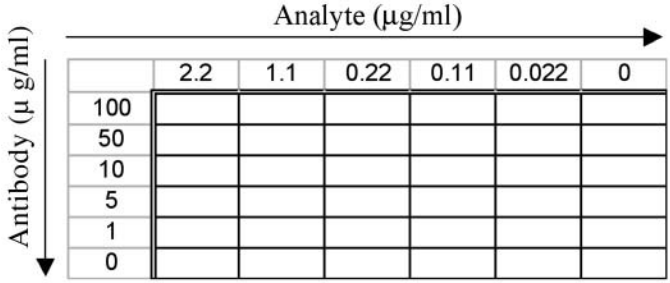

Fig. 2. Diagram of 2D matrix for determining optimal antibody and analyte concentration for maximal agglutination.

samples. For instructional purposes, suppose that the physiological range of interest for the analyte under investigation is 2.2–0.022 µg/mL. A reasonable range of standards would then be 2.2, 1.1, 0.22, 0.11, 0.022, and 0 µg/mL in 100 m*M* PBS. This will be the range used throughout the rest of the protocol.

5. Set up a two-dimensional (2D) matrix of cuvets, such that there is a a cuvet for each antibody-nanoshell and analyte pair (*see* **Fig. 2** and **Note 8**).
6. In each row, add 252 µL of nanoshells at the appropriate antibody concentration as outlined in **step 5**.
7. Add 420 µL PBS to each cuvet. This step places the antibody-nanoshell conjugates in a physiological buffer, a step that is necessary to promote optimal antibody activity. Doing so prior to assembly of OPSS-PEG-antibody and PEG-SH would cause premature aggregation of the particles.
8. Record the A^{720} for each cuvet. This is the absorbance at $t = 0$.
9. Add 28 µL of analyte of appropriate concentration to each sample in the matrix, paying careful attention to the time when the analyte was added to each sample.
10. Record the decrease in absorbance over time (e.g., 10, 30, 60 min).
11. By plotting the percentage decrease in absorbance from $t = 0$, there should be an optimal antibody concentration and time point that provides a quantitative, log-linear reduction in absorbance over the concentration range of interest. Record this concentration and the elapsed time.

3.5. Whole-Blood Immunoassay

After optimization of the assay in saline, the system is ready to be performed in whole blood. This assay is very similar in design to the saline assay performed in **Subheading 3.4.**, with a few minor adjustments of volume and time that are necessary because the whole-blood specimens already contain the analyte and are not spiked (*see* **Note 9**).

3.5.1. Preparation of Reagents and Samples

The optimal preparation of antibody-nanoshell conjugate was determined in **Subheading 3.4.2.** The same preparation is used in the whole-blood assay;

steps 1 and **2** from **Subheading 3.4.3.** therefore need to be repeated and scaled up. To determine the degree of scale-up, consider that assaying one blood sample will require about 3 mL of nanoshells (this includes all standards and controls). Suppose that only one blood sample requires analysis. This would require 3 mL of nanoshells/assay × 1 assay = 3 mL of antibody-nanoshells. The original protocol outlined in **steps 2** and **3** from **Subheading 3.4.2.** makes 2.222 mL of antibody-nanoshells. Therefore, a scale-up of twofold would prepare sufficient amounts of conjugate (4.444 mL).

1. In 100 m*M* PBS, serially dilute a standard solution of analyte, spanning the range of interest for the assay (e.g., 2.2, 1.1, 0.22, 0.11, 0.022, 0 μg/mL). This is the same preparation as that in **step 4** of **Subheading 3.4.2.**
2. Collect the blood. This procedure requires two blood specimens. In tube 1, collect the analyte-free sample of blood for the standards, and in tube 2 collect the patient's specimen containing analyte of unknown concentration. Both samples should be freshly drawn and heparinized (10 U/mL).
3. Prepare lysis buffer working solution by mixing 1.5 mL of lysis buffer with 1.0 mL of protease inhibitor cocktail.
4. Lyse both the analyte-free blood and the blood specimen by mixing 3.75 mL of the whole blood from **step 3** with 1.25 mL of lysis buffer working solution. Vortex until the blood is completely lysed, changing from a turbid solution to a clear red (about 1 min). After lysis, add an additional 6.25 mL of 100 m*M* PBS to each blood specimen.

3.5.2. Running of Standards

1. Zero the spectrometer using a solution of 280 μL of PBS and 420 μL of blood lysate from tube 1.
2. Set up 1 cuvet for each standard. To each of these, add 252 μL of nanoshells and 420 μL of the blood lysate from tube 1.
3. Add 28 μL of the corresponding standard to each cuvet. Mix thoroughly.
4. Measure the A^{720} precisely 20 s after mixing each sample. Then record the A^{720} at the optimal time of completion, as determined in **step 11** from **Subheading 3.4.2.**

3.5.3. Running of Samples

1. Zero the spectrometer using a solution of 280 μL of PBS and 420 μL of blood lysate from tube 2.
2. For each sample, add 420 μL of blood lysate from tube 2 to a cuvet containing 28 μL of PBS. This should be done in triplicate ($n = 3$).
3. Add 252 μL of nanoshells to each cuvet. Measure the A^{720} precisely 20 s after mixing each sample. Then record the A^{720} at the optimal time of completion, as determined in **step 11** of **Subheading 3.4.2.**

3.5.4. Analysis

1. Prior to setting up a standard curve from the data in **Subheading 3.5.2.**, divide all standard concentrations by 5 (i.e., 2.2, 1.1, . . . μg/mL now becomes 0.44,

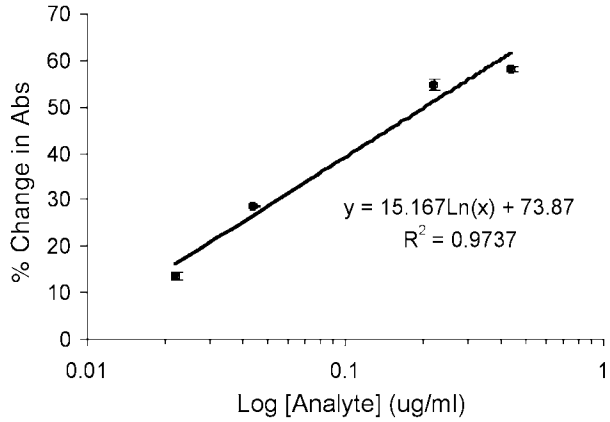

Fig. 3. Standard curve depicting log-linear behavior of antibody-nanoshell agglutination in presence of analyte.

0.22, . . .). Doing so accounts for the dilutions and volumes used in this study. The standard data now represents the original concentration of analyte in the 100% whole-blood specimen.
2. Fit a logarithmic curve to the data in **Subheading 3.5.2.** (*see* **Fig. 3**).
3. Using this trend, extrapolate the original sample concentrations in **Subheading 3.5.3.**

4. Notes

1. Although these particles are resonant at 720 n*M* and perform well in whole blood, nanoshells with resonances anywhere between 700 and 900 n*M* should also perform well in whole blood.
2. This protocol outlines one specific recipe for a 106-n*M* core; however, a core diameter ranging anywhere between 95 and 110 n*M* would suffice. What is more important is that the particles be monodisperse; that is, their standard deviation should be <10% of the particle diameter.
3. Results from this procedure are highly sensitive to reagent volumes. Increasing amounts of either NH_4OH or TEOS typically produce larger particles. In addition, improved results can be achived if the TEOS is distilled prior to reacting.
4. Most UV-vis spectrometers are incapable of detecting an absorbance beyond 2.0. To make this measurement, a fraction of the solution is removed and diluted 10-fold prior to measurement. The stock solution concentration is then adjusted until the 10-fold dilution reads 1.2.
5. When choosing the appropriate antibody for this assay, one needs to be mindful of whether the antibody is polyclonal or monoclonal. Although monoclonal antibodies (MAbs) are typically more specific, they only bind to one epitope. Hence, two separate MAbs will have to be used, with each binding to a separate epitope on the analyte. Using a polyclonal antibody, however, requires only one preparation.

6. A number of different molecular weight PEG compounds have been examined to assess nanoshell stability in a saline environment. Studies to date have shown that PEG with a mol wt of <5000 fails to stabilize the nanoparticles. Although larger PEG compounds (10,000 and 20,000) also stabilize the nanoshells, they are not recommended for this application. Larger PEG chains will sterically deter antibody-antigen binding on the nanoshell surface.
7. The use of excessive quantities can also promote nanoshell aggregation, a phenomenon that may be owing to steric exclusion forces.
8. This experiment is designed such that it can be performed in a standard 1-cm cuvet, which, although available in most laboratories, requires large volumes of sample and nanoshells. It should, however, be possible to perform this assay on a much smaller scale (on a 96-well tray perhaps), permitting rapid, high-throughput screening of multiple samples.
9. **Suheading 3.5.1., step 1** can be performed well in advance of the whole-blood immunoassay. Preliminary studies show that antibody-nanoshell conjugates can be stored for weeks with minimal loss of activity (in the absence of preservatives). The purchase of, or advance preparation of, the conjugates makes the remaining whole-blood assay (**Subheading 3.5.**) a simple technique capable of completion within 1 h.

Acknowledgments

We wish to thank the National Science Foundation, the MURI program administered by the Army Research Office, and the Robert. A. Welch Foundation for financial support.

References

1. Hirsch, L. R., Jackson, J. B., Lee, A., Halas, N. J., and West, J. L. (2003) A whole blood immunoassay using gold nanoshells. *Anal. Chem.* **75,** 2377–2381.
2. Averitt, R. D., Sarkar, D., and Halas, N. J. (1997) Plasmon resonance shifts of Au-coated Au_2S nanoshells: insight into multicomponent nanoparticle growth. *Phys. Rev. Lett.* **78,** 4217–4220.
3. Oldenberg, S. J., Averitt, R. D., Westcott, S. L., and Halas, N. J. (1998) Nanoengineering of optical resonances. *Chem. Phys. Lett.* **288,** 243–247.
4. Duff, D. G., Baiker, A., and Edwards, P. P. (1993) A new hydrosol of gold clusters, 1: formation and particle size variation. *Langmuir* **9,** 2301–2309.
5. Stöber, W., Fink, A., and Bohn, E. (1968) Controlled growth of monodisperse silica spheres in the micron size range. *J. Coll. Interf. Sci.* **26,** 62–69.

9

Assays for Selection of Single-Chain Fragment Variable Recombinant Antibodies to Metal Nanoclusters

Jennifer Edl, Ray Mernaugh, and David W. Wright

Summary

The protocols herein describe colony-lift and fluorescent immunoassays that were used to identify bacterial colonies that produced single-chain fragment variable (ScFv) recombinant antibodies reactive with zero-state silver. A large (approx 2.9-billion member) phage-displayed antibody library was panned against zero valent silver. Bacterial colonies obtained after two rounds of selection were either lifted onto nitrocellulose filters or picked to individual wells of 384-well microtiter culture plates. Colonies lifted onto filters were placed onto zero valent silver-coated filters and induced to produce soluble ScFv antibodies. ScFv antibodies, expressed by individual colonies, that bound to silver nanocluster-coated filters were detected using an anti-ScFv antibody conjugated to horseradish peroxidase and a chemiluminescent substrate. Colonies picked to 384-well micotiter culture plates were induced to express soluble ScFv antibodies. ScFv antibodies in bacterial periplasmic extract were transferred from 384-well culture plates to 384-well assay plates containing zero-state silver particles and an anti-ScFv antibody conjugated to a fluorescent dye. ScFv antibodies, expressed by individual bacterial clones, that bound to zero valent silver nanoparticles in 384-well assay plates were detected using an FMAT 8100 fluorescent plate reader. The colony-lift and fluorescent immunoassays detected ScFv antibodies reactive with zero valent silver. Similar assay formats should also be useful to detect bacterially expressed recombinant antibodies or proteins to other nanoclusters.

Key Words

Single-chain fragment variable (ScFv); recombinant antibodies; horseradish peroxidase; Anti-E tag antibody; silver-coated membrane; nanoparticles.

1. Introduction

The design of readily programmable, structurally well-defined biological interfaces for inorganic materials represents a significant challenge toward realizing the promise of bionanotechnology. Encouraging approaches have used

From: *Methods in Molecular Biology, vol. 303: NanoBiotechnology Protocols*
Edited by: S. J. Rosenthal and D. W. Wright © Humana Press Inc., Totowa, NJ

oligonucleotide-functionalized nanoparticles ***(1)***, genetically engineered viruses ***(2–4)***, the iron-storage protein ferritin ***(5,6)***, and several classes of polypeptides inspired by naturally occurring biomineralization systems ***(7,8)***. Additionally, several reports have demonstrated the identification of effective nanoparticle-forming peptides via combinatorial means including phage display ***(9)***, rolling mutagenesis ***(10)***, and synthetic spatially addressable libraries ***(8)***.

Recombinant antibodies reactive with antigens, silver nanoparticles, and so on can be detected using a variety of different assays. The following protocols describe two such assays that were used to detect single-chain fragment variable (ScFv) recombinant antibodies reactive with silver nanoparticles. The "silver nanoparticles" used in these assays were actually aggregates of nanoparticles. Because the purpose of these assays was to detect ScFv antibodies reactive with zero-state silver metal free of any organic or inorganic surface-bound molecules, the particles were not treated with reagents to obtain true nanoparticles.

The ScFv recombinant antibodies used in the assays were cloned into the Amersham-Pharmacia pCANTAB5E phagemid expression vector to produce a recombinant phage antibody library that contained approx 2.9×10^9 members. The ScFv antibodies assayed were obtained from bacterial isolates that stemmed from two to three rounds of phage antibody library selection on silver nanoparticles. ScFv antibodies expressed by *Escherichia coli* using pCANTAB5E display a short peptide tag (E-tag) recognized by the Anti-E tag monoclonal antibody (MAb). The Anti-E tag MAb can be conjugated to or labeled with various reporter molecules such as horseradish peroxidase (HRP) or fluorescent dyes such as FMAT™ Blue Monofunctional Dye. The HRP- or dye-conjugated Anti-E tag antibody will bind to any E-tagged ScFv antibodies that interact with silver nanoparticles in an assay. The HRP conjugated to the Anti-E tag antibody can be used to catalyze a substrate reaction to produce a color- or light-emitting (chemiluminescent) signal that can be detected using a microtiter plate reader, film, or light-capturing device. The fluorescent dye conjugated to the Anti-E tag antibody can be detected with a fluorescence microtiter plate reader. If the HRP or dye reporter molecules are present when the assay is read, then the Anti-E MAb is bound to E-tagged ScFv antibodies that interact with silver nanoparticles.

In the colony-lift assay described in **Subheading 3.1.** (**Fig. 1**), bacterial colonies that contain and express E-tagged ScFv antibodies are placed onto nitrocellulose membranes and set on bacterial culture medium ***(11)***. The colony membranes are subsequently placed on top of a silver nanoparticle-coated membrane permeated with bacterial culture medium that induces bacterial ScFv expression. ScFv antibodies expressed by the bacterial colonies diffuse through the colony filters and onto the silver nanoparticle-coated membrane. After incubation, the silver nanoparticle-coated membrane is washed to remove unbound ScFv

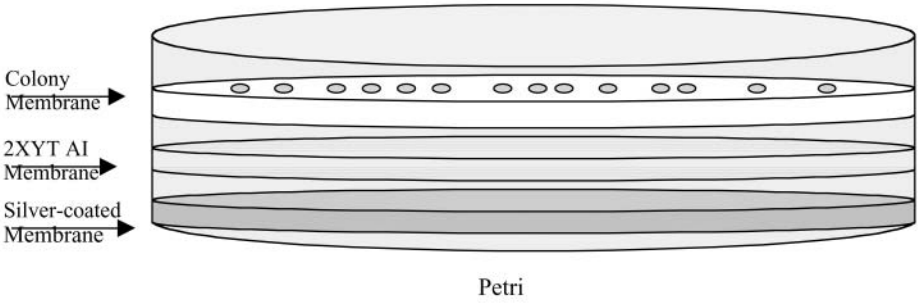

Fig. 1. Schematic diagram of a colony lift on silver-coated nitrocellulose. The silver-coated membrane is placed top side up on the bottom of a Petri dish followed by the 2XYT AI-moistened membrane and the colony-containing membrane.

antibodies and probed with Anti-E tag antibody conjugated with HRP (Anti-E/HRP). Unbound Anti-E/HRP is removed by washing. The membrane is then exposed to an HRP chemiluminescence substrate that emits a light signal that produces a black spot on photographic film wherever the Anti-E/HRP binds to ScFv antibodies that interact with silver nanoparticles. The colony-membrane and the photographic film can then be aligned to determine which bacterial colonies express ScFv antibodies reactive with silver nanoparticles.

The Applied Biosystems FMAT™ 8100 HTS System is a microtiter plate reader that uses a microscopic lens to focus on and detect a fluorescent signal present only on the bottom of a well in a microtiter plate. In the assay described in **Subheading 3.2.**, the silver nanoparticles are combined in a microtiter well with Anti-E antibody conjugated to FMAT Blue and ScFv antibodies in bacterial culture medium. The silver nanoparticles settle to the bottom of the well on incubation. The FMAT 8100 is then used to detect FMAT Blue Anti-E bound to ScFv antibodies that have interacted with silver nanoparticles present on the bottom of the microtiter wells.

2. Materials

1. 2XYT bacterial broth culture medium: Dissolve 5 g of NaCl, 10 g of Bacto™ Yeast Extract, and 17 g of Bacto™ Tryptone in 1 L of double-deionized water. Filter the medium into sterile disposable plastic bottles using a peristaltic pump and a 0.2-µm filter device. The medium can be stored at room temperature for 6–12 mo.
2. 2XYT AG agar medium: Add 15 g of granulated agar to 1 L of bacterial culture medium in a 2-L Erlenmeyer flask. Autoclave at 121°C, 15 psi for 15 min to dissolve the agar. Allow the agar medium to cool to 45°C. Add 20 g of D(+)-glucose and 100 mg of ampicillan and mix. Pour approx 30 mL of agar medium into each of 30 sterile 150 × 15 mm plastic Petri dish. Allow the agar medium to cool

overnight, and store at 4°C until needed in a closed plastic bag or container. Plates can be stored at 4°C for 1 mo.

3. 2XYT AI medium: Add 100 mg of filter-sterilized ampicillin and 238.31 mg of filter-sterilized isopropyl-β-D-thiogalactoside to 1 L of sterile bacterial culture medium. Store at 4°C until needed. The medium can be stored at 4°C for 1 mo.
4. 2XYT AG with glycerol: Add 16 mL of a 50% (v/v) filtered glycerol solution to 34 mL of 2XYT AG, mix, and then store at 4°C. This medium can be stored at 4°C for 1 mo.
5. 1X TES: To a 1-L graduated cylinder add 171.15 g of sucrose; 200 mL of 1 *M* Tris, pH 8.0; and 1 mL of 0.5 *M* EDTA. Add double-distilled deionized water to 1 L, and then mix. To prepare 1/5X TES, add 200 mL of 1X TES and 800 mL of double-deinonized water to a 1-L graduated cylinder and mix. Filter-sterilize 1X TES and 1/5X TES using a 0.2-µm filter unit. Store at 4°C.
6. Phosphate-buffered saline (PBS): To a 1-L graduated cylinder, add 1.44 g of sodium phosphate dibasic anhydrous, 8 g of sodium chloride, 0.2 g of potassium chloride, and 0.24 g of potassium phosphate. Add double-distilled deionized water to 1 L, and then mix to dissolve.
7. 0.1% Tween in PBS (PBS/T): Add 1 mL of polyoxyethylene-sorbitan monolaurate (Tween-20, Sigma cat. no. P-7949, St. Louis, MO) to 1 L of PBS and mix.
8. 0.1 *N* Nitric acid in double-deionized water.
9. Silver, nanosize-activated powder (Aldrich cat. no. 48,405-9).
10. HRP/Anti-E tag conjugate (Amersham cat. no. 27-9413-01).
11. FMAT Blue Monofunctional Dye/Anti-E tag conjugate. Prepare conjugate according to the manufacturer's instructions using the Anti-E Tag Antibody (Amersham cat. no. 27-9412-01) and an FMAT™ Blue Monofunctional Dye kit (Applied Biosystems cat. no. 432851).
12. 384-Well black, clear-bottomed microtiter plates for use with the FMAT 8100 HTS System (Applied Biosystems cat. no. 4315481).
13. 384-Well polystyrene plates.
14. 384-Pin polypropylene replicator.
15. Protran® pure nitrocellulose transfer and immobilization membranes (132-mm, 0.45-µm pore size) (Schleicher and Schuell cat. no. 10402525).
16. SuperSignal® West Pico Chemiluminescent Substrate (Pierce cat. no. 24080).
17. Scientific imaging film and cassette (8- × 10-in).
18. Required instrumentation: multichannel pipet, 30°C incubator, film developer, FMAT 8100 HTS System, and clinical centrifuge equipped with microtiter plate carriers.

3. Methods

3.1. Colony Lift

1. Day 1: Spread bacteria to obtain individual colonies to be assayed for ScFv activity on 2XYT AG plates (*see* **Note 1**). Invert the plates and incubate at 30°C overnight in a humidified container.

2. Day 2: Use a multichannel pipet to add 75 µL of 2XYT AG medium to each well of a Nunc 384-well plate.
3. Aseptically pick or transfer individual colonies from the 2XYT AG agar plates to individual wells of the 384-well plate containing 2XYT AG medium. Incubate the plate at 30°C overnight in a humidified container. This is the master plate.
4. Day 3: Use a pen or pencil to mark a 132-mm nitrocellulose membrane so that it can be oriented later on. The side of the membrane marked will be the top side of the membrane.
5. Use a 384-pin replicator to transfer a small amount of bacterial culture medium from each well of the 384-well master plate to the top side of the 132-mm nitrocellulose membrane. Wrap the 384-well master plate in plastic wrap and store at 4°C until needed.
6. Place the 132-mm membrane top side up onto a 2XYT AG agar plate and incubate at 37°C for 6 h.
7. Place a second 132-mm nitrocellulose membrane in PBS/T for 30 min. The Tween-20 in PBS/T will block the membrane and prevent proteins from sticking nonspecifically.
8. Remove the second nitrocellulose membrane from the PBS/T and allow to air-dry briefly. Place the dried membrane in a sterile 150-mm Petri dish, and moisten with 2XYT AI.
9. Drain excess 2XYT AI medium from the nitrocellulose membrane (AI membrane). The AI membrane will be used in **step 16**.
10. Weight out 10 mg of silver nanosize-activated powder and place in a sterile 15-mL conical centrifuge tube. Add 1 mL of 0.1 *N* nitric acid. Centrifuge the silver at full speed for 5 min. Decant and discard the nitric acid. Add 1 mL of double-deionized water and centrifuge at full speed for 5 min. Decant and discard the water. Add 1 mL of double-deionized water. Check the pH. If the pH is still acidic, repeat the wash steps with water until the pH is 5.0–8.0.
11. Dilute the silver from **step 11** in 2 mL of PBS to a final concentration of 10 µg/mL. Transfer the silver solution to a sterile Petri dish.
12. Using a pen or pencil, designate a third 132-mm nitrocellulose membrane as a silver-coated membrane.
13. Place the silver-coated membrane face or label-side down onto the silver solution in the Petri dish until moistened. Remove the membrane, invert, and let air-dry.
14. Place the silver-coated membrane in PBS/T for 30 min.
15. Remove the silver-coated membrane and allow to air-dry briefly. Place the silver-coated membrane label side up in a sterile Petri dish, and moisten with 2XYT AI.
16. Drain excess 2XYT AI medium from the silver-coated membrane, and place the AI membrane on top of the silver-coated membrane. Then place the colony membrane top side up (from **step 9**) on top of the AI membrane (*see* **Fig. 1**). Incubate the plate inverted in a humidified container at 30°C for 3 h (*see* **Note 3**).
17. Transfer the colony membrane to a fresh 2XYT AG plate. Store at 4°C. Discard the AI membrane.

18. Wash the silver-coated membrane with PBS/T using three 10-min washes. The silver-coated membrane can be wrapped in a plastic wrap and stored at 4°C overnight, if needed.
19. Dilute HRP/Anti-E tag conjugate 1:8000 in PBS/T. Incubate the silver-coated membrane in this solution for 1 h at room temperature with gentle shaking.
20. Wash the silver-coated membrane with PBS/T using three 10-min washes. Rinse the membrane for 10 s with double-deionized water.
21. Combine equal volumes of chemiluminescent peroxide solution and luminol/enhancer solution according to the manufacturer's instructions.
22. Place the washed membrane into the chemiluminescent substrate for 5 min. Place the silver-coated membrane top side up into a photographic film cassette and cover with plastic wrap. Place the photographic film onto the membrane for varying lengths of time (*see* **Note 4**). Then develop the film. Black areas on the film correspond to bacterial colonies that produce ScFv recombinant antibodies reactive with silver on the membrane (**Fig. 2**).
23. Align the photographic film and colony membrane from **step 18**.
24. Using a sterile pipet tip or toothpick, transfer individual bacterial colonies that give a positive black signal on the film to individual sterile centrifuge tubes containing 500 µL of 2XYT AG with glycerol. Store bacterial isolates as glycerol stocks at –70°C until needed.

3.2. FMAT™ Analysis

1. Add 100 µL of 2XYT AI to each well of a Nunc 384-well plate. This is the replica plate.
2. Dip a 384-pin replicator into the 384-well master plate (*see* **Subheading 3.1., step 3**), remove, and then place into the 384-well replica plate. Incubate the replica plate in a humidified container at 30°C overnight.
3. Centrifuge the replica plate at 500*g* for 10 min. Invert the replica plate over a biohazard bag and flick out the culture supernatant.
4. Using a multichannel pipet, add 40 µL of 1X TES to each well of the 384-well plate followed by 60 µL of 1/5X TES to each well of the plate. Incubate on ice for 1 h.
5. Prepare silver nanosize-activated powder as described in **Subheading 3.1., step 10**.
6. Dilute the silver to 10 µg/mL in PBS/T. Using a multichannel pipet, add 25 µL of diluted silver to each well of a 384-well clear-bottomed black plate (FMAT plate).
7. Using a multichannel pipet, transfer 25 µL of periplasmic extract (prepared in **step 4**) from each well of the 384-well replica plate to the corresponding wells of the FMAT plate.
8. Dilute FMAT Blue Monofunctional Dye/Anti E tag conjugate to 0.75 µg/mL in PBS/T. Using a multichannel pipet, add 25 µL of diluted antibody conjugate to each well of the FMAT plate.
9. Incubate the plate for 2.5 h at room temperature in the dark.
10. Use an FMAT 8100 HTS System to read the microtiter plate. The microtiter plate reader will detect the FMAT Blue Monofunctional Dye/Anti E tag conjugate bound to ScFv recombinant antibodies reactive with silver nanoparticles.

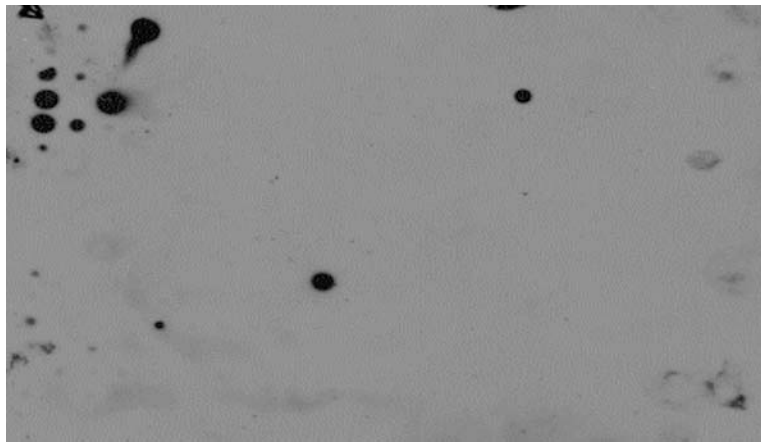

Fig. 2. Photographic film after development of a colony-lifted, silver-coated membrane. Black areas on the film correspond to bacterial colonies that produce ScFv recombinant antibodies reactive with silver on the membrane.

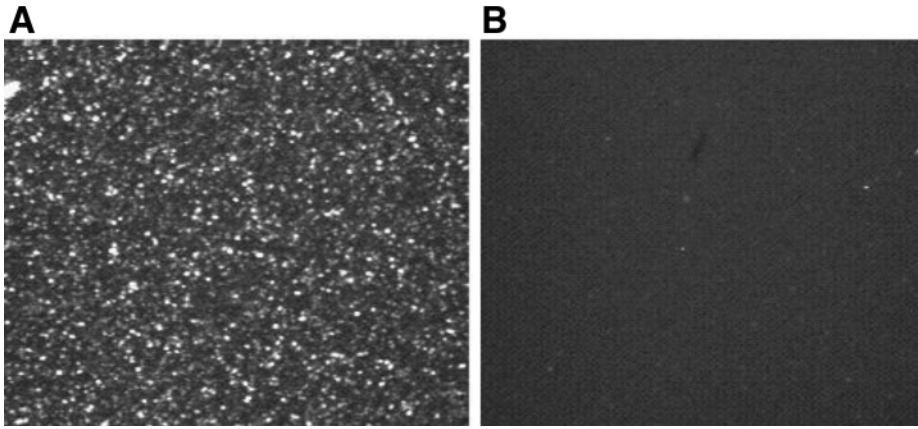

Fig. 3. FMAT results for ScFv on silver nanoparticles: **(A)** detail of ScFv M5, which reacted with silver nanoparticles; **(B)** detail of ScFv G1, which did not react with silver nanoparticles.

11. Based on FMAT analysis results, identify wells from the master plate containing bacterial clones that produce ScFv reactive with silver nanoparticles (**Fig. 3**).
12. Using a micropipet equipped with a sterile pipet tip, transfer 10–30 µL of bacterial culture from positive clones in the master plate to sterile centrifuge tubes containing 500 µL of 2XYT AG with glycerol, mix, and then store at –70°C as glycerol stocks until needed.

4. Notes

1. Multiple dilutions should be performed, since colony numbers will vary from one preparation to another.
2. A humidified container is prepared by lining a sealable plastic container with wet paper towels. Petri dishes, microtiter plates, and so on placed in the container will not dry out during incubation or storage.
3. An 18-gage needle should be used to punch holes through all membrane layers in order to line up the membranes in subsequent steps.
4. Depending on the sensitivity of the substrate and concentration of the ScFv antibodies, the photographic film exposure time will vary. It is best to start with 30 s, but film may need to be exposed for 5 min or longer.

References

1. Storhoff, J. J. and Mirkin, C. A. (1999) Programmed materials synthesis with DNA. *Chem. Rev.* **99,** 1849–1862.
2. Douglas, T. and Young, M. (1999) Virus particles as templates for materials synthesis. *Adv. Mater.* **11,** 679–681.
3. Lee, S. W., Mao, C., Flynn, C. E., and Belcher, A. M. (2002) Ordering of quantum dots using genetically engineered viruses. *Nano. Lett.* **296,** 892–895.
4. Douglas, T., Strable, E., Willits, D., Aitouchen, A., Liberia, M., and Young, M. (2002) Protein engineering of a viral cage for constrained nanomaterials synthesis. *Adv. Mater.* **14,** 415–418.
5. Douglas, T. and Stark, V. (2000) Nanophase cobalt oxyhydroxide mineral synthesized within the protein cage of ferritin. *Inorg. Chem.* **39,** 1828–1830.
6. Mark, A., Willits, D., Mosolf, J., Young M., and Douglas, T. (2002) Protein cage constrained synthesis of ferromagnetic iron oxide nanoparticles. *Adv. Mater.* **14,** 1562–1565.
7. Weiner, S. and Addadi, L. (1997) Design strategies in mineralized biological materials. *J. Mater. Chem.* **7,** 689–702.
8. Spreitzer, G., Whitling, J. M., Madura, J. D., and Wright, D. W. (2000) Peptide encapsulated CdS nanoclusters from a combinatorial ligand library. *J. Chem. Soc. Chem. Commun.* **209,** 210.
9. Whaley, S. R., English, D. S., Hu, E. L., Barbara, P. F., and Belcher, A. M. (2000) Selection of peptides with semiconductor binding specificity for directed nanocrystal assembly. *Nature* **405,** 665–668.
10. Brown, S., Sarikaya, M., and Johnson, E. (2000) A genetic analysis of crystal growth. *J. Mol. Biol.* **299,** 725–735.
11. Rodenburg, C. M., Mernaugh, R. L., Bilbao, G., and Khazaeli, M. B. (1998) Production of a single chain anti-CEA antibody from the hybridoma cell line T84.66 using a modified colony-lift selection procedure to detect antigen-positive ScFv bacterial clones. *Hybridoma* **17,** 1–8.

10

Surface-Functionalized Nanoparticles for Controlled Drug Delivery

Sung-Wook Choi, Woo-Sik Kim, and Jung-Hyun Kim

Summary

Nanoparticles have been extensively investigated in drug-delivery systems. Especially, the effectiveness of the surface-functionalized nanoparticles, which consist of copolymers with functional molecules, is well demonstrated. This chapter describes the complete technique for the preparation of surface-functionalized nanoparticles. Tetracycline with an affinity to bone was chosen as a model material for surface functionalization. There are two steps for the preparation of tetracycline-modified nanoparticles. The first step is the conjugation of poly(D,L-lactide-co-glycolic acid) with tetracycline via carbodiimide chemistry and is the most often employed. Three kinds of techniques—the emulsification-diffusion method, nanoprecipitation, and the dialysis method—are used for nanoparticle formation of the resulting copolymer. Prepared nanoparticles having a size <200 nm and a hydrophilic surface layer can be applied for bone-specific drug delivery.

Key Words

Surface-functionalized nanoparticles; carbodiimide chemistry; poly(D,L-lactide-co-glycolic acid); tetracycline; emulsification-diffusion method; nanoprecipitation method; dialysis method; bone-specific drug delivery.

1. Introduction

Well-designed functional nanoparticles are of great interest for drug-delivery systems. Functional nanoparticles suitable for biomedical applications are defined as polymeric particles with submicron size having the characteristics of protective ability of encapsulated therapeutic agents, avoidance of the reticuloendothelial system, long circulation time in the body, and site-specific delivery with the targeting moiety. The size of the nanoparticles as well as their surface properties is the crucial factor for practical in vivo study. Numerous works ***(1–4)*** have recommended the nanoparticle (less than 100 nm diameter) with

From: *Methods in Molecular Biology, vol. 303: NanoBiotechnology Protocols*
Edited by: S. J. Rosenthal and D. W. Wright

the hydrophilic surface, which can minimize opsonization and subsequent clearance by the macrophage.

Surface-functionalized nanoparticles have been proven to be useful in controlled-release ***(5)*** and site-specific delivery. Many researchers have demonstrated site-specific delivery using surface-functionalized nanoparticles with a high affinity to target sites ***(6–8)***. In this chapter, bone-specific drug delivery using surface-functionalized nanoparticles is discussed. Poly(D,L-lactide-co-glycolic acid) (PLGA) was used as a biodegradable polymer, which is approved for in vivo use by the Food and Drug Administration. Tetracycline was chosen as a model functional molecule because it has a strong affinity for adsorption to calcium phosphate ***(9)*** and thus can serve as a targeting moiety for the bone-specific drug-delivery system. Detailed procedures for the conjugation of tetracycline to PLGA and the three kinds of methods for nanoparticle formation are described.

2. Materials

1. PLGA (lactic acid:glycolic acid ratio of 75:25, mol wt = 10,000; Wako, Saitama, Japan).
2. Ethyl acetate.
3. Acetone.
4. Diethyl ether.
5. Dimethylformamide (DMF).
6. Tubular dialysis membrane (mol wt cutoff = 12,000 g/mol).
7. Poloxamer 188.
8. Homogenizer (Omni, Waterbury, CT).
9. Tetracycline (store at 0°C).
10. Hydroxyapatite (HA).
11. HCl.
12. *N*-Hydroxysuccinimide (NHS).
13. Dicyclohexylcarbodiimide (DCC).
14. Phosphate-buffered saline (PBS) (pH 7.4).
15. Syringe filter (0.45-μm pore size).
16. Pyrene.

3. Methods

Complete techniques on the conjugation of tetracycline to PLGA and nanoparticle formation of conjugated polymer are described. The overall procedures for the preparation of functionalized nanoparticles are introduced in **Subheading 3.1.** (*see* **Fig. 1**) and the detailed steps follow. Tetracycline, chosen as a functional molecule, is conjugated to the PLGA via carbodiimide chemistry (**Subheading 3.2.**). Then the resulting conjugated polymer is formed into nanoparticles by three different methods (**Subheding 3.3.**). Finally, the specific affinity of tetracycline-modified nanoparticles to HA is examined (**Subheading 3.4.**).

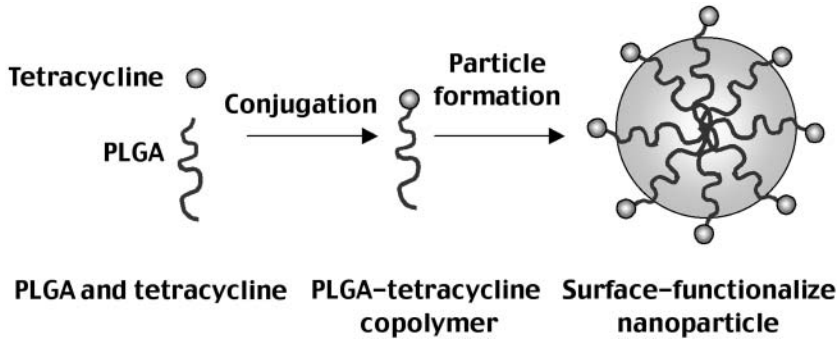

Fig. 1. Overall procedure for preparation of surface-functionalized nanoparticle.

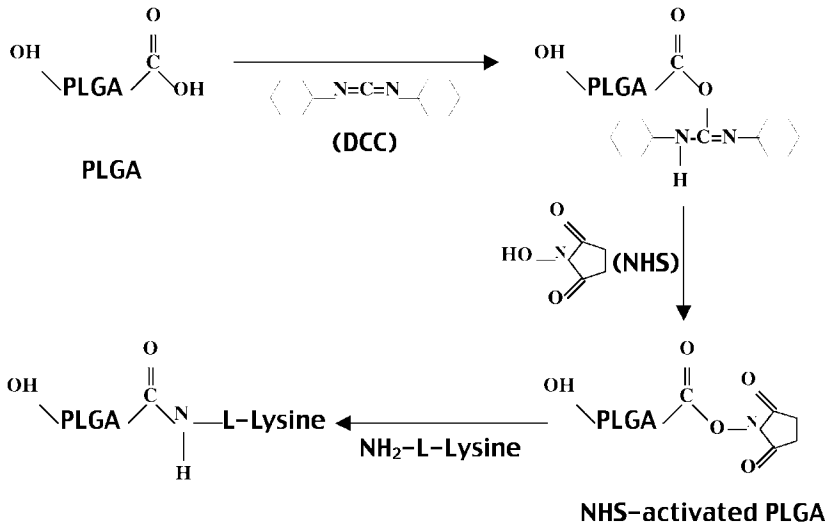

Fig. 2. Schematic diagram of conjugation of PLGA-tetracycline copolymer.

3.1. Surface-Functionalized Nanoparticles

3.1.1. Conjugation

Carbodiimide chemistry is well known and often used for the amide bond reaction between the carboxyl group and primary (or secondary) amine group ***(10,11)***. Conjugation between PLGA and tetracycline is shown schematically in **Fig. 2**. The carboxyl group of PLGA is activated with NHS in the presence of DCC. After the addition of tetracycline, NHS is replaced with tetracycline to form the PLGA-tetracycline-conjugated polymer.

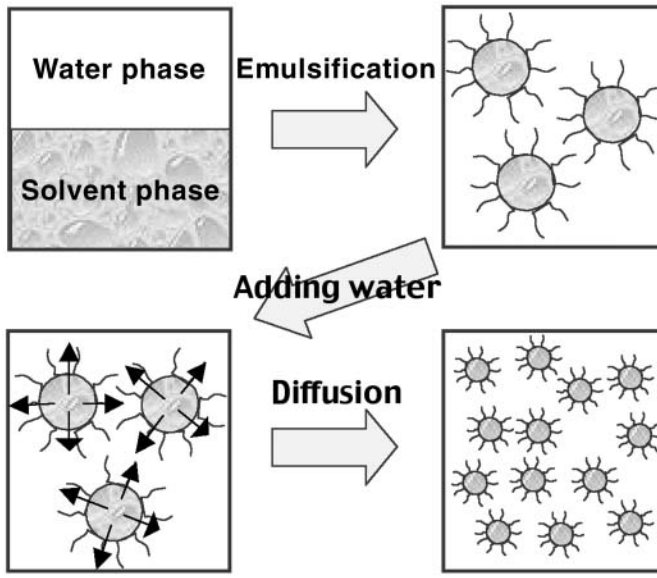

Fig. 3. Nanoparticle preparation by emulsification-diffusion method.

3.1.2. Emulsification-Diffusion Method

Many researchers ***(13–16)*** have studied the emulsification-diffusion method developed by Leroux et al. ***(12)***. The use of partially water-miscible solvent, which allows the additional diffusion of solvent, is the unique characteristic of the emulsification-diffusion method. After homogenization, oil and water phases are in a state of mutual saturation. However, the addition of water leads to interfacial turbulence at the interface of the oil and water phases, which allows the diffusion of solvent into continuous water phase ***(13)***. In this stage, PLGA is aggregated in the form of nanoparticles (*see* **Fig. 3**).

3.1.3. Nanoprecipitation Method

The nanoprecipitation method is very simple for the preparation of nanoparticles ***(17–19)***. Briefly, polymer is dissolved in volatile water-miscible solvent, and then the polymer solution is injected into the water phase through a syringe under stirring (*see* **Fig. 4**, left). In some cases, polymer solution is added dropwise into an aqueous phase ***(18,19)***. The particle formation is dominated by the solvent diffusion. The rapid diffusion of solvent is assumed to result in the reduction of nanoparticle size.

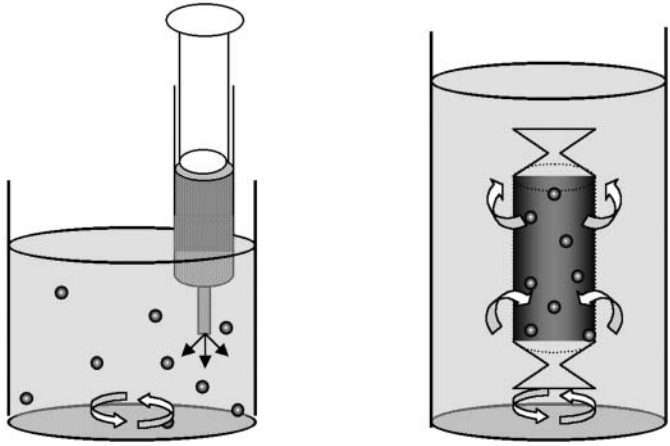

Fig. 4. Schematic illustration of nanoprecipitation (**left**) and dialysis method (**right**).

3.1.4. Dialysis Method

Micellar nanoparticles can be prepared by the dialysis method without any other surfactants ***(20–22)***. The polymer is first dissolved in water-miscible solvents, and then the polymer solution is dialyzed against the water. During the dialysis process, micellar nanoparticles are induced and the organic solvent is removed by water exchange (*see* **Fig. 4**, right). The employed solvent significantly affects the size and size distribution of the micellar nanoparticles. The mutual miscibilities of a polymer, solvent, and water are assumed to be the key factors ***(22)***.

3.2. Conjugation Between PLGA and Tetracycline

The PLGA used in this procedure has a hydroxyl group and a carboxyl group at its terminal ends (*see* **Note 1**).

1. Dissolve 1 g (0.1 mmol) of PLGA in 20 mL of acetone.
2. For activation of the carboxyl group of PLGA, add 0.1 g (0.5 mmol) of DCC and 0.06 g (0.5 mmol) of NHS to the polymer solution.
3. Stir the solution overnight at room temperature.
4. Filter the PLGA solution through a syringe filter to remove the precipitated dicyclohexylurea (byproduct of the reaction).
5. After the evaporation of 5 mL of acetone, precipitate the PLGA solution in cold diethyl ether to remove the unreactants and dry under a vacuum oven (*see* **Note 2**).
6. Dissolve 0.088 g (0.2 mmol) of tetracycline in 10 mL of acetone/0.1 mL of HCl.
7. Dissolve 1 g of the NHS-activated PLGA in 20 mL of acetone.

8. Add the 10 mL of tetracycline solution (**step 6**) to the NHS-activated PLGA solution (**step 7**) under stirring.
9. To remove the insoluble particulates, filter the mixed solution through a syringe filter and stir the mixed solution for 5 h.
10. Precipitate the resulting polymer solution in cold diethyl ether and dry under a vacuum oven.

3.3. Preparation of Functional Nanoparticles

After the conjugation of tetracycline to PLGA, the next step is the nanoparticle formation of the resulting copolymer. The three preparative methods are detailed next. Pyrene is used as a hydrophobic dye for the assay of the concentration of nanoparticles (*see* **Notes 3–5**).

3.3.1. Emulsification-Diffusion Method

1. Dissolve 0.2 g of the prepared PLGA-tetracycline polymer and 0.001 g of pyrene in 10 mL of ethyl acetate, and dissolve 1 g of Poloxamer 188 in 20 mL of pH 7.4 PBS.
2. Add 10 mL of the organic solution to 20 mL of PBS containing Poloxamer 188.
3. After 1 min, emulsify the mixed solution using a high-speed homogenizer at 12,000 rpm for 7 min.
4. Add 80 mL of PBS to the resulting oil/water emulsion under moderate stirring. The rapid diffusion of solvent into water occurs and the nanoparticles are formed in 5 min.
5. Stir the nanoparticle suspension for 5 h to evaporate the solvent (*see* **Fig. 5**).

3.3.2. Nanoprecipitation

1. Dissolve 0.1 g of PLGA-tetracycline copolymer and 0.001 g of pyrene in 10 mL of acetone.
2. Dissolve 0.5 g of Poloxamer 188 in 50 mL of PBS.
3. Inject the polymer solution (**step 1**) through the needle of a syringe into stirred PBS containing poloxamer with the needle dipped in the PBS. Nanoparticle forms immediately.
4. Stir the nanoparticle suspension for 5 h to evaporate the acetone.
5. Filter the nanoparticle suspension through a syringe filter to remove some large aggregates.

3.3.3. Dialysis Method

1. Dissolve 0.02 g of PLGA-tetracycline copolymer and 0.001 g of pyrene in 10 mL of DMF.
2. Fill the tubular dialysis membrane with the polymer solution, and dialyze against PBS for 3 h using a dialysis membrane.
3. Exchange the PBS at intervals of 2–4 h for 24 h.

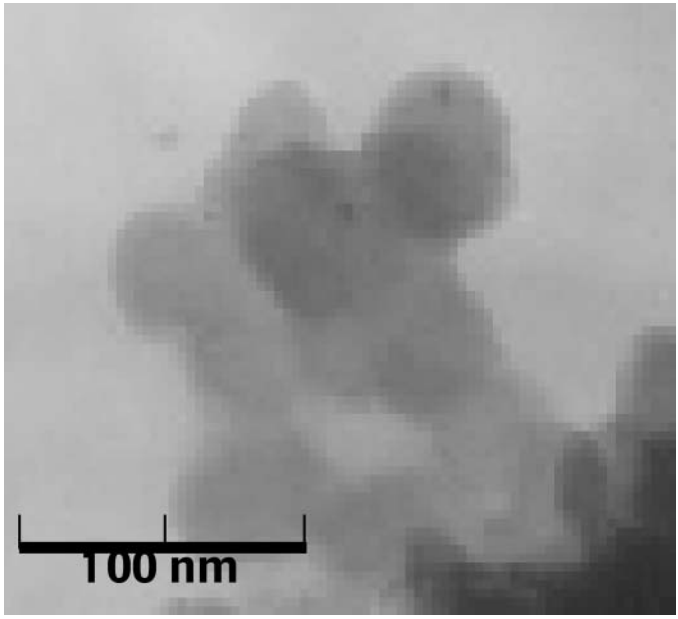

Fig. 5. Transmission electron microscopy image of PLGA nanoparticles prepared by emulsification-diffusion method.

3.4. Characterization of Tetracycline-Modified Nanoparticles

HA is used as a substitute for in vitro bone study because it is inorganic material existing in only hard tissues (bone and teeth), not in soft tissues ***(9)***. In this section, the amount of adsorption of tetracycline-modified nanoparticle to HA is examined to verify the specific affinity to bone (*see* **Fig. 6**). Pyrene is incorporated into nanoparticles as a hydrophobic dye (*see* **Notes 6–8**).

1. Prepare various concentrations of HA dispersions (0.01, 0.02, 0.03, and 0.04 g/mL).
2. Add 1 mL of the tetracycline-modified nanoparticle suspension (prepared by the emulsification-diffusion method in **Subheading 3.3.1.**) to each of the HA dispersions (**step 1**).
3. Agitate the mixed dispersions for 2 h.
4. Filter each of the mixed dispersions through a syringe filter.
5. Measure the concentration of tetracycline-modified nanoparticles using an ultraviolet spectrophotometer at 335 nm.

4. Notes

1. The used PLGA polymer has two functional groups such as a hydroxyl (—OH) group and a carboxyl (—COOH) group ***(23)***. In this chapter, carbodiimide

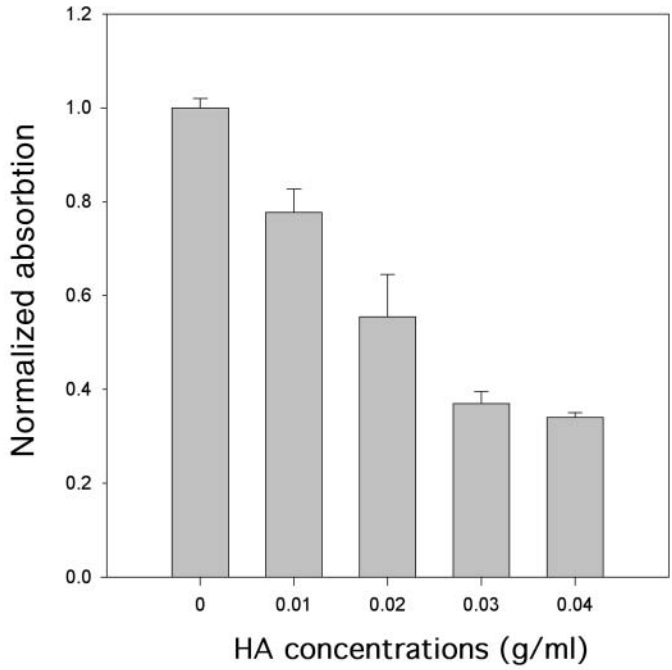

Fig. 6. Affinity of tetracycline-modified nanoparticles on HA.

chemistry is employed for the conjugation between PLGA and tetracycline, but many other methods are available to bind the functional molecule to polymer. Bromo-*tris*(pyrrolidino)-phosphonium hexafluorophosphate (PyBrop) ***(23)***, thionyl chloride ***(24)***, *p*-nitrophenyl chloroformate ***(25)***, and carbonyldiimidazole ***(26)*** are the representative coupling agents to produce amide or ester bond. The solubilities of polymer, functional molecule, and coupling agent should be taken into account for successful reaction.

2. For precipitation of the polymer solution in cold ethyl ether, the polymer solution should be concentrated by the evaporation of solvent. Otherwise, the precipitated polymer will disperse in ethyl ether and form into small particulate. In such a case, the suspension should be centrifuged to obtain the resulting polymer.
3. In the emulsification-diffusion method, the effects of process variables and the thermodynamic parameters (diffusion coefficients and solvent-polymer interaction parameter) on the particle size are investigated ***(13,16)***. The rapid diffusion of solvent is very important for the reduction of particle size. Ultrasonication in the emulsification step and the addition of heated water (about 50°C) in the diffusion step are effective at reducing the particle size, because the diffusion coefficient is proportional to temperature in Kelvin ***(13)***.
4. Volatile water-miscible solvents such as acetone and tetrahydrofuran are mainly used in the nanoprecipitation method to facilitate the removal of solvents. How-

ever, in the dialysis method all of the water-miscible solvents can be employed, because particle formation and removal of solvents occur simultaneously. The lower concentration of polymer in solvent leads to a smaller nanoparticle.

5. Generally, the size range of nanoparticles formed by the emulsification-diffusion method is 50–150 nm. Nanoparticles formed by the nanoprecipitation method are assumed to be more aggregates than micelles, having a particle size >100 nm. The dialysis method can produce micellar nanoparticles ranging from 25 to 200 nm owing to the formation of micelles.
6. Poloxamers used as surfactants are not biodegradable because they have ether, not ester, linkage although they are well known as biocompatible materials. Consequently, they may remain in the body after administration. Therefore, the nanoparticle without surfactant is thought to be suitable for clinical applications.
7. For incorporation of hydrophobic drug into nanoparticles ***(27–31)***, target hydrophobic molecules are dissolved in the organic phase containing polymer and then the nanoparticles are prepared. Incorporation efficiency is determined by the process variables and the solubility of target molecules in the used organic solvent.
8. Tetracycline-modified nanoparticles have been demonstrated to have a great affinity with HA (*see* **Fig. 6**) and thus can be employed for a potential bone-specific drug carrier. The functional molecule with the specific affinity to some organs, cells, or diseases can be utilized as the guide material for targeted drug-delivery systems ***(8,32–34)***.

Acknowledgment

We acknowledge the financial support of the Korea Institute of S&T Evaluation and Planning (National Research Laboratory Program, 2000-N-NL-01-C-032).

References

1. Cammas, S., Suzuki, K., Sone, C., Sakurai, Y., Kataoka, K., and Okano, T. (1997) Thermo-responsive polymer nanoparticles with a core-shell micelle structure as site-specific drug carriers. *J. Control. Release* **48,** 157–164.
2. Löbenberg, R., Araujo, L., Briesen, H. V., Rodgers, E., and Kreuter, J. (1998) Body distribution of azidothymidine bound to hexyl-cyanoacrylate nanoparticles after i.v. injection to rats. *J. Control. Release* **50,** 21–30.
3. Dunn, S. E., Brindley, A., Davis, S. S., Davies, M. C., and Illum, L. (1994) Polystyrene-poly(ethylene glycol) (PS-PEG2000) particles as model system for site specific drug delivery. 2. The effect of PEG surface density on the in vitro cell interaction and in vivo biodistribution. *Pharm. Res.* **11,** 1016–1022.
4. Stolnik, S., Illum, L., and Davis, S. S. (1995) Long circulation microparticulate drug carriers. *Adv. Drug Deliv. Rev.* **16,** 195–214.
5. Yoo, H. S., Lee, K. H., Oh, J. E., and Park, T. G. (2000) In vitro and in vivo anti-tumor activities of nanoparticles based on doxorubicin–PLGA conjugates. *J. Control. Release* **68,** 419–431.

6. Calvo, P., Gouritin, B., Brigger, I., Lasmezas, C., Deslys, J. P., Williams, A., Andreux, J. P., Dormont, D., and Couvreur, P. (2001) PEGylated polycyanoacrylate nanoparticles as vector for drug delivery in prion diseases. *J. Neurosci. Methods* **111,** 151–155.
7. Li, Y. P, Pei, Y. Y., Zhou, Z. H., Zhang, X. Y., Gu, Z. H., Ding, J., Zhou, J. J., and Gao, X. J. (2001) PEGylated polycyanoacrylate nanoparticles as tumor necrosis factor-a carriers. *J. Control. Release* **71,** 287–296.
8. Wroblewski, S., Berenson, M., Kopeckova, P., and Kopecek, J. (2001) Potential of lectin-*N*-(2-hydroxypropyl)methacrylamide copolymer-drug conjugates for the treatment of pre-cancerous conditions. *J. Control. Release* **74,** 283–293.
9. Misra, D. N. (1991) Adsorption and orientation of tetracycline on hydroxyapatite. *Calcif. Tissue Int.* **48,** 362–367.
10. Valuev, I. L., Chupov, V. V., and Valuev, L. I. (1998) Chemical modification of polymers with physiologically active species using water-soluble carbodiimides. *Biomaterials* **19,** 41–43.
11. Kim, I. S., Jeong, Y. I., Cho, C. S., and Kim, S. H. (2000) Core-shell type polymeric nanoparticles composed of poly(L-lactic acid) and poly(*N*-isopropylacrylamide). *Int. J. Pharm.* **211,** 1–8.
12. Leroux, J. C., Cozens, R., Roesel, J. L., Galli, B., Kubel, F., Doelker, E., and Gurny, R. (1995) Pharmacokinetics of a novel HIV-1 protease inhibitor incorporated into biodegradable or enteric nanoparticles following intravenous and oral administration to mice. *J. Pharm. Sci.* **84,** 1387–1391.
13. Kwon, H. Y., Lee, J. Y., Choi, S. W., Jang, Y., and Kim, J. H. (2001) Preparation of PLGA nanoparticles containing estrogen by emulsification–diffusion method. *Colloids Surf. A: Physicochem. Eng. Aspects* **182,** 123–130.
14. Quintanar-Guerrero, D., Allémann, E., Fessi, H., and Doelker, E. (1999) Pseudolatex preparation using a novel emulsion–diffusion process involving direct displacement of partially water-miscible solvents by distillation. *Int. J. Pharm.* **188,** 155–164.
15. Berton, M., Allémann, E., Stein, C. Y., and Gurny, R. (1999) Highly loaded nanoparticulate carrier using an hydrophobic antisense oligonucleotide complex. *Eur. J. Pharm. Sci.* **9,** 163–170.
16. Choi, S. W., Kwon, H. Y., Kim, W. S., and Kim, J. H. (2002) Thermodynamic parameters on poly(L,D-lactide-co-glycolide) particle size in emulsification–diffusion process. *Colloids Surf. A: Physicochem. Eng. Aspects* **201,** 283–289.
17. Schubert, M. A. and Müller-Goymann, C. C. (2003) Solvent injection as a new approach for manufacturing lipid nanoparticles—evaluation of the method and process parameters. *Eur. J. Pharm. Biopharm.* **55,** 125–131.
18. Panagi, Z., Beletsi, A., Evangelatos, G., Livaniou, E., Ithakissios, D. S., and Avgoustakis, K. (2001) Effect of dose on the biodistribution and pharmacokinetics of PLGA and PLGA–mPEG nanoparticles. *Int. J. Pharm.* **221,** 143–152.
19. Vittaz, M., Bazile, D., Spenlehauer, G., Verrecchia, T., Veillard, M., Puisieux, F., and Labarre, D. (1996) Effect of PEO surface density on long-circulating PLA-PEO nanoparticles which are very low complement activators. *Biomaterials* **17,** 1553–1643.

20. Kwon, G. S., Naito, M., Yokoyama, M., and Okano, T. (1995) Physical entrapment of adriamycin in AB block copolymer micelles. *Pharm. Res.* **12,** 192–195.
21. Lasic, D. D. (1992) Mixed micelles in drug delivery. *Nature* **355,** 279–280.
22. Kim, S. Y., Shin, I. G., Lee, Y. M., Cho, C. S., and Sung, Y. K. (1998) Methoxy poly(ethylene glycol) and ε-caprolactone amphiphilic block copolymeric micelle containing indomethacin: II. Micelle formation and drug release behaviours. *J. Control. Release* **51,** 13–22.
23. Oh, J. E., Nam, Y. S., Lee, K. H., and Park, T. G. (1999) Conjugation of drug to poly(D,L-lactic-co-glycolic acid) for controlled release from biodegradable microspheres. *J. Control. Release* **57,** 269–280.
24. Aksoy, S., Tumturk, H., and Hasirci, N. (1998) Stability of α-amylase immobilized on poly(methyl methacrylate-acrylic acid) microspheres. *J. Biotechnol.* **60,** 37–46.
25. Yoo, H. S. and Park, T. G. (2001) Biodegradable polymeric micelles composed of doxorubicin conjugated PLGA–PEG block copolymer. *J. Control. Release* **70,** 63–70.
26. Kim, I. S. and Kim, S. H. (2001) Evaluation of polymeric nanoparticles composed of cholic acid and methoxy poly(ethylene glycol). *Int. J. Pharm.* **226,** 23–29.
27. Ryu, J. G., Jeong, Y. I., Kim, I. S., Lee, J. H., Nah, J. W., and Kim, S. H. (2000) Clonazepam release from core-shell type nanoparticles of poly(o-caprolactone): poly(ethylene glycol): poly(o-caprolactone) triblock copolymers. *Int. J. Pharm.* **200,** 231–242.
28. Kim, S. Y., Ha, J. C., and Lee, Y. M. (2000) Poly(ethylene oxide)-poly(propylene oxide)-poly(ethylene oxide)/poly(e-caprolactone) (PCL) amphiphilic block copolymeric nanospheres II. Thermo-responsive drug release behaviors. *J. Control. Release* **65,** 345–358.
29. Jeon, H. J., Jeong, Y. I., Jang, M. K., Park, Y. H., and Nah, J. W. (2000) Effect of solvent on the preparation of surfactant-free poly(D,L-lactide-co-glycolide) nanoparticles and norfloxacin release characteristics. *Int. J. Pharm.* **207,** 99–108.
30. Allen, C. Maysinger, D., and Eisenberg, A. (1999) Nano-engineering block copolymer aggregates for drug delivery. *Colloids Surf. B: Biointerfaces* **16,** 3–27.
31. Nakanishi, T., Fukushima, S., Okamoto, K., Suzuki, M., Matsumura, Y., Yokoyama, M., Okano, T., Sakurai, Y., and Kataoka, K. (2001) Development of the polymer micelle carrier system for doxorubicin. *J. Control. Release* **74,** 295–302.
32. Cho, C. S., Cho, K. Y., Park, I. K., Kim, S. H., Sasagawa, T., Uchiyama, M., and Akaike, T. (2001) Receptor-mediated delivery of all trans-retinoic acid to hepatocyte using poly(L-lactic acid) nanoparticles coated with galactose-carrying polystyrene. *J. Control. Release* **77,** 7–15.
33. Dawson, G. F. and Halbert, G. W. (2000) The in vitro cell association of invasin coated polylactide-co-glycolide nanoparticles. *Pharm. Res.* **17,** 1420–1425.
34. Stella, B., Arpicco, S., Peracchia, M. T., Desmaele, D., Hoebeke, J., Renoir, M., D'Angelo, J., Cattel, L., and Couvreur, P. (2000) Design of folic acid–conjugated nanoparticles for drug targeting. *J. Pharm. Sci.* **89,** 1452–1464.

11

Screening of Combinatorial Peptide Libraries for Nanocluster Synthesis

Joseph M. Slocik and David W. Wright

Summary

A significant challenge in bionanotechnology is the discovery of effective biological interfaces that allow inorganic nanoscale materials to mimic effectively their biological counterparts. Much like *de novo* design of proteins, the rational design of such interfaces is a daunting task. An alternative approach is to screen libraries of peptides, inspired by known biological examples of such hybrid protein–material interfaces, for peptide ligands capable of not only stabilizing a size-discrete population of nanoclusters, but providing the requisite biological compatibility. The protocol described in this chapter is an approach for the simultaneous screening of spatially addressable combinatorial libraries for the stabilization of a variety of metal sulfide, metal oxide, and zero-valent nanoclusters. Additionally, the screening process allows the researcher to characterize the resulting nanoclusters in terms of a variety of physical properties. Ultimately, an informatics structure–function analysis may be performed in order to elucidate specific properties of the ligand sets, which provides access to certain desired material characteristics.

Key Words

Combinatorial chemistry; nanocluster synthesis; biomimetic nanoclusters; peptide-encapsulated nanoclusters; spatially addressable combinatorial library; metal sulfide nanoclusters; zero-valent nanoclusters.

1. Introduction

A major objective in achieving robust, functional nanodevices is the development of the requisite chemistry to assemble larger architectures through control of the interfaces and distribution of nanocomponents. Biological systems offer important insights into possible approaches to the problems encountered in the synthesis of extended materials ***(1)***. The array of materials produced by biological systems include laminate composites and ceramics such as bone, teeth, and shells ***(2)***; magnetic materials such as the forms of magnetite found

From: *Methods in Molecular Biology, vol. 303: NanoBiotechnology Protocols*
Edited by: S. J. Rosenthal and D. W. Wright

in magnetobacteria and the brains of migratory animals ***(3)***; novel silver or cadmium sulfide nanoclusters produced as a result of heavy metal detoxification mechanisms by bacteria ***(4,5)***; and arrays of precisely fabricated diffracting architectures resulting in the multitude of intense colors observed in insects and birds ***(6)***. Consequently, there has been increasing interest in the use of biomolecules to control the synthesis of nanoparticles in a biomimetic fashion.

The relationship of ligand structure to chemical and physical properties of the resulting cluster is a central theme in nanoscale chemistry. Advances in a number of areas, such as catalysis and sensor discovery, highlight the utility of complexes with well-designed structural, electronic, and stereochemical features. Unfortunately, the rational design of ligands for functional nanoclusters remains extremely empirical, especially if novel physical and chemical properties are desired. Increasingly, combinatorial chemistry is emerging as a viable approach for the identification of such novel ligands (**Fig. 1**) ***(7)***. In this chapter, we present our approach for screening peptides ***(8,9)***, derived from a spatially addressed peptide library, for the ability to stabilize novel biologically compatible and functional nanoscale materials.

2. Materials

2.1. Nanocluster Synthesis

1. Peptide libraries: There are three primary approaches to the development of synthetic ligand libraries ***(10)***. Conventional serial approaches result in "one-at-a-time ligands." Although this method provides a high level of control over the compounds entering the screening process, it results in a low throughput of potential compounds. Pooled synthesis combinatorial approaches represent the other end of the spectrum. Methods such as the "split-pool" approach yield an extremely large number of compounds but present challenges of purity and deconvolution of assay screens. An intermediate approach is the parallel synthesis of an array of compounds in a spatially addressable format. For the purpose of this protocol, the library used is a spatially addressable library that has been synthesized using the Mimotopes peptide on a pen system ***(11)***. Peptide synthesis yielded approx 1–4 µmol of each target ligand. Control peptides were >97% pure by high-performance liquid chromatography and mass spectrometry. It should be emphasized that any well-designed library will suffice as the basis of the assay screen. Subsequently, the individual members of the peptide library were screened simultaneously for the ability to stabilize a wide spectrum of nanoparticles, followed by screens to evaluate the physical properties of the resulting materials. Lyophilized peptides were dissolved in 1.0 mL of 0.1% trifluoroacteic acid (TFA), resulting in a final peptide stock solution with a concentration of 1.0–4.0 m*M*.
2. Aqueous solvents: Prepare 0.01 *M* HCl, 0.1% TFA, and double-deionized water filtered by reverse osmosis and ion-exchange cartridges (MODULAB water

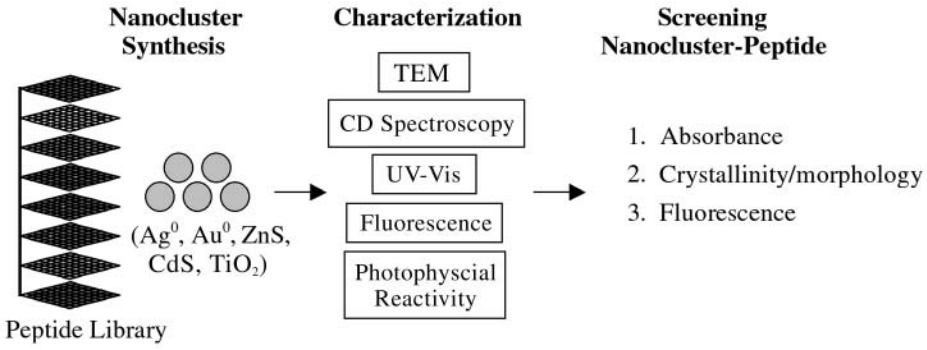

Fig. 1. Total possible number of permutations varied over three binding positions and eight amino acids to comprise peptide library.

systems) in 500-mL total volumes. Store the 0.1% TFA in a glass bottle. After solvent preparation, degas each solvent for 30 min with N_2 on a Schlenk line (*see* **Note 1**). Then cycle the solvents into a glove box and store.

3. 0.01 *M* Phosphate buffer, pH 6.0 (*see* **Note 2**): Dissolve 0.1648 g of sodium phosphate dibasic Na_2HPO_4 and 0.6050 g of sodium phosphate monobasic NaH_2PO_4 in 500 mL of double-deionized water. Adjust the pH to 6.0 with 1 or 2 drops of 1 *M* HCl. Degas the buffer with N_2 for 30 min prior to storage in a glove box.
4. Stock solutions of metal ions at a concentration of 5 m*M*: In four 10-mL glass vials, weigh 0.00718 g of $ZnSO_4$, 0.00521 g of $CdSO_4$, 0.00425 g of $AgNO_3$, and 0.00984 g of $HAuCl_4 \cdot 3H_2O$. Cycle into a glove box through the antechamber (*see* **Note 3**). In the glove box, dissolve $ZnSO_4$ and $CdSO_4$ in 5.00 mL of 0.01 *M* HCl. Dissolve $AgNO_3$ and $HAuCl_4 \cdot 3H_2O$ in 5.00 mL of double-deionized water. Store the $HAuCl_4 \cdot 3H_2O$ covered with aluminum foil (light sensitive) in a refrigerator at 4°C. Additionally, cover the $AgNO_3$ solution with aluminum foil (light sensitive).
5. Titanium (IV) isopropoxide ($Ti([CH_3]_2CHO)_4$) solution: Pipet 7.3 µL of $Ti([CH_3]_2CHO)_4$ in 5.00 mL of absolute ethanol in a separate vial to yield a 5 m*M* solution under nitrogen (*see* **Note 4**). Store under N_2 in a glove box to avoid all humidity. $Ti([CH_3]_2CHO)_4$ is readily hydrolyzed and will instantly precipitate as TiO_2 in even the slightest levels of humidity; it is extremely sensitive to moisture. Make solution daily as needed.
6. 5 m*M* Stock solution of inorganic sulfide: Dissolve 0.00195 g of Na_2S in 5.00 mL of double-deionized water in a glove box by first weighing out the appropriate amount of Na_2S in a glass vial and then transferring to the glove box. Keep refrigerated and prepare once a week.
7. 5 m*M* Stock solution of sodium borohydride reductant: Dissolve 0.00189 g of $NaBH_4$ in 10.00 mL of double-deionized water under nitrogen. Prepare daily; $NaBH_4$ loses reducing power over time.

2.2. Screening of Library Peptides

1. Basic ultraviolet-visible (UV-Vis) spectrophotometer, either scanning or equipped with a photodiode array. To increase throughput, an Agilent 8453 spectrophotometer model with a multicell holder can be employed.
2. Varian Cary Eclipse fluorometer, to screen the set of metal sulfide nanoclusters (ZnS and CdS) for fluorescence.
3. Aviv model 215 CD spectrometer equipped with a thermoelectric cell holder accessory, to perform circular dichroism (CD) spectroscopy.
4. Phillips CM20 transmission electron microscope operating at 200 kV and coupled with an energy-dispersive X-ray spectrometer, to provide physical characterization of the nanoclusters.
5. Methylviologen dye, to examine the semiconducting nanoclusters of ZnS, CdS, and TiO_2 for photophysical reactivity. Prepare a 12.5 m*M* methylviologen solution by pipetting 12.5 µL of a 0.01 *M* methylviologen solution with 1 mL of 0.1 *M* NaOH in a 10-mL volumetric flask and diluting with double-deionized water. Cover the methylviologen solution with aluminum foil (sensitive to light) and store in a glove box.

3. Methods

3.1. Nanocluster Synthesis With Library Peptides

Each nanocluster type (Au^0, Ag^0, ZnS, CdS, and TiO_2) is synthesized in triplicate to yield a total of 15 reactions carried out for each peptide (*see* **Note 5**). All nanocluster reactions are performed in the anaerobic environment of a glove box according to the general reaction scheme in **Fig. 2**.

3.1.1. Reductive Synthesis of Ag^0 and Au^0 Nanoclusters

1. Add 1.00 mL of 10 m*M* phosphate buffer, pH 6.0, to six 10-mL glass vials.
2. To each vial, pipet 10.0 µL of the 3.7 m*M* peptide solution.
3. To a set of three labeled vials, add 4.8 µL of $AgNO_3$ stock solution. To the remaining set, add 4.8 µL of $HAuCl_4 \cdot 3H_2O$ stock solution (*see* **Note 6**).
4. Add a micro stir bar to each vial.
5. Wait 15 min after adding metal ions to the peptide to allow for the formation of a metal-peptide precursor complex.
6. Pipet 9.6 µL of 5 m*M* sodium borohydride to all vials to initiate reduction.
7. Cover the vials in aluminum foil and stir for 4 h.

3.1.2. Sulfide Addition Synthesis of ZnS and CdS Nanoclusters

1. To six vials, add 1.00 mL of 10 m*M* phosphate buffer, pH 6.0.
2. Add 10.0 µL of a library peptide to all vials.
3. To a set of three vials, pipet 4.8 µL of the 5 m*M* stock solutions of $ZnSO_4$ or $CdSO_4$.

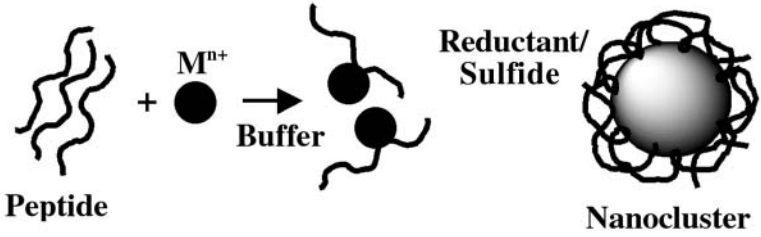

Fig. 2. Nanocluster synthesis scheme with peptide library.

4. Add a micro stir bar to each vial.
5. After 15 min, add 4.8 µL of 5 m*M* Na_2S to all six vials to yield a final peptide concentration of 3.6289×10^{-5} *M*.
6. Cover the vials with aluminum foil and stir for 4 h.

3.1.3. Condensation Synthesis of TiO_2 Nanoclusters

1. To the last set of three labeled vials, add 1.00 mL of 10 m*M* phosphate buffer, pH 6.0.
2. Pipet 10.0 µL of peptide into each vial.
3. Dispense 4.8 µL of 5 m*M* stock solution of $Ti([CH_3]_2CHO)_4$ to each peptide-containing vial.
4. Add a micro stir bar, cover with aluminum foil, and stir for 4 h.

3.2. Screening Library

3.2.1. Secondary Structure of Peptide Ligand

During the 4-h nanocluster reaction period, perform the following preliminary studies on the free peptide: individual CD spectrum and temperature unfolding study.

1. Pipet 5.0 µL of peptide in 0.5 mL of 10 m*M* phosphate buffer, pH 6.0. Transfer the peptide solution to a strain-free CD quartz cell with a 1-cm path length.
2. Examine the peptide for a secondary structure using a CD spectrometer to scan the sample from 190 to 260 nm with 0.5-nm steps averaging 2 s at every step to obtain the CD spectra of the free peptides. After spectra are collected, convert all raw data to molar ellipticity (units of degrees•cm^2/dmol) by dividing by the concentration and the path length of the cell.
3. If there is a secondary structure of interest, obtain a melting profile of the free peptide over the temperature range of 5 to 85°C at 10°C intervals. Most commercial CD instruments have an appropriate programmable interface. Use this to program the thermal denaturation experiment beginning at 5°C using a 15-min temperature equilibration period at each new temperature (*see* **Note 7**).

3.2.2. Characterization of Peptide-Encapsulated Nanoclusters

On completion of synthesis, perform a methylviologen reduction assay while the reactions are under nitrogen. Perform this assay on the CdS, ZnS, and TiO_2 nanoclusters.

1. In a glove box, mix 100 µL of the crude nanocluster reaction with 800 µL of the 12.5 m*M* methylviologen basic solution in a 1.00-mL cuvet with a rubber stopper. Put the cuvet in a foil-covered beaker and remove from the glove box. Obtain a UV-Vis spectrum of the solution and identify λ_{max}. Using a fluorometer, excite the sample at λ_{max} for 10 min without acquiring data (set the excitation monochromator and scan parameters, but do not start the scan). After irradiation, carefully remove the sample from the fluorometer and place back in the foil-covered beaker. Take a UV-Vis spectrum of the sample against an air blank (*see* **Note 13**). The appearance of peaks in the spectrum at 398 and 600 nm indicates a positive result for the photodriven reduction of methylviologen.
2. Remove all 15 reaction vials from the glove box and obtain UV-Vis absorbance spectra using a 1.00-mL cuvet (*see* **Note 8**).
3. Additionally, obtain CD spectra for all nanocluster reactions following above parameters (*see* **Note 9**).
4. If there is a secondary structure of interest on the nanoparticle surface, select the most representative sample that exhibits reproducibility from the triplicate CD spectra and obtain a CD melting profile from 5 to 85°C using a temperature macro (**Fig. 3**). Repeat the temperature experiment with all five nanoclusters (*see* **Note 10**).
5. Examine the clusters of CdS and ZnS for fluorescence. Perform an emission scan on nanoclusters by exciting samples at the absorbance maximum determined in the UV-Vis spectrum. Start the scan range at 10 nm above the excitation wavelength and stop the scan at 750 nm. As needed, adjust the photomultiplier tube detector voltage to the highest value, and set the excitation and emission slits to 5 nm (*see* **Note 11**).
6. Study the physical characteristics of the nanoclusters by transmission electron microscopy (TEM). Prepare TEM grids (200-mesh quantifoil copper grids from SPI supplies) by pipetting 2 drops of the crude aqueous nanocluster reaction onto a grid for each different nanocluster (*see* **Note 13**). Obtain a size distribution histogram from the TEM micrograph by manually measuring 50–100 particles in the bright-field image (**Fig. 4**).

3.2.3. Evaluation Criteria for Nanocluster-Peptide Screens

Inspect the morphology and crystallinity of nanocluster populations in the TEM micrographs for uniformity and appearance. Nanoclusters should appear spheroidal or faceted. An absence of these physical features is indicative of ineffectual stabilization of nanocluster, and the reaction would be considered unsuccessful.

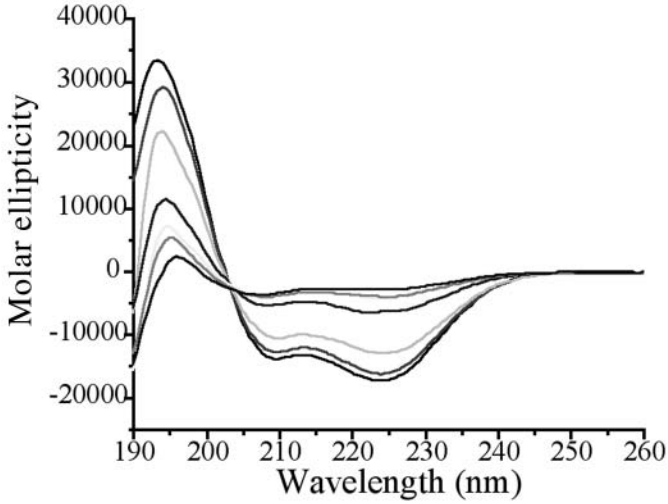

Fig. 3. CD spectra of ZnS-(HHH) obtained over temperature range of 25–85°C.

The CdS and ZnS nanoclusters should fluoresce near 530 and 440 nm, respectively, as broad peaks. Lack of fluorescence suggests poor stabilization of nanoparticles by screened ligand.

Each type of nanocluster should exhibit characteristic absorbance maxima λ_{max} (*see* **Note 8**). Lack of the characteristic quantum confined absorbance for semiconductor nanoclusters or plasmon resonance absorption features for noble metal nanoclusters is indicative of an unsuccessful reaction.

After identifying the peptide-nanocluster "hits," reaction conditions may be optimized for specific peptide-encapsulated nanocluster combinations.

4. Notes

1. Solvents can also be purged using an HPLC buffer purge system with helium for 30 min or frozen/thawed under vacuum to remove dissolved gases.
2. Phosphate buffer provides the pH desired as well as less signal to noise in CD spectra. Consequently, the peptides exhibit maximal helicity and the effects of the nanocluster surface are obscured in more basic pH, so pH 6.0 was chosen.
3. Use a Kimwipe and rubber band to cap the vials, preventing oxygen from being trapped.
4. Make sure the pipet tip is in the ethanol before dispensing; otherwise, TiO_2 is likely to form.
5. Nanocluster reactions are done in triplicate to ensure reproducibility. It should be emphasized that the nanocluster reaction conditions represent an averaged set of conditions expected to work for the widest possible variety of nanoclusters screened. This does not imply that the reaction conditions for nanocluster formation are

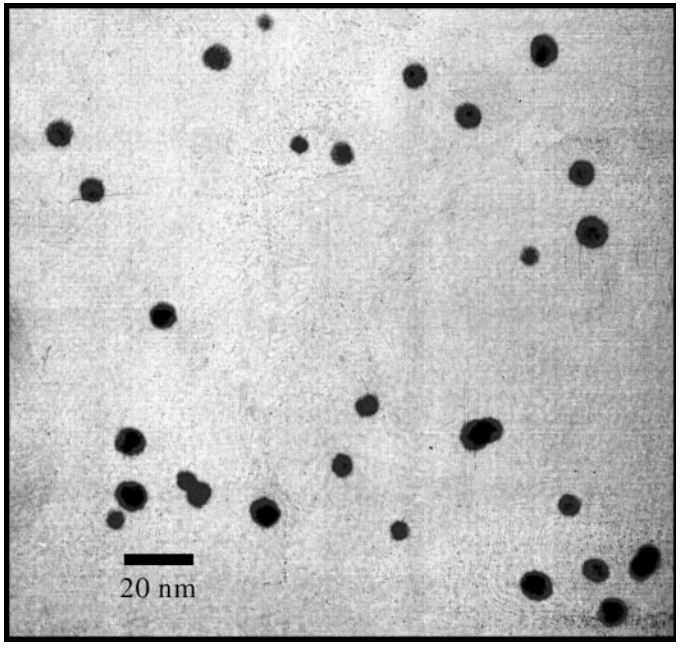

Fig. 4. Bright-field TEM micrograph of representative sample of Au^0-(HAA) nanoparticles in 10 m*M* phosphate buffer, ph 6.0, and at magnification of ×310,000.

necessarily optimized. Once "hits" have been identified, the specifics of the reaction space for any nanocluster/peptide combination should be systematically optimized.

6. The addition of metal and peptide is in a 1:1.25 mole ratio.
7. Thermal denaturation experiments take approx 3.5 h.
8. When transferring cuvets from the fluorometer to the UV-Vis spectrophotometer, do not disturb the sample by mixing or shaking. Any convection of sample will cause the assay to fail, because the trapped holes on the nanocluster surface will recombine with the reduced methylviologen and oxidize the dye, resulting in loss of characteristic absorption features.
9. Examine UV-Vis spectra for the characteristic absorbance of each cluster type. The zero-valent metal nanoclusters have strong plasmon absorption benchmarks indicative of formation at about 400–460 nm for Ag^0 and 500–550 nm for Au^0. The metal sulfides exhibit λ_{max} at about 260–300 nm less than their bulk band-gap energy.
10. Superimpose CD spectra from the reactions performed in triplicate to confirm reproducibility.
11. Plot temperature data by measuring the molar ellipticity at 222 nm for each subsequent temperature; this yields a plot of temperature vs helicity.

12. Depending on the fluorometer model available, scan parameters such as slit widths, detector voltages, and scan averaging times may need to be optimized.
13. After approx 30 s of immersing the grid, remove the grid from the droplets and air-dry for several minutes. There are a number of techniques for preparing samples, but this allows enough of the sample to deposit onto the grid for observation.

References

1. Mann, S. (ed.) (1996) *Biomimetic Materials Chemistry*, VCH, New York.
2. Heuer, A. H., Fink, D. J., Laraia, V. J., et al. (1992) Innovative materials processing strategies: a biomimetic approach. *Science* **255,** 1098–1105.
3. Kirschvink, J. L., Jones, D. S., and Macfadden, J. B. (eds.). (1985) *Magnetite Biomineralization and Magnetoreception in Organisms: A New Biomagnetism*, Plenum, New York.
4. Klaus, T., Joerger, R., Olsson, E., and Granqvist, C.-G. (1999) Silver-based crystalline nanoparticles, microbially fabricated. *Proc. Natl. Acad. Sci. USA* **96,** 13,611–13,614.
5. Dameron, C. T., Reese, R. N., Mehra, R. K., Kortan, A. R., Carroll, P. J., Steigerwald, M. L., Brus, L. E., and Winge, D. R. (1989) Biosynthesis of cadmium sulphide quantum semiconductor crystallites. *Science* **338,** 596–597.
6. Srinivasarao, M. (1999) Nano-optics in the biological world: beetles, butterflies, birds and moths. *Chem. Rev.* **99,** 1935–1961.
7. Jandeleit, B., Schaefer, D. J., Powers, T. S., Turner, H. W., and Weinberg, W. H. (1999) Combinatorial materials and catalysis. *Angew. Chem. Int. Ed.* **38,** 2494–2532.
8. Spreitzer, G., Whitling, J. M., Madura, J. D., and Wright, D. W. (2000) Peptide-encapsulated CdS nanoclusters from a combinatorial ligand library. *J. Roy. Soc. Chem. Commun.* 209–210.
9. Whitling, J. M., Spreitzer, G., and Wright, D. W. (2000) A combinatorial and informatics approach to CdS nanoclusters. *Adv. Mat.* **12,** 1377–1380.
10. Czarnik, A. W. and DeWitt, S. H. (eds.). (1997) *A Practical Guide to Combinatorial Chemistry*, American Chemical Society, Washington, DC.
11. Pirrung, M. C. (1997) Spatially addressable combinatorial libraries. *Chem. Rev.* **9,** 473–489.

12

Structural DNA Nanotechnology

An Overview

Nadrian C. Seeman

Summary

Structural DNA nanotechnology uses unusual DNA motifs to build target shapes and arrangements. These unusual motifs are generated by reciprocal exchange of DNA backbones, leading to branched systems with many strands and multiple helical domains. The motifs may be combined by sticky-ended cohesion, involving hydrogen bonding or covalent interactions. Other forms of cohesion involve edge sharing or paranemic interactions of double helices. A large number of individual species have been developed by this approach, including polyhedral catenanes, such as a cube and a truncated octahedron; a variety of single-stranded knots; and Borromean rings. In addition to these static species, DNA-based nanomechanical devices have been produced that are targeted ultimately to lead to nanorobotics. Many of the key goals of structural DNA nanotechnology entail the use of periodic arrays. A variety of two-dimensional DNA arrays have been produced with tunable features, such as patterns and cavities. DNA molecules have been used successfully in DNA-based computation as molecular representations of Wang tiles, whose self-assembly can be programmed to perform a calculation. Structural DNA nanotechnology appears to be at the cusp of a truly exciting explosion of applications, which can be expected to occur by the end of the current decade.

Key Words

Holliday junctions; branched DNA; DNA nanotechnology; sticky-ended cohesion; double crossover molecules; triple crossover molecules; paranemic cohesion; edge sharing; reciprocal exchange; DNA complementarity.

1. Introduction

The year 2003 is the 50th anniversary of the Watson-Crick ***(1)*** model for double helical DNA. The impact of this model during the past half century has been immense. Indeed, the double helix has become a cultural icon of our

From: *Methods in Molecular Biology, vol. 303: NanoBiotechnology Protocols*
Edited by: S. J. Rosenthal and D. W. Wright © Humana Press Inc., Totowa, NJ

civilization in much the same way that the pyramids of Egypt, the temples of Greece, the cathedrals of medieval Europe, and the Great Wall of China were icons of previous eras. The simplicity and elegance of the molecule that nature evolved to perpetuate and express genetic information, have revolutionized genetics and have had a similar impact in other areas ranging from medicine to forensics. All of these applications are predicated on the complementarity of the two strands of DNA, rooted in the hydrogen-bonded base pairing between adenine (A) and thymine (T) and between guanine (G) and cytosine (C). The DNA double helix is inherently a nanoscale object; its diameter is about 20 Å (2 nm) and the separation of the bases is 3.4 Å; the helical periodicity is 10–10.5 nucleotide (nt) pairs per turn, or approx 3.5 nm per turn. Here, I discuss making complex materials with nanoscale features from DNA; this pursuit is termed *structural DNA nanotechnology*.

What purposes would be served by producing DNA-based constructs? It is expected that these systems can be applied to several practical ends. The initial motivating goal for this research is that spatially periodic networks are crystals. If stick-figure crystalline cages can be built on the nanometer scale, they could be used to orient other biological macromolecules as guests inside those cages, thereby rendering their three-dimensional (3D) structures amenable to diffraction analysis ***(2)***. This notion is illustrated in **Fig. 1A**, which shows a DNA "box" hosting macromolecular guests. Similarly, the same types of crystalline arrays could be used to position and orient components of molecular electronic devices with nanometer-scale precision ***(3)***. An example of this type of application is shown in **Fig. 1B**. Two DNA branched junctions have pendent from them a nanowire. When their sticky ends cohere, the nanowires are organized as well. DNA-based nanomechanical devices can lead to a nanometer-scale robotics and to very smart materials, materials that respond to specific stimuli by particular spatial transitions. Structural DNA nanotechnology creates motifs that can be useful for DNA-based computation and for the algorithmic assembly of materials ***(4)***. Algorithmic assembly holds great promise for the highly controlled construction of materials with designed features and target sizes in one, two, or three dimensions.

A key, if often unnoticed, feature of the double helix is that its axis is linear, not in the geometric sense of being a straight line, but in the topological sense that it is unbranched. The biological relevance of this fact is that only a linear complement to a DNA strand is well defined ***(5)***. This point is illustrated in **Fig. 2**. In **Fig. 2A**, a DNA duplex molecule is illustrated, in which each base of strand 2 is paired to strand 1. By contrast, **Fig. 2B** shows a molecule in which strand 2 contains a hairpin that produces a 3-arm branched junction. Every base in strand 1 has a complement in strand 2, just as in **Fig. 2A**. However, the complement is not well defined. The third (horizontal) arm of the junction could have

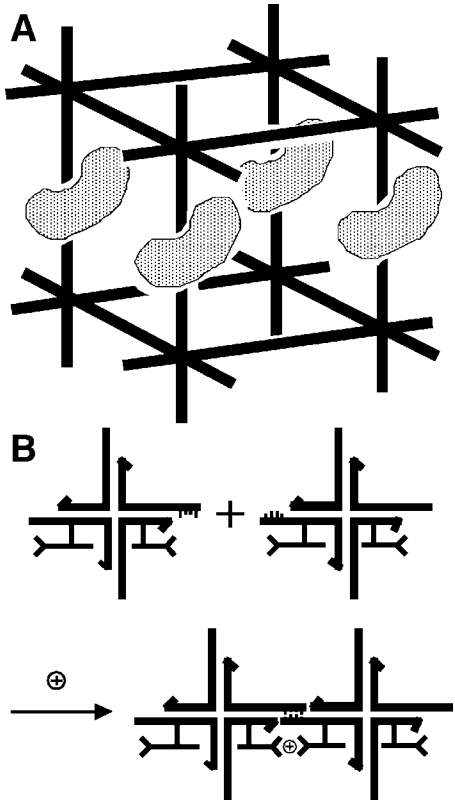

Fig. 1. Applications of DNA periodic arrays. **(A)** Biological macromolecules organized into a crystalline array are depicted. A cubelike box motif is shown, with sticky ends protruding from each vertex. Attached to the vertical edges are biological macromolecules that have been aligned to form a crystalline arrangement. The idea is that the boxes are to be organized into a host lattice by sticky ends, thereby arranging the macromolecular guests into a crystalline array, amenable to diffraction analysis. **(B)** Nanoelectronic circuit components organized by DNA are deposited. Two DNA branched junctions are shown, with complementary sticky ends. Pendent from the DNA are molecules that can act as molecular wires. The architectural properties of the DNA are seen to organize the wirelike molecules, with the help of a cation, which forms a molecular synapse.

any length, without affecting the complementarity of strand 2 for strand 1. Thus, the replication protocol used by DNA polymerase would not be effective in replicating this structure exactly, even though it would produce complements to the individual strands. Nevertheless, biology does use branched DNA as ephemeral intermediates in the processes of replication, recombination, and repair.

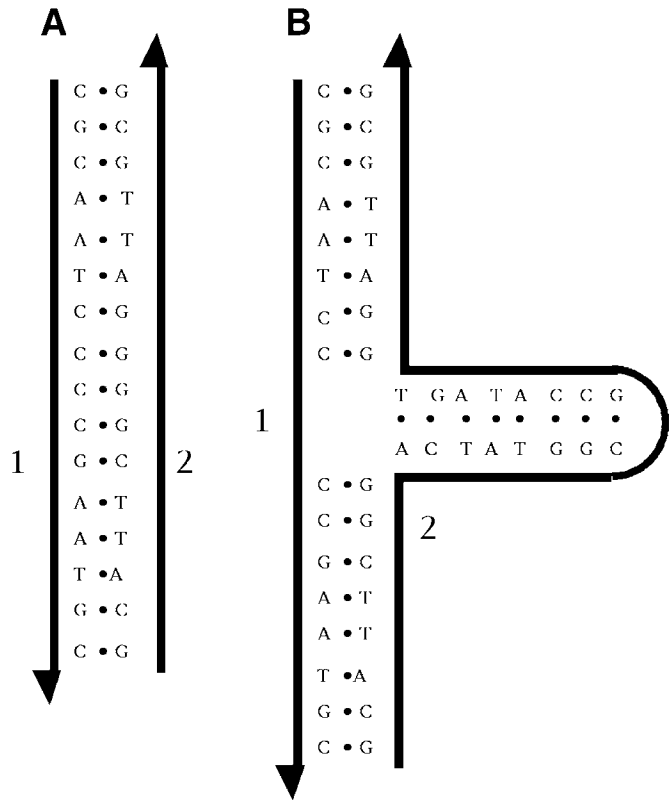

Fig. 2. Inexact complementarity in branched DNA. **(A)** A DNA duplex with its strands numbered 1 and 2 is shown. **(B)** A 3-arm branched junction with its strands also labeled 1 and 2 is shown; strand 1 is identical to strand 1 in (A). Every nucleotide of strand 1 in (B) is complemented by a nucleotide in strand 2 in (B), but there are many nucleotides in the branch whose sequences are irrelevant to the complementarity between strands 2 and 1. The only well-defined complement to strand 1 is strand 2 of (A).

Regardless of the difficulties that branched DNA might present as genetic material, it is extremely valuable for structural DNA nanotechnology, because linear DNA molecules do not lead to inherently interesting arrangements of DNA in two or three dimensions. Genetic engineers have used sticky-ended cohesion and ligation for nearly 30 yr to produce linear recombinant DNA molecules ***(6)***. These molecules are of value for their sequences and the gene products to which they can lead, but structurally speaking, they consist of long lines or circles, perhaps including some catenanes or knots. However, if one combines sticky-ended cohesion with branched DNA species, it is possible to

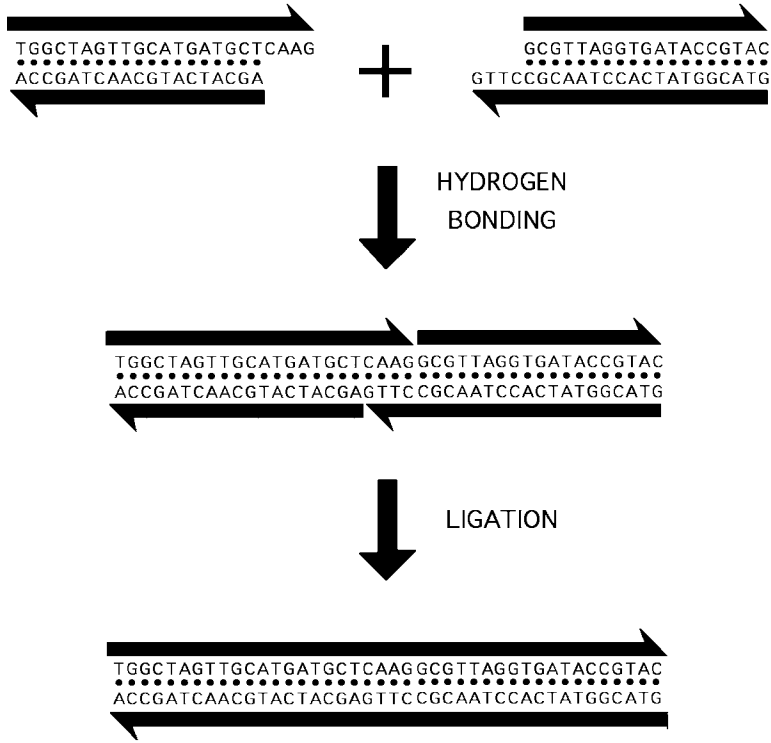

Fig. 3. Sticky-ended cohesion. **(Top)** Two linear double helical molecules of DNA are shown. The black lines terminating in half arrows indicate the antiparallel backbones. The half-arrows also indicate the 5′→3′ directions of the backbones. The right end of the left molecule and the left end of the right molecule have single-stranded extensions ("sticky ends") that are complementary to each other. **(Middle)** Under the proper conditions, these molecules bind to each other specifically by hydrogen bonding. **(Bottom)** The molecules can be ligated to covalency by the proper enzymes and cofactors.

produce many complex structures and topologies with relatively little effort. **Figure 3** illustrates the nature of sticky-ended cohesion: two double helices with complementary single-stranded overhangs will cohere to form a complex under the appropriate solution conditions.

The recognition of one strand of DNA by another strand is common to many types of DNA nanotechnology and to molecular biology. The special feature of *structural* DNA nanotechnology is that it takes advantage of the well-defined structure at the point where the two helices cohere. **Figure 4** shows the crystal structure of a DNA decamer that forms continuous helices within the periodic lattice ***(7)***. In contrast to many other crystals of DNA decamers, these decamers

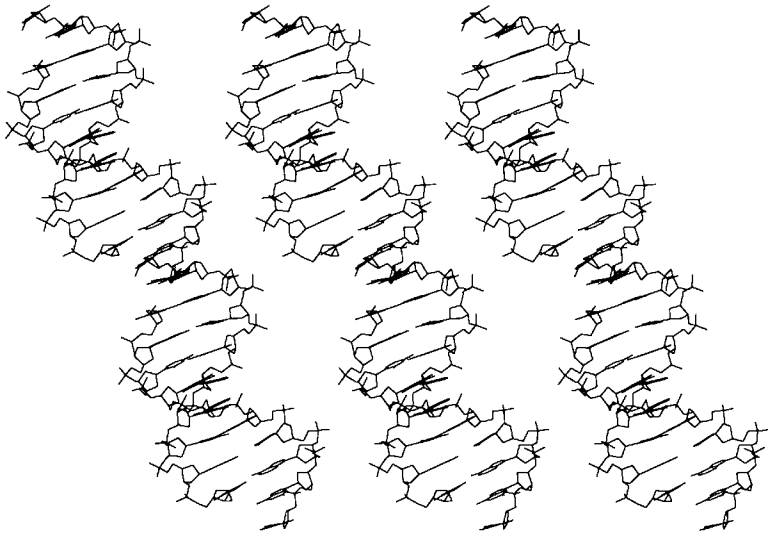

Fig. 4. Crystal structure of infinite DNA helices held together by sticky ends. Shown are three DNA double helices that consist of an infinite repeat of a decamer. The decamers are held together by complementary sticky ends, flanked by breaks in the DNA backbone. The key point is that the DNA around the sticky ends is the same as the rest of the DNA; it is all B-DNA, so the structure of any sticky-ended complex is known with high precision.

are held together by sticky ends at their 5′ ends. The key point of the crystal structure is that the 3D conformation of the DNA in the vicinity of the sticky end is the same as the rest of it; it is all B-DNA, the classic structure. Thus, if two DNA molecules are held together by sticky ends, and one knows the coordinates of one of them, then one knows the coordinates of the one to which it is binding by sticky-ended cohesion. This fact is exploited extensively in structural DNA nanotechnology. If one wished to use some other biologically based recognition system, such as antibody-antigen interactions, it would be possible, but one would have to work out the spatial relationships of the two partners in the binding reaction for every pair, say, by a crystal structure. By contrast, the many possible DNA sticky ends (4^N for N-base sticky ends) have structures that are virtually identical. Other modes of cohesion are being introduced into structural DNA nanotechnology. These include paranemic crossover (PX) cohesion ***(8)*** and edge sharing ***(9)***. However, the structural parameters of these forms of cohesion can only be estimated at this time.

It is easy to generate branched DNA molecules by the logic used in biological systems—reciprocal exchange of strands ***(10)***. An example of reciprocal

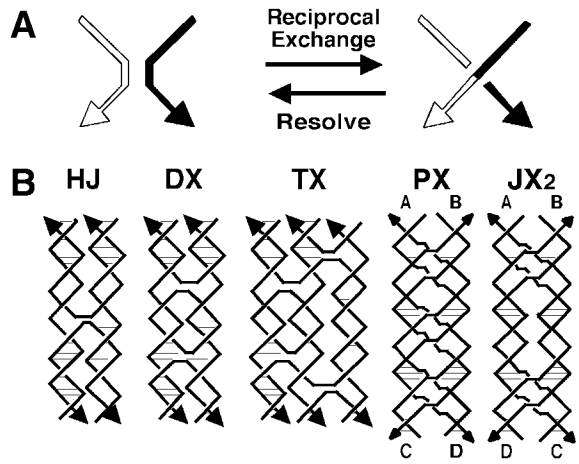

Fig. 5. Motif generation and sample motifs. **(A)** Reciprocal exchange of DNA backbones. Two strands are shown on the left, one filled and one unfilled. Following reciprocal exchange, one strand is filled-unfilled, and the other strand is unfilled-filled. **(B)** Key motifs in structural DNA nanotechnology. On the left is an HJ, a 4-arm junction that results from a single reciprocal exchange between double helices. To its right is a DX molecule, which results from a double exchange. To the right of the DX is a TX molecule, which results from two successive double reciprocal exchanges. The HJ and the DX and TX molecules all contain exchanges between strands of opposite polarity. To the right of the TX molecule is a PX molecule, where two double helices exchange strands at every possible point where the helices come into proximity. To the right of the PX molecule is a JX_2 molecule that lacks two of the crossovers of the PX molecule. The exchanges in the PX and JX_2 molecule are between strands of the same polarity.

exchange is shown in **Fig. 5A**, where a filled strand and an outlined strand trade portions of their strands. **Figure 5B** illustrates a number of motifs derived in this fashion that have proved to be important in structural DNA nanotechnology. At the left is the Holliday junction (HJ), the biological intermediate in genetic recombination ***(11)***, which results from a single reciprocal exchange between double helices. To its right is the double crossover (DX) molecule ***(12)***, an intermediate in meiosis ***(13)***, which is derived by two exchanges between double helices. On the right of the DX molecule is the triple crossover (TX) molecule, which is generated by two reciprocal exchanges between a helix of the DX molecule and another double helix ***(14)***. The two strands of the double helix have opposite polarities. Exchange can occur between strands of the same polarity or strands of opposite polarity. The HJ, DX, and TX molecules shown are all illustrated to have been the result of exchanges between

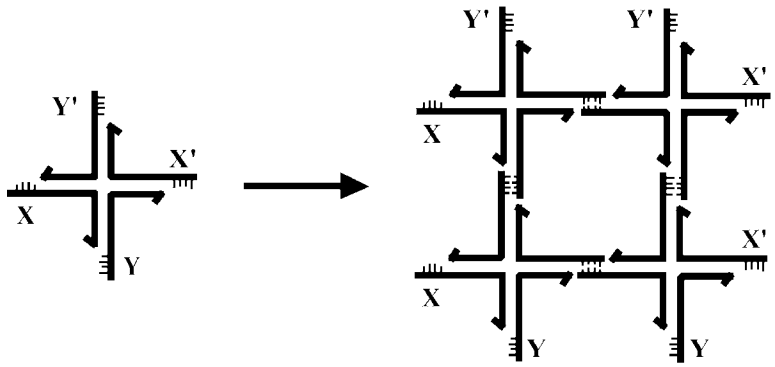

Fig. 6. Combination of branched motifs and sticky ends. At the left is a 4-arm branched junction with sticky ends, labeled X and its complement X′, and Y and its complement Y′. On the right, four such molecules are combined to produce a quadrilateral. The sticky ends on the outside of the quadrilateral are available so that the structure can be extended to form a 2D lattice.

strands of opposite polarity. The PX structure on the right of the TX molecule illustrates crossovers between strands of the same polarity ***(10)***. Exchange in the PX motif occurs at every possible point where the strands are juxtaposed. The JX_2 variant to the right of the PX molecule lacks two crossovers in the middle; it has been used in a robust nanomechanical device ***(15)***.

Figure 6 illustrates the HJ single crossover junction structure in a convenient branched arrangement, much like the intersection of two roads. Each of the four double helical arms has been tailed by a sticky end. The arrangement on the right shows four of these junctions assembled to form a quadrilateral by sticky-ended cohesion. In addition to the sticky ends that pair within each edge of the quadrilateral, sticky ends are visible on the outside of the structure, so that this arrangement could be extended to yield two-dimensional ***(20)*** crystalline arrays. It is important to realize that the parallel-line representation of DNA used in **Fig. 6** is only a convenience. The double helical nature of DNA really makes this a 3D system, rather than a 2D system. Thus, in principle, branched DNA molecules tailed in sticky ends can be assembled into 3D objects and lattices.

Why use DNA for this purpose? The key reason has already been discussed: sticky-ended cohesion of DNA is the most predictable *intermolecular* interaction of any known molecular system, in the senses of affinity, diversity, and structure. In addition, convenient automated chemistry exists for the synthesis of DNA molecules of particular sequences, both conventional nucleotides and specially derivatized variants, such as biotinylated nucleotides or branched

residues. There are numerous enzymes that can be used with DNA: ligases to join cohesive ends covalently ***(6)***, restriction enzymes that can be used both synthetically ***(16)*** and analytically ***(17,18)***, exonucleases for the removal of failure products ***(17)***, and topoisomerases that can be used to diagnose topological problems ***(19)***. DNA is a relatively stiff molecule, with a persistence length of about 50 nm under standard conditions ***(20)***. There is an external code on DNA so that its sequence may be read from the grooves, even though the double helix is intact ***(21)***. The functional group density of DNA is very high; thus, it may be derivatized at a density limited only by the nucleotide repeat. In addition, the gene therapy and antisense enterprises have produced large numbers of variants on the theme of DNA (e.g., *see* **ref. *22***); although it is most convenient to prototype nanoconstructs with DNA, many applications are likely to benefit from the use of variants such as peptide nucleic acids ***(23)***.

How does one choose sequences for DNA constructs? The key to any successful molecular engineering approach is to design the components of a construction not just so that they are capable of yielding the product, but also to ensure, insofar as possible, that no other product will be competitive with the target. Ultimately, one must estimate the thermodynamics of all possible sequences and select the one most likely to lead to the intended product ***(24)***. Empirically, I have found that adequate sequences can be generated by the approximation to this approach called sequence symmetry minimization, which is shown in **Fig. 7** ***(2,25)***. This drawing illustrates a 4-arm junction; its arms are each 8 nt long, so each of its strands contains 16 nt. One divides the 16 nt into a series of overlapping elements (13 tetramers in this case). One insists that each of these elements, such as the boxed CGCA and GCAA, be unique. In addition, one also insists that any element that spans a bend (such as the boxed CTGA) not have its simple contiguous Watson-Crick complement (TCAG) anywhere in the sequence. With these constraints, competition with the target octamers can come only from trimers, such as the ATG sequences in the dashed boxes. It should be clear that this approach assumes that double helices are the most favorable structures that DNA can form, and that maximizing double helix formation will lead to the successful formation of branch points. The success of this method relies on the cooperativity of DNA double helix formation.

2. DNA Objects

Individual branched junctions have been constructed containing 3 ***(26)***, 4 ***(24)***, 5, and 6 arms ***(27)***. A variety of studies have shown that the angles between the arms appear to be flexible ***(26,28,29)***. Consequently, the earliest constructions consisted of topological targets, rather than targets with specific 3D geometries. Both the level of control and the proofs of these structures are on the topological level. The connectivity of an object is the number of vertices

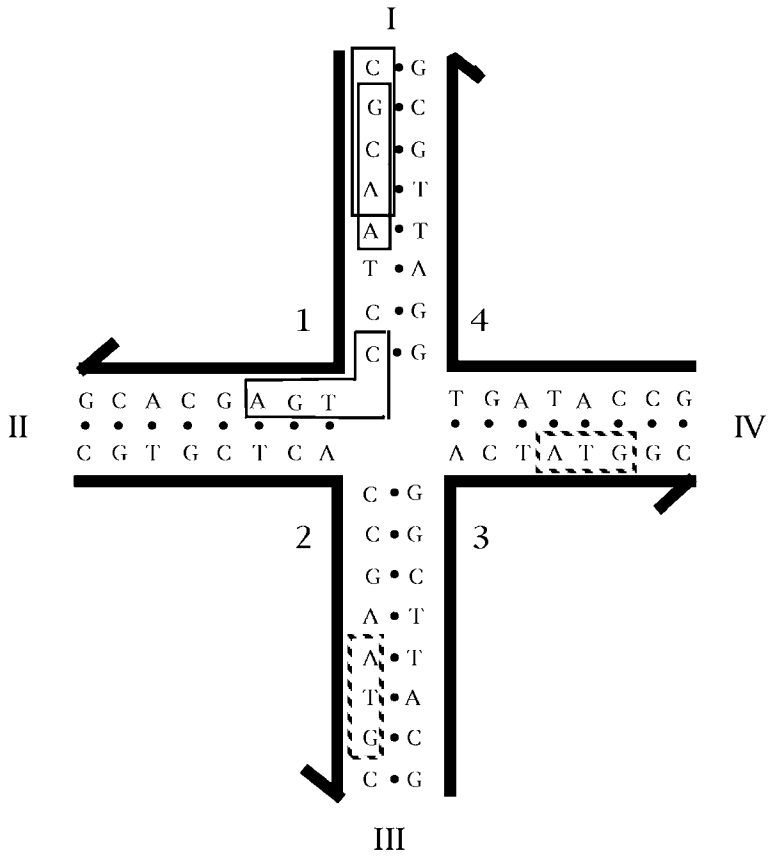

Fig. 7. Sequence Symmetry Minimization produces a stable DNA branched junction. The junction shown is composed of four strands of DNA, labeled with Arabic numerals. The half arrows indicate the 3′ end of each strand. Each strand is paired with two other strands to form double helical arms; the arms are numbered with Roman numerals. The dots between the bases indicate the hydrogen-bonded base paring that forms the double helices. The sequence of this junction has been optimized to minimize symmetry and non-Watson-Crick base pairing. Because there is no homologous twofold sequence symmetry flanking the central branch point, this junction cannot undergo the branch migration isomerization reaction. At the upper part of arm I, two of the 52 unique tetrameric elements in this complex are boxed; these are CGCA and GCAA. At the corner of strand 1, the sequence CTGA is boxed. This is 1 of 12 sequences in the complex (3 on each strand) that span a junction. The complements to each of these 12 sequences are not present. Whereas tetrameric elements have been used to assign the sequence of this molecule, there is redundancy in the molecule among trimers, such as the ATG sequences shown in the dashed boxes.

to which every vertex is bonded via the edges. The first object with a nontrivial connectivity of 3 or greater was a DNA molecule whose helix axes were connected like the edges of a cube ***(17)***. The edges consisted of DNA double helices, and the vertices corresponded to the branch points of 3-arm junctions. There were two turns per edge, so each face consisted of a cyclic single strand linked twice to each of its four neighbors, forming a hexacatenane. Every edge of this molecule (shown in **Fig. 8A**) contains a unique restriction site. It was constructed in solution, and proof of synthesis consisted of restricting the final hexacatenane to target subcatenanes ***(17,30)***.

In the next development, a truncated octahedron was also constructed from DNA ***(18)***, this time using a solid-support-based method ***(16)***. This molecule (shown in **Fig. 8B**) is also a complex catenane. There are 14 faces to a truncated octahedron, so this molecule is a 14-catenane, with six strands corresponding to square faces and eight strands corresponding to hexagonal faces. Although the truncated octahedron is a 3-connected object, it was constructed with 4-arm junctions (not shown), in the hope that the extra helices could be used to connect the polyhedra into a macromolecular version of zeolite A. Enough material was produced to demonstrate the synthesis, but not to use it as starting material for lattice construction.

In addition to these polyhedral catenanes, a series of strictly topological targets has been produced. Knots and catenanes are characterized by the set of nodes seen when they are projected into a plane. The half turn of DNA corresponds to such a node in any topological target. Consequently, it is easy to produce virtually any knot from DNA, with negative nodes being produced by conventional right-handed B-DNA and positive nodes being derived from left-handed Z-DNA ***(31)***. **Figure 8C** illustrates a trefoil knot with negative nodes, and **Fig. 8E** a trefoil knot with positive nodes. **Figure 8D** shows a figure-8 knot with two negative nodes and two positive nodes. All of these knots (and an unknotted circle) have been produced from one strand of DNA by changing ligation conditions. The strand contained two regions that could turn into Z-DNA, but with different propensities: at non-Z-promoting conditions, the knot with negative nodes was produced; at conditions that weakly promote the B-Z transition, the figure-8 knot was produced; and at strongly Z-promoting conditions, the trefoil with positive nodes was produced ***(32)***. **Figure 8F** illustrates Borromean rings built from the combination of a right-handed B-DNA 3-arm junction connected to a left-handed Z-DNA 3-arm junction ***(33)***. Borromean rings have a special property: when any ring in a set of Borromean rings is cut, all the rings fall apart. This is an extremely difficult topology to produce from conventional organometallic systems, but it was relatively easy to make it from DNA.

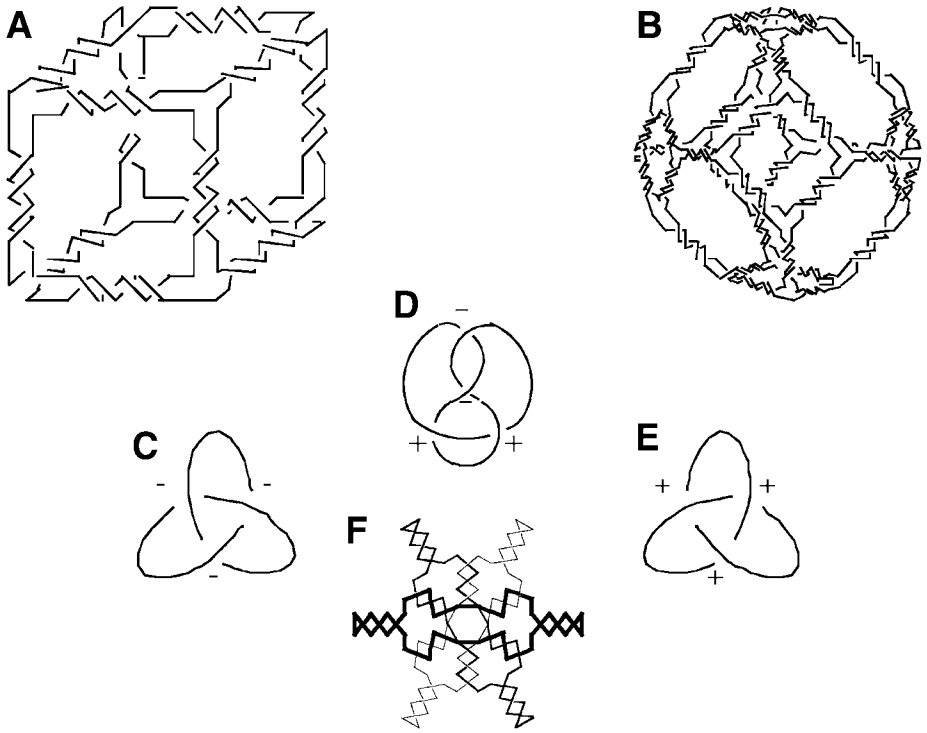

Fig. 8. Ligated products from flexible DNA components. **(A)** Stick cube and **(B)** stick truncated octahedron. The drawings show that each edge of the two figures contains two turns of double helical DNA. The twisting is confined to the central portion of each edge for clarity, but it actually extends from vertex to vertex. Both molecules are drawn as though they were constructed from 3-arm junctions, but the truncated octahedron has been constructed from 4-arm junctions, which has been omitted for clarity. **(C–E)** Deliberate knots constructed from DNA. The signs of the nodes are indicated: (C) a trefoil knot with negative nodes; (D) a figure-8 knot; (E) a trefoil knot with positive nodes. **(F)** Borromean rings. Scission of any of the three rings shown results in the unlinking of the other two rings.

3. DNA Arrays

Being able to produce a series of topological targets, such as the knots, Borromean rings and polyhedral catenanes are of interest, but the greatest value will be derived when a variety of species can be attached to each other, particularly if functionality is associated with them. The essence of structural DNA nanotechnological goals is to place specific functional species at particular loci, using the architectural properties of DNA. Functionality includes the use of periodic DNA arrays to scaffold molecular arrangements in other species,

alogorithmic assemblies that perform computations, and the development of DNA-based nanomechanical devices.

In addition to the intermolecular specificity described in **Subheading 1.**, the key architectural property that is needed to build and demonstrate these arrays and devices is high structural integrity in the components; even if their associations are precise, the assembly from marshmallow-like components will not produce well-structured materials. As noted above, single-branched junctions, such as the HJ structure in **Fig. 6**, are relatively flexible. Fortunately, the DX molecule is considerably more rigid, apparently stiffer than double helical DNA ***(34,35)***. The TX and PX molecules appear to share this rigidity ***(14,15)***. Consequently, it has been possible to use these molecules as the building blocks of both arrays and devices. Arrays are expected to be useful as the scaffolding for the heteromolecules shown in **Fig. 1**, as the basis of DNA computation by self-assembly, and as frameworks to mount DNA nanomechanical devices.

Figure 9 illustrates 2D arrangements that entail the use of DX molecules to produce periodic patterns. **Figure 9A** illustrates a two-component array that can tile the plane. One tile is a DX molecule labeled **A** and the second is a DX molecule labeled **B***. **B*** contains another DNA domain that projects out of the plane of the helix axes. This other domain can serve as a topographic marker for the atomic force microscope when the **AB*** array is deposited onto the surface of mica. The dimensions of the two DX tiles in **Fig. 9A** are about 4 nm high × 16 nm wide × 2 nm thick. Thus, the **B*** markers in the 2D array shown should appear as stripelike features separated by approx 32 nm, which has been confirmed by experiment. **Figure 9b** shows a four-tile arrangement that should produce stripes separated by approx 64 nm, also confirmed by experiment ***(36)***. Thus, it is possible to design and produce patterns using DNA components; these patterns contain predictable features, based on the sticky-ended cohesion of individual motifs. The patterns can be modified by the enzymatic addition or removal of these features; nonenzymatic addition has also been demonstrated ***(37)***. In addition to forming arrays from DX molecules, it is possible to produce periodic arrays from TX molecules ***(14)***. A variety of DNA parallelograms also have been used to produce 2D arrays ***(38–40)***. These motifs are produced by combining four HJ-like branched junctions. Unlike the DX, TX, and PX molecules, the two domains of the HJ molecule are not parallel to each other. As a function of the sequence and backbone connections at the crossover point, they adopt angles of approx 60° ***(38)***, approx –70° ***(39)***, or approx 40° ***(40)***, thus producing a diversity of parallelogram angles.

4. DNA Nanomechanical Devices

Nanomechanical action is a central target of nanotechnology. The first DNA-based devices were predicated on structural transitions of DNA driven by small

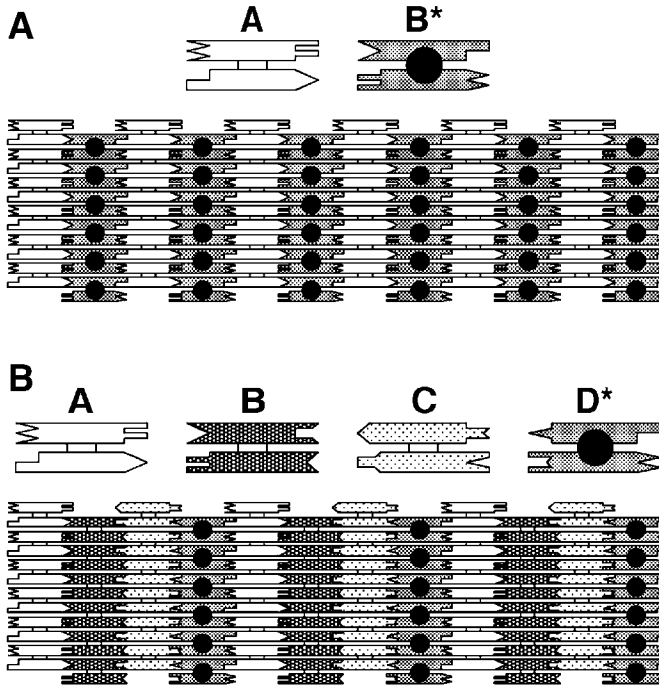

Fig. 9. Tiling the plane with DX molecules. **(A)** Two-tile pattern. The two helices of the DX molecule are represented schematically as rectangular shapes that terminate in a variety of shapes. The terminal shapes are a geometrical representation of sticky ends. The individual tiles are shown at the top of the figure; the way tiles fit together using complementary sticky ends to tile the plane is shown at the bottom. The molecule labeled **A** is a conventional DX molecule, but the molecule labeled **B*** contains a short helical domain that protrudes from the plane of the helix axes; this protrusion is shown as a black dot. The black dots form a stripelike feature in the array. The dimensions of the tiles are 4×16 nm in this projection. Thus, the stripelike features should be about 32 nm apart. **(B)** Four-tile pattern. The same conventions apply as in **(A)**. The four tiles form an array in which the stripes should be separated by about 64 nm, as confirmed by atomic force microscopy.

molecules. The initial DNA device entailed the extrusion of a DNA cruciform structure from a cyclic molecule ***(41)***. The system consisted of a DNA circle (approx 300 nt) that contained a branch point capable of assuming five different positions, because there were four symmetric nucleotides at its base; the symmetry was eliminated beyond that point. The device is illustrated in **Figure 10**. The position of the branch point was controlled by the addition or removal of an intercalating dye that changes the supercoiling. This system was not very

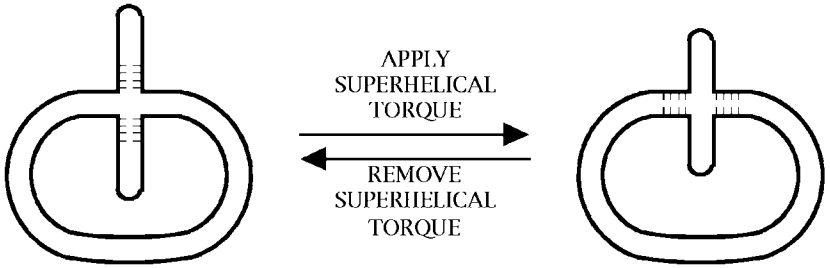

Fig. 10. Torsionally driven DNA device. On the left is a DNA circle that contains a fixed branch. There are four symmetric nucleotide pairs at the base of the branch, and these can undergo branch migration. With the normal twist of the DNA in the circle, the nucleotides are extruded from the circle. However, when the twist is decreased by the addition of ethidium, the nucleotide branch migrates to become part of the circle.

convenient to operate, and the large size of the DNA circle made it unwieldy to handle. Nevertheless, it demonstrated that DNA could form the basis of a two-state mechanical system.

The second DNA-based device (**Fig. 11A**) was a marked advance. It was relatively small and included two rigid components, DX molecules like those used to make the arrays in **Fig. 9**. The basis of the device was the transition between right-handed (conventional) B-DNA and left-handed Z-DNA. There are two requirements for the formation of Z-DNA: a "proto-Z" sequence capable of forming Z-DNA readily (typically a $[CG]_n$ sequence), and conditions (typically high salt or molecules like $Co[NH_3]_6^{3+}$ that emulate the presence of high salt) to promote the transition ***(42)***. The sequence requirement provides control over the transition in space, and the requirement for special conditions provides control over the transition in time. As shown in **Fig. 11A**, the device consists of two DX molecules connected by a $(CG)_{10}$ double helical shaft that provides the proto-Z sequence. In B-promoting conditions, both of the DX helices not collinear with the shaft are on the same side of the shaft. In Z-promoting conditions, one of these helices ends up on the other side of the shaft. This difference is the result of converting a portion of the shaft to Z-DNA, which rotates one DX motif relative to the other by 3.5 turns. The movement was demonstrated by fluorescence resonance energy transfer (FRET) measurements that respond to the difference between dye separations on the DX motifs ***(43)***.

The reason that the B-Z device is not the ultimate DNA-based nanomechanical device is that it is activated by an unspecific molecule, $Co(NH_3)_6^{3+}$. Consequently, a number of such devices, embedded in an array, would all respond similarly, although some chemical nuance might be available to obtain

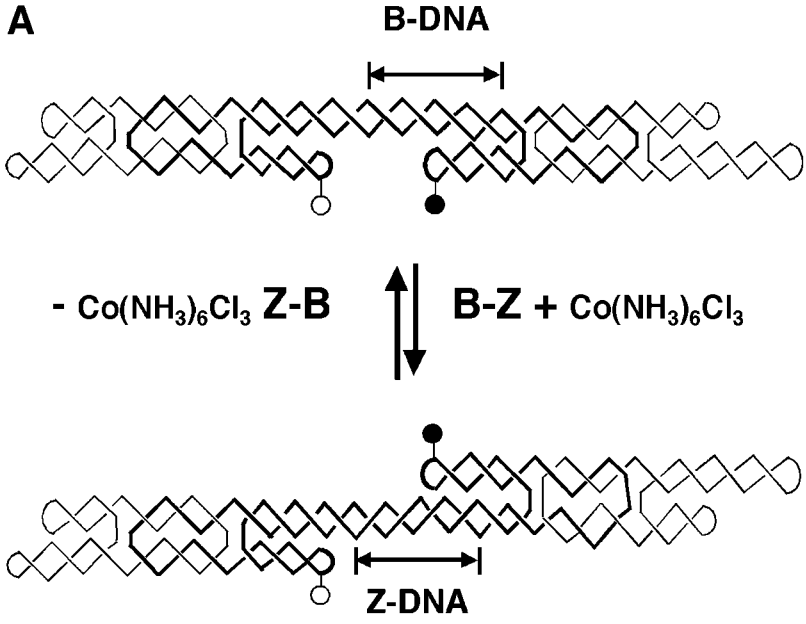
A
B-DNA
- Co(NH3)6Cl3 Z-B
B-Z + Co(NH3)6Cl3
Z-DNA

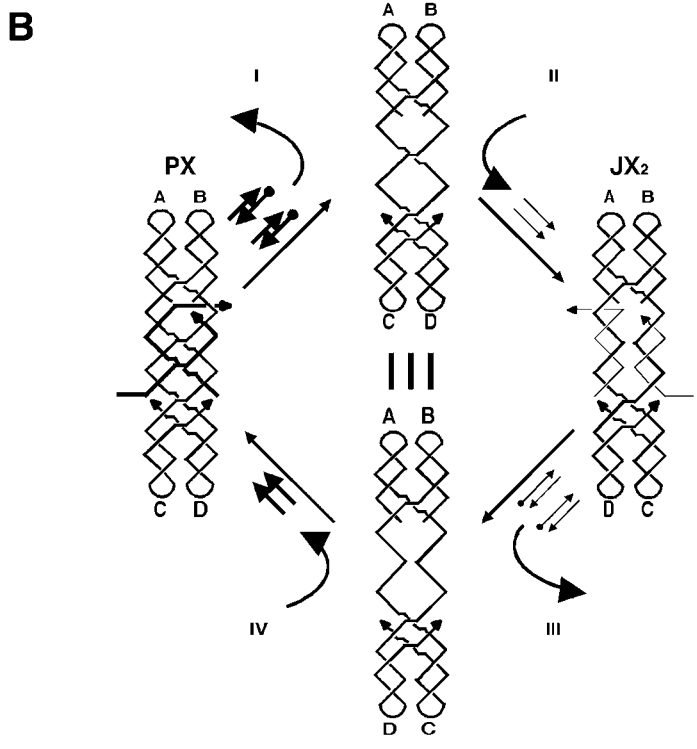
B
A B
I
II
PX
JX2
A B
C D
C D
A B
A B
D C
D C
IV
III

differential responses ***(32)***. Thus, N two-state devices would result in essentially two structural states; clearly it would be of much greater utility to have N distinct two-state devices capable of producing 2^N structural states. It is evident that a sequence-dependent device would be an appropriate vehicle for the goal of achieving multiple states; Yurke et al. ***(44)*** worked out the method for manipulating sequence-dependent devices. It entails setting the state of a device by the addition of a "set" strand that contains an unpaired tail. When the full complement to the set strand is added, the set strand is removed, and a different set strand may be added. This system has been adapted to the PX and JX_2 motifs (**Fig. 5**) ***(15)***. **Figure 11B** shows how these two states can be interconverted by the removal of one pair of set strands (processes I and III) and the addition of the opposite pair (processes II and IV). The tops and bottoms of the two states differ by a half rotation, as seen by comparing the A and B labels at the tops of the molecules, and the C and D labels at the bottoms of the molecules. A variety of devices can be produced by changing the sequences of the regions where the set strands bind.

Fig. 11. *(See opposite page)* DNA-based nanomechanical devices. **(A)** Device predicated on B-Z transition. The molecule consists of two DX molecules, connected by a segment containing proto-Z-DNA. The molecule also consists of three cyclic strands, two on the ends, drawn with a thin line, and one in the middle, drawn with a thick line. The molecule contains a pair of fluorescent dyes to report their separation by FRET. One is represented as a solid circle, and the other as an open circle. In the upper molecule, the proto-Z segment is in the B conformation, and the dyes are on the same side of the central double helix. In the lower molecule, the proto-Z segment is in the Z conformation, and the dyes are on opposite sides of the central double helix. At the top and bottom, the two vertical lines flanking the conformation descriptor indicate the length of the proto-Z-DNA and its conformation. **(B)** Sequence-dependent device. This device uses two motifs, PX and JX_2. The labels A, B, C, and D on both show that there is a 180° difference between the wrappings of the two molecules. Two strands are drawn as thick lines at the center of the PX motif, and two strands are drawn with thin lines at the center of the JX_2 motif; in addition to the parts pairing to the larger motifs, each has an unpaired segment. These strands can be removed and inserted by the addition of their total complements (including the segments unpaired in the larger motifs) to the solution; these complements are shown in processes I and III as strands with black dots (representing biotins) on their ends. The biotins can be bound to magnetic streptavidin beads so that these species can be removed from solution. Starting with the PX, one can add the complement strands (process I), to produce an unstructured intermediate. Adding the set strands in process II leads to the JX_2 structure. Removing them (III) and adding the PX set strands (IV) completes the machine cycle. Many different devices could be made by changing the sequences to which the set strands bind.

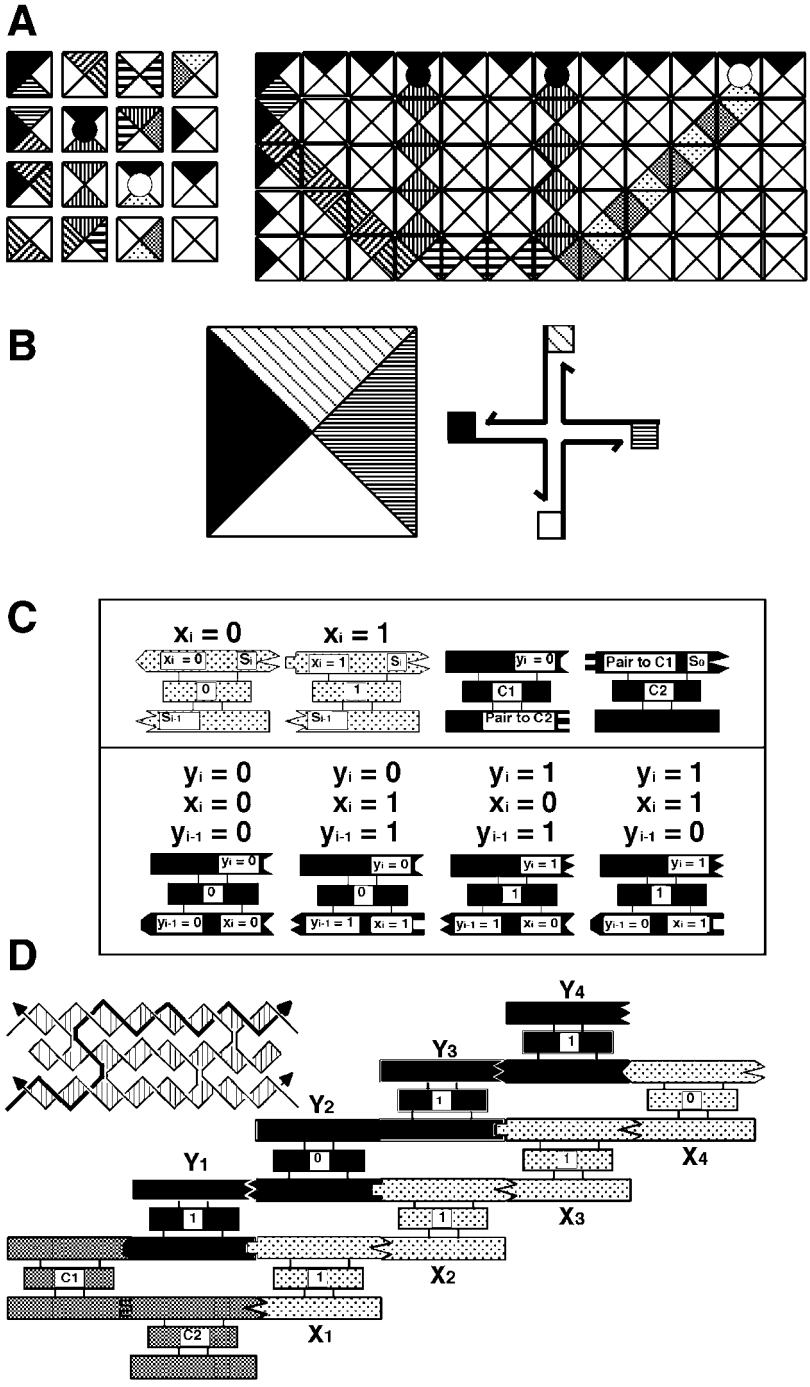
A
B
C
$x_i = 0$
$x_i = 1$
$y_i = 0$
Pair to C1
C1
C2
Pair to C2
$y_i = 0$ $x_i = 0$ $y_{i-1} = 0$
$y_i = 0$ $x_i = 1$ $y_{i-1} = 1$
$y_i = 1$ $x_i = 0$ $y_{i-1} = 1$
$y_i = 1$ $x_i = 1$ $y_{i-1} = 0$
D
Y_4
Y_3
Y_2
Y_1
X_4
X_3
X_2
X_1
C1
C2

5. DNA-Based Computation

In 1994, Leonard Adleman ***(45)*** founded experimental DNA-based computation. His approach is different from the use of DNA to scaffold nanoelectronic component assembly, suggested in **Fig. 1**. Instead, Adleman combined the information in DNA molecules themselves, using standard biotechnological operations (ligation, polymerase chain reaction, gel electrophoresis, and sequence-specific binding to derivatized beads) to solve a Hamiltonian path problem. This is a problem related to the traveling salesman problem (What is the optimal route for a salesman to visit *N* cities?). In the Hamiltonian path problem, there is a defined start point and end point, and an incomplete set of routes between the cities; the problem is to establish whether there is a path between the start point and end point that visits all the cities. The idea behind DNA-based computation is that there exist certain classes of computational problems for which the parallelism of molecular assembly overcomes the slow speed of the required macroscopic manipulations. Many varieties of DNA-based computation have been proposed, and a number of them have been tested experimentally for relatively small cases. Space does not permit discussion of all of them.

Nevertheless, there is one approach to DNA-based computation that is relevant to our discussion of structural DNA nanotechnology. This was a method

---

Fig. 12. *(see opposite page)* DNA-based computation. **(A)** Wang tiles. On the left is a group of 16 Wang tiles. The edges of the tiles are flanked by a variety of patterns. These tiles assemble into the mosaic on the right according to the rule that each edge in the mosaic is flanked by the same pattern. The mosaic represents a calculation, adding 4 to 7 to obtain 11. The two addends are in the top row in the fourth and seventh column. The path through the calculation begins in the upper left corner and continues on a diagonal until it encounters the vertical column in the fourth column. The path then switches to horizontal until the seventh column and then switches again to the diagonal, terminating in the eleventh column. (After **ref. *46***.) **(B)** Relationship between Wang tiles and branched junctions. The shadings are the same in both the tile and the sticky ends of the junction, indicating that the sticky ends on a branched junction can emulate a Wang tile. **(C)** Components of a cumulative XOR calculation. TX tiles are shown as rectangles ending in sticky ends represented geometrically. The input *x* tiles are shown at the upper left, and the value of the tile is shown in the central domain. Initiator tiles C1 and C2 are shown in the upper right and the four possible *y* tiles are shown in the bottom row. The inputs of the *y* tiles is shown on their bottom domains. **(D)** Self-assembled tiles. The strand structure of the TX tiles is illustrated on the upper left, with the reporter strand drawn with a thicker line. The assembly of tiles in a prototype calculation is shown, using the components illustrated in (C). The input 1, 1, 1, 0 produces an output of 1, 0, 1, 1 by successive binding of *y* tiles into the double sites created as the array assembles.

suggested by Winfree ***(4)***, who noticed that the system described above, branched junctions with sticky ends, could be a way to implement computation by "Wang tiles" on the molecular scale. This is a system of tiles whose edges may contain one or more different markings; the tiles self-assemble into a mosaic according to the local rule that all edges in the mosaic are flanked by the same marking. Such a form of assembly can be shown to emulate the operation of a Turing machine, a general-purpose computer ***(46)***. A group of Wang tiles is shown on the left of **Fig. 12A**, and an assembly of Wang tiles is shown on the right. The relationship between the sticky ends of a branched junction and the markings on a Wang tile is shown in **Fig. 12B**.

This form of DNA-based computation has been prototyped successfully in a 4-bit cumulative exclusive OR (XOR) calculation ***(47)***. The XOR calculation yields a 1 if the two inputs are different, and a 0 if they are the same. **Figure 12C** shows the components of this calculation. Each component is a TX molecule, schematized as three rectangles with geometrical shapes on their ends to represent complementarity. The input bits are "*x*" tiles (upper left), and the output bits are "*y*" tiles (bottom), and there are two initiator tiles, C1 and C2, as well (upper right). The upper left corner of **Fig. 12D** shows the strand structure of the TX tiles; each strand contains a "reporter strand" (drawn with a thicker line); the value of *x* and *y* tiles is set to 0 or 1, depending on whether the tile contains a *Pvu*II or *Eco*RV restriction site, respectively. The y_i tiles perform the gating function; there are four of them, corresponding to the four possible combinations of 0 and 1 inputs. The input involves the bottom domain (**Fig. 12C**). The assembly of periodic arrays discussed in **Subheading 3.** entails competition between correct and incorrect tiles for particular positions; by contrast, the competition here is between correct and partially correct tiles. For example, the $y_{i-1} = 0$ sticky end on the leftmost tile is the same as the y_{i-1} sticky end on the rightmost tile. In the cumulative XOR calculation, $y_i = \text{XOR}\ (x_i, y_{i-1})$. The implementation of this formula is shown in **Fig. 12D**. The x_i tiles and the initiators are given longer sticky ends than the y_i tiles, so they assemble a template first when the tiles are cooled. This creates a double site where the υ_1 tile can bind. This binding creates the double site where the y_2 tile can bind, and so on. When the assembly is complete, the reporter strands are ligated together, creating a long strand that connects the input to the output through the initiator tiles. Partial restriction analysis of the resulting strand reveals that the correct answer is obtained almost exclusively.

6. Conclusion

This chapter discussed the current state of structural DNA nanotechnology, emphasizing the individual components, their assembly into objects and

topological targets as well as into periodic and algorithmic arrays, and their manipulation as nanomechanical devices. Where is the field going? The achievement of several key near-term goals will move structural DNA nanotechnology from an elegant structural curiosity to a system with practical consequences. First among these goals is the extension of array-making capabilities from 2D to 3D, particularly with high order. Likewise, heterologous molecules must be incorporated into DNA arrays, so that the goals both of orienting biological macromolecules for diffraction purposes and of organizing nanoelectronic circuits may be met. DNA nanorobotics awaits the incorporation of the PX-JX_2 device into arrays. Algorithmic 3D assembly will lead ultimately to very smart materials, particularly if combined with nanodevices. Hierarchical systems must ultimately be developed, as well as the combination of arrays with aptamers for sensor applications. The development of self-replicating systems using branched DNA appears today to be somewhat oblique ***(48,49)***, but it nevertheless represents an exciting challenge that will significantly economize on the preparation of these systems and increase their development by in vitro evolution. Currently, structural DNA nanotechnology is a biokleptic pursuit, stealing genetic molecules from biological systems; ultimately, it must advance from biokleptic to biomimetic, not just using the central molecules of life, but improving on them, without losing their inherent power as central elements of self-assembled systems.

Acknowledgments

I am grateful to all of my students, postdocs, and collaborators for their contributions to the founding of structural DNA nanotechnology. This research was supported by grants GM-29554 from the National Institute of General Medical Sciences, N00014-98-1-0093 from the Office of Naval Research; DMI-0210844, EIA-0086015, DMR-01138790, and CTS-0103002 from the National Science Foundation, and F30602-01-2-0561 from DARPA/AFSOR.

References

1. Watson, J. D. and Crick, F. H. C. (1953) A structure for deoxyribose nucleic acid. *Nature* **171,** 737–738.
2. Seeman, N. C. (1982) Nucleic acid junctions and lattices. *J. Theor. Biol.* **99,** 237–247.
3. Robinson, B. H. and Seeman, N. C. (1987) The design of a biochip. *Protein Eng.* **1,** 295–300.
4. Winfree, E. (1996) On the computational power of DNA annealing and ligation, in *DNA Based Computing* (Lipton, E. J. and Baum, E. B., eds.), American Mathematical Society, Providence, RI, pp. 199–219.
5. Seeman, N. C. (2000) In the nick of space: generalized nucleic acid complementarity and the development of DNA nanotechnology. *Synlett* **2000,** 1536–1548.

6. Cohen, S. N., Chang, A. C. Y., Boyer, H. W., and Helling, R. B. (1973) Construction of biologically functional bacterial plasmids *in vitro*. *Proc. Nat. Acad. Sci. USA* **70,** 3240–3244.
7. Qiu, H., Dewan, J. C., and Seeman, N. C. (1997) A DNA decamer with a sticky end: the crystal structure of d-CGACGATCGT. *J. Mol. Biol.* **267,** 881–898.
8. Zhang, X., Yan, H., Shen, Z., and Seeman, N. C. (2002) Paranemic cohesion of topologically-closed DNA molecules. *J. Am. Chem. Soc.* **124,** 12,940–12,941.
9. Yan, H. and Seeman, N. C. (2003) Edge-sharing motifs in DNA nanotechnology. *J. Supramol. Chem.* **1,** 229–237.
10. Seeman, N. C. (2001) DNA nicks and nodes and nanotechnology. *Nano Lett.* **1,** 22–26.
11. Holliday, R. (1964) A mechanism for gene conversion in fungi. *Genet. Res.* **5,** 282–304.
12. Fu, T.-J. and Seeman, N. C. (1993) DNA double crossover structures. *Biochem.* **32,** 3211–3220.
13. Schwacha, A. and Kleckner, N. (1995) Identification of double Holliday junctions as intermediates in meiotic recombination. *Cell* **83,** 783–791.
14. LaBean, T., Yan, H., Kopatsch, J., Liu, F., Winfree, E., Reif, J. H., and Seeman, N. C. (2000) The construction, analysis, ligation and self-assembly of DNA triple crossover complexes. *J. Am. Chem. Soc.* **122,** 1848–1860.
15. Yan, H., Zhang, X., Shen, Z., and Seeman, N. C. (2002) A robust DNA mechanical device controlled by hybridization topology. *Nature* **415,** 62–65.
16. Zhang, Y. and Seeman, N. C. (1992) A solid-support methodology for the construction of geometrical objects from DNA. *J. Am. Chem. Soc.* **114,** 2656–2663.
17. Chen, J. and Seeman, N. C. (1991) The synthesis from DNA of a molecule with the connectivity of a cube. *Nature* **350,** 631–633.
18. Zhang, Y. and Seeman, N. C. (1994) The construction of a DNA truncated octahedron. *J. Am. Chem. Soc.* **116,** 1661–1669.
19. Qi, J., Li, X., Yang, X., and Seeman, N. C. (1996) The ligation of triangles built from bulged three-arm DNA branched junctions. *J. Am. Chem. Soc.* **118,** 6121–6130.
20. Hagerman, P. J. (1988) Flexibility of DNA. *Ann. Rev. Biophys. Chem.* **17,** 265–286.
21. Seeman, N. C., Rosenberg, J. M., and Rich, A. (1976) Sequence specific recognition of double helical nucleic acids by proteins. *Proc. Nat. Acad. Sci. USA* **73,** 804–808.
22. Freier, S. M. and Altmann, K.-H. (1997) The ups and down of nucleic acid duplex stability. *Nucleic Acids Res.* **25,** 4229–4243.
23. Nielsen, P. E., Egholm, M., Berg, R. H., and Buchardt, O. (1991) Sequence selective recognition of DNA by strand displacement with a thymine-substituted polyamide. *Science* **254,** 1497–1500.
24. Kallenbach, N. R., Ma, R.-I., and Seeman, N. C. (1983) An immobile nucleic acid junction constructed from oligonucleotides. *Nature* **305,** 829–831.
25. Seeman, N. C. (1990) *De novo* design of sequences for nucleic acid structure engineering. *J. Biomol. Struct. Dynanics* **8,** 573–581.

26. Ma, R. I., Kallenbach, N. R., Sheardy, R. D., Petrillo, M. L., and Seeman, N. C. (1986) Three arm nucleic acid junctions are flexible. *Nucleic Acids Res.* **14,** 9745–9753.
27. Wang, Y., Mueller, J. E., Kemper, B., and Seeman, N. C. (1991) The assembly and characterization of 5-arm and 6-arm DNA junctions. *Biochemistry* **30,** 5667–5674.
28. Petrillo, M. L., Newton, C. J., Cunningham, R. P., Ma, R.-I., Kallenbach, N. R., and Seeman, N. C. (1988) Ligation and flexibility of four-arm DNA junctions. *Biopolymers* **27,** 1337–1352.
29. Eis, P. S. and Millar, D. P. (1993) Conformational distributions of a four-way DNA junction revealed by time-resolved fluorescence resonance energy transfer. *Biochemistry* **32,** 13,852–13,860.
30. Chen, J. and Seeman, N. C. (1991) The electrophoretic properties of a DNA cube and its sub-structure catenanes. *Electrophoresis* **12,** 607–611.
31. Seeman, N. C. (1992) The design of single-stranded nucleic acid knots. *Mol. Eng.* **2,** 297–307.
32. Du, S. M., Stollar, B. D., and Seeman, N. C. (1995) A synthetic DNA molecule in three knotted topologies. *J. Am. Chem. Soc.* **117,** 1194–1200.
33. Mao, C., Sun, W., and Seeman, N. C. (1997) Assembly of Borromean rings from DNA. *Nature* **386,** 137–138.
34. Li, X., Yang, X., Qi, J., and Seeman, N. C. (1996) Antiparallel DNA double crossover molecules as components for nanoconstruction. *J. Am. Chem. Soc.* **118,** 6131–6140.
35. Sa-Ardyen, P., Vologodskii, A. V., and Seeman, N. C. (2003) The flexibility of DNA double crossover molecules. *Biophys. J.* **84,** 3829–3837.
36. Winfree, E., Liu, F., Wenzler, L. A., and Seeman, N. C. (1998) Design and self-assembly of two-dimensional DNA crystals. *Nature* **394,** 539–544.
37. Liu, F., Sha, R., and Seeman, N. C. (1999) Modifying the surface features of two-dimensional DNA crystals. *J. Am. Chem. Soc.* **121,** 917–922.
38. Mao, C., Sun, W., and Seeman, N. C. (1999) Designed two-dimensional DNA Holliday junction arrays visualized by atomic force microscopy. *J. Am. Chem. Soc.* **121,** 5437–5443.
39. Sha, R., Liu, F., Millar, D. P., and Seeman, N. C. (2000) Atomic force microscopy of parallel DNA branched junction arrays. *Chem. Biol.* **7,** 743–751.
40. Sha, R., Liu, F., and Seeman, N. C. (2002) Atomic force measurement of the inter-domain angle in symmetric Holliday junctions. *Biochemistry* **41,** 5950–5955.
41. Yang, X., Vologodskii, A. V., Liu, B., Kemper, B., and Seeman, N. C. (1998) Torsional control of double stranded DNA branch migration. *Biopolymers* **45,** 69–83.
42. Rich, A., Nordheim, A., and Wang, A. H.-J. (1984) The chemistry and biology of left-handed Z-DNA. *Ann. Rev. Biochem.* **53,** 791–846.
43. Mao, C., Sun, W., Shen, Z., and Seeman, N. C. (1999) A DNA nanomechanical device based on the B-Z transition. *Nature* **397,** 144–146.
44. Yurke, B., Turberfield, A. J., Mills, A. P. Jr., Simmel, F. C., and Neumann, J. L. (2000) A DNA-fuelled molecular machine made of DNA. *Nature* **406,** 605–608.

45. Adleman, L. (1994) Molecular computation of solutions to combinatorial problems. *Science* **266,** 1021–1024.
46. Grünbaum, B. and Shephard, G. C. (1986) *Tilings & Patterns*, Freeman, New York.
47. Mao, C., LaBean, T., Reif, J. H., and Seeman, N. C. (2000) Logical computation using algorithmic self-assembly of DNA triple crossover molecules. *Nature* **407,** 493–496.
48. Seeman, N. C. (1991) The construction of 3-D stick figures from branched DNA. *DNA Cell Biol.* **10,** 475–486.
49. Eckardt, H. E., Naumann, K., Pankau, W. M., Rein, M., Schweitzer, M., Windhab, N., and von Kiedrowski, G. (2002) Chemical copying of connectivity. *Nature* **420,** 286.

13

Nanostructured DNA Templates

Jeffery L. Coffer, Russell F. Pinizzotto, and Young Gyu Rho

Summary

We have developed methods for nanostructure fabrication relying on the size and shape of a polynucleotide to dictate the overall structure of an assemblage of individual semiconductor nanoparticles. Use of the circular plasmids pUCLeu4 and $\phi\chi$ 174 when anchored to a suitably derivatized substrate yields arrays of semiconductor nanoparticles matching the shapes of the biopolymer stabilizer. The viability of the methodology was confirmed using high-resolution transmission electron microscopy and selected-area electron diffraction.

Key Words

pUCLeu4; $\phi\chi$ 174; plasmid; semiconductor nanoparticles; cadmium sulfide; templates.

1. Introduction

The use of polynucleotides for nanostructure fabrication ***(1–3)*** is a useful development in a rapidly expanding area of interdisciplinary nanoscale science in which biological systems are used to control the size, shape, orientation, assembly, and so on of the material ***(4)***. The final nanostructures also indirectly mirror DNA structure without the necessity of shadowing or staining techniques ***(5)***. Ideally, if semiconducting materials are fabricated using this strategy, the resulting composite also provides an interface for future hybrid device platforms applicable to DNA-based computation ***(6)***. In principle, an almost unlimited number of nanostructures can be formed using DNA molecules of various sizes, shapes, and composition as structural templates for additional synthesis ***(7)***. The simplest choices include quantum wires, assembled using nucleotides 2–50 kb in length; quantum rings, analogous to quantum corrals, assembled using covalently closed circular polynucleotides known as plasmids; and quantum dots formed directly from small DNA fragments of 30 bp or less (or, alternatively, condensed larger DNA molecules) ***(8–11)***. Based on some of the more

From: *Methods in Molecular Biology, vol. 303: NanoBiotechnology Protocols*
Edited by: S. J. Rosenthal and D. W. Wright © Humana Press Inc., Totowa, NJ

complex DNA topologies described in the literature (e.g., knots, crosses) ***(12)***, other more elaborate motifs can also be envisioned.

In this chapter, we provide protocols for the formation of networks of quantum-confined cadmium sulfide nanoparticles (Q-CdS) formed using circular plasmid DNA molecules anchored to a solid substrate. By varying the deposition sequence and/or reactant concentrations, two extreme morphologies are illustrated: isolated rings of Q-CdS/plasmid DNA and weblike arrays of Q-CdS/plasmid DNA. Overall, the topology of the DNA bound to the solid substrate acts as a template to control the overall shape of the self-assembled nanoparticle structure.

2. Materials

1. Carbon rods, spectroscopic grade (less than 2-ppm impurities).
2. Copper grids for transmission electron microscopy (TEM), 400 mesh.
3. Cadmium perchlorate, $Cd(ClO_4)_2 \cdot 6H_2O$.
4. Hydrogen sulfide, H_2S (99.5%).
5. Plasmid DNA, pUCLeu4 and $\phi\chi$ 174 RF II.
6. Ultrapure water, 18 MΩ quality.

3. Methods

The methods outlined next describe the properties of the specific plasmids used as templates, proper preparation of the carbon-coated copper grids necessary for TEM analysis, and fabrication of the CdS nanostructures on the plasmid templates. In addition, typical results for some of the procedures, as determined in our laboratories, are presented.

3.1. Synthesis and Purification of Plasmid Templates

pUCLeu4 DNA was generously provided by Dr. Robert M. Pirtle of the University of North Texas. pUCLeu4 DNA was generated by cloning a human DNA fragment (781-bp *Kpn*I-*Sst*I) encompassing a leucine $tRNA_{AAG}$ gene as a foreign DNA into pUC19 vector DNA (**Fig. 1A**). A large amount of pUCLeu4 plasmid DNA, produced by *Escherichia coli*, was extracted from the bacterial cells by an alkaline procedure and treated with RNases A and T_1 to degrade the bacterial RNA. The bacterial RNA was extracted with phenol:chloroform (1:1) and chloroform:isoamyl alcohol (24:1) and precipitated with cold ethanol. The chromosomal bacterial DNA and degraded RNA were removed from the pUCLeu4 plasmid DNA by high-performance liquid chromatography on an anion-exchange column using an NaCl gradient ***(13)***.

According to polyagarose gel electrophoresis, approx 70% of the undigested pUCLeu4 plasmid DNA synthesized with this method was supercoiled. The supercoiled pUCLeu4 plasmid DNA molecules were treated to generate the

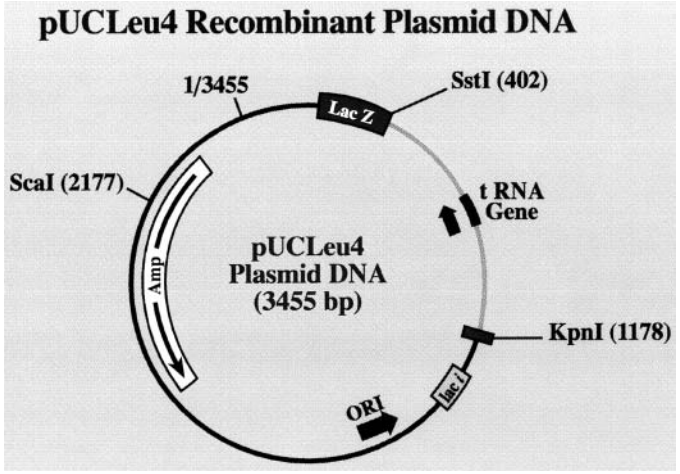

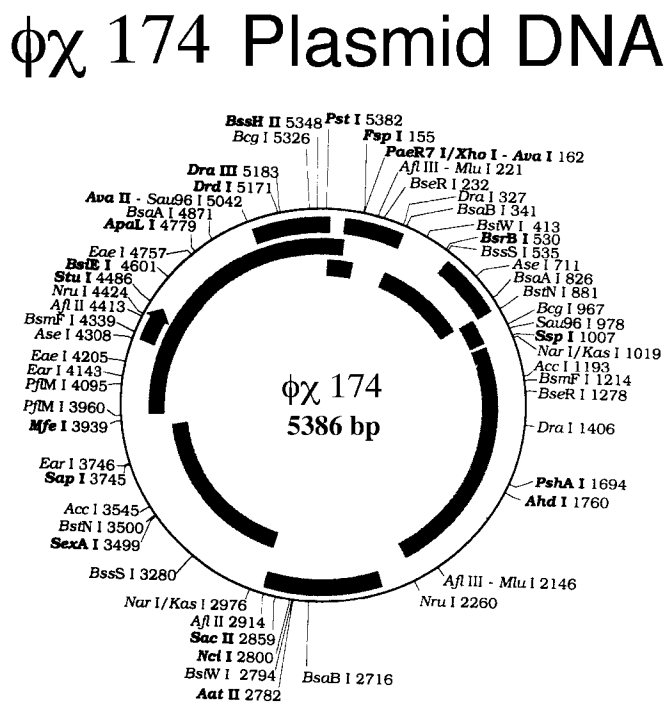

Fig. 1. Composition maps for plasmids **(**top**)** pUCLeu4 and **(**bottom**)** X 174 RF II utilized as templates.

relaxed circular form for use as templates. The population of relaxed circular DNA present can be enhanced by cutting and rejoining one of the 3′ or 5′ phosphodiester bonds using DNA topoisomerase I enzyme.

The plasmid $\phi\chi$ 174 RF II was obtained commercially from New England Biolabs (Beverly, MA). It is a larger plasmid vector containing 5386 nucleotides and is approx 1.83 μm in circumference (for the relaxed, open circular conformation).

3.2. Fabrication and Preparation of Ultrathin Carbon-Coated TEM Grids

3.2.1. Fabrication of Carbon Substrate

Since the scale of the Q-CdS/DNA semiconductor structures is in the nanometer regime, very fine and flat substrate surfaces are necessary for TEM analysis. Microstructural characterization of the carbon films was started because commercial carbon films have many artifacts that can make TEM analysis difficult, and potentially nondiagnostic of the resulting nanostructures. In particular, some of these microstructures, formed during film fabrication, are similar in size and shape to the microstructure of Q-CdS/linear DNA. In the initial stages of our experiments, these artifacts were misleading. Therefore, the carbon films used for TEM substrates were fabricated in our laboratory and always examined before use as substrates.

The thin carbon films that were the primary substrates used for these experiments were fabricated using a JEOL JEE-4X evaporator operating at 2×10^{-6} torr. As a carbon source for the evaporator, one side of a carbon rod was sharpened to approx 1 mm in diameter for a length of 6–8 mm using a fine file (*see* **Note 1**). Carbon evaporation is achieved by resistively heating the contact area of two sharpened carbon rods, so the thin carbon tip makes it easier to control the evaporation process. The carbon rods were positioned about 10–15 cm above the specimen stage. Freshly cleaved mica, with the fresh side facing upward toward the carbon source, was placed on the specimen stage (underneath the carbon rods) using tweezers. When preparations were complete, the work chamber was evacuated for 1 h to reduce the vacuum level to lower than 2×10^{-6} torr. When high vacuum was achieved, the mica substrate was covered with a shutter and the heating current increased slowly until the tip of the carbon rod began to glow red. After a few seconds, the particles that were generated during the sharpening of the carbon rod were removed. The shutter was then opened and the heating current increased to evaporate the carbon. The current was increased as slowly as possible until the tips of the carbon rods glowed white so that the carbon

films were deposited by evaporation and not by arcing, which produces many carbon fragments. Depending on the height of the carbon rods, but after two or three evaporation cycles with each approx 20–30 s long, carbon film deposition was complete.

3.2.2. Preparation of Carbon Substrates on Cu TEM Grids

The carbon films were placed on acetone-cleaned 400-mesh Cu TEM grids. The grids were placed shiny side up on a wire mesh that was in steam-sterilized distilled water contained in a Buchner funnel or a dish that could be drained. The carbon film was separated from the mica substrate by dipping the mica into water and floating off the carbon film. The TEM grids were coated by aligning the separated carbon film on top of the TEM grids and then draining the water. The wire mesh was picked up with tweezers and placed on filter paper to remove the water remaining on both the wire mesh and the TEM grids. The carbon-coated grids were used within 30 min, before they were completely dry, or after complete drying, depending on the type of experiment performed (*see* **Note 2**).

3.3. Preparation of Q-CdS/pUCLeu4 or Q-CdS/ϕχ 174 RF II Samples

The range of fabrication strategies for quantum-confined cadmium sulfide nanoparticles on DNA templates is outlined in **Fig. 2**. All routes entail four basic steps: (1) preparation of both DNA and Cd ion solutions at the requisite concentrations, (2) formation of a plasmid–cadmium ion complex, (3) adsorption onto a solid support, and (4) reaction with a gaseous sulfide source. These steps are typically followed in the order listed, but the option exists for switching steps 2 and 3 if desired (*see* **Subheading 3.3.5.**).

3.3.1. Preparation of DNA and Cd^{2+} Solutions

In a typical experiment, approx 2 mL of 2 m*M* DNA (the amount of DNA is defined on a per-nucleotide basis) was prepared from the original concentration of about 2 mg/mL. To prepare this target molar nucleotide concentration of 2 m*M*, a 10-µL aliquot of 2 mg/mL DNA solution was taken via microliter syringe and diluted with 10 mL of distilled deionized water in a 50-mL flask. The DNA solution was thoroughly mixed by shaking it manually for approx 10 min. The concentration of the diluted solution was measured spectrophotometrically using an ε value of 6600 M^{-1} cm^{-1} at an absorption wavelength of 260 nm. In a separate beaker, 100 m*M* $Cd(ClO_4)_2 \cdot 6H_2O$ solution was freshly prepared from the solid, which was dissolved slowly by shaking for approx 10 min. To make 2 mL of 2 m*M* cadmium ion solution from this stock 100 m*M* Cd^{2+} solution, 40 µL of the 100 m*M* solution was diluted in 1.96 mL of distilled deionized water.

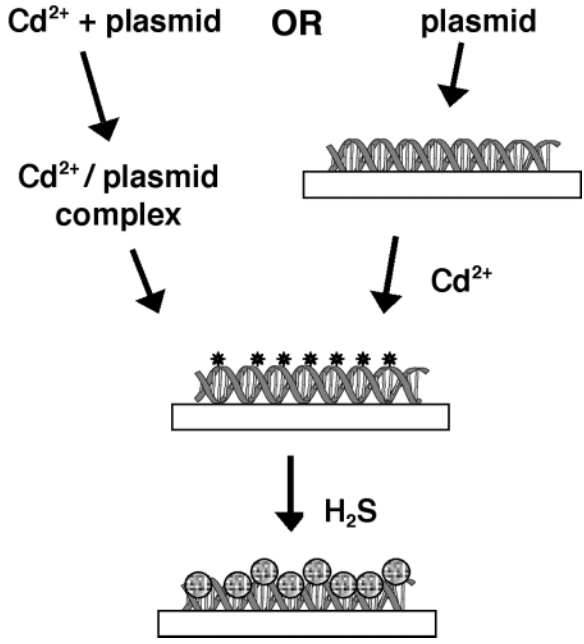

Fig. 2. Routes to semiconductor nanostructure formation using DNA templates.

Some experiments entail the variation of cadmium ion concentration in nanostructure formation. In these experiments, two strategies were explored: (1) an overall lower loading of nanostructures on a given support, and (2) in one of these diluted nanostructures a large excess of cadmium ion to nucleotide. For the former, 2 mL of a 2 m*M* Cd^{2+} solution is mixed with 2 mL of 5 μg/mL (approx 15 μ*M* in nucleotide) pUCLeu4 plasmid DNA or, alternatively, 2 mL of a 1 μg/mL solution (approx 3 μ*M* in nucleotide) for the case of the φχ 174 RF II. In the latter example, 2 mL of 2 μ*M* Cd^{2+} is mixed with 2 mL of 5 μg/mL pUCLeu4 plasmid DNA or 1 μg/mL of 2 mL φχ 174 RF II DNA, close to a target ratio of 1:1.

3.3.2. Mixing of Cd^{2+} and DNA in Solution

Formation of cadmium metal ion/DNA complexes was carried out by mixing the two previously prepared solutions of Cd^{2+} and plasmid DNA in a 1:1 ratio in a 10-mL beaker. The mixed solution was stirred with a pipet by squeezing the solution in and out of it for 2 to 3 min to mix the Cd^{2+} and DNA homogeneously. The beaker was shaken slowly for approx 10 min to maximize the interaction between the cadmium ions and the DNA.

3.3.3. Reactant Adsorption Onto Solid Supports and Reaction With Sulfide

Samples were prepared on the previously described thin amorphous carbon films to make characterization straightforward. One to two microliters of 2 m*M* Cd^{2+}/DNA (at a 1:1 DNA to Cd^{2+} ratio) was dropped onto carbon film/copper TEM grids using a microliter syringe. Excess solution was blotted from the side or bottom of the grid with a sharp corner of a piece of filter paper (*see* **Note 3**). The carbon-coated TEM grids were prepared as described in **Subheading 3.2.2.** and used within 30 min, but before the carbon films were completely dry. After air-drying, the samples were placed on antistatic polyshield paper and placed in a vial that could be sealed with a rubber septum. The samples were exposed to H_2S by adding this gaseous reagent into the vial using a gas tight microliter syringe. The reaction was allowed to proceed for approx 30 min to 1 h to form Q-CdS particles on DNA.

3.3.4. Cd^{2+}/DNA Deposition by Floating Grids in Solutions

To alter the relatively high concentration of supercoiled DNA and the high density of netlike microstructures found over large, localized areas, in these experiments, the carbon-coated TEM grid was placed on the Cd^{2+}/DNA complex instead of dropping the mixture onto the TEM grid. In this way, the Cd^{2+}/DNA complexes can be anchored uniformly over the carbon film by adsorption.

The concentrations and the Cd^{2+}/DNA ratio (2 μ*M* and 2 m*M* cadmium solutions with either 5 μg/mL of pUCLeu4 plasmid DNA or 1 μg/mL of ϕχ 174 RF II DNA) were the same as described in **Subheading 3.3.1.** Preparation and mixing of these solutions were the same as described previously (*see* **Note 4**).

One or two drops of the well-mixed Cd^{2+}/DNA complexes were dropped on a clean glass slide using a Pasteur pipet. Using tweezers, carbon-coated TEM grids were placed on the complex solution with the carbon-coated side down. Approximately 1 or 2 min later, the grid was picked up and placed on filter paper with the carbon film side up to remove the excess water. After air-drying for approx 30 min, the grids were exposed to H_2S gas as described in **Subheading 3.3.3.** Either wet or dry carbon films can be used with this deposition method.

3.3.5. Sequential Addition of DNA and Cd^{2+} to Carbon Surfaces

To prevent extensive entanglement of the CdS/DNA structures in some experiments, DNA molecules were anchored onto the carbon film first, and then the grids with the attached DNA were dipped in Cd^{2+} solution to allow the Cd^{2+} ions to interact with the DNA molecules directly (*see* **Note 5**).

Two sets of samples with two different DNA concentrations, 5 and 0.5 µg/mL, were prepared by dipping them into a 2 m*M* cadmium ion solution. The DNA and cadmium solutions were prepared as described in **Subheading 3.3.** One or two drops of DNA solution was dropped onto a clean glass slide with a Pasteur pipet. Carbon-coated TEM grids were placed on the DNA solution, and after 1 or 2 min the grids were picked up and placed on filter paper to remove the excess water. The samples were air-dried for 6–10 min, then dipped very slowly into cadmium solution one by one, while trying not to disturb the solution, to reduce washing away of the DNA from the grid. After approx 3–5 min, the grids were placed on filter paper with the carbon film side up and air-dried for approx 30 min. The grids were then exposed to H_2S gas for approx 30 min, as described in **Subheading 3.3.3.**

3.4. Characterization

3.4.1. Instrumentation

Both analytical transmission electron microscopy (AEM) and high-resolution election microscopy (HREM) can be used for microstructural characterization of the Q-CdS/DNA mesostructures. The mesoscale semiconductor structures are imaged using a combination of bright-field, dark-field, and high-resolution electron microscopy. In our previous experiments, analytical electron microscopy, X-ray energy dispersive spectroscopy for elemental chemical analysis, and selected-area electron diffraction for phase identification were performed using both a JEOL 100 CX and a JEOL 200 CX operating at 100 and 200 kV, respectively. Lattice imaging of Q-CdS particles on DNA was performed using a Hitachi H-9000 high-resolution electron microscope with a demonstrated lattice resolution of 1 Å operating at an accelerating voltage of 300 kV. Q-CdS nanoparticle sizes and size distributions were determined using HREM micrographs. Some samples were examined both with and without metal shadowing.

3.4.2 Results

Figure 3 illustrates the type of structure observed when the procedure in **Subheading 3.2.2.** is followed, i.e., adding microliter amounts of 2 m*M* Cd^{2+}/nucleotide complex onto carbon film/copper TEM grids using a microliter syringe. The dark ring observed is an assembly of quantum confined cadmium sulfide nanoparticles on a circular pUCLeu4 template. Since DNA is a biopolymer with relatively low electron density, plasmids are not observed alone in the TEM. With this particular variant of the method, CdS nanoparticles are observed not only on the plasmid, but also on the carbon surface as well, since excess Cd^{2+} is not completely removed. This particular Q-CdS ring structure is

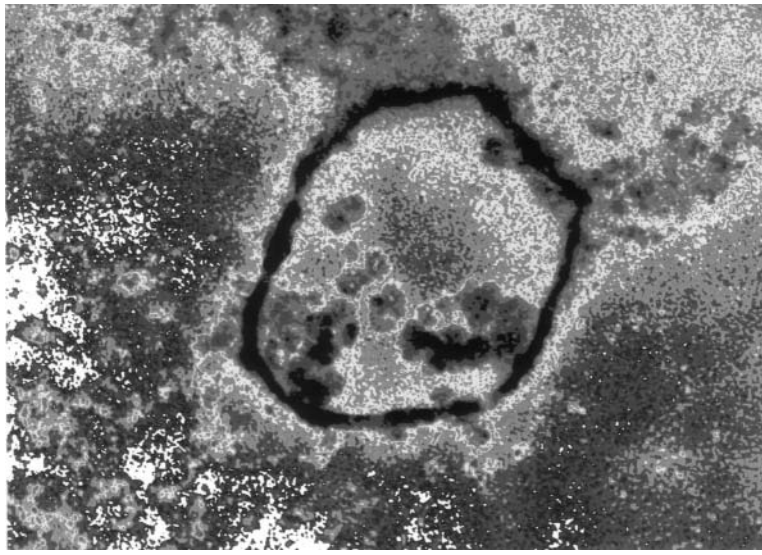

Fig. 3. Bright-field TEM micrograph of circular plasmid pUCLeu4 DNA molecule that has served as nucleation site for ring of Q-CdS nanoparticles. The measured circumference of the ring (1.2 μm) closely matches the predicted value of the relaxed circular conformation of the plasmid DNA molecule.

approx 10 nm thick and 700 nm long. HREM confirms that the dark ring comprises an assembly of randomly oriented, closely packed CdS nanoparticles, with an average size of approx 5 nm (**Fig. 4**). The elemental composition is confirmed by concomitant energy dispersive X-ray analysis (showing the expected presence of cadmium and sulfur), and selected-area electron diffraction measurements verify that the phase of the material is the cubic form of cadmium sulfide.

To circumvent nonselective Cd^{2+} binding, as well as to reduce the number of CdS structures templating on supercoiled DNA, two specific strategies have proven useful. One involves the flotation of the carbon surfaces in an aqueous solution containing the plasmid and cadmium ions; if a large excess of Cd^{2+} (say, 1000-fold) is present, then extensive aggregation of the CdS/plasmid occurs, resulting in numerous "weblike" structures across the surface of the film (**Fig. 5**). The other option is to decouple the Cd^{2+}- and plasmid-binding events and add them individually to the carbon surface, rather than collectively as a complex (*see* **Subheading 3.3.5.**). This method produces a relatively more dispersed series of Q-CdS rings across the surface (**Fig. 6**).

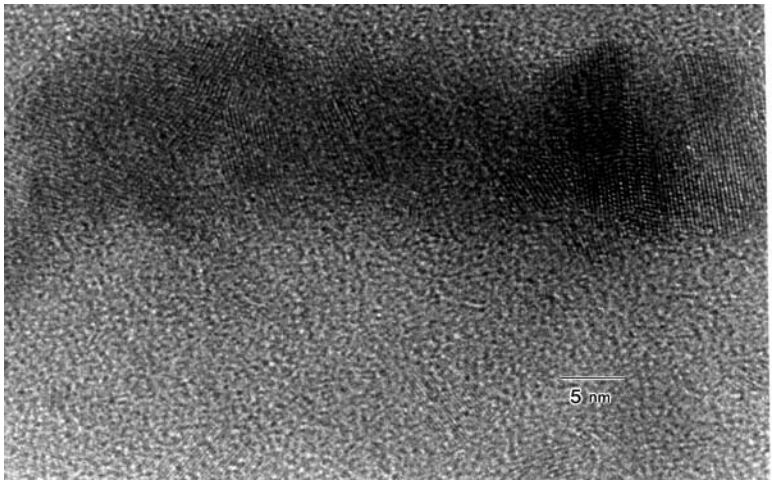

Fig. 4. HREM image of one section of Q-CdS/DNA ring. The ring consists of numerous nanoparticles with different orientations.

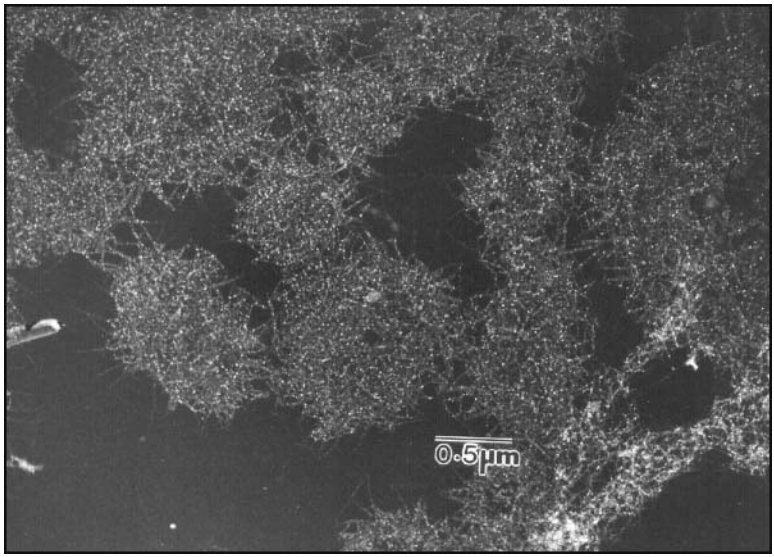

Fig. 5. Bright-field TEM image of weblike pattern of CdS nanostructures induced by cadmium ion-induced plasmid aggregation. Control experiments using Cd^{2+} bound to this plasmid under comparable conditions (and imaged with the assistance of metal shadowing) confirm that this is the case. Note the presence of the individual CdS nanocrystals (showing up as small white spots in the image).

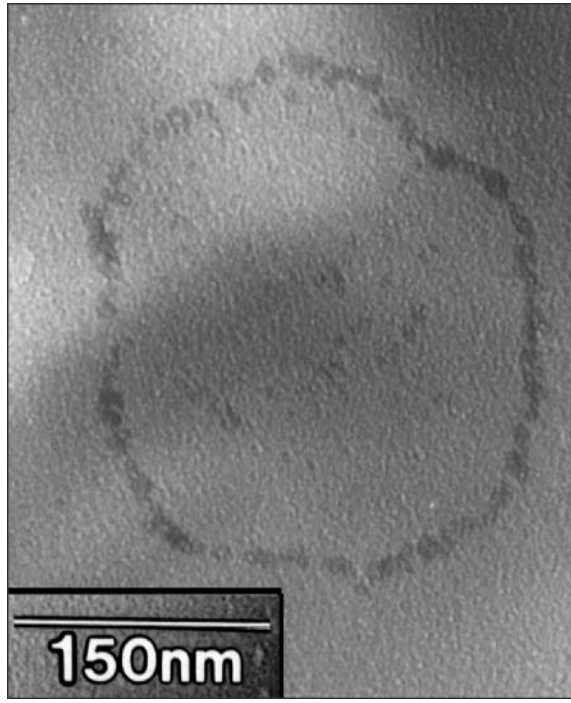

Fig. 6. Discrete "necklace" of CdS nanocrystals formed by separate addition of plasmid to a carbon surface, followed by cadmium ion addition and H_2S exposure.

4. Notes

1. If the diameter of the tip is too large or the tip is sharpened into a conical shape without making it long enough, the thin tip area may be burnt off before achieving the required film thickness
2. For example, wet carbon films were used when the DNA was deposited using the dropping method (*see* **Subheading 3.3.3.**), and dry carbon substrates were used when the DNA was deposited by floating the grids on the DNA or Cd^{2+}/DNA solutions (as described in **Subheading 3.3.4.**).
3. Because of the hydrophobic nature of the carbon film and the surface tension of the water drop, the deposition of the Cd^{2+}/DNA complexes onto the carbon-coated TEM grids was extremely difficult. The carbon films usually broke owing to these effects, but breakage can be reduced by using wet carbon films.
4. In the method that employs floating the TEM grids on the complex solution, it is imperative that freshly mixed Cd^{2+} solutions be used for satisfactory results.
5. The amount 5 μg/mL of DNA was used because we anticipated that many of the DNA molecules attached to the carbon film would be washed away when the grids were dipped into the cadmium solution. A high cadmium concentration,

2 m*M*, was used to reduce the interaction time to reduce the removal of DNA from the grids.

References

1. Alivasatos, A. P., Johnsson, K., Peng, X., Wilson, T., Loweth, C., Bruchez, M., and Schultz, P. (1996) Organization of nanocrystal molecules using DNA. *Nature* **382,** 609–611.
2. Mirkin, C., Letsinger, R., Mucic, R., and Storhoff, J. (1996) A DNA-based method for rationally assembling nanoparticles into macroscopic materials. *Nature* **382,** 607–609.
3. Coffer, J., Bigham, S., Li, X., Rho, Y., Pinizzotto, R., Pirtle, R., and Pirtle, I. (1996) Dictation of the shape of mesoscale semiconductor nanoparticle assemblies by plasmid DNA. *Appl. Phys. Lett.* **69,** 3851–3853.
4. Mann, S. (1993) Molecular tectonics in biomineralization and biomimetic materials chemistry. *Nature* **365,** 499–505.
5. Rho, Y. G. (1996) PhD dissertation, University of North Texas, Denton, TX.
6. Winfree, E. (1996) in *DNA Computers, Proceedings of a DIMACS Workshop*, (Lupton, R. and Baum, E., eds.), American Mathematical Society, pp. 199–219.
7. Coffer, J. L. (1997) Approaches for generating mesoscale patterns of semiconductor nanoclusters. *J. Cluster Sci.* **8,** 159–178.
8. Coffer, J. L. and Chandler, R. R. (1991) Nucleotides as structural templates for the self-assembly of quantum-confined CdS clusters. *Mater. Res. Soc. Symp. Proc.* **206,** 527–531.
9. Coffer, J. L., Bigham, S. R., Pinizzotto, R. F., and Yang, H. (1992) Characterization of quantum-confined CdS nanocrystallites stabilized by deoxyribonucleic acid. *Nanotechnology* **3,** 69–76.
10. Bigham, S. R. and Coffer, J. L. (1995) The influence of adenine content on the properties of Q-CdS clusters stabilized by polynucleotides. *Colloids Surfaces* **95,** 211–219.
11. Chandler, R. R., Bigham, S. R., and Coffer, J. L. (1993) Preparation and spectroscopic analysis of semiconductor colloids. *J. Chem. Ed.* **70,** A7–A10.
12. Seeman, N. C. (2003) DNA in a material world. *Nature* **421,** 427–431.
13. Chang, Y. N., Pirtle, I. L., and Pirtle, R. M. (1986) Nucleotide sequence and transcription of a human tRNA gene cluster with four genes. *Gene* **48,** 165–174.

14

Probing DNA Structure With Nanoparticles

Rahina Mahtab and Catherine J. Murphy

Summary

Semiconductor nanoparticles, also known as quantum dots, are receiving increasing attention for their biological applications. These nanomaterials are photoluminescent and are being developed both as dyes and as sensors. Here we describe our "sensor" use of quantum dots to detect different intrinsic DNA structures. Structural polymorphism in DNA may serve as a biological signal in vivo, highlighting the need for recognition of DNA structure in addition to DNA sequence in biotechnology assays.

Key Words

DNA; oligonucleotides; quantum dots; semiconductor; nanoparticles.

1. Introduction

The overall double helical structure of DNA has been known since the 1950s ***(1,2)***, but since the 1980s it has become increasingly recognized that local DNA structure and dynamics can affect its function ***(3–7)***. The DNA duplex, as a result of chemical damage or by virtue of its intrinsic sequence, may exhibit bends, loops, bulges, kinks, and other unusual structures on a few-base-pair-length scale ***(5,8–15)***.

Characterization of local DNA structure can be done, of course, by traditional nuclear magnetic resonance or X-ray crystallographic methods (***[14]***; This article describes the features of the Protein Data Bank, the standard database to search and download crystal structures, NMR structures, and some theoretical structures of biological macromolecules, including DNA: http://www.rcsb.org/pdb/. Rutgers University also maintains the Nucleic Acid Database for DNA/RNA sequence and structure searching: http://ndbserver.rutgers.edu/NDB/ndb.html.). A powerful alternative approach—should the DNA samples not be amenable to characterization by these methods—is to bind a probe to the DNA target, and use the optical

From: *Methods in Molecular Biology, vol. 303: NanoBiotechnology Protocols*
Edited by: S. J. Rosenthal and D. W. Wright © Humana Press Inc., Totowa, NJ

properties of the probe to infer the nature of local DNA structure or dynamics ***(15)***. Common examples of such probes include fluorescent intercalators ***(15)***.

A more unusual example of an optical probe for DNA is an inorganic nanoparticle ***(16–20)***. Nanoparticles are materials that have diameters on the 1- to 100-nm scale and are therefore in the size range of proteins. Nanoparticles made of inorganic materials such as semiconductors and metals have unusual, size-dependent optical properties in this size range ***(16–20)***. In particular, semiconductor nanoparticles are known as "quantum dots" because they exhibit "particle-in-a-box" quantum confinement effects at the nanoscale ***(16–20)***. CdSe and CdS nanoparticles can be made by a number of routes in the 2- to 8-nm size range, and these nanoparticles are photoluminescent in the visible, with wavelength maxima that depend on size and surface group ***(16–20)***. Some researchers have used CdSe quantum dots as inorganic dyes for biological labeling assays ***(21–28)***. We have used CdS nanoparticles as protein-sized probes of local DNA structure ***(29–34)***. In this chapter, we describe how we make our nanoparticles and how titration experiments are performed with unusual DNAs, and we give examples of the typical data and results.

2. Materials

1. Anhydrous Na_2S (Alfa), NaOH (Aldrich), sodium polyphosphate (Aldrich), 2-mercaptoethanol (Aldrich), and $Cd(NO_3)_2 \cdot 4H_2O$ (Aldrich) for CdS nanoparticle synthesis: these are used as received. Sodium nitrate is obtained from either Fisher or Aldrich. Deionized and purified water (Continental Water Systems) is used for all solutions.
2. Tris buffer (5 m*M* tris hydrochloride; 5 m*M* NaCl, pH 7.2) and tris-EDTA buffer (10 m*M* tris hydrochloride; 1 m*M* EDTA dipotassium salt; 200 m*M* KCl, pH 8.0): prepare from Sigma-Aldrich or Fisher compounds for DNA solutions.
3. Oligonucleotides. These can be obtained commercially from many different companies; we have used Operon, MWG Biotech, and Midland Certified Reagents.
4. Stir plate.
5. pH meter.
6. Ultraviolet (UV) blacklight.
7. Spectrofluorometer, for acquiring data.
8. High-performance liquid chromatograph, for purifying DNA (unnecessary if one purchases purified DNA).
9. Heat block or hot water bath, to anneal DNA.

3. Methods

3.1. Synthesis of "Unactivated" CdS Nanoparticles Stabilized by Polyphosphate

CdS nanoparticles are prepared with reagent weights based on a final concentration of 2×10^{-4} *M* (*see* **Note 1**).

1. In a three-necked flask held over a stir/heat plate, place a stir bar and 100 mL of deionized water, and degas the water by bubbling nitrogen gas through it for 15 min.
2. Maintain a blanket flow of nitrogen through the rest of this procedure.
3. Add 6.2 mg of cadmium nitrate tetrahydrate, $Cd[NO_3]_2 \cdot 4H_2O$ to the flask, with stirring.
4. Add 12.1 mg of sodium polyphosphate to the flask, with stirring.
5. Insert a pH meter into the flask and check the pH of the aqueous solution. Adjust the pH to 9.8 by adding small amounts of 0.1 *M* NaOH via a pipet.
6. Stir the solution vigorously.
7. Weigh out 1.6 mg of anhydrous sodium sulfide (Na_2S) and dissolve it in 2 mL of water. Immediately add this solution dropwise to the three-necked flask. The reaction mixture should become light yellow.
8. Continue stirring for 20 min.
9. Adjust the pH of the solution to 10.3 with 0.1 *M* NaOH. The reaction has produced approx 4-nm CdS nanoparticles, surface capped with polyphosphate. Size can be checked by transmission electron microscopy. The solution should be stored under nitrogen in the dark. If one irradiates the solution with a UV blacklight, dull pinkish yellow emission will be observed. If one desires to "activate" the nanoparticles with Cd(II) (*see* **Subheading 3.2.**), the solution should remain undisturbed for 24 h.

3.2. Activation of CdS Nanoparticles With Cd(II)

The solution of CdS made in **Subheading 3.1.** should remain undisturbed for 24 h after its synthesis. Prepare a solution of 0.01 *M* $Cd(NO_3)_2$ tetrahydrate (*see* **Note 2**). Then monitor the photoluminescence of the unactivated CdS solution while adding drops of 0.01 *M* $Cd(NO_3)_2$ tetrahydrate solution to it. The CdS solution before activation has an emission peak maximum at approx 550 nm. As the activation progresses, a new peak appears at approx 440 nm and the intensity of this peak increases. Addition of Cd(II) is continued until this new peak at 440 nm has reached its maximum intensity. Toward the end, addition of Cd(II) is done very carefully, and the emission spectrum is checked after each addition of 1 or 2 drops, because if more Cd(II) is added than what is required for maximum activation, the photoluminescence of the activated CdS solution will decrease.

During activation the pH of the solution decreases. After activation is complete, the pH of the solution is brought back to 10.3 with 0.1 *M* NaOH. The "activated" CdS solution has a very bright pinkish white glow under UV light. The nanoparticles should not have changed in size and now are coated with a loose "web" of Cd(II). This activation procedure can be performed with other divalent metal salt solutions as well.

3.3. Synthesis of 2-Mercaptoethanol-Capped CdS

The synthesis of 2-mercaptoethanol-capped CdS produces nanoparticles that bear —SCH_2CH_2OH groups that are ionically neutral compared with the

activated ones from **Subheading 3.2.** As before, CdS nanoparticles are prepared with reagent weights based on a final concentration of 2×10^{-4} *M*.

1. In a three-necked flask held over a stir/heat plate, place a stir bar and 100 mL of deionized water, and degas the water by bubbling nitrogen gas through it for 15 min.
2. Maintain a blanket flow of nitrogen through the rest of this procedure.
3. Add 6.2 mg of $Cd(NO_3)_2 \cdot 4H_2O$ and 1.4 µL of mercaptoethanol to the water, with stirring.
4. Insert a pH meter into the flask and check the pH of the aqueous solution. Adjust the pH to 9.8 by adding small amounts of 0.1 *M* NaOH via a pipet.
5. Stir the solution vigorously.
6. Weigh out 1.6 mg of Na_2S and dissolve it in 2 mL of water. Immediately add this solution dropwise to the three-necked flask. The reaction mixture should remain colorless.
7. Continue stirring for 20 min.
8. Adjust the pH of the solution to 10.3 with 0.1 *M* NaOH. The colorless solution, which glows yellow-green when viewed under UV light, contains CdS nanoparticles surface coated with mercaptoethanol. The nanoparticle diameter should be approx 4 nm. The solution should be stored in the dark under nitrogen (*see* **Note 3**).

3.4. DNA Purification by High-Performance Liquid Chromatography and Annealing

One must decide what sequences of DNA one wishes to probe and choose control DNAs that are allegedly "normal" compared with the "unusual" one that is of interest. DNAs can be commercially obtained and purified; here we describe our procedures for purification and annealing.

In our experiments, we choose the sequences 5′-GGGTCCTCAGCTTGCC-3′ and complement as a "straight" duplex, 5′-GGTCCAAAAAATTGCC-3′ and complement as a "bent" duplex, the self-complementary 5′-GGTCATGGCC ATGACC-3′ as a "kinked" duplex. We have also examined single-stranded DNAs (ssDNAs) that fold up into unusual structures, such as 5′-CGGCGGCGGCG GCGGCGGCGG-3′, $d(CGG)_7$, and 5′-CCGCCGCCGCCGCCGCCGCCG-3′, $d(CCG)_7$. These are commercially purchased and received as a dried-down pellet ("trityl off") on a 1-µmol scale.

Oligonucleotides are purified by high-performance liquid chromatography (HPLC) on a C_8 or C_{18} reverse-phase column with a triethylammonium acetate/acetonitrile gradient, collected and dried down, and redissolved in tris buffer (5 m*M* tris hydrochloride; 5 m*M* NaCl, pH 7.2) for duplex DNAs (*see* **Note 4**). The exact nature of the HPLC gradient can vary, depending on the user's DNA and HPLC.

For annealing duplex DNAs, equal amounts of the complementary single strands are mixed together in Eppendorf tubes and placed in a boiling water

bath or a heat block. The heat is turned off and the mixture is allowed to cool down to room temperature. Ultraviolet (UV)-visible melting temperature experiments confirm that the duplexes are double stranded (T_m approx 50°C in the stated buffer at approx 1 m*M* nucleotide concentration).

For annealing unusual ssDNAs into their folded states, the literature must be consulted closely for the proper ionic strength conditions. In the case of the d(CGG) and d(CCG) triplet repeats, which are similarly purified by reverse-phase HPLC, the proper buffer is tris-EDTA. These oligonucleotides are annealed at 90°C in a heating block for 10 min, allowed to cool gradually to room temperature, and then allowed to cool down further to 4°C for 48 h to obtain the properly folded structures, which can be confirmed by circular dichroism spectroscopy and melting temperature experiments.

3.5. Titrations of Cd(II)-Activated CdS With Duplex DNAs

Binding of DNA to cationic Cd(II)-activated quantum dots is monitored by photoluminescence spectroscopy. The DNA quenches the emission of the nanoparticle solution, and from such data equilibrium binding constants can be obtained.

1. Place 200 µL of a 2×10^{-4} *M* activated CdS solution into a quartz cuvet, and place the cuvet in a spectrofluorometer. Ensure that the size of the excitation light beam in the fluorometer matches the sample size; we have used small 400-µL cuvets instead of the standard 1-cm, 3-mL cuvets.
2. Using an excitation wavelength of 350 nm, which is absorbed by the CdS nanoparticles but not by the DNA, acquire an emission spectrum from 400–800 nm. Slit widths and detector settings will vary by instrument, but for our spectrofluorometer (SLM-AMINCO 8100) we use 4-nm slits.
3. Take a 5-µL aliquot of an approximately millimolar (nucleotide) DNA solution in tris buffer (*see* **Note 4**) and add it to the 200 µL of CdS solution. Mix by inverting the stoppered cuvet several times, and record the emission spectrum.
4. Wait 30 min, and repeat **step 3** until the photoluminescence of the CdS is completely quenched (*see* **Note 5**).
5. Repeat **steps 3** and **4** for different DNAs. Do all of these photoluminescence titrations in a single day, and without changing the spectrofluorometer parameters.
6. Repeat **steps 3** and **4** for a buffer solution without DNA, as a control for any loss of photoluminescence intrinsic to the CdS sample. Typically, this is a minor effect. DNA titration experiments with other DNAs in other buffers (e.g., the triplet repeat sequences mentioned in **Subheading 3.4.**) with the proper buffer control can be performed analogously.

To calculate binding constants of the DNA to the nanoparticles, first integrate the areas under the photoluminescence spectra data curves. From **Fig. 1**, one could integrate the entire area under the curves from 400 to 800 nm, or one

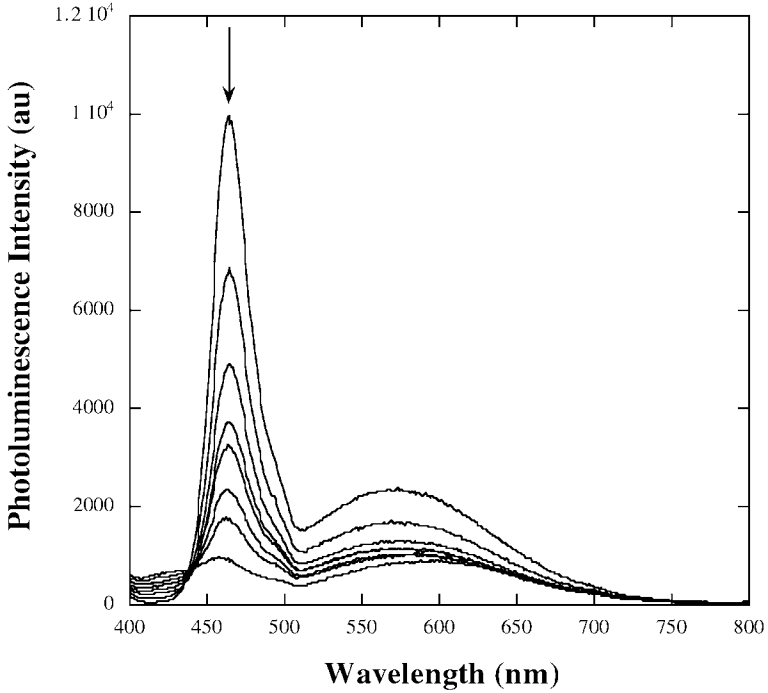

Fig. 1. Raw photoluminescence titration data for Cd(II)-activated CdS nanoparticles, made as described in the text, with a 32mer duplex DNA in tris buffer. The top spectrum is the original Cd(II)-activated CdS data; subsequent addition of DNA decreases the intensity. The peak at approx 570 nm corresponds to the "unactivated" CdS, and the approx 460 nm peak corresponds to the Cd(II)-CdS "activated" species.

could use only the "surface-sensitive" peak at 460 nm. In the latter case, integrating the area from approx 440–510 nm would be appropriate.

Should buffer alone quench the emission of the nanoparticles more than approx 5% of the amount of DNA quenching, the DNA data must be corrected. To do this, *I*(corrected) = *I*(DNA) – *I*(buffer), in which *I*(corrected) is the corrected integrated photoluminescence intensity for a given concentration of DNA; *I*(DNA) is the raw integrated intensity for a given concentration of DNA, as in **Fig. 1**; and *I*(buffer) is the raw integrated intensity for the same volume of buffer that goes with the given DNA concentration.

We have used the Frisch-Simha-Eirich (FSE) adsorption isotherm, which physically corresponds to a long polymer adsorbing to a flat surface in short segments, to extract binding constants from our data ***(35)***. Other models, of course, may be used. The FSE isotherm takes the form

$$[\theta \exp(2K_1\theta)]/(1 - \theta) = (KC)^{1/\upsilon} \quad (1)$$

in which θ, the fractional surface coverage of DNA on the nanoparticles, is equated to fractional change in photoluminescence (i.e., $\theta = [I(\text{DNA}) - I_0]/[I(\text{DNAfinal}) - I_0]$, in which I(DNA) is the corrected integrated intensity of the CdS emission at a particular DNA concentration; I_0 is the initial CdS photoluminescence integrated intensity without DNA; and I(DNAfinal) is the corrected integrated intensity of the CdS emission at the highest [most quenched] DNA concentration); C is the DNA concentration; K_1 is a constant that is a function of the interaction of adsorbed polymer segments, which we manually fit; K is the equilibrium constant for the binding of DNA to the nanoparticle; and υ corresponds to the average number of segments attached to the surface, which has no physical meaning in our system, and is allowed to mathematically float.

Plots of $[\theta \exp(2K_1\theta)]/(1 - \theta)$, with varying values for K_1, vs C are constructed, and fits to a "power" function in the software (Kaleidagraph or Excel) yield values for K and υ. We have generally found that $K_1 = 0.5$ gives the best fits to our data, and υ does not generally vary much.

With the oligonucleotides referred to in **Subheading 3.4.** as "straight," "bent," or "kinked," the binding constants we obtained to 4 nm Cd(II)-CdS nanoparticles were 1000, 4200, and 7200 M^{-1}, respectively. In this case, the kinked DNA was thought to have a larger bend angle than the bent DNA, and the trend from our data suggests that the more bent the DNA, the tighter it binds to a curved surface. In the case of triplet repeat DNAs of unknown structures, we observed that they bound to our particles in much higher salt buffers, under conditions in which normal duplex DNA did not bind to the particles. This suggests that these unknown structures either were more able to wrap about a curved surface than duplex DNA, or perhaps were less sensitive to electrostatics in binding to the nanoparticles, possibly because of increased van der Waals interactions.

3.6. Time Trace Experiments

In this experiment, one can examine the kinetics of DNA binding to nanoparticles. The amount of DNA needed to quench all of the CdS emission in a 200-µL sample is determined in the titration experiments in **Subheading 3.5.**

In a fresh cuvet is placed 200 µL of the colloidal CdS solution, and the cuvet is placed in a fluorometer. The excitation wavelength is set to 350 nm, and the emission monochromator is set to the CdS emission maximum wavelength, approx 460 nm in **Fig. 1**. Then the amount of DNA calculated to quench all of the CdS emission in a 200-µL sample is added all at once. The emission intensity at 460 nm is recorded every 10 s over a period of 300 s. Control experiments are run by adding the appropriate volume of buffer without the DNA.

The kinetics of adsorption can be fit by many models, none of which are really representative of the physical system (small DNA, large "molecule" binding). In general, one must assume that the DNA is either free or bound to CdS, and if bound to CdS will quench its emission. To estimate association rate constants, we have fit data to von Hippel's formulation for protein-DNA binding kinetics for very long DNAs ***(36)***. The integrated rate equation is

$$\left[\frac{1}{(R)-(O)}\right] \ln\left\{\frac{(O)\,[(R)-(RO)]}{(R)\,[(O)-(RO)]}\right\} = k_a t \qquad (2)$$

in which R is the concentration of free particle, O is the concentration of the free DNA, RO is the concentration of bound DNA (i.e., the concentration of the CdS–DNA complex), t is the time, and k_a is the association rate constant. In this treatment, binding is viewed as a simple second-order association reaction that has a negligible dissociation rate, which might not be the case in our system. This model does not fit our data that well, likely because its assumptions of infinitely long DNA and tight binding constants are not appropriate for our system. We retained the assumptions we made for fitting our luminescence data to the FSE adsorption isotherm: namely, that all DNA is either free or bound, and that fractional change in luminescence is proportional to the fraction of DNA that is bound. We have also assumed in the von Hippel treatment that one bound duplex is sufficient to quench the emission for a given particle. Readers may choose other kinetics models for their own situations.

3.7. Reverse Salt Titrations

In this experiment, we add salt to a premade DNA–nanoparticle complex and dissociate the complex. From the data we can extract the electrostatic contribution of binding between the two species ***(31,37–39)***.

1. To the standard 200 µL of Cd(II)-activated CdS solution in a cuvet, add sufficient DNA to quench approx 75% of the emission (from **Subheading 3.5.**).
2. Prepare a stock solution of 0.25 *M* $NaNO_3$.
3. Add known amounts of the $NaNO_3$ stock solution, in microliter aliquots, to the CdS-DNA solution, and record the photoluminescence spectrum after each aliquot addition, using the same parameters as before. The intensity of CdS emission increases on salt addition, reversing the quenching observed with DNA. Sodium nitrate is preferred to sodium chloride because of the tendency of Cd(II) to make complex ions with Cl^- (e.g., $[CdCl_4]^{2-}$). Sufficiently high salt concentrations cause precipitation of the nanoparticles.
4. From the data, construct a plot of equilibrium constant K as a function of salt concentration, and extract from that the contribution that electrostatics makes to the overall DNA-nanoparticle binding. To do this, make the same assumptions

about free and bound DNA as in the time trace experiments, at each salt concentration; calculate the free DNA and bound DNA; and estimate the "free" particle concentration from the photoluminescence integrated intensities. Once that is obtained, a plot of log K vs log [Na^+] should produce a straight line with a slope corresponding to the number of counterions released as the nanoparticle and DNA bind ***(31,37–39)***. Once the number of counterions released is known, calculate the contribution of this electrostatic component to the overall binding according to

$$\Delta G_{electro} = (\text{no. of counterions released})(RT)\ \ln[Na^+] \quad (3)$$

in which $\Delta G_{electro}$ is the portion of the free-energy change that is owing to electrostatics, at a given sodium ion concentration [Na^+]; R is the gas constant; and T is the temperature.

4. Notes

1. The quantum dots prepared as described here are not "passivated," meaning that they are not coated with a material (ZnS, or another higher-band-gap semiconductor, or silica) that will insulate the quantum dot from its environment and render its emission stable and bright regardless of the surrounding medium. In the kind of experiments described here, the intensity of the photoluminescence of the quantum dots should be sensitive to the environment. Hence, control experiments with buffer alone, and standard DNAs, are required.
2. We have activated with Zn(II) and Mg(II) as well; the resulting CdS nanoparticles act similarly, but not identically, with DNA.
3. In the synthesis of thiol-capped CdS, as in **Subheading 3.3.**, other thiols may give different optical properties. For example, we have used L-cysteine as a thiol, and the resulting CdS solution appears pale yellow and glows bright yellow under UV light.
4. The ionic strength of the buffer is lower than that of a typical tris buffer, because the nanoparticles associate electrostatically with the DNA, and a salt concentration that is too high will screen the binding.
5. It is important during the course of the titration to make sure that equilibrium has been reached at each DNA concentration along the way; hence, the 30-min waiting period between spectra.

References

1. Watson, J. D. and Crick, F. H. C. (1953) A structure for deoxyribonucleic acid. *Nature* **171,** 737–738.
2. Franklin, R. E. and Gosling, R. G. (1953) Molecular configuration of sodium thymonucleate. *Nature* **171,** 740–741.
3. Goodman, S. D. and Nash, H. A. (1989) Functional replacement of a protein-induced bend in a DNA recombination site. *Nature* **341,** 251–254.
4. Perez-Martin, J. and Espinosa, M. (1994) Correlation between DNA bending and transcriptional activation at a plasmid promoter. *J. Mol. Biol.* **241,** 7–17.

5. Fry, M. and Loeb, L. A. (1994) The fragile X syndrome d(CGG)n nucleotide repeats form a stable tetrahelical structure. *Proc. Natl. Acad. Sci. USA* **91,** 4950–4954.
6. Marathias, V. M., Jerkovic, B., and Bolton, P. H. (1999) Damage increases the flexibility of duplex DNA. *Nucleic Acids Res.* **27,** 1854–1858.
7. Kelley, S. O. and Barton, J. K. (1999) Electron transfer between bases in double-helical DNA. *Science* **283,** 375–381.
8. Wells, R. D. and Harvey, S. C. (eds.). (1988) *Unusual DNA Structures*, Springer-Verlag, New York.
9. Hagerman, P. J. (1990) Sequence-directed curvature of DNA. *Annu. Rev. Biochem.* **59,** 755–781.
10. Crothers, D. M., Haran, T. E., and Nadeau, J. G. (1990) Intrinsically bent DNA. *J. Biol. Chem.* **265,** 7093–7096.
11. Goodsell, D. S., Kopka, M. L., Cascio, D., and Dickerson, R. E. (1993) Crystal structure of CATGGCCATG and its implications for A-tract bending models. *Proc. Natl. Acad. Sci. USA* **90,** 2930–2934.
12. Calladine, C. R. and Drew, H. R. (1997) *Understanding DNA*, 2nd ed., Academic, San Diego.
13. Moore, H., Greenwell, P. W., Liu, C.-P., Arnheim, N., and Petes, T. D. (1999) Triplet repeats form secondary structures that escape DNA repair in yeast. *Proc. Natl. Acad. Sci. USA* **96,** 1504–1509.
14. Berman, H. M., Westbrook, J., Feng, Z., Gilliland, G., Bhat, T. N., Weissig, H., Shindyalov, I. N., and Bourne, P. E. (2000) The protein data bank. *Nucleic Acids Res.* **28,** 235–242.
15. Murphy, C. J. (2001) Photophysical probes of DNA sequence-directed structure and dynamics. *Adv. Photochem.* **26,** 145–217.
16. Weller, H. (1993) Quantized semiconductor particles: a novel state of matter for materials science. *Adv. Mater.* **5,** 88–95.
17. Alivisatos, A. P. (1996) Perspectives on the physical chemistry of semiconductor nanocrystals. *J. Phys. Chem.* **100,** 13,226–13,239.
18. Alivisatos, A. P. (1996) Semiconductor clusters, nanocrystals, and quantum dots. *Science* **271,** 933–937.
19. Murphy, C. J. and Coffer, J. L. (2002) Quantum dots: a primer. *Appl. Spectrosc.* **56,** 16A–27A.
20. Murphy, C. J. (2002) Optical sensing with quantum dots. *Anal. Chem.* **74,** 520A–526A.
21. Bruchez, M. Jr., Moronne, M., Gin, P., Weiss, S., and Alivisatos, A. P. (1998) Semiconductor nanocrystals as fluorescent biological labels. *Science* **281,** 2013–2016.
22. Chan, W. C. W. and Nie, S. (1998) Quantum dot bioconjugates for ultrasensitive nonisotopic detection. *Science* **281,** 2016–2018.
23. Mattousi, H., Mauro, J. M., Goldman, E. R., Anderson, G. P., Sundar, C. V., Mikulec, F. V., and Bawendi, M. G. (2000) Self-assembly of CdSe-ZnS quantum dot bioconjugates using an engineered recombinant protein. *J. Am. Chem. Soc.* **122,** 12,142–12,150.

24. Pathak, S., Choi, S.-K., Arnheim, N., and Thompson, M. E. (2001) Hydroxylated quantum dots as luminescent probes for in situ hybridization. *J. Am. Chem. Soc.* **123,** 4103–4104.
25. Gerion, D., Pinaud, F., Williams, S. C., Parak, W. J., Zanchet, D., Weiss, S., and Alivisatos, A. P. (2001) Synthesis and properties of biocompatible, water-soluble silica-coated CdSe/ZnS semiconductor quantum dots. *J. Phys. Chem. B* **105,** 8861–8871.
26. Han, M. Y., Gao, X. H., Su, J. Z., and Nie, S. (2001) Quantum-dot-tagged microbeads for multiplexed optical coding of biomolecules. *Nat. Biotechnol.* **19,** 631–635.
27. Rosenthal, S. J., Tomlinson, A., Adkins, E. M., Schroeter, S., Adams, S., Swafford, L., McBride, J., Wang, Y. Q., DeFelice, L. J., and Blakely, R. D. (2002) Targeting cell surface receptors with ligand-conjugated nanocrystals. *J. Am. Chem. Soc.* **124,** 4586–4594.
28. Wang, S. P., Mamedova, N., Kotov, N. A., Chen, W., and Studer, J. (2002) Antibody/antigen immunocomplex from CdTe nanoparticle bioconjugates. *Nano Lett.* **2,** 817–822.
29. Mahtab, R., Rogers, J. P., and Murphy, C. J. (1995) Protein-sized quantum dot luminescence can distinguish between "straight," "bent" and "kinked" oligonucleotides. *J. Am. Chem. Soc.* **117,** 9099–9100.
30. Mahtab, R., Rogers, J. P., Singleton, C. P., and Murphy, C. J. (1996) Preferential adsorption of a "kinked" DNA to a neutral curved surface: comparisons to and implications for nonspecific DNA-protein interactions. *J. Am. Chem. Soc.* **118,** 7028–7032.
31. Mahtab, R., Harden, H. H., and Murphy, C. J. (2000) Temperature- and salt-dependent binding of long DNA to protein-sized quantum dots: thermodynamics of "inorganic protein"–DNA interactions. *J. Am. Chem. Soc.* **122,** 14–17.
32. Lakowicz, J. R., Grycynski, I., Grycynski, Z., Nowaczyk, K., and Murphy, C. J. (2000) Time-resolved spectral observations of cadmium-enriched cadmium sulphide nanoparticles and the effects of DNA oligomer binding. *Anal. Biochem.* **280,** 128–136.
33. Murphy, C. J. and Mahtab, R. (2000) Detection of unusual DNA structures with nanoparticles. *Proc. SPIE* **3924,** 10–16.
34. Gearheart, L., Caswell, K. K., and Murphy, C. J. (2001) Recognition of hypermethylated triplet repeats *in vitro* by cationic nanoparticles. *J. Biomed. Opt.* **6,** 111–115.
35. Simha, R., Frisch, H. L., and Eirich, F. R. (1953) The adsorption of flexible macromolecules. *J. Phys. Chem.* **57,** 584–589.
36. Winter, R. B., Berg, O. G., and von Hippel, P. H. (1981) Diffusion-driven mechanisms of protein translocation on nucleic acids. III. The E. coli lac repressor-operator interaction: kinetic measurements and conclusions. *Biochemistry* **20,** 6961–6977.
37. Anderson, C. F. and Record, M. T. Jr. (1995) Salt–nucleic acid interactions. *Annu. Rev. Phys. Chem.* **46,** 657–700.

38. Record, T. M. Jr. and Spolar, R. S. (1990) Some thermodynamic principles of non-specific and site-specific protein-DNA onteractions, in *The Biology of Nonspecific Protein-DNA Interactions* (Revzin, A., ed.), CRC Press, Boca Raton, FL.
39. Haq, I., Lincoln, P., Suh, D., Norden, B., Chowdhry, B. Z., and Chaires, J. B. (1995) Interaction of Δ and L-$[Ru(phen)_2dppz]^{2+}$ with DNA: a calorimetric and equilibrium binding study. *J. Am. Chem. Soc.* **117,** 4788–4796.

15

Synthetic Nanoscale Elements for Delivery of Materials Into Viable Cells

Timothy E. McKnight, Anatoli V. Melechko, Michael A. Guillorn, Vladimir I. Merkulov, Douglas H. Lowndes, and Michael L. Simpson

Summary

Arrays of vertically aligned carbon nanofibers (VACNFs) provide structures that are well suited for the direct integration and manipulation of molecular-scale phenomena within intact, live cells. VACNFs are fabricated via a combination of microfabrication techniques and catalytic plasma-enhanced chemical vapor deposition. In this chapter, we discuss the synthesis of VACNFs and detail the methods for introducing these arrays into the intracellular domain of mammalian cells for the purpose of delivering large macromolecules, specifically plasmid DNA, on a massively parallel basis.

Key Words

Carbon nanofibers; gene delivery; material delivery; cellular interfacing; tethered genes.

1. Introduction

Because they reside at the same size scale as the biomolecular machines of cells, engineered nanoscale devices may provide the means to construct new tools for monitoring and manipulating cellular processes. The ideal tools would interface directly with subcellular, biomolecular processes, allowing the control of these processes while also providing transduction of responses with both spatial and temporal resolution. Ultimately, this interfacing might be performed without adversely affecting cell viability or functionality. Investigators have highlighted this interface of nanotechnology and biotechnology through the use of nonbleaching fluorescent nanocrystals in place of dyes as a means of monitoring cellular processes ***(1–3)***. Pulled-glass capillaries with nanoscale tips have been implemented for cellular and subcellular electrophysiological stimulus and monitoring ***(4)*** and for manipulating intracellular material using microinjection

From: *Methods in Molecular Biology, vol. 303: NanoBiotechnology Protocols*
Edited by: S. J. Rosenthal and D. W. Wright © Humana Press Inc., Totowa, NJ

of membrane-impermeable molecules (e.g., proteins, DNA) ***(5)***. Conventionally, these devices have required manipulating cells one at a time while visualizing the process under a microscope and, thus, provide a serial interface to individual cells. Parallel embodiments of these devices have been fabricated using silicon microfabrication methods ***(6)***, but as with all micromachining techniques, there are limitations to the ultimate size scale and density of features (tip radii and spacing of the silicon needles) and to the choice of substrate materials (i.e., parallel embodiments not easily fabricated on transparent substrates convenient for cell culture). By contrast, recent advances in the synthesis of nanomaterials, including carbon nanofibers and carbon nanotubes, can avoid these limitations and provide the means to construct massively parallel, addressable functional nanoscale devices including chemically specific atomic force microscope probes ***(7,8)***, electrochemical probes ***(9)***, and electromechanical manipulators ***(10)***. Within this family of structures, carbon nanofibers are particularly well suited for the construction of intracellular devices because of the ability to control their synthesis exquisitely. Deterministic arrays of closely spaced (pitch ≥ 1 μm) vertically aligned carbon nanofibers (VACNFs) ***(11–13)*** may be grown on a wide variety of substrates (including quartz and glass slides) with wide bases that provide mechanical strength while still generating a small diameter tip (≥5-nm tip radius) appropriate for insertion directly into cells.

Here we describe the steps for fabricating functional VACNF devices and for implementing these devices in a first step toward molecular-scale integration with live cells. As a demonstration, these devices are used to introduce exogenous material (e.g., nanofiber-scaffolded plasmid DNA) into viable cells. While providing a novel and effective method for gene delivery, the functional insertion of nanofiber-scaffolded DNA has exciting potential for ultimately providing a nanoscale genomic interfacing platform (*see* **Note 1**).

2. Materials

2.1. Nanofiber Synthesis

1. Photoresist (Shipley).
2. Si wafers (Silicon Quest).
3. Ni slugs (Goodfellows).
4. Acetone and isopropanol.
5. Dry nitrogen.
6. Acetylene (Matheson gases).
7. Ammonia (Matheson gases).

2.2. Nanofiber-Mediated Material Delivery

1. Plasmid DNA: pd2EYFP-N1 (Clontech) or pgreenlantern-1.
2. 100 m*M* 2-(*N*-morpholino)ethane sulfonic acid (MES) buffer adjusted to pH 4.5–4.8 with NaOH (Sigma-Aldrich).

3. 1-Ethyl-3-(3-dimethylaminopropyl) carbodiimide (EDC) (Sigma-Aldrich).
4. Phosphate-buffered saline (PBS) or other serum-free and dye-free cell suspension buffer.
5. Eppendorf microcentrifuge tubes (1.5 mL) or equivalent.
6. Sylgard 184 two-part poly(dimethylsiloxane) (PDMS) kit (Dow Corning, Midland, MI).
7. Propidium iodide (Sigma-Aldrich).

3. Methods

3.1. Synthesis of VACNFs

VACNFs are synthesized deterministically using catalytically controlled, direct current (DC) plasma-enhanced chemical vapor deposition ***(11,12,14)***. VACNFs grow from catalyst particles (e.g., Ni) deposited onto a substrate at predefined locations when placed onto a cathode of a glow discharge system (**Fig. 1**) at elevated temperature (e.g., 700°C) in a flow of acetylene and ammonia. Carbon species decompose at the surface of the catalyst particle, and free carbon atoms diffuse through it and are incorporated into a growing nanostructure between the particle and the substrate ***(15)***. Such nanofibers, which have a catalyst particle at the tip, grow oriented along the electric field lines ***(13,16)***. Thus, the orientation can be determined by the direction of the field. The lateral dimensions of the nanofibers are determined by the size of the catalytic particle, and their length can be precisely controlled by the growth time. Growth conditions can be manipulated to control the shape of the nanofibers (e.g., conical vs cylindrical) ***(13)*** and to control the chemical composition of material deposited on the walls (e.g., amorphous carbon or silicon nitride) ***(17)***. We provide next the specific steps for the synthesis of VACNFs suitable for functional integration into viable cells. An example of such an array is shown in **Fig. 2**.

3.1.1. Patterning of Substrate

1. Spin a photoresist or an electron beam resist (depending on whether photolithography or electron beam lithography is used, respectively) on the surface of a silicon wafer and process according to the manufacturer's guidelines.
2. Expose and develop a pattern so that the resist is removed from the areas where the carbon nanofibers will be grown.

Specific details depend on the lithography tool and resist. For a general overview of the processes, readers are referred to **ref. *18***. For transfection of mammalian cells, such as Chinese hamster ovary (CHO) cells, the pattern is an array of dots that are 0.5 μm in diameter arranged on a square grid with 5-μm spacing ***(19)***. Additional grid lines every 100 μm and indexing numbers are helpful to track transfected cells ***(20)***.

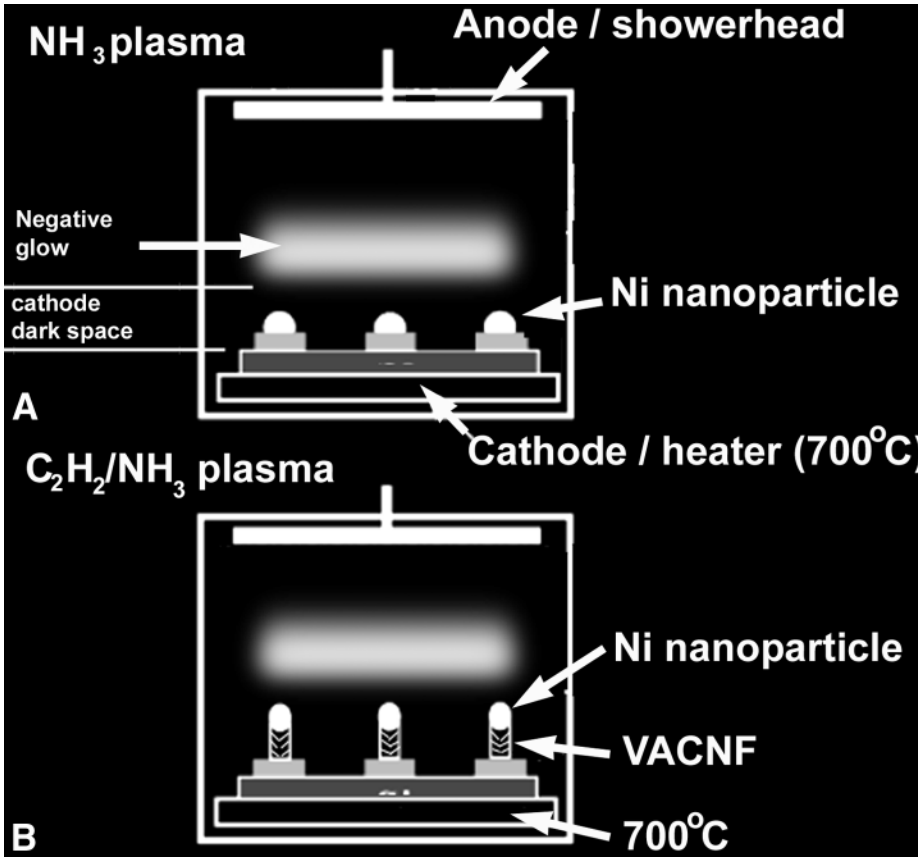

Fig. 1. Schematic representation of the PECVD process for growing vertically aligned carbon nanofibers. **(A)** Catalyst pretreatment/nanoparticle formation; **(B)** Growth of carbon nanofibers.

3.1.2. Deposition of Catalyst

1. Load patterned wafers into a physical vapor deposition chamber, and after an appropriate vacuum is achieved (10^{-7} torr), deposit 20 nm of Ni.

3.1.3. Lifting Off of Excess Metal

1. Place a metallized wafer in a glass dish filled with acetone, cover the dish with a looking-glass cover to prevent evaporation of acetone, and soak it for 30–60 min.
2. Ultrasonicate for 30 s.
3. Remove the wafer from the dish but do not let the acetone dry out, and while holding the wafer with tweezers above the dish immediately rinse the wafer with

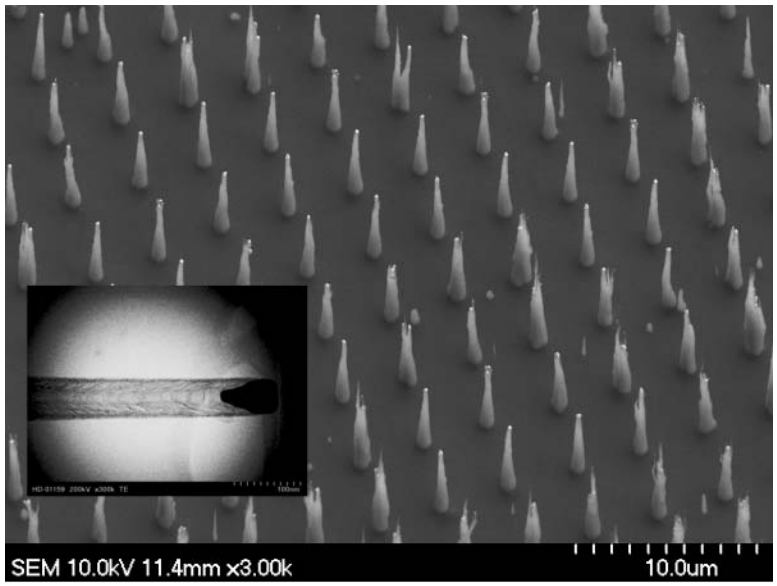

Fig. 2. Typical array of VACNFs suitable for integration with viable cells; **(inset)** transmission electron microscope image of nanofiber.

a spray of acetone to remove metal particulates. Wash the acetone by spraying the wafer with isopropanol.

4. Blow-dry with N_2.

3.1.4. Growth of Carbon Nanofibers

Growth parameters such as gas flows, pressure, and plasma current will vary depending on the particular chamber setup, type of substrate, chamber and substrate size, and catalyst pattern.

1. Mount a wafer on top of the heater-cathode of a DC plasma enhanced chemical vapor deposition (PECVD) system.
2. Evacuate the chamber until a vacuum below 0.1 torr is achieved.
3. Set the substrate temperature controller to 700°C.
4. Introduce ammonia by opening the automatic valve and set the flow to 80 standard cubic centimeters per minute (sscm) and pressure to 3 torr.
5. When the temperature reaches 700°C, introduce acetylene at 20 sccm.
6. Ten seconds after opening the acetylene valve, start DC plasma discharge by turning on the high voltage. Set the high-voltage power supply to constant current mode with the current set to 350 mA.
7. Continue growth for 60 min to produce 6-μm-long fibers.

8. Terminate growth by turning off the high voltage.
9. Turn off the gas flow, open the pressure control valve to pump down the chamber, turn off the heater, and wait until the wafer is cooled down to at least below 300°C before removing.

3.2. Spotting of Nanofiber Arrays With Plasmid DNA

For DNA delivery applications, VACNF arrays must be surface modified with DNA prior to cellular interfacing. VACNF arrays may be spotted with DNA or DNA may be covalently linked to the nanofibers ***(19,20)***. The former procedure relies on physiadsorption of DNA on the nanofiber surface during spotting, and release of this DNA once the nanofiber has been introduced via penetration into the intracellular domain. Nanofiber surface composition is an important factor that influences both adsorption and release of material. We have found that bare carbon nanofibers are poor DNA carriers. They are typically hydrophobic ***(21)*** and, thus, do not wet easily with aqueous DNA solutions. Furthermore, DNA is only weakly held on the surface of bare carbon nanofibers, apparently often being shed prior to introduction of the nanofiber within a cell. By contrast, nanofibers that are synthesized under conditions that redeposit silicon nitride on the sidewalls of the growing structure ***(26)*** are found to promote strong adsorption of DNA during spotting but release at least some of this material once the structure is introduced into a cell. The specific steps for spotting DNA on VACNF arrays are as follows:

1. To promote wetting of prepared nanofiber arrays, expose the array samples to a 30-s radio-frequency (RF) oxygen plasma etch process (RF power = 115 W, pressure = 350 torr, oxygen flow rate = 50 sccm).
2. In a chemical fume hood, cleave large samples into 5-mm^2 chips using a diamond scribe to make straight cleavage lines across the surface being broken. Snap at the scored line by placing the line directly over a rigid, straight edge and tapping the side to be broken at an edge, *not* on the fibered surface.
3. Following all cleavage procedures, rinse the samples in a spray of distilled water to eliminate debris.
4. Spot 5-mm^2 fiber arrays samples with 1 to 2 µL of plasmid DNA at concentrations of 10–500 ng/µL. Ideally, plasmid DNA should be suspended in water, as opposed to conventional buffering solutions, in order to avoid the formation of salt crystals during the subsequent drying step.
5. Air-dry each spotted sample in a sterile culture hood. Typically, this takes approx 10 min under normal laboratory humidity.

3.3. Covalent Modification of Fibers With Plasmid DNA

To provide more control over the fate of introduced genes than that provided by the physisorption/desorption mechanism of spotting, delivered material may be physically tethered to the nanofiber scaffold. Covalent attachment of plasmid

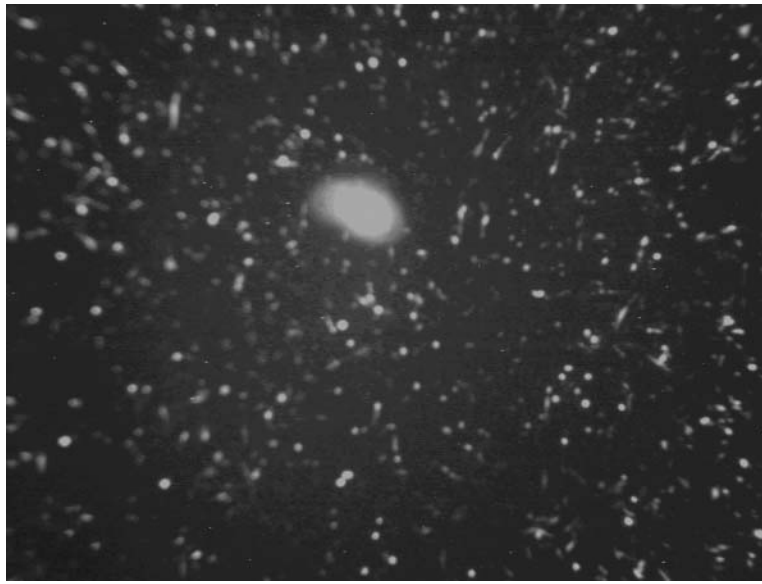

Fig. 3. Fluorescent micrograph of green fluorescent protein (GFP) expression in CHO cells 1 d after integration with fiber array covalently derivatized with pgreenlantern-1, a GFP reporter plasmid.

DNA is achieved using a condensation reaction between primary amines of DNA bases and carboxylic acid sites on the nanofiber surface. Using this method, the DNA may attach at multiple locations, and the sites of attachment within the DNA cannot be specified. As such, it is likely that much of the plasmid DNA will be rendered transcriptionally inactive, because attachment at sites within the active coding region of the plasmid will interfere with polymerase access and function. Nonetheless, this technique has provided transcriptionally active, bound plasmid using a 5081-bp plasmid with a 30% active coding region (pgreenlantern-1; **Fig. 3**).

For highest yield, it is recommended that plasmid DNA be suspended only in water. Both Tris and EDTA of TE DNA buffers contain reactive groups that will interfere with the EDC condensation reaction of DNA onto the carboxylic acid sites of fibers. The specific steps for covalent attachment of DNA to VACNF arrays are as follows:

1. Provide or increase the number of carboxylic acid sites on the fiber surfaces by exposing array samples to a 5-min RF oxygen reactive ion etch (RIE). A typical oxygen RIE recipe for a Trion etcher is a pressure of 350 mt, an RIE power of 115 W, and an oxygen flow of 50 sccm. This step may be conducted on either discrete samples or large (wafer-scale) nanofiber arrays.

2. In a chemical fume hood, cleave large samples into 5-mm^2 chips using a diamond scribe to make straight cleavage lines across the surface being broken. Snap at the scored line by placing the line directly over a rigid, straight edge and tapping the side to be broken at an edge, *not* on the fibered surface.
3. Following all cleavage procedures, rinse the samples in a spray of distilled water to eliminate debris.
4. Place individual 5-mm^2 array samples into 1.5-mL Eppendorf tubes, taking care to handle the samples by the edges. The curve of the Eppendorf tube will protect the fibered surface from contact with the tube walls.
5. Dispense 500 µL of 0.1 *M* MES, pH 4.5 buffer containing 10 mg of EDC to cover each fibered sample in its reaction tube. Ensure that the fibered surface is wetted and remains submerged and does not harbor trapped air bubbles.
6. If a control sample is desired in order to evaluate the effects of covalently attached vs nonspecifically adsorbed DNA on fibers, dispense 500 µL of 0.1 *M* MES, pH 4.5 buffer containing noO EDC to cover the control samples in their reaction tubes. Ensure that the fibered surfaces are wetted and remain submerged and do not harbor trapped air bubbles.
7. Add 1 µg of plasmid DNA in water to each sample, triturating the dispensed fluid to disperse into the solution.
8. Agitate these reaction tubes on an orbital shaker for at least 2 h at room temperature, ideally overnight, to allow the reaction to run to completion.
9. Aspirate each reaction mixture with a Pasteur pipet, taking care not to touch the fibered surface.
10. Rinse each reaction tube in two, 1-mL aliquots of PBS and then soak in 1 mL of PBS for 1 h at 37°C.
11. Rinse each reaction tube in two, 1-mL aliquots of deionized water.
12. Dry each sample prior to use.

3.4. Preparation of Microcentrifuge Spin Tubes

For some cell types, fiber penetration into a cell may be achieved by centrifuging the cells down onto the vertical array of nanofibers. A modified Eppendorf tube may be implemented for rapid cell-fiber interfacing with a benchtop microcentrifuge. Because microcentrifuges typically employ rotors that hold tubes at a 45° angle, the modified Eppendorf tube is designed to feature a 45° slanted surface such that a small (approx 5 × 5 mm) VACNF array chip may be positioned on the slant normal to centrifugal force. The specific steps for constructing a modified Eppendorf tube are as follows:

1. Wearing appropriate chemical protection gloves and glasses, prepare approx 10 mL of PDMS by mixing 10 g of component A (Sylgard 184; Dow Corning) with 1 g of Sylgard 184 curing agent. Avoid generating excessive bubbles during mixing by using a gentle folding motion with a flat, stainless steel weigh spatula.
2. Place the mixed PDMS solution into a 10-mL syringe to allow convenient dispensing of aliquots of the PDMS solution.

3. Dispense 0.5 mL of the PDMS solution into each 1.5-mL Eppendorf tube to be modified. Cap each tube after filling.
4. Place the filled Eppendorf tubes in a microcentrifuge, carefully rotating each tube so that each tube's lid hinge is positioned pointing away from the centrifuge rotor's center. This positioning will be used each time the spin tube is implemented in order to orient the tube properly.
5. Spin the centrifuge for 12 h at 2000*g* and ambient temperature. If the centrifuge features a heater, cure time may be reduced to 30 min at 65°C. During this time, the PDMS in each tube will slant and cure, forming a semirigid, planar surface normal to the centrifuge's radial vector.
6. Open each tube, place the tubes in a beaker, cap the beaker with aluminum foil and autoclave indicator tape, and sterilize the lot in an autoclave.
7. Following sterilization, dry any excess moisture by placing in a drying oven (temperature not to exceed 95°C).

3.5. Interfacing of Cells Onto Carbon Nanofiber Arrays

Fiber penetration and material delivery into a cell appears to be a multistep procedure. For small dye molecules, simply centrifuging the cell onto fibers for brief intervals (minutes) at high pelleting forces (approx 1000*g*) can provide cell loading. For DNA delivery, centrifugation and a subsequent press step is much more effective than centrifugation alone, perhaps providing improved penetration of nanofibers across the nuclear membrane barrier (**Fig. 4**). Although some success at cell-fiber interfacing has been achieved simply by allowing cells to settle out of suspension onto fibers and then performing a press, interfacing effectiveness and material delivery to the nucleus is improved by first centrifuging cells onto the fibers. Centrifuge parameters will likely vary for different cell types, and these should be adjusted and optimized appropriately. For CHO cells, pelleting forces of 600*g* for 30 s to 1 min are effective if followed by a subsequent press step.

Following centrifugation of cells onto fibers, a subsequent press step dramatically improves fiber penetration into the intracellular domain. This press step should be performed on a relatively flat surface (<1 μm surface roughness) that is compatible with the cells being studied. Ideally, to increase the effectiveness of the press step for the entire chip surface, the surface should be somewhat flexible and compliant. An autoclavable dish that has been partially filled with PDMS, as described next, works well as a stamping pad.

3.5.1. Preparation of Sterile, Compliant Pressing Surface

1. Wearing appropriate chemical protection gloves and glasses, prepare approx 2 mL of PDMS for each stamping pad to be used by mixing 2 g of component A (Sylgard 184; Dow Corning) with 0.2 g of Sylgard 184 curing agent. Avoid

Fig. 4. Mouse myeloma cell (SP2/O-AG12) cultured for 3 d after centrifuging and pressing onto a 5-µm spaced nanofiber forest. This cell grows in suspension culture and does not attach and stretch out onto the fibers or fiber substrate.

generating excessive bubbles during mixing by using a gentle folding motion with a flat, stainless steel weigh spatula. If excessive bubbles are formed during mixing, place the mixture in a centrifuge tube and spin at more than 100*g* for 5 min. This will effectively remove air bubbles from the mix.
2. Pour the PDMS mixture into an autoclavable dish (more than 35 mm in diameter) such that at least 1 mm of PDMS solution covers the entire bottom of the dish.
3. Cure the PDMS by placing the dish on a flat surface at 65°C for at least 30 min.
4. Autoclave the stamping dish to sterilize.

3.5.2. Optimization of Centrifugation Parameters

Prior to interfacing cells to nanofiber arrays, cells must be suspended in serum- and dye-free buffer solutions. Medium constituents, and particularly serum, can have mitogenic effects on cells if administered directly to the intracellular domain. Thus, for all cell-interfacing procedures, cells should be washed of their medium and resuspended in PBS, or other buffers appropriate to the cell being studied.

Centrifugation parameters can be optimized by using a membrane-impermeant DNA intercalating stain to monitor membrane rupture (an indicator for fiber penetration) and membrane resealing (required for cell recovery). Ideal centrifugation parameters will result in a high probability of

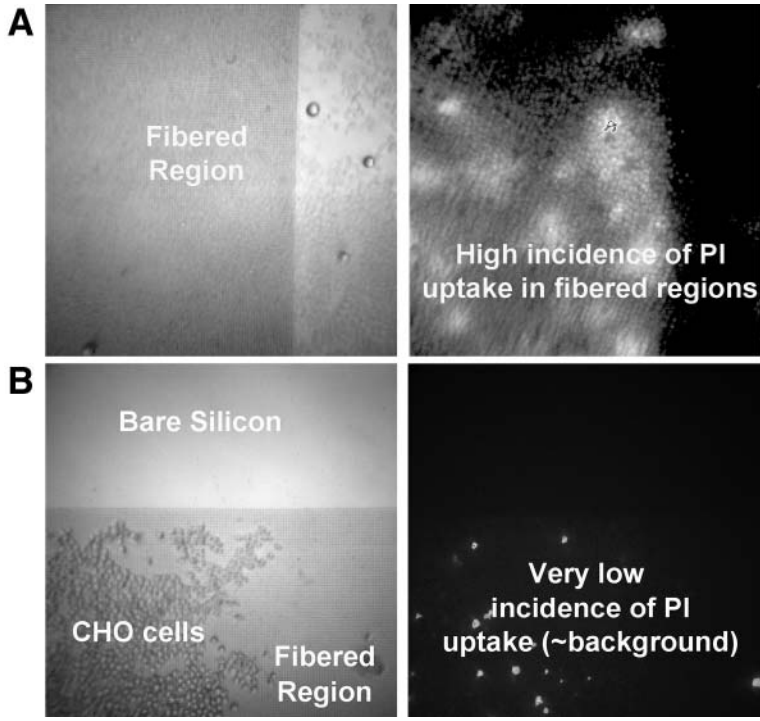

Fig. 5. PI uptake in cells centrifuged onto nanofiber arrays. **(A)** When cells are centrifuged onto fibers in the presence of impermeant PI, the dye passes the plasma membrane and stains DNA/RNA within the cell. **(B)** If PI is added to the system 5 min after the centrifugation procedure, it is excluded from the intracellular domain, apparently owing to resealing of the plasma membrane following fiber penetration.

membrane rupture, but also a high probability of membrane resealing, such that manipulated cells remain viable after the interfacing procedure. These tests can be performed using centrifugation trials with a membrane-impermeant stain in solution during centrifugation (to evaluate membrane rupture), and with this stain added to solution approx 5 min after centrifugation (to evaluate membrane resealing or general cell recovery). Propidium iodide (PI) and ethidium homodimer are both effective impermeant dyes (**Fig. 5**). Both, however, are suspected mutagens and should be handled with caution. The specific steps for optimizing centrifugation parameters are as follows:

1. Using appropriate laboratory safety procedures, prepare a 1 m*M* stock solution of either PI or ethidium homodimer.
2. Prepare cells for interfacing by suspending adherent cell types (scraping or trypsinization as appropriate) and washing all types free of medium, dyes, and

serum using pelleting and resuspension. Resuspend in a cell-specific buffer, such as PBS, at a dilution that will provide the desired monolayer coverage for a 1-cm^2 surface area using 0.5 mL of cells. Approximately 30 mL of cells will allow 10 different centrifugation trials.

3. In the following steps, work with only one set of samples at a time for each spin setting to be evaluated. Each set will consist of three samples with dye in the solution during the spin, and three samples with dye added to the solution after the spin. Label these P1, P2, and P3 for "penetration," and R1, R2, and R3 for "resealing."
4. Place the fibered samples into the PDMS slant of modified Eppendorf tubes such that the unfibered back side of the substrate is flat on the PDMS surface in the center of the tube.
5. Triturate the cell suspension to resuspend the cells before each trial, and place 0.5 mL of the cell suspension in each sample tube.
6. Add 5 μL of the 1 m*M* solution of dye to three of the samples labeled P1, P2, and P3. Triturate to mix.
7. Close all the samples and load into a microcentrifuge. Ensure that the samples are loaded opposite to one another in order to balance the microcentrifuge. Also ensure that the lid hinge of each tube is positioned pointing outward from the center of the centrifuge (as they were positioned during fabrication) such that the slant of the PDMS is oriented appropriately. The slant of the PDMS should be oriented straight up and down when loaded correctly.
8. Spin for the desired force and time. Trial 1 should be set at a time and force typical for gentle pelleting of the cell line studied. Subsequent trials will increase either or both of these parameters.
9. Following the spin, wait 5 min.
10. Carefully aspirate the solution from the P1, P2, and P3 samples and carefully add 0.5 mL of neat PBS.
11. Add 5 μL of the 1 m*M* solution of dye to the three samples labeled R1, R2, and R3.
12. Incubate for 5 min plus the centrifugation time, in order to incubate the R samples for the same amount of time the P samples were incubated with dye.
13. Carefully aspirate the solution from the R1, R2, and R3 samples and carefully add 0.5 mL of neat PBS.
14. Remove the samples from all six modified Eppendorf tubes, and observe the surfaces of each sample with an epifluorescent microscope equipped with a TRITC filter set (535/610).
15. Repeat **steps 4–14** until an optimized centrifugation protocol is achieved in which P samples result in high numbers of dyed cells (indicating potential penetration by fibers into cells), but R samples maintain very low numbers of dyed cells (indicating resealing of the membrane following puncture). Note that depending on the cell line, culture conditions, and harvesting techniques, membrane penetration and resealing may not be mutually obtained. Ultimately, to

achieve puncture merely using centrifugation, pelleting conditions may be too extreme to allow cell resealing and recovery. In this case, a more gentle spin protocol should be combined with a subsequent press step to provide potential DNA delivery.

3.5.3. Increasing of Fiber/Cell Integration by Pressing

If the press step is employed, it must be implemented as quickly as possible following centrifugation in order to minimize additional trauma to the cells that may result owing to membrane attachment to the fiber surface and subsequent shear of these attached domains during the press step. The specific press steps are as follows:

1. Immediately following centrifugation, carefully remove the chip from the spin tube with fine-nosed tweezers. Grasp the chip by its edges with the tweezers. Do not clasp the fibered surface.
2. Gently place the chip face down on the PDMS stamping pad, and gently press the back surface of the chip using a force approximately equivalent to writing with a pencil. Minimize lateral movement of the chip on the PDMS surface so as not to shear fibers and cells from the substrate.
3. Immediately remove the chip from the PDMS surface and place face up in a culture dish.
4. Place sufficient buffer solution in the culture dish to submerge the chip.
5. Allow the cells to recover in buffer solution for at least 15 min.
6. Aspirate the buffer solution from the culture dish and replace with growth medium.
7. Incubate under appropriate growth conditions for the cell line being studied.

4. Notes

1. The procedures discussed describe the steps for delivery of material, in this case plasmid DNA, into cells. There are many other potential applications of functionally integrated nanostructures into viable cells that can be realized if more extensive postgrowth processing of the VACNFs is performed. In essence, the VACNF is a high-aspect-ratio, mechanically and chemically robust conductor of electrons that can be deterministically produced on any substrate compatible with the PECVD growth process. Use of large-scale growth reactors created the opportunity to synthesize high-quality VACNFs in precisely defined locations on substrates compatible with microelectronic device manufacturing equipment (e.g., 100-mm-diameter round Si and quartz wafers). Consequently, it was discovered that VACNFs are compatible with many of the standard microfabrication techniques used in the production of integrated circuits and microelectromechanical systems ***(9,22–26)***. Although a comprehensive description of microfabrication techniques for VACNF substrates is beyond the scope of this discussion, we briefly describe next some of the more useful processing steps.

a. Perhaps the most fundamental operation is the deposition of thin films on VACNF arrays. We have examined the effect of SiO_2 and amorphous Si deposition onto VACNF using rf PECVD. We found that these layers could be uniformly deposited onto the fibers, resulting in a conformal coating. Physical vapor deposition techniques including sputtering and electron beam evaporation have also been used successfully for this purpose. This provided us with a mechanism to modify the surface of the VACNF. Of particular interest was the coating of dielectric layers onto the VACNF that could be selectively removed from regions of the fiber with subsequent microfabrication processes. This provides the ability to control the amount of the fiber body capable of participating in electron transport independent of the aspect ratio or geometry of the fiber.
b. Once material has been deposited onto a substrate, typically some sort of patterning is performed. Photolithography has long been established as the standard workhorse technique used in the microelectronics industry for this purpose. This process involves the patterning of ultraviolet–sensitive polymer layers (photoresists). Photoresists are typically spin cast onto substrates at speeds ranging from 1000 to 6000 rpm. Simple experiments involving the deposition of photoresist layers with a thickness between 200 nm and 2 μm demonstrated that even high-aspect-ratio VACNFs survive this processing. Not only can a photoresist be applied to substrates with VACNF on them, but it can be exposed and developed using well-established techniques. Moreover, a photoresist can be stripped from substrates containing fibers using a combination of organic solvents and ultrasonic agitation with no damage to the structural integrity of the VACNF.
c. Once a pattern has been exposed in a layer of photoresist and developed, it is transferred into the substrate by either the addition or removal of material, referred to as additive or subtractive pattern transfer, respectively. In the case of subtractive pattern transfer, some form of etching is used to remove the desired layer or layers from the patterned area. These processes include various forms of plasma-based etching along with wet chemical etching. Material deposited onto a VACNF can be removed using several combinations of these techniques without significantly damaging the fiber. The fact that the VACNF is composed of graphitic carbon provides it with a robust body that can withstand bombardment of ions during plasma-based processes and any sort of chemical reaction with the exception of those designed to attack carbonaceous materials.
d. The processing techniques just described have resulted in the fabrication of several microscale structures that exploit the unique nanoscale properties of the VACNF ***(9,22–26)***. A process for passivating the body of the fibers with an insulating thin film while leaving the tips electrically and electrochemically active was developed for the fabrication of electrochemical probes with high spatial resolution (**Fig. 6**). This technology was then combined with a process for creating individually electrically addressable VACNFs on an insulating substrate to produce arrays of high-aspect-ratio electrochemical probes ***(9)***.

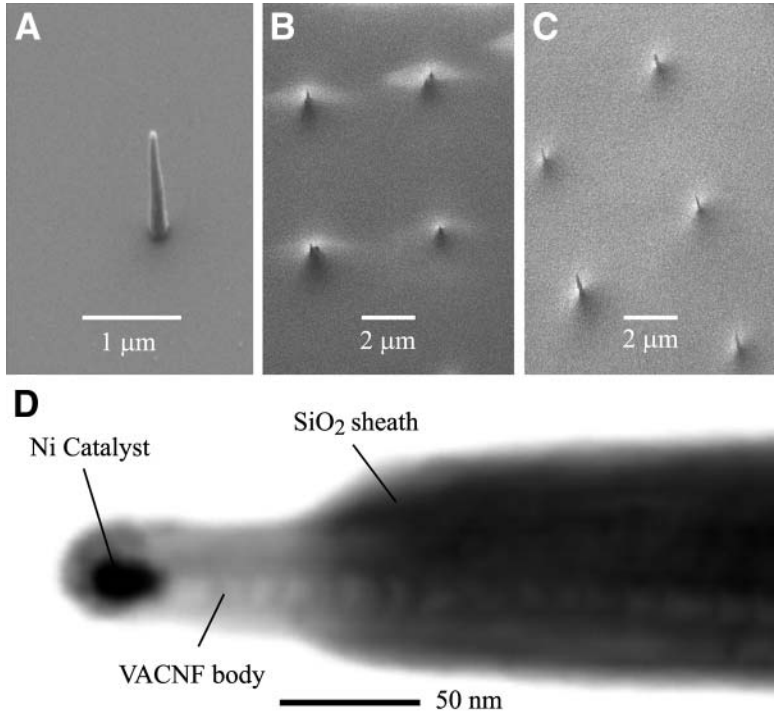

Fig. 6. **(A)** VACNF grown on Si passivated conformally with thin film of SiO_2; **(B)** array of passivated VACNF following spin coating of photoresist; **(C)** array after a brief RIE, liberating tip while leaving body passivated; **(D)** scanning transmission electron micrograph of passivated VACNF following tip release described in **(C)**. The VACNF tip extends beyond the oxide sheath, producing a nanometer-scale electrochemically active surface.

e. Chemical mechanical polishing is frequently used in microelectronic circuit manufacturing to planarize substrate morphology. This technique can also be applied to films deposited onto VACNF. Conformal layers of SiO_2 have been successfully planarized without damaging the VACNF. Continuation of this process has been shown to remove sections of the VACNF at the same rate as the SiO2, leaving the exposed fiber core coplanar with the surrounding oxide topography. This strategy has enabled the synthesis of coplanar electrode arrays for electrochemical applications in which many fibers perform transduction in a parallel fashion.
f. The VACNF can also be used as a sacrificial template for the creation of vertically oriented nanofluidic devices ***(24,26)***. In this process, arrays of VACNF are grown on either Si or Si_3N_4 membranes. The fibers are coated with a thin conformal film using PECVD or low pressure chemical vapor deposition

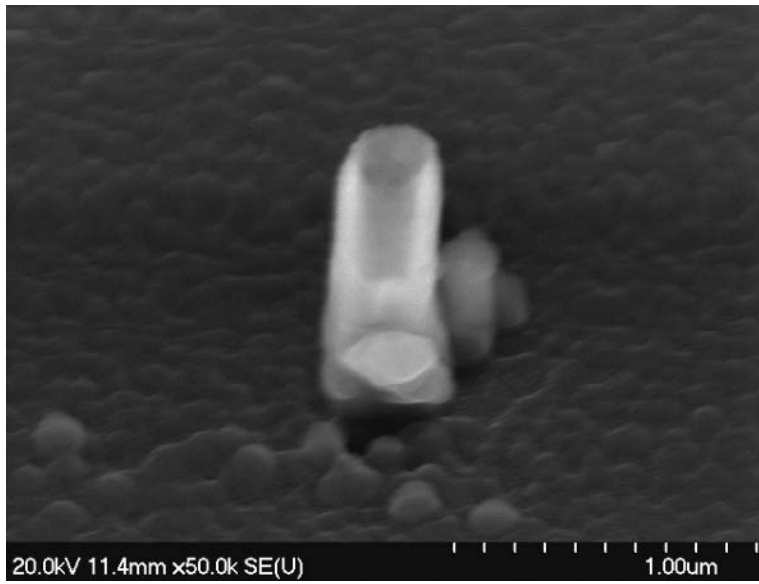

Fig. 7. SiO_2 nanopipe formed using VACNF as sacrificial template.

(LPCVD). The tips of the fibers are liberated using the process described in **Note 1.d.** for the individual electrochemical probes. Following removal of the remaining photoresist, the substrates are subjected to a brief etch in nitric acid to remove the Ni catalyst particle at the tip. An O_2 RIE is used to remove the body of the fiber from the thin film tube encasing it. Once the body of the fiber has been entirely removed, the bottom of the tube can be opened, creating a nanometer-sized pipe structure, or nanopipe (**Fig. 7**). These types of structures have been used in fluid transport experiments involving DNA and fluorescent intercalating dyes ***(26)***.

The combination of the growth, postgrowth processing, and interfacing techniques described in this chapter provides a set of unique tools for direct interaction with cellular processes at the molecular scale. There is a great deal of promise in the application of such high-volume, yet precisely engineered devices to problems of biological interest. Perhaps as these tools evolve further, they will eventually be as significant within biological fields as they have been for semiconductor electronics.

References

1. Chan, W. C. W. and Nie, S. M. (1998) Quantum dot bioconjugates for ultrasensitive nonisotopic detection. *Science* **281(5385),** 2016–2018.
2. Bruchez, M., Moronne, M., Gin, P., Weiss, S., and Alivisatos, A. P. (1998) Semiconductor nanocrystals as fluorescent biological labels. *Science* **281(5385),** 2013–2016.

3. Dubertret, B., Skourides, P., Norris, D. J., Noireaux, V., Brivanlou, A. H., and Libchaber, A. (2002) In vivo imaging of quantum dots encapsulated in phospholipid micelles. *Science* **298(5599),** 1759–1762.
4. Wightman, R. M., Jankowski, J. A., Kennedy, R. T., Kawagoe, K. T., Schroeder, T. J., Leszczyszyn, D. J., Near, J. A., Diliberto, E. J., and Viveros, O. H. (1991) Temporally resolved catecholamine spikes correspond to single vesicle release from individual chromaffin cells. *Proc. Natl. Acad. Sci. USA* **88(23),** 10,754–10,758.
5. Knoblauch, M., Hibberd, J. M., Gray, J. C., and van Bel, A. J. E. (1999) A galinstan expansion femto syringe for microinjection of eukaryotic organelles and prokaryotes. *Nat. Biotechnol.* **17(9),** 906–909.
6. McAllister, D. V., Allen, M. G., and Prausnitz, M. R. (2000) Microfabricated microneedles for gene and drug delivery. *Annu. Rev. Biomed. Eng.* **2,** 289–313.
7. Wong, S. S., Joselevich, E., Woolley, A. T., Cheung, C. L., and Lieber, C. M. (1998) Covalently functionalized nanotubes as nanometre-sized probes in chemistry and biology. *Nature* **394(6688),** 52–55.
8. Woolley, A. T., Guillemette, C., Cheung, C. L., Housman, D. E., and Lieber, C. M. (2000) Direct haplotyping of kilobase-size DNA using carbon nanotube probes. *Nat. Biotechnol.* **18(7),** 760–763.
9. Guillorn, M. A., McKnight, T. E., Melechko, A., Merkulov, V. I., Britt, P. F., Austin, D. W., Lowndes, D. H., and Simpson, M. L. (2002) Individually addressable vertically aligned carbon nanofiber-based electrochemical probes. *J. Appl. Phys.* **91(6),** 3824–3828.
10. Kim, P. and Lieber, C. M. (1999) Nanotube nanotweezers. *Science* **286(5447),** 2148–2150.
11. Ren, Z. F., Huang, Z. P., Xu, J. W., Wang, J. H., Bush, P., Siegal, M. P., and Provencio, P. N. (1998) Synthesis of large arrays of well-aligned carbon nanotubes on glass. *Science* **282(5391),** 1105–1107.
12. Merkulov, V. I., Lowndes, D. H., Wei, Y. Y., Eres, G., and Voelkl, E. (2000) Patterned growth of individual and multiple vertically aligned carbon nanotubes. *Appl. Phys. Lett.* **76(24),** 3555–3557.
13. Merkulov, V. I., Guillorn, M. A., Lowndes, D. H., Simpson, M. L., and Voelkl, E. (2001) Shaping carbon nanostructures by controlling the synthesis process. *Appl. Phys. Lett.* **79(8),** 1178–1180.
14. Ren, Z. F., Huang, Z. P., Wang, D. Z., Wen, J. G., Xu, J. W., Wang, J. H., Calvet, L. E., Chen, J., Klemic, J. F., and Reed, M. A. (1999) Synthesis and characterization of Cu_2O nanowires. *Appl. Phys. Lett.* **75(8),** 1086–1088.
15. Baker, R. T. K., (1989) Catalytic growth of carbon filaments. *Carbon* **27(3),** 315–323.
16. Merkulov, V. I., Melechko, A. V., Guillorn, M. A., Lowndes, D. H., and Simpson, M. L. (2001) Alignment mechanism of carbon nanofibers produced by plasma-enhanced chemical-vapor deposition. *Appl. Phys. Lett.* **79(18),** 2970–2972.
17. Melechko, A. V., McKnight, T. E., Hensley, D. K., Guillorn, M. A., Borisevich, A. Y., Merkulov, V. I., Lowndes, D. H., and Simpson, M. L. (2003) Large-scale synthesis of arrays of high-aspect-ratio rigid vertically aligned cabon nanofibers. *Nanotechnology* **14(9),** 1029–1035.

18. Madou, M. J. (2002) *Fundamentals of Microfabrication: The Science of Miniaturization*, CRC Press, New York.
19. McKnight, T. E., Melechko, A. V., Griffin, G. D., Guillorn, M. A., Merkulov, V. I., Serna, F., Hensley, D. K., Doktycz, M. J., Lowndes, D. H., and Simpson, M. L. (2003) Functional intracellular integration of synthetic nanostructures with viable cells for non-inheritable genetic modification. *Nanotechnology* **14,** 551–556.
20. McKnight, T. E., Melechko, A. V., Hensley, D. K., Mann, D. G. J., Griffin, G. D., and Simpson, M. L. (2004) Intracellular integration of synthetic nanostructures with viable cells for controlled biochemical manipulation. *Nano Lett.* **4,** 1213–1219.
21. Lau, K. K. S., Bico, J., Teo, K. B. K., Chhowalla, M., Amaratunga, G. A. J., Milne, W. I., McKinley, G. H., and Gleason, K. K. (2003) Superhydrophobic carbon nanotube forests. *Nano Lett.* **3(12),** 1701–1705.
22. Guillorn, M. A., Melechko, A. V., Merkulov, V. I., Ellis, E. D., Simpson, M. L., Baylor, L. R., and Bordonaro, G. J. (2001) Microfabricated field emission devices using carbon nanofibers as cathode elements. *J. Vacuum Sci. & Technol. B* **19(6),** 2598–2601.
23. Guillorn, M. A., Melechko, A. V., Merkulov, V. I., Hensley, D. K., Simpson, M. L., and Lowndes, D. H. (2002) Self-aligned gated field emission devices using single carbon nanofiber cathodes. *Appl. Phys. Lett.* **81(19),** 3660–3662.
24. Melechko, A. V., McKnight, T. E., Guillorn, M. A., Austin, D. W., Ilic, B., Merkulov, V. I., Doktycz, M. J., Lowndes, D. H., and Simpson, M. L. (2002) Nanotype fabrication using vertically aligned carbon nanofiber templates. *J. Vacuum Sci. Technol. B* **20(6),** 2730–2733.
25. Zhang, L., Melechko, A. V., Merkulov, V. I., Guillorn, M. A., Simpson, M. L., Lowndes, D. H., and Doktycz, M. J. (2002) Controlled transport of latex beads through vertically aligned carbon nanofiber membranes. *Appl. Phys. Lett.* **81(1),** 135–137.
26. Melechko, A. V., McKnight, T. E., Guillorn, M. A., Merkulov, V. I., Ilic, B., Doktycz, M. J., Lowndes, D. H., and Simpson, M. L. (2003) Vertically aligned carbon nanofibers as sacrificial templates for nanofluidic structures. *Appl. Phys. Lett.* **82(6),** 976–978.

16

Real-Time Cell Dynamics With a Multianalyte Physiometer

Sven E. Eklund, Eugene Kozlov, Dale E. Taylor, Franz Baudenbacher, and David E. Cliffel

Summary

A technique for simultaneously measuring changes in extracellular glucose, lactate, and oxygen concentrations in conjunction with acidification rates on a Cytosensor™ Microphysiometer is described. Platinum electrodes are inserted into the standard Cytosensor plunger head and modified with enzymes and biocompatible polymeric films. The lactate and glucose oxidase enzymes catalyze the reaction of lactate and glucose. An end product of these catalyses, H_2O_2, is measured amperometrically. Extracellular oxygen is also measured amperometrically, while the acidification rate is measured potentiometrically by the Cytosensor. Useful information is obtained during the Cytosensor stop-flow cycles, which produce increasing or decreasing peaks, owing to the production of lactic and carbonic acid and consumption of glucose and oxygen by the cells. Fabrication of the modified sensor head and deposition of the electrode films is detailed, and the operation of the technique is described and illustrated by the simultaneous measurement of all four analytes during the addition of 20 m*M* fluoride to mouse fibroblast cells.

Key Words

Cellular physiology; Cytosensor™; Microphysiometer; enzyme electrodes; oxygen; acidification; multianalyte; Nafion.

1. Introduction

Living cells represent the ultimate nanoscale analytical detectors based on their nanostructured protein receptors coupled directly to cell metabolism and function. Significant advances in nanobiotechnology research at this point have been made in artificially re-creating the sensing strategies found in cell membranes. Despite this progress, the components of the living cell remain the most complex of all nanostructured devices. One approach is to use cell physiology

From: *Methods in Molecular Biology, vol. 303: NanoBiotechnology Protocols*
Edited by: S. J. Rosenthal and D. W. Wright © Humana Press Inc., Totowa, NJ

as an analytical platform by coupling the quick response of cell receptors to the cell's energy metabolism.

New classes of biosensors have been used to determine the physiological response of cells to various chemical environments and toxic agents by detecting changes in extracellular analyte concentrations ***(1–3)***. Since the responses are related to the metabolic activity of the cells, they can be used to screen the cellular responses to various agents such as drugs and toxins. The simplest case would be the determination of a single analyte indicative of metabolic activity. However, if responses are obtained simultaneously from multiple analytes, these biosensors offer a multidimensional approach to the elucidation of cellular metabolic pathways and responses to chemical and biological agents.

Although there are many analytes in metabolism to choose from, the choice is normally limited to those that are directly involved in the energy-producing pathways within the cell and that can be measured in the extracellular environment: oxygen consumption, glucose consumption, lactic acid production, and acidification rate (which is a combination of lactic acid and carbonic acid release). Using glucose and oxygen as inputs and lactate and acidification as outputs, real-time cell dynamics can be described by this simple model of metabolic physiology. The two major pathways in this model can be described as anaerobic, in which lactic acid is produced by the cells, and aerobic, in which extracellular glucose and oxygen are eventually converted into carbon dioxide (carbonic acid) and water. Acidification, measured potentiometrically, and oxygen concentration, measured amperometrically, can be determined directly. Glucose and lactate concentrations can be determined indirectly by measuring the H_2O_2 produced by selective catalysis of these analytes with glucose oxidase (GOX) and lactate oxidase (LOX), respectively ***(4)***. Cellular physiological responses to a particular agent can then be inferred from the direction and magnitude of the change in these analytes. In addition, constructing dose–response curves for specific agents would be analogous to analytical calibration curves.

Karube and colleagues ***(5,6)*** first described indirect detection of an agent by using the change in the oxygen consumption rates of yeast cells exposed to a wide variety of physiological agents. This technique, which measured oxygen concentration amperometrically by a Clark electrode, was never commercialized as an analytical instrument. The Cytosensor™ Microphysiometer, however, has been commercialized and used for a large number of cellular studies ***(7–11)*** in which the change in pH in the extracellular environment is related to metabolic signals from the cell. However, this does not provide multidimensional extracellular measurements, which are more useful to characterize cellular response to chemical stimulations such as drugs and toxins, nor can the internal dynamics of the cell metabolic pathways be investigated.

Measurements detecting species such as oxygen ***(12,13)***, glucose ***(4,14)***, and lactate ***(4)*** have been made at modified platinum electrodes. By incorporating similarly modified electrodes into the Cytosensor Microphysiometer, producing a multianalyte sensor head, measurements can be made simultaneously in conjunction with acidification rates, and a broader picture of cellular physiology can be realized. This technique presents the methodology to simultaneously measure the change in extracellular glucose, lactate, and oxygen concentrations in conjunction with acidification rates in response to metabolic agents. These measurements help to elucidate cellular activity in response to drugs and toxins and to help distinguish between aerobic and anaerobic metabolic pathways.

The Cytosensor Microphysiometer operates via a program in which a cell medium (usually RPMI-1640) is pumped through a cell chamber (containing approx 3×10^5 cells) in a series of flow and stop-flow cycles. During the stop-flow cycles, the solution in the chamber is stationary and the acidification in the cell chamber changes at a rate comparable to the number and activity of the cells. This rate is measured by the instrument using a light-addressable potentiometric sensor ***(9)***. Once a baseline cellular activity is achieved, a metabolic agent is introduced and the change in acidification rate is recorded.

The technique of multianalyte determination takes advantage of the Cytosensor Microphysiometer technology by measuring the change in glucose, oxygen, and lactate concentrations in conjunction with the Cytosensor Microphysiometer acidification rates. Amperometric curves for glucose, lactate, and oxygen are obtained by applying appropriate potentials at the modified platinum electrodes while running the acidification rate program. When the stop-flow cycle begins, the current begins to decrease or increase, depending on whether the analyte is being consumed or produced by the cells. The raw data (**Fig. 1**) appear similar to the Cytosensor acidification raw data but generally have curved slopes, and instead of measuring the slope of the change in pH in negative microvolts per second, the area of the resultant peaks during the stop-flow cycle (in Coulombs of charge), or the difference in peak heights, is plotted vs time and is proportional to the analyte concentration. The Coulombs of charge for the glucose and lactate can be converted into concentrations by an *in situ* addition of known quantities of analyte, usually at the end of the experiment, thereby internally calibrating the sensors. The oxygen consumption can be estimated by assuming the baseline current as the ambient oxygen concentration and extrapolating to zero.

The GOX- and LOX-modified platinum electrodes themselves are coated with a solution containing the enzyme, bovine serum albumin (BSA), and the crosslinking agent glutaraldehyde. The chemical reactions catalyzed at the respective enzyme electrodes can be simply described as

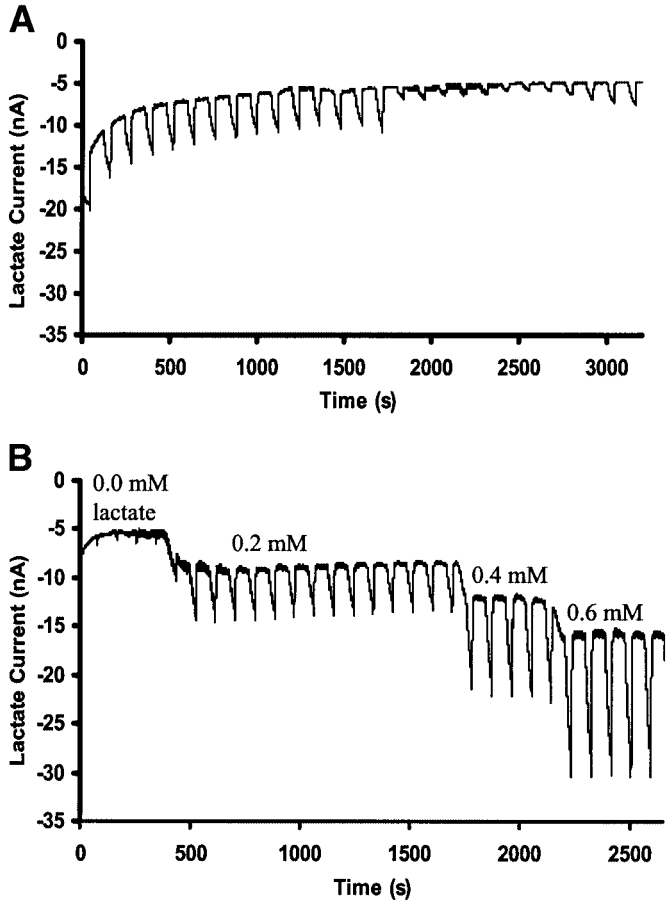

Fig. 1. Modified lactate electrode response in Cytosensor Microphysiometer with **(A)** approx 3×10^5 CHO cells (with 20 m*M* NaF added at 1800 s and stopped at 2700 s) and **(B)** additions of 0.2 m*M* lactate. The medium used in both cases was RPMI-1640.

$$\text{glucose} + O_2 + H_2O \rightarrow \text{gluconic acid} + H_2O_2 \quad (1)$$

and

$$\text{lactate} + O_2 + H_2O \rightarrow \text{pyruvate} + H_2O_2 \quad (2)$$

The platinum electrodes are set at a potential that will oxidize the H_2O_2 product back to water and oxygen (usually +0.6 V vs the Ag/AgCl reference electrode), and so any change in glucose or lactate concentration will be seen as a change in H_2O_2 concentration. These films give rapid time response and very high currents in the concentration ranges of the target analytes: glucose (10 m*M* in

RPMI-1640) and lactate (roughly 0.3 m*M* scale with approx 3×10^5 fibroblast cells at an acidification rate of –200 to –250 μV/s). These currents approach the region where Michaelis-Menten kinetics giving rise to nonlinear sensors would need to be considered. Fortunately, it is easy to modify the enzyme loading on the electrode so that the concentrations of interest are in a linear response range of the modified electrode, i.e., in the more linear portion of the Michaelis-Menten curve. This modification is achieved by adding a diffusion barrier to the electrodes in the form of a Nafion film. Nafion also has the benefit of adding resistance to biofouling, because the Nafion is negatively charged and very unreactive. The Nafion is diluted before coating the LOX membrane so that it does not completely block the negatively charged lactate ions from diffusing through the membrane.

The lactate response raw data for Chinese hamster ovary (CHO) cells exposed to 20 m*M* NaF is shown in **Fig. 1A**, where the peaks represent the increase in current owing to cellular lactate production during the stop-flow cycle of the Cytosensor Microphysiometer program. When NaF was added at 1800 s, cellular lactate production was suppressed, shown as a decrease in the peak area (or height). The cellular lactate production resumed when NaF was stopped. The effect of 0.2 m*M* lactate additions as a calibration are shown in **Fig. 1B**, although lactate (and glucose) additions are usually added at the end of the experiment. Since the lactate and glucose current responses are fairly linear, simple two-point calibration curves are generally sufficient to convert the Coulombs of charge (or peak height current differences) to concentrations. The oxygen concentration can be estimated by extrapolating from the baseline current, assumed to be ambient oxygen at 0.24 m*M*. The acidification rate data can be directly imported from the Cytosensor Microphysiometer program. Note that in determining concentrations of analytes, any analyte additions to the flow medium, such as the lactate additions shown in **Fig. 1B**, produce an increasing baseline during the flow cycle on each successive addition. However, when analyte concentration changes are owing to cellular activity, such as the lactate in **Fig. 1A**, the baseline during the flow cycle generally does not change when the analyte concentration increases or decreases, because the baseline concentration in solution does not change in the vicinity of the electrode until the analyte concentration gradient from the cells during the stop-flow cycle reaches the electrode. Peak currents during stop-flow may therefore be more representative of the actual analyte concentration because they are not affected by the time for the concentration gradient from the cells, whether decreasing or increasing, to reach the electrode. This has been found to be especially true for the lactate determination, in which the difference in lactate concentration calculated from peak heights was two to three times larger than that calculated from areas. However, there

may be times when it is difficult to analyze the peak height owing to a nonstandard peak shape, especially for glucose consumption.

The effect of 20 m*M* NaF on fibroblast cells is illustrated in **Fig. 2**, which shows the changes in the extracellular concentrations of glucose, lactate, and oxygen and the acidification rate. Fluoride shut down the metabolic activity of the cells, shown as an increase in the glucose and oxygen concentrations (the cells are using less) and as a decrease in the lactate concentration and acidification rate (the cells are producing less). Once the fluoride was removed, the cells appeared to recover nearly to their previous metabolic state.

2. Materials

2.1. Equipment

1. Cytosensor Microphysiometer instrument and all corresponding materials necessary for measuring acidification rates (Molecular Devices, Sunnyvale, CA).
2. CHI 1030 Multipotentiostat (CH Instruments, Austin, TX) with a PC to run the instrument and accompanying software.
3. Aqueous reference electrode, Ag/AgCl (can be obtained from CH Instruments).

2.2. Membrane Solution Reagents

1. GOX (*Aspergillus niger*; Sigma, St. Louis, MO).
2. LOX (from *Pediococcus* species; Sigma).
3. BSA (Fraction V, 96%; Sigma).
4. Glutaraldehyde (glutaric dialdehyde), 25% solution in water.
5. 1 m*M* Phosphate buffer, pH 7.0.
6. Phosphate-buffered saline (PBS): 1 m*M* Phosphate; 100 m*M* NaCl, pH 7.0.
7. Triton X-100.
8. Nafion solution: perfluorsulfonic acid–PTFE copolymer, 5% (w/w) solution from Alfa Aesar.

2.3. Sensor Head Materials

1. Cytosensor Microphysiometer plunger heads with four holes drilled lengthwise through the body to accommodate the platinum wires.
2. Platinum wire, 24 gage (0.51-mm diameter) and 36 gage (0.127-mm diameter).
3. Hysol® Epoxy-Patch® structural adhesive (1c; Dexter).

Fig. 2. *(opposite page)* Modified sensor head response to changes in extracellular **(A)** glucose, **(B)** lactate, **(C)** oxygen concentrations and the **(D)** Cytosensor Microphysiometer-measured acidification rate on addition of 20 m*M* NaF to approx 3×10^5 fibroblast cells. NaF addition began at 1700 s and was stopped at 2800 s. The medium was RPMI-1640 with a 60-s flow cycle and a 30-s stop-flow cycle. The curves in (A–C) have been baseline corrected. Details of the effects of NaF on fibroblasts have been published ***(15)***.

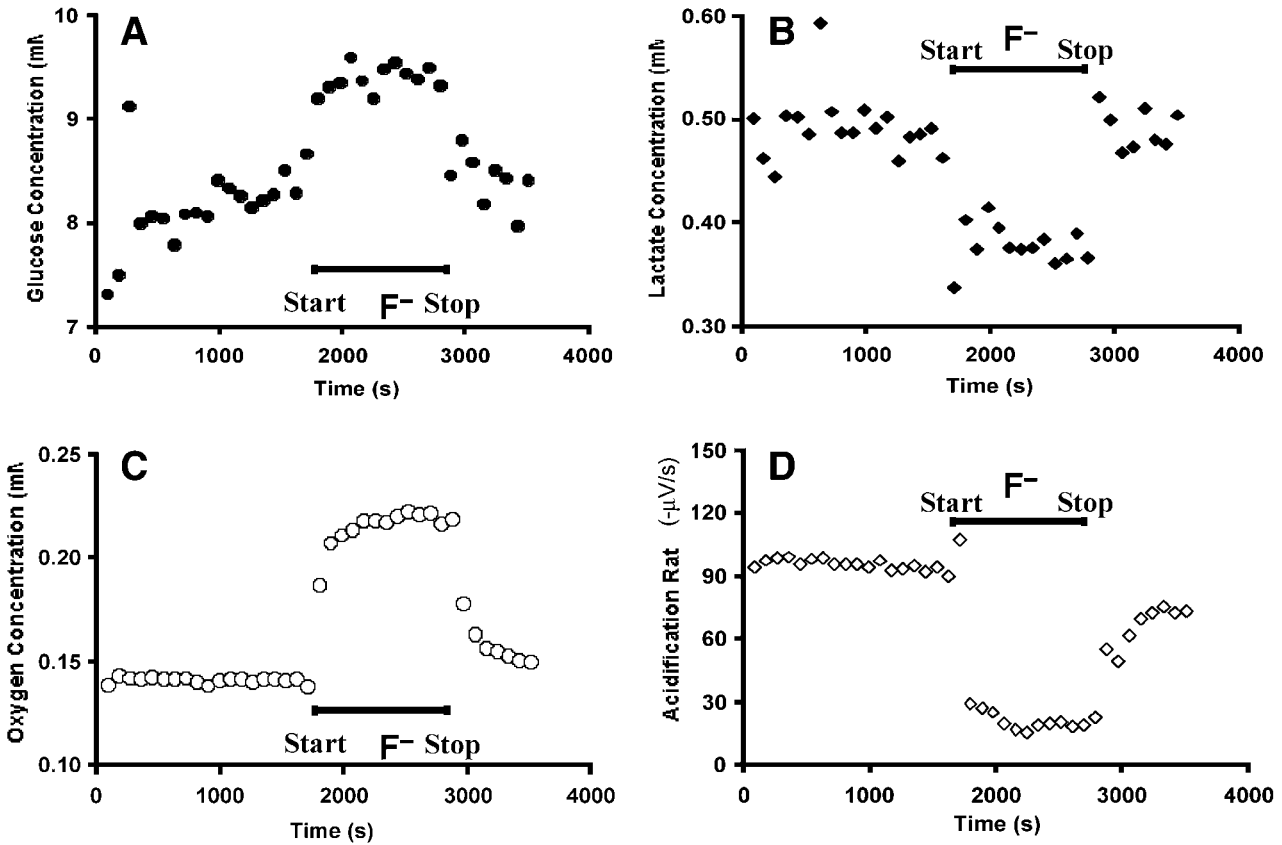
A
Glucose Concentration (mM
10
9
8
7
Start F⁻ Stop
0
1000
2000
3000
4000
Time (s)
B
Lactate Concentration (mM
0.60
0.50
0.40
0.30
Start F⁻ Stop
0
1000
2000
3000
4000
Time (s)
C
Oxygen Concentration (mM
0.25
0.20
0.15
0.10
Start F⁻ Stop
0
1000
2000
3000
4000
Time (s)
D
Acidification Rat (-μV/s)
150
120
90
60
30
0
Start F⁻ Stop
0
1000
2000
3000
4000
Time (s)

4. Brass crimp connectors (CCD-202-1-SP; SPC Technology).
5. Polyurethane (Crystal Clear 200 or harder version, from Smooth-On).
6. Silver epoxy (Epo-Tek®, Epoxy Technology®, Billerica, MA).
7. Diamond-polishing compounds (1, 6, and 15 µ, Metadi II, from Buehler).
8. Cotton-tipped swabs.

2.4. Cell Lines

1. CHO cells M3WT4 (American Type Culture Collection [ATCC] no. CRL-1981).
2. Mouse sc fibroblast cells A9 L HD2 S.C.18 (ATCC no. CRL-10255).

3. Methods

3.1. Construction and Preparation of Sensor Heads

3.1.1. Physical Modifications to Sensor Head

1. Insert four platinum wires (24 gage; *see* **step 2** for the smaller oxygen electrode) in holes drilled lengthwise through a Cytosensor Microphysiometer plunger head **(***see* **Note 1**). Then seal them at the surface with Hysol Epoxy-Patch and allow to harden for the recommended time **(Fig. 3) (***see* **Note 2**).
2. For the oxygen electrode, the smaller platinum wire (36 gage) can be attached to the larger platinum wire with silver epoxy before sealing in the electrode **(Fig. 3)**. To do this, leave the 24-gage platinum wire approx 3 mm below the surface of the sensor face, fill with a small amount of silver epoxy, then insert a short piece of the smaller platinum wire. The wire can be sealed with Hysol Epoxy-Patch after the silver epoxy hardens (*see* **Note 3**).
3. Solder crimp connectors to the platinum wires at the back.
4. Attach a rubber collar, and then pour freshly mixed polyurethane into the back of the sensor head. Before the polyurethane hardens, insert a wooden stick in the center of the back of the sensor head to form a hole for the Cytosensor plunger arm to fit. The wooden stick can easily be removed before complete hardening of the polyurethane (*see* **Note 5**). Allow the polyurethane to harden for the recommended time. This provides electrical insulation and mechanical strength for the crimp connectors (*see* **Note 5**).
5. Polish the electrodes with sandpaper glued to a machined brass jig that fits over the electrode area alone, minimizing damage to the O-ring seat (**Fig. 2**). Then rub diamond-polishing compound over the electrodes with cotton-tipped applicators to achieve a fine polish (*see* **Note 6**).

3.1.2. Preparation of Oxidase-BSA Coating Solution

1. In a small vial, weigh out 5 mg of GOX.
2. Add 500 µL of 1 m*M* phosphate buffer containing 0.02% (v/v) Triton X-100 and dissolve the GOX.
3. Thoroughly dissolve 50 mg of BSA in the mixture (*see* **Note 7**).
4. Add 5 µL of the 25 wt% glutaraldehyde solution and mix well (*see* **Note 8**).
5. Repeat this process for the LOX solution, except use approx 2.5 mg of LOX (*see* **Note 9**).

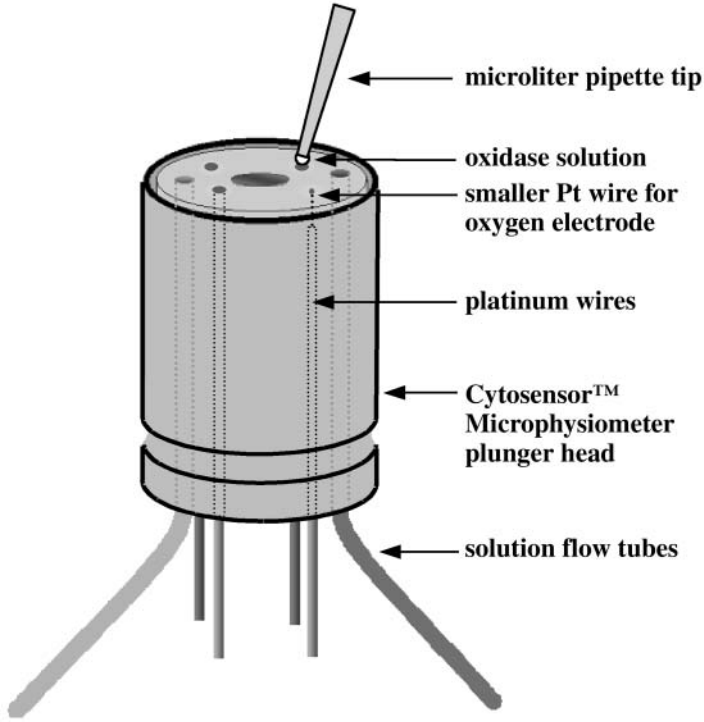

Fig. 3. Modified sensor head for use in Cytosensor Microphysiometer. The four platinum electrodes are shown placed around a center electrode. The center iron electrode comes as part of the plunger head before the modifications and is the counter-electrode for the acidification measurements. The smaller of the four platinum electrodes is used for oxygen measurements. Deposition of the oxidase solution, whether GOX/BSA, LOX/BSA, or Nafion, is shown by the droplet from the microliter pipet tip.

3.1.3. Coating of Modified Sensor Head Electrodes

1. Draw a small amount of the coating solution into a 10 µL plastic pipet tip.
2. Gently force the solution out of the tip by pressing a finger (moistened for good seal) at the back of the pipet tip, and allowing a partial droplet to form at the tip. Touch the droplet to the electrode area (**Fig. 3**) and allow it to cover the electrode but minimize droplet spread outside of the electrode area as much as possible (*see* **Note 10**).
3. Let dry for approx 30 min in room air.
4. After drying, coat the GOX-BSA membrane with a droplet (using the pipet tip as in **step 2**) of 5% Nafion solution, and allow it to dry for 10–15 min before use.

5. Coat the LOX-BSA membrane with three or four droplets of a Nafion solution consisting of 1 part (v/v) 5% Nafion solution to 9 parts ethanol.
6. Coat the smaller of the four electrodes (oxygen electrode) with a droplet of 5% Nafion solution.
7. Store the sensor heads at 4°C with the sensor ends immersed in 50 m*M* phosphate buffer (pH 7.0).

3.1.4. Testing of Sensor Quality

1. Insert the sensor end only of the sensor head into a small glass bottle containing 10 mL of a stirred, 1 m*M* PBS solution.
2. Connect the leads of the CHI 1030 to the electrodes as described in **Subheading 3.2.**, except using a separate Ag/AgCl aqueous reference electrode (this can be obtained from CH Instruments).
3. Run the same amperometric program as described in **Subheading 3.3.1.** for the CHI 1030.
4. When the current approaches a steady state, add successive aliquots of solutions of glucose (200 µL of a 0.1 *M* solution = 2 m*M*) or lactate (50 µL of a 0.1 *M* solution = 0.5 m*M*) and observe the increase in current. The currents should be roughly 5–10 nA/m*M* for glucose (up to 10 m*M* glucose) and 50–100 nA/m*M* for lactate (up to 2 m*M* lactate), depending on the quality of the coatings.

3.2. Attachment of Modified Sensor Head to Cytosensor Microphysiometer

The Cytosensor Microphysiometer program is used in the usual manner for obtaining acidification rates and controls the flow/stop-flow cycles. The CHI 1030 is run in conjunction with this to obtain the glucose, lactate, and oxygen concentration data. However, the only shared electrode between the instruments is the reference electrode. The CHI 1030 connects to the other electrodes separately from the Cytosensor Microphysiometer.

1. Insert the seated cells into the Cytosensor Microphysiometer in the usual manner for obtaining acidification rates, except replace the usual plunger with the modified sensor head.
2. Attach the CHI 1030 leads 1 (green), 2 (yellow), and 3 (yellow) directly to the GOX, LOX, and oxygen electrodes, respectively, on the modified sensor head.
3. Attach the counterelectrode lead (red) to the remaining platinum electrode on the modified sensor head.
4. Attach the reference electrode lead (white) to the reference electrode on the Cytosensor Microphysiometer instrument.

3.3. Standard Operating Procedure

3.3.1. CHI 1030 Program Parameters

1. Select the amperometric *i-t* curve program from the technique menu.
2. Select the program setup and insert the following parameters:

a. Electrode 1, GOX: Init E = +0.6 V, Sample Interval = 0.2 s, Sampling Time = length of experiment (recommend at least 10,000 s), Quiet Time = 0 s, Scales During Run = 1, Sensitivity = 1.e-007.
b. Electrode 2, LOX: Init E = +0.6 V, Sensitivity = 1.e-007; check "on" box.
c. Electrode 3, Oxygen: Init E = –0.45 V, Sensitivity = 1.e-007; check "on" box.

3.3.2. Initial Preparations

Once the cells are inserted into the modified sensor head and the electrodes are attached the Cytosensor program can be started to determine the quality of the connections and activity of the cells. *See* **Note 11** for the Cytosensor Microphysiometer program parameters.

The Cytosensor Microphysiometer should return a "no problem" signal to ensure good electrical connections. The cells should be fairly active—the larger the acidification rate, the more active the cells, and the larger the signal change that will be generated for the sensors. However, this may vary between cell types. Best results have been obtained with acidification rates approx –200 μV/s or greater.

The modified sensor head should also be tested briefly with the amperometric *i-t* curve program described in **Subheading 3.3.1.** to ensure that the CHI 1030 leads have good connections and that the sensors are working properly. Be sure that the sensor head plunger hole is dry. Then with the Cytosensor Microphysiometer pumps running, select "run" on the CHI 1030 and observe the currents. The GOX and LOX electrodes give negative currents and the oxygen electrode gives positive, all of which begin to decrease to a steady state (ideally in the 10- to 40-nA range).

Once both programs are functioning properly, they can then be started simultaneously. Mark the difference in the starting time or some common point during the run, and let them run until the cells have adjusted to the environment, i.e., achieve a steady baseline with respect to the acidification rate (*see* **Note 12**).

3.3.3. Addition of Metabolic Agent and Calibration Standards

1. Add metabolic agents either during a stop-flow cycle or near the start of a flow cycle. This allows the agent to begin taking effect before the next measurement (i.e., stop-flow cycle) (*see* **Note 13**).
2. After the desired number of cycles under metabolic agent flow, switch back to regular RPMI flow without the metabolic agent, and allow the cells to recover to a steady state for a desired number of cycles.
3. For construction of the calibration curve to convert the peak areas to concentrations, at the end of the experiment, add to the flow solution standard additions of lactate to change the concentration by 0.2 m*M* and glucose to change the concentration by 0.5 m*M* for each aliquot.

4. Remove the cells and repeat the experiment. This serves as a background check on the effect of the metabolic agent on the electrodes themselves in the absence of cells.

3.4. Data Accumulation and Calibration

1. Model the area or height of the peaks during stop-flow in Coulombs as measured against the flow baseline as directly proportional to the concentration.
2. Use the standard additions of glucose and lactate at the end of the experiment to construct a calibration curve of peak current (measured from the current baseline) or Coulombs of charge (also measured from the current baseline) vs concentration.
3. Estimate the oxygen concentration by extrapolating from ambient as a baseline. This may require measurement of the dissolved oxygen in the bulk solution if it is not known or it may be assumed. Then take the oxygen response (in Coulombs during stop-flow) of the sensor head in the absence of cells as the ambient oxygen concentration, and use a two-point calibration.
4. Convert all files to .TXT files and import into a spreadsheet program such as Excel for data analysis. This includes the acidification rate data from the Cytosensor Microphysiometer.

4. Notes

1. The wires should not touch the center electrode that comes with the plunger, should run the length of the sensor body, and should be electrically insulated. It may be helpful to bevel the holes at the surface before inserting the wires and filling with epoxy. When depositing epoxy around the electrode, it is useful to push the wire a few millimeters above the surface, depositing epoxy, then pulling the wire back down. This helps to ensure good adhesion of the epoxy to the platinum wire.
2. The silver epoxy can be deposited into the hole by filling a small, disposable syringe needle with some of the silver epoxy and then injecting it into the hole. To prevent the silver epoxy from making a silver electrode by being exposed at the surface, the hole with the silver epoxy can be beveled slightly with a larger drill bit after the silver epoxy has been injected. This will remove excess silver epoxy around and near the surface before the smaller platinum wire is inserted.
3. Polyurethane can also be used as the sealant. However, a version that is harder than Crystal Clear 200 is recommended. Make sure that the sensor head crimp connectors will not touch the plunger arm. They should be angled out similar to the flow tubing when the polyurethane sealant is used and before it hardens.
4. A Teflon rod has been used as well, which can be left in for the duration of hardening, since the material does not stick to it, and the Teflon is easily removed later. The wooden stick can also be drilled out. In addition, it is possible that the material could just be drilled out of the back after the hardening process, but having the wooden stick in provides a soft channel for the drill bit to follow and thus minimizes any possible damage to the tubing or crimp connectors from the drill bit.

5. Hysol Epoxy-Patch or some other insulating and hardening epoxy can be used in place of the polyurethane.
6. Alumina-polishing compound (Buehler) could be used in place of the diamond. Be careful not to grind the electrode surface area too far below the plunger lip/O-ring seat. This causes the electrodes to be too far from the cells when placed in the cup and, hence, an increase in the diffusion distance. In this case, the solution stop-flow cycle would have to be increased in proportion to the increased diffusion distance, i.e., beyond a practical time in order to measure a signal. The closer the electrodes to the cell membrane, the better and more rapid the signal response.
7. The more powdery versions of BSA go more easily and quickly into solution. The flakier BSA works but takes much longer to dissolve fully.
8. Be sure to mix thoroughly the glutaraldehyde into the solution. This prevents concentrated regions of the glutaraldehyde, which can cause portions of the mixture to gel early.
9. Because LOX is expensive and the solution has a tendency to gel more quickly, depending on how accurately the amount of glutaraldehyde was added, as many heads as possible should be prepared at one time for coating, because the solutions do not last more than 1 d. We found that storage of the solutions in a freezer or refrigerator overnight does not preserve them. Because the GOX is much cheaper, it can be used to practice making the solutions and applying the coatings before the LOX is used. Once coated on the electrodes, however, the coatings can last for 1 mo or longer.
10. If the coating spreads too far outside the sensor head area, the current is too high and it will be difficult to control the linear response even with the Nafion layers. In addition, excess H_2O_2 will be produced outside the platinum electrode area and may adversely affect the cells.
11. The Cytosensor Microphysiometer program can be set up to run 90 s flow, and 30 s stop-flow. This program may vary widely, but note that the shorter the stop-flow cycle, the less time for the analyte concentration gradient from the cells to reach the electrodes, so at least a 30-s stop-flow cycle is recommended as a minimum. In attempting to shorten the overall experiment time, we found that no adverse effects could be detected on reducing the 90-s flow cycle to 60 s.
12. There will be a slight amount of noise visible on the Cytosensor display, but it has no adverse effect on the determination of acidification rate. However, care should be taken not to allow any solution to get into the plunger hole of the sensor head, because this can cause unacceptable electrical noise between the two instruments. Water in the plunger hole is the main cause of bad signals and can easily get in when the tubing running to the reference electrode is disconnected while the solution is still flowing or during insertion of the sensor head into the cell holder. Drying with absorbent tissue usually removes the water.
13. The time for a metabolic agent to begin to affect the cells and to what extent will vary widely depending on the particular agent itself and the type of cells used. This includes the recovery period, if any, as well.

Acknowledgments

This work was supported in part by the Defense Advanced Research Projects Agency (N66001-01-C-8064), the Vanderbilt Institute for Integrative Biosystems Research and Education, and Vanderbilt University.

References

1. Cliffel, D., Baudenbacher, F. J., Wikswo, J. P., Eklund, S., Balcarcel, R. R., and Gilligan, J. M. (2003) Device and methods for detecting the response of a plurality of cells to at least one analyte of interest. *PCT Int. Appl.*, 123.
2. Eklund, S. E., Cliffel, D. E., Kozlov, E., Prokop, A., Wikswo, J., and Baudenbacher, F. (2003) Modification of the Cytosensor™ Microphysiometer to simultaneously measure extracellular acidification and oxygen consumption rates. *Anal. Chim. Acta* **496,** 93–101.
3. Wilson, G. S. (ed.). (2003) Bioelectrochemistry, in *Encyclopedia of Electrochemistry*, vol. 9 (Bard, A. J. and Stratmann, M., eds.), Wiley-VCH, Weinheim, pp. 309–340.
4. Yang, Q., Atanasov, P., and Wilkins, E. (1998) An integrated needle-type biosensor for intravascular glucose and lactate monitoring. *Electroanalysis* **10,** 752–757.
5. Karube, I. (1987) Micro-organism based sensors, in *Biosensors: Fundamentals and Applications* (Turner, A., Karube, I., and Wilson, G. S., eds.), Oxford University Press, Oxford, UK, pp. 471–480.
6. Karube, I., Matsunaga, T., and Suzuki, S. (1979) Microbioassay of nystatin with a yeast electrode. *Anal. Chim. Acta* **109,** 39–44.
7. Parce, J. W., Owicki, J. C., Kercso, K. M., Sigal, G. B., Wada, H. G., Muir, V. C., Bousse, L. J., Ross, K. L., Sikic B. I., and McConnell, H. M. (1989) Detection of cell-affecting agents with a silicon biosensor. *Science* **246,** 243–247.
8. Owicki, J. C., Parce, J. W., Kercso, K. M., Sigal, G. B., Muir, V. C., Venter, J. C., Fraser, C. M., and McConnell, H. M. (1990) Continuous monitoring of receptor-mediated changes in the metabolic rates of living cells. *Proc. Natl. Acad. Sci. USA* **87,** 4007–4011.
9. Owicki, J. C., Bousse, L. J., Hafeman, D. G., Kirk, G. L., Olson, J. D., Wada, H. G., and Parce, J. W. (1994) The light-addressable potentiometric sensor: principles and biological applications. *Annu. Rev. Biophys. Biomol. Struct.* **23,** 87–113.
10. Hafner, F. (2000) Cytosensor Microphysiometer: technology and recent applications. *Biosens. Bioelectronics* **15,** 149–158.
11. Jonnala, R. R. and Buccafusco, J. J. (2001) Inhibition of nerve growth factor signaling by peroxynitrile. *J. Neurosci. Res.* **63,** 27–34.
12. Tammesveski, K., Kikas, T., Tenno, T., and Niinistö, L. (1998) Preparation and characteriztion of platinum coatings for long life-time BOD biosensor. *Sens. Actuators* **47,** 21–29.

13. Paliteiro, C., Pereira, M. L., and Jorge, A. M. (1991) Oxygen reduction on platinum electrodes coated with Nafion. *Electrochim. Acta* **9,** 507–523.
14. Sittampalam, G. and Wilson, G. S. (1982) Amperometric determination of glucose at parts per million levels with immobilized glucose oxidase. *J. Chem. Ed.* **59,** 70–73.
15. Eklund, S., Taylor, D., Kozlov, A., Prokop, A., and Cliffel, D. (2004) A microphysiometer for simultaneous measurement of changes in extracellular glucose, lactate, oxygen, and acidification rate. *Anal. Chem.* **76,** 516–527.

Index

METHODS IN MOLECULAR BIOLOGY™ • 303
SERIES EDITOR: *John M. Walker*

NanoBiotechnology Protocols

Edited by

Sandra J. Rosenthal *and* **David W. Wright**
The Department of Chemistry, Vanderbilt University, Nashville, TN

The combination of nanoscience and biotechnology promises to yield revolutionary biological insights, ranging from receptor function to drug discovery to personal medicine. In *NanoBiotechnology Protocols,* hands-on experts in nanomaterial synthesis and application describe in detail the key experimental techniques currently employed in novel materials synthesis, dynamic cellular imaging, and biological assays. The authors emphasize diverse strategies to synthesize and functionalize the use of nanoparticles for biological applications. Additional chapters focus on the use of biological components (peptides, antibodies, and DNA) to synthesize and organize nanoparticles to be used as a building block in larger assemblies. These new materials make it possible to image cellular processes for longer durations, leading to high throughput cellular-based screens for drug discovery, drug delivery, and diagnostic applications. Highlights include overview chapters on quantum dots and DNA nanotechnology, and cutting-edge techniques in the emerging nanobiotechnology arena. A value-added compact disk containing color figures is included. The protocols follow the successful *Methods in Molecular Biology*™ series format, each offering step-by-step laboratory instructions, an introduction outlining the principle behind the technique, lists of the necessary equipment and reagents, and tips on troubleshooting and avoiding known pitfalls.

Illuminating and cross-disciplinary, *NanoBiotechnology Protocols* enables novice and experienced researchers alike to quickly come up to speed with both nanomaterials preparation and the use of nanomaterials in biological and medicinal applications.

FEATURES

- **State-of-the-art techniques to synthesize and functionalize the use of nanoparticles**
- **Overview chapters on quantum dots and DNA nanotechnology**
- **Diverse strategies to synthesize and functionalize nanoprobes for biological applications**
- **Introductory review chapters for novices new to nanobiotechnology**
- **High throughput cellular-based screens for drug discovery and diagnostic applications**
- **Tricks of the trade and notes on troubleshooting and avoiding known pitfalls**

CONTENTS

Methods in Molecular Biology™ • 303
NANOBIOTECHNOLOGY PROTOCOLS
ISBN: 1-58829-276-2 E-ISBN: 1-59259-901-X
ISSN: 1064–3745 humanapress.com

ISBN 1-58829-276-2
9 781588 292766 90000